HIGH PERFORMANCE POLYESTER-BASED MATERIALS

A thesis submitted in part fulfilment of the degree of Doctor of Philosophy

STEPHEN MICHAEL JONES

Department of Chemistry

2015

Abstract

Biaxially oriented films produced from semi-crystalline, semi-aromatic polyesters are utilised extensively as components within various applications, including the specialist packaging, flexible electronic and photovoltaic markets. However, the thermal performance of such polyesters, specifically poly(ethylene terephthalate) (PET) and poly(ethylene-2,6-naphthalate) (PEN), is inadequate for several applications that require greater dimensional stability at higher operating temperatures. The work described in this project is therefore primarily focussed upon the copolymerisation of rigid comonomers with PET and PEN, in order to produce novel polyester-based materials that exhibit superior thermomechanical performance, *with* retention of crystallinity, to achieve biaxial orientation.

Rigid biphenyldiimide comonomers were readily incorporated into PEN and poly(butylene-2,6-naphthalate) (PBN) via a melt-polycondensation route. For each copoly(ester-imide) series, retention of semi-crystalline behaviour is observed throughout entire copolymer composition ratios. This phenomenon may be rationalised by cocrystallisation between isomorphic biphenyldiimide and naphthalenedicarboxylate residues, which enables statistically random copolymers to melt-crystallise despite high proportions of imide sub-units being present. In terms of thermal performance, the glass transition temperature, T_g, linearly increases with imide comonomer content for both series. This facilitated the production of several high performance PEN-based biaxially oriented films, which displayed analogous drawing, barrier and optical properties to PEN. Selected PBN copoly(ester-imide)s also possess the ability to either melt-crystallise, or form a mesophase from the isotropic state depending on the applied cooling rate.

An equivalent synthetic approach based upon isomorphic comonomer crystallisation was subsequently applied to PET by copolymerisation with rigid diimide and Kevlar®-type amide comonomers, to afford several novel high performance PET-based copoly(ester-imide)s and copoly(ester-amide)s that all exhibited increased T_gs. Retention of crystallinity was achieved in these copolymers by either melt-crystallisation or thermal annealing. The initial production of a semi-crystalline, PET-based biaxially oriented film with a T_g in excess of 100 °C was successful, and this material has obvious scope for further industrial scale-up and process development.

Declaration of original authorship

I confirm that this is my own work and the use of all material from other sources has been properly and fully acknowledged.

_____ Stephen Michael Jones

Acknowledgements

I would first like to thank my supervisors, Prof. Howard Colquhoun (University of Reading) and Dr. Stephen Sankey (DuPont Teijin Films), for all of the support and guidance offered to me throughout the course of the research project. This has enabled the development of my chemistry knowledge and transferrable skills due to the faith and encouragement given.

With research being conducted at both the University of Reading and DuPont Teijin Films, there are many other people that have contributed to this research project. In Reading, I would like to thank past and present members of the HMC group for their support in the lab and positive influence towards the work environment. I am also grateful to Nick Spencer and Dr. Kenneth Shankland (both XRD), and to Martin Reeves (MS) for their technical assistance.

The industrial-scale synthesis and film-production work undertaken at Wilton was performed with contributions from Dave Turner, James Kelly, Robert Welford, Dr. Kieran Looney and Megan Todd of DuPont Teijin Films, Alan Patterson of Cordell and Roy Valentine of High Force Research. Furthermore, I wish to thank Joe Perkins (NMR), Dave Stocks (rheology), Andrew Broadhurst (DMA) and Simon Young (GPC) of Intertek who provided invaluable characterisation data.

This PhD project was fully funded by DuPont Teijin Films, who provided both direct financial support and also, as indicated above, substantial technical contributions to the progress of the research.

Finally, I am grateful for the continual support given by my family and girlfriend Rachel, without whom the completion of this thesis would not have been possible.

Table of contents

List of abbreviations

3HB	3-Hydroxybutyrate
3HV	3-Hydroxyvalerate
A	Cross-sectional area
AFP	Aromatic fluorinated polyarylate
AR	Bisphenol-A aryl carbonate
BB	Biphenyl-4,4'-dicarboxylic acid
BHBN	Bis(4-hydroxybutyl)-2,6-naphthalate
BHEI	*N*,*N*'-Bis-[*p*-(2-hydroxyethoxycarbonyl)phenyl]-biphenyl-3,4,3',4'-tetracarboxydiimide
BHEN	Bis(2-hydroxyethyl)-2,6-naphthalate
BHET	Bis(2-hydroxyethyl)terephthalate
BHTA	*N*,*N*'-bis(2-hydroxyethyl)terephthalamide
BPDA	Biphenyl-3,4,3',4'-tetracarboxylic dianhydride
$CHCl_3$	Chloroform
CHDM	1,4-Cyclohexylenedimethylene terephthalate
C_p	Heat capacity
CTE	Coefficient of thermal expansion
Đ	Dispersity (polydispersity index)
DEG	Diethylene glycol
DMA	Dynamic mechanical analysis
DMAc	*N*,*N*-Dimethylacetamide
DMF	*N*,*N*-Dimethylformamide
DMN	2,6-Dimethylnaphthalate
DMSO	Dimethyl sulfoxide
DMT	Dimethyl terephthalate
DPM	4,4'-Bis-[(4-carbo-2-hydroxyethoxy)-phthalimido]diphenylmethane
dQ/dt	Heat flow
DSC	Differential scanning calorimetry
dT/dt	Heating rate
DTF	DuPont Teijin Films U.K Ltd.
E	Elastic modulus
EG	Ethylene glycol

ETB	Elongation to break
F	Load
f(t,T)	Kinetic heat flow component
f''(t,T)	Thermodynamic heat flow component
G'	Storage modulus
G''	Loss modulus
GPC	Gel permeation chromatography
HBA	*ρ*-Hydroxybenzoic acid
HFIP	1,1,1,3,3,3-Hexafluoro-2-propanol
η_{inh}	Inherent viscosity
IR	Infrared spectroscopy
IV	Intrinsic viscosity
K	Empirical parameter
k	Overall crystallisation rate constant
L_c	Lamellar thickness
l_o	Initial film length
LTO	Linear Tape Open
MAF	Mobile amorphous fraction
M_n	Number-average molecular weight
$Mn(OAc)_2.4H_2O$	Manganese (II) acetate tetrahydrate
M_w	Weight-average molecular weight
M_z	Z-average molecular weight
N	Number of polymeric products
n	Avrami exponent
N_0	Number of monomer molecules
NDA	2,6-Naphthalenedicarboxylic acid
NDC	2,6-Naphthalene dicarboxylate
NMR	Nuclear magnetic resonance spectroscopy
$\bar{n}_{PEN}$	Number-average PEN sequence length
OLED	Organic light emitting diode
OTR	Oxygen transmission rate
p	Number of functional groups reacted
PBN	Poly(butylene-2,6-naphthalate)

PBT	Poly(1,4-butylene terephthalate)
PC	Polycarbonate
PDI	*N*,*N*'-Bis-(2-hydroxyethyl) pyromellitimide
PEEK	Polyetheretherketone
PEN	Poly(ethylene-2,6-naphthalate)
PES	Polyethersulfone
PET	Poly(ethylene terephthalate)
PI	Polyimide
PV	Photovoltaic
RAF	Rigid amorphous fraction
$\mathbf{R_{wp}}$	Weighted-profile R value
$\mathbf{Sb_2O_3}$	Antimony trioxide
SSP	Solid state polymerisation
$\boldsymbol{t_0}$	Crystallisation onset time
$\boldsymbol{t_{0.5}}$	Crystallisation half-time
T2T	*N*,*N*'-Bis(*p*-carbomethoxybenzoyl)ethanediamine
T4T	*N*,*N*' Bis(*p*-carbomethoxybenzoyl)butanediamine
TA	Terephthalic acid
$\boldsymbol{T_{cc}}$	Cold crystallisation temperature
$\boldsymbol{T_d}$	Degradation temperature
TFA	Trifluoroacetic acid
$\boldsymbol{T_g}$	Glass transition temperature
$\boldsymbol{T_g}$*	Maximum glass transition temperature
TGA	Thermogravimetric analysis
$\boldsymbol{T_i}$	Isothermal temperature
TLT	Total light transmission
$\boldsymbol{T_m}$	Crystalline melting temperature
$\boldsymbol{T_m}^\circ$	Equilibrium melting point
UV	Ultraviolet
$\boldsymbol{V_c}$	Relative volumetric transformed fraction
$\boldsymbol{W_c}$	Crystalline mass fraction
WVTR	Water vapour transmission rate
XRD	X-ray diffraction

$\boldsymbol{X_n}$	Number-average degree of polymerisation
$\boldsymbol{X_w}$	Weight-average degree of polymerisation
$\boldsymbol{\gamma}$	Lamellar thickening factor
$\boldsymbol{\Delta H(t)}$	Maximum enthalpy value
$\boldsymbol{\Delta H_{cc}}$	Enthalpy of cold crystallisation
$\boldsymbol{\Delta H_f}$ **or** $\boldsymbol{\Delta H_m}$	Enthalpy of fusion
$\boldsymbol{\Delta H_f^\circ}$ **or** $\boldsymbol{\Delta H_m^\circ}$	Enthalpy of fusion for a crystal at the T_m°
$\boldsymbol{\Delta H_{total}}$	Cumulative enthalpy value
$\boldsymbol{\Delta H_u}$	Heat of fusion per comonomer unit
$\boldsymbol{\Delta S_m}$	Entropy of melting
$\boldsymbol{\varepsilon}$	Strain
$\boldsymbol{\eta^*}$	Complex viscosity
$\boldsymbol{\rho_a}$	Amorphous density
$\boldsymbol{\rho_c}$	Crystalline density
$\boldsymbol{\sigma}$	Specific fold-surface free energy or tensile stress
$\boldsymbol{\chi}$	Degree of randomness
$\boldsymbol{\chi_c}$	Degree of crystallinity

Chapter 1
Introduction

1.1 Research motivation

Thermoplastic, semi-aromatic, semi-crystalline polyesters have become ubiquitous in modern life since the initial discovery of poly(ethylene terephthalate) (PET) by Whinfield and Dickson in 1941.[1,2] Such polyesters exhibit high mechanical, thermal and electrical performance and may be readily processed into fibre, moulded or film form at a low manufacturing cost relative to alternative polymers. This has ensured their utilisation in many applications incorporating blow-moulded bottles, clothing fibres and biaxially oriented film. The global demand for PET resin is expected[3] to reach ~ 21 million tonnes in 2015, emphasising the global significance of this product market.

DuPont Teijin Films U.K Ltd. (DTF) is the world leader in the supply of PET and poly(ethylene-2,6-naphthalate) (PEN) biaxially oriented film (Figure 1.1), with a current global turnover exceeding $1.5 bn p.a.[4] The current portfolio of DTF manufactured polyester film is featured within various products including photovoltaic (PV) modules, electrical insulation components and specialist food packaging. However, despite this clear demand for polyester film, the relatively poor thermal performance and stability of PET and PEN in comparison to thermoplastic polymers such as polyetheretherketone (PEEK) is inhibiting future product innovation.[5–7]

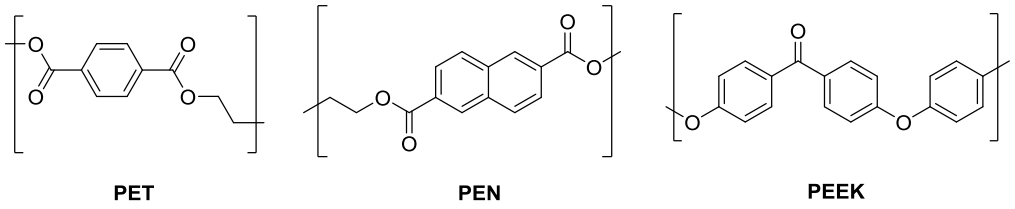

Figure 1.1 Molecular structures of poly(ethylene terephthalate) (PET), poly(ethylene-2,6-naphthalate) (PEN) and polyetheretherketone (PEEK).

For example, it is desirable for commercial organic electronic devices to be printed on plastic substrates in the field of flexible electronics to benefit from a continuous, high-speed printing process utilising PET support film. As illustrated in Figure 1.2 by an organic light emitting diode (OLED) variant, plastic-based flexible displays offer more aesthetic product portfolios and greater processing volumes than glass equivalents.[8,9] The industrial-scale production of such products is not currently achievable, as the upper working temperatures of polyester film

are below the required temperatures for the deposition of electro-active components. Furthermore, the subsequent thermal annealing and soldering steps that ensures the correct operation of such devices are also performed at inoperable temperatures. PET, in particular, is also relatively permeable to water vapour and oxygen, substances that are critically damaging to PV modules and hence shorten the associated product lifetimes.

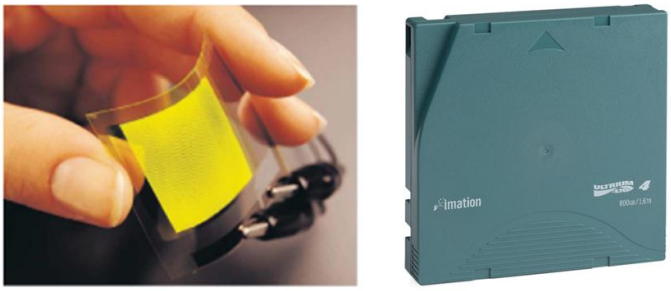

Figure 1.2 Photograph of a flexible organic light emitting diode (OLED) display (left, reproduced with permission from W. A. MacDonald[10]), juxtaposed with a photograph of a data cartridge consisting of Linear Tape Open (LTO) format magnetic storage tape (right).

In view of the greater thermal performance PEN exhibits over PET, it is preferentially utilised in applications, which require more demanding operating temperatures e.g. within magnetic recording media for high density data storage and electronic circuitry for hydrolysis resistant automotive wiring. An increase in data storage, defined as a greater density or capacity of information, in the Linear Tape Open (LTO) format[11] may be progressively achieved upon this transition to a superior performing film. The control of dimensional reproducibility in biaxially oriented polyester film is also critical for the long-term performance of such applications. This property ensures that film expansion and contraction is minimal throughout the thermal processing steps of multilayer composite structures, which are also utilised in flexible electronic displays. It is reasonable to assume that any additional increase in thermal or dimensional stability relative to PEN would enable a greater incorporation of polyester-based biaxially oriented film in data storage and analogous applications.

The aim of this research project is therefore to improve the thermomechanical performance of PET and PEN biaxially oriented film, for future incorporation in the applications previously discussed. A more comprehensive overview of the project objectives will be presented at the end of Chapter 1. This is preceded by a literature review which will: analyse the current routes to synthesise PET and PEN in polymer and film form; discuss the structure-property relationships of semi-aromatic, semi-crystalline polyesters; and give an evaluation of previous attempts to improve the thermomechanical performance of polyesters.

1.2 Chemistry of polyesters

1.2.1 Step-growth polymerisation

Polyesters are synthesised by the polycondensation of monomer molecules; defined as the repeated reaction between two reactive functional groups to form a single functional group accompanied with the loss of a small-molecule condensate.[12] In context, this typically involves the esterification reaction of diol and dicarboxylic acid comonomers of the *xx* and *yy* type to produce water as a byproduct, where *x* and *y* represent the respective functional groups that may react with one other.

The polycondensation reaction is a form of step-growth polymerisation, of which the general progression scheme is illustrated in Figure 1.3. It is observed that two monomers initially react to form a dimer, which then may react further with another monomer and so forth. A functional group of any *z*-mer may then react with another functional group of any other *z*-mer to progressively form the polymer chain, where *z* is the number of structural repeating units within the polymer. The rate of increase in molecular weight is therefore relatively slow in comparison to addition (chain-growth) polymerisation.

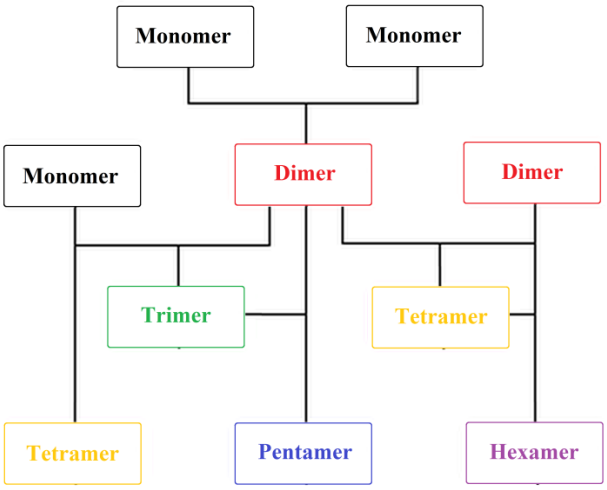

Figure 1.3 General molecular weight progression for a step-growth polymerisation.[13]

The extent of a polycondensation reaction i.e. the achieved molecular weight, may be described by the Carothers equation[14] (Equation 1.1), where X_n is the number-average degree of polymerisation, N_0 is the number of monomer molecules, N is the number of polymeric products and p is the number of functional groups reacted. The degree of polymerisation can therefore be monitored by measuring the conversion of monomer units:

Equation 1.1

$$X_n = \frac{N_0}{N} = \frac{N_0}{N_0(1-p)} = \frac{1}{(1-p)}$$

It is reported[15] that there are three requirements for the synthesis of high molecular weight linear polymers from difunctional monomers: the stoichiometric balance of monomers; a high degree of monomer purity; and a high yielding polymerisation reaction. With respect to Equation 1.1, it is clear that a high molecular weight will only be obtained as *p* tends to 1, at the end of the reaction. This becomes increasingly harder to achieve as the polymerisation progresses (even under the assumption of using stoichiometric and pure monomers) due to the difficulty in maintaining stoichiometric equivalence; the decreasing frequency of chain-end groups encountering reactive sites and increasing interference from side reactions.

The molecular weight distribution, X_w/X_n, of a step-growth polymer may be calculated from Equation 1.2, where X_w is the weighted average degree of polymerisation. This measure may also be defined as the dispersity, Đ, and is observed to increase with respect to *p* and tends to a maximum value of 2 when *p* approaches 1. In contrast to chain-growth polymerisation, step-growth polymers therefore generally possess a greater Đ due to the statistical distribution of polymer chain lengths formed in a step-wise manner.

Equation 1.2

$$\frac{X_w}{X_n} = 1 + p$$

A copolymer may be formed if two comonomers, defined as A and B, possess different chemical structures (aside from the reactive functional groups). Figure 1.4 illustrates the three categories of copolymer that may arise from the step-growth copolymerisation of A and B *xy*-type comonomers, in terms of comonomer sequence distribution within the copolymer chain. Flory[16] stated that the step-growth kinetics of a mono-esterification reaction are equivalent to the polycondensation analogue, assuming equal reactivity of the respective functional groups. If the relative amounts of the *xy*-type comonomers therefore differ, then a random copolymer is most commonly observed whereby A and B are statistically distributed within the copolymer chain according to their relative content.

If two comonomers of the *xy*-type are copolymerised in equal ratios,[17] an alternating copolymer may be formed comprising A and B in an alternating sequence. This sequence may also be considered as an AB homopolymer structure given the increased ordering. A block copolymer, defined as when the copolymer chain consists of repeated long sequences of A followed by long sequences of B, is rarely observed in step-growth polymers because of the kinetic theory previously discussed. Some examples of block copolymers, as detailed by Woody *et al.*[18] have been synthesised via the reaction of dihalides with appropriately

substituted difunctional groups. However, this type of polymer remains outside of the scope of the present research project and will not be detailed further.

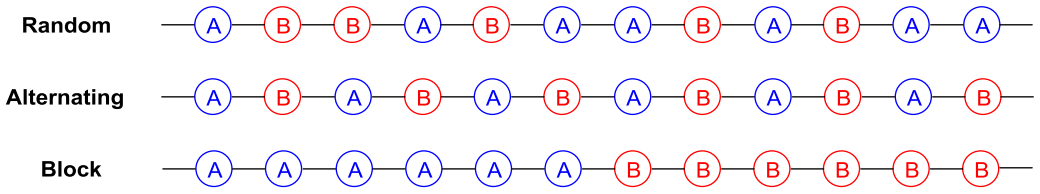

Figure 1.4 Comparative sequence distributions for an AB-type copolymer of the *xy*-type following step-growth polymerisation.

The repeated esterification reaction in the synthesis of polyesters proceeds via the reversible $A_{AC}2$ mechanism. As illustrated in Scheme 1.1, this initially occurs through the nucleophilic attack of a diol on the carboxylic acid carbonyl group of a diacid. Water is then removed as a leaving group following intramolecular proton transfer, to afford the ester product. The equilibrium constant for polyester formation is relatively small in comparison to that for the reverse reaction,[13] so that water and/or other low molecular weight byproducts must be concurrently removed in order to achieve high molecular weight polyesters.

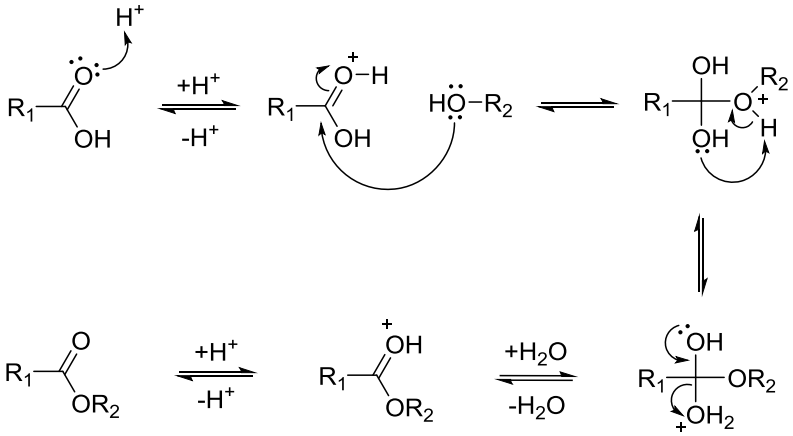

Scheme 1.1 The $A_{AC}2$ mechanism for esterification/hydrolysis and transesterification/glycolysis.[19]

1.2.2 Industrial synthesis of PET and PEN

The industrial synthesis of semi-crystalline, semi-aromatic polyesters is achieved[20] in two steps: esterification and polycondensation. For PET and PEN, the polycondensation step involves the linear step-growth polymerisation of bis(2-hydroxyethyl) terephthalate (BHET) or bis(2-hydroxyethyl)-2,6-naphthalate (BHEN), respectively. The esterification step may occur by two different routes: transesterification and direct esterification. In this section, discussion of the synthetic routes is focussed upon PET, with reference given to PEN where differences are observed.

BHET may be formed by the transesterification reaction of dimethyl terephthalate (DMT) with ethylene glycol (EG) (Scheme 1.2). The reaction is carried out at temperatures between 170 and 210 °C (190-230 °C for BHEN) with an excess of EG[21] (1:2.2 DMT:EG) in order to drive the reaction equilibrium forward. Metal acetates (Mn, Pb, Co, Zn) are typically utilised[22–24] as catalysts, though a large number of alternatively derivatised metals have also been reported.[25,26] The reaction kinetics were observed[27] to be third order overall, being first order with respect to DMT or 2,6-dimethylnaphthalate (DMN), EG and the catalyst. There is still significant debate regarding the catalytic mechanism, with different proposals made by Fontana,[27] Walker[28] and Choi *et al*.[29] It is generally considered that the reaction proceeds via the formation of a metal alcoholate, yet the formation and contribution of oligomers remains poorly understood.[20]

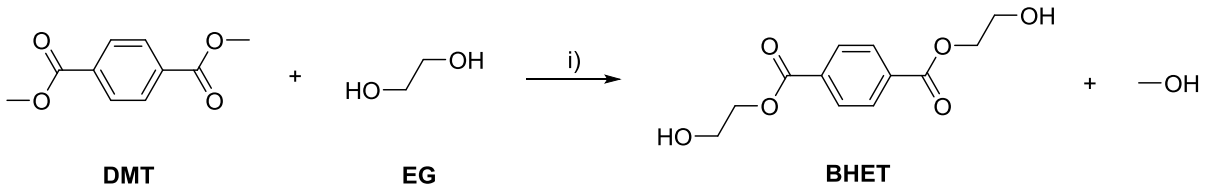

Scheme 1.2 Transesterification of PET, where DMT = dimethyl terephthalate, EG = ethylene glycol and BHET = bis(2-hydroxyethyl) terephthalate. Experimental conditions: i) 170-210 °C, metal acetate catalyst.

The by-product of the transesterification reaction is methanol, which is a clear disadvantage of this synthesis route in terms of waste production on an industrial-scale. This safety concern may be avoided by synthesising BHET via the *direct* esterification of terephthalic acid (TA) with EG (Scheme 1.3). This route is now therefore preferred for the industrial manufacture of PET,[30] facilitated by the increasing commercial availability of pure TA. Furthermore, the direct esterification route has reduced catalytic requirements and consumption of EG (1:1.5 TA:EG), resulting in lower synthetic costs in comparison to the transesterification reaction detailed in Scheme 1.2.

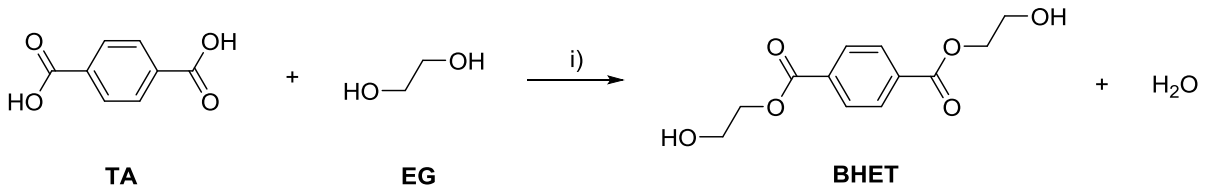

Scheme 1.3 Direct esterification of PET, where TA = terephthalic acid. Experimental conditions: i) 230-260 °C, under vacuum (< 1 mbar).

The direct esterification of TA is performed at temperatures between 230-260 °C under pressure (~ 3 bar),[31–33] in order to increase the solubility of TA in EG. As the carboxylic acid groups in TA act as both a reagent and catalyst,[34] no external catalysts are required. However,

Ti(IV) butoxide catalysts may also be used in order to reduce the reaction time.[35,36] The solubility of 2,6-naphthalenedicarboxylic acid (NDA) in EG is relatively poor, resulting in low reaction rates, so that the transesterification route is still preferred for PEN.

Scheme 1.4 illustrates the melt-polycondensation reaction of BHET, the second step in the synthesis of PET. This is performed under vacuum (< 1 mbar) at high temperatures (up to 290 °C or 300 °C for PET or PEN, respectively), to ensure the concurrent removal of EG by distillation. Antimony trioxide (Sb_2O_3) is the most commonly utilised[37] polycondensation catalyst due to its high commercial availability and low acidity.

Despite Ti(IV) catalysts possessing a greater catalytic activity than Sb(III) equivalents, their usage is restricted because they promote side reactions which give a yellow discolouration to the final polymer.[38] The mechanism of Sb_2O_3 catalysis is still debated within the literature,[23,39] but reaction is postulated to occur via metal coordination to either the ester carbonyl or terminal hydroxyl functional groups. Stevenson *et al.*,[40] Challa[41] and Santacesaria[42] *et al*. claim that monomeric BHET forms an inactive complex with Sb_2O_3, so that only oligomeric BHET contributes to the formation of PET.

It is also known[25] that Sb_2O_3 has a negative impact on polymer stability, in addition to the contribution of unwanted side products that will be discussed later in more detail. The introduction of phosphorus-based stabilisers, such as phosphoric acid, triphenylphosphate and triphenylphosphite, at the polycondensation stage is observed[43–45] to increase the thermal stability and visible appearance of PET. The mechanism by which this occurs is still unknown, but is thought to occur by the inhibition of polycondensation catalysts.[26]

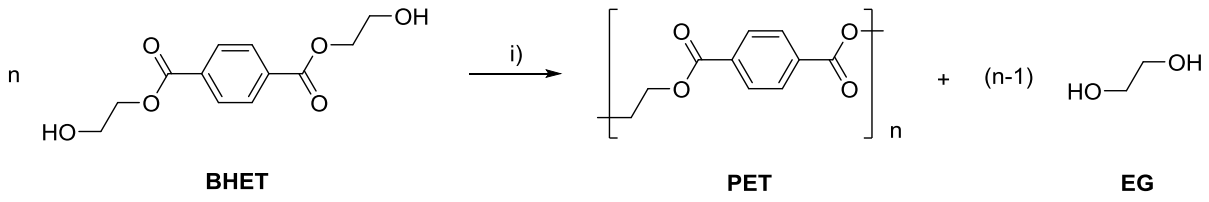

BHET **PET** **EG**

Scheme 1.4 Polycondensation of PET. Experimental conditions: i) 270-290 °C, 1-3 h, Sb_2O_3, phosphorus-based stabiliser.

The polycondensation reaction is continued until the desired molecular weight is achieved. This may be monitored by and correlated with the intrinsic melt viscosity (IV) of the reaction melt,[46] estimated by the torque exerted on the melt stirrer, which increases as the polycondensation progresses. An IV of 0.60-0.65 dL g^{-1} (M_n < 20,000 Da) is required for the processing of PET into biaxially oriented film, and may be produced from the discussed

melt-polycondensation route. However, this range of molecular weight must be increased for applications such as bottle grade and technical fibres that require an IV of 0.90 dL g^{-1} or greater.[47] High molecular weight polyesters cannot be produced industrially via the melt-polycondensation route, as the accompanied increase in IV renders the polymer inextrudable and lowers the diffusion and exchange coefficients necessary for the sufficient removal of EG.[48] Furthermore, the long reaction times and increased temperatures required to obtain improved molecular weights increases the risk of degradative side reactions.

However, the molar mass of condensation polymers such as PET may be increased further by solid-state polymerisation (SSP). SSP may therefore be considered as an additional, but not isolated, synthesis step of PET and is generally performed ~ 10-50 °C below the crystalline melting temperature, T_m, of the polymer but significantly higher than the glass transition temperature, T_g.[49] An inert atmosphere of dry nitrogen, or a vacuum, is used to prevent oxidative degradation. As illustrated in Scheme 1.5, the synthetic chemistry for achieving progressive chain growth is identical to that under melt-polycondensation conditions. Thus, SSP may proceed by transesterification or direct esterification reactions via the removal of hydroxyl and carboxyl end groups respectively, in the amorphous regions of the polyester.

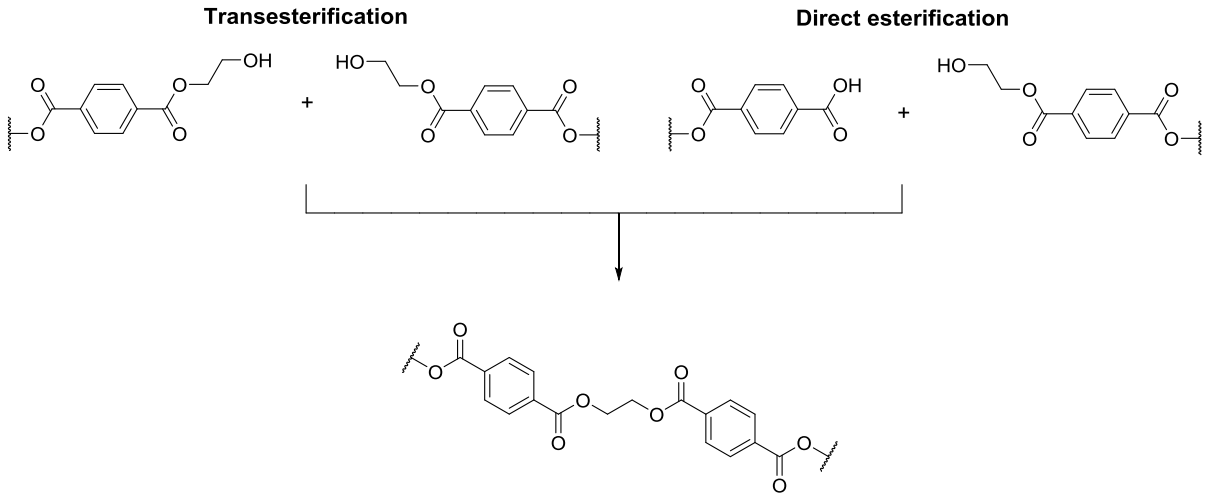

Scheme 1.5 Further transesterification and polycondensation reactions of PET by solid state polymerisation (SSP).

It is reported[50] that the theoretical SSP reaction rate is determined by several conditions: diffusion of the chain-end groups in the solid phase; diffusion of the byproducts (EG and water) through the solid phase; and the removal of byproducts in the gas phase. In practice, the observed SSP reaction rate is mainly dependent on the sole parameter that may be controlled (the use of a dynamic vacuum to aid the removal of byproducts), but is still slower

than the equivalent melt-polycondensation reaction. This is due to the limited mobility of polymer chains in the solid phase, which simultaneously decreases as the SSP reaction progresses and thus the level of crystallinity in the polymer increases.

1.2.2.1 Side and degradation reactions

The synthesis of semi-crystalline, semi-aromatic polyesters by the melt-polycondensation route is accompanied by several side reactions, which are to the detriment of the molecular weight and the subsequent quality of the final polymer. Among those reactions of concern is the formation of diethylene glycol[51,52] (DEG), as extensively studied by Chen *et al.*,[53–56] which primarily occurs during the polycondensation stage. It is reported that for each mol% increase of DEG with respect to PET, the T_m of PET is reduced by 5 °C.[57] In the context of this project, the introduction of flexible DEG units would also decrease the T_g and therefore reduce the thermomechanical performance of any synthesised polymer.

As illustrated in Scheme 1.6, the formation of DEG is most likely to occur by the etherification of two hydroxyl groups on separate EG molecules. This may occur either in the free form of EG (top), when terminally bound to the polymer chain (middle) or through a combination of both mechanisms (below). Otton *et al.*[58] demonstrated that the formation rate of DEG was fastest between the reaction of free and terminal EG, aided by intramolecular assistance from the ester carbonyl group which accelerates the nucleophilic substitution reaction.[19] An alternative mechanism was previously suggested by Hovenkamp *et al.*,[59] who claimed that DEG was formed by the reaction of the ester carbonyl group with EG to afford DEG and TA. This route appears less probable due to the opposing consensus in the literature and the unusual nature of a primary alcohol reacting with the ester of a weak organic acid.

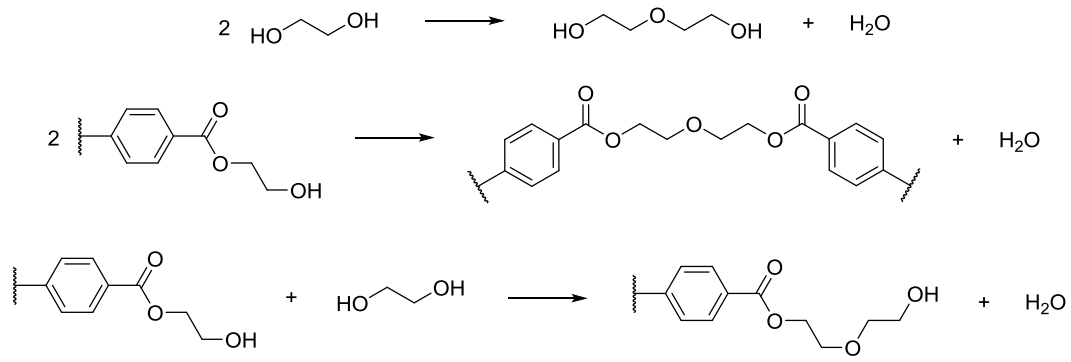

Scheme 1.6 Different possible routes to the formation of diethylene glycol (DEG)[53] residues in the synthesis of PET.

The content of DEG in commercial PET is typically between 1-3.6 mol%[23] and is observed to vary depending on the polymerisation conditions used. However, DEG is always present in

the final polymer as it possesses an almost identical reactivity, lower volatility and higher boiling point in comparison to EG (235 against 197 °C).[31] The final content level of DEG in PET may therefore only be controlled rather than inhibited. It is also noted that the formation of DEG is greater when utilising the DMT transesterification route towards PET synthesis, due to the because of increased hydroxyl functionality in the starting reagents.

PET also contains between 2-3 mol% of oligomers in either linear or cyclic form.[19] Unlike DEG, short-chain oligomers may be removed from the final polymer by solvent extraction (but this is generally more applicable to laboratory-scale syntheses than for industrial purposes). Oligomers are mainly formed during the synthesis of PET, but may also be produced under drying and processing conditions from additional exposure to heat.[60] Linear oligomers arise from incomplete esterification reactions whereby methyl ester groups inhibit chain growth. West *et al.*[61] demonstrated that the formation probability of short-chain linear oligomers is no larger than that for longer PET chains, suggesting it becomes increasingly difficult to eliminate oligomers through chain-growth polymerisation after formation.

Peebles *et al.*[62] first proposed that cyclic oligomer formation occurred via a cyclodepolymerisation reaction, as illustrated in Scheme 1.7. At constant temperature, it was observed that the reaction rate is linearly dependent upon decreasing molecular weight and therefore increasing hydroxyl end group concentration. This mechanism was later supported by Ha *et al.*[63] and de Freire *et al.*[64]

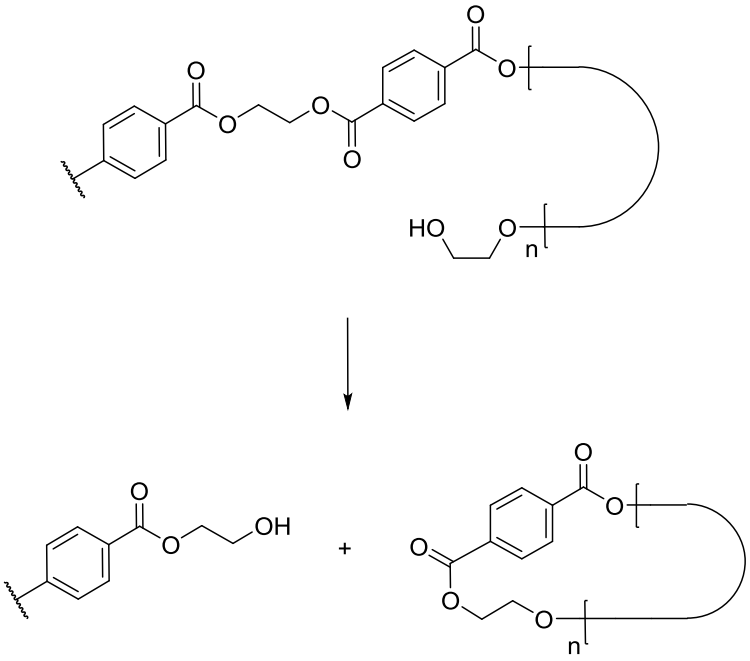

Scheme 1.7 Formation of cyclic oligomers in the synthesis of PET.[47]

The degradation of semi-aromatic, semi-crystalline polyesters leads to the deterioration of many properties due to changes in chemical functionality. Degradation usually occurs after the polyester has been subjected to external stimuli which include: heat (thermal); light (photo-oxidative); oxygen (oxidative) and weathering (hydrolytic).[31] In particular, the topics of photo-oxidative[65–67] and hydrolytic[68–70] degradation have been extensively covered within the literature and will not be further discussed as they principally occur post-synthesis.

With reference to the present project, the issue of thermal degradation is most prevalent and is reported to occur primarily during the melt-polymerisation step. The rate of thermal degradation rises with increasing reaction times and temperatures, particularly above 300 °C.[71] Thermo-oxidative degradation may also occur during synthesis or other extrusion methods, but is substantially reduced if an inert atmosphere is maintained.

The primary thermal decomposition process for PET is reported[72] to produce terminal vinyl groups which in turn cause discolouration and reduced molecular weight in the final polymer. This mechanism was initially proposed by Pohl *et al.*[73] to occur as illustrated in Scheme 1.8, and this was subsequently supported by further studies[44,74–76] which monitored the degradation products of PET and relevant model compounds as a function of temperature. It is observed that the chain scission of ester linkages in this ionic mechanism proceeds via an intramolecular β-hydrogen abstraction reaction through a six-membered transition state.

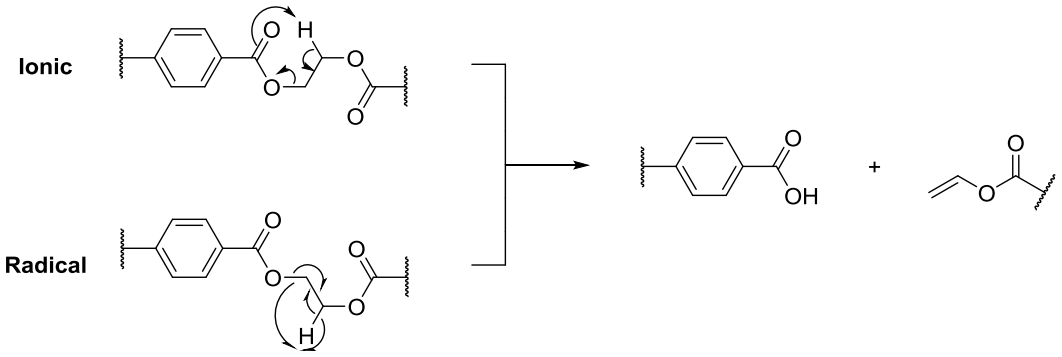

Scheme 1.8 Proposed primary thermal decomposition processes of PET.[73,77]

Alternative radical-based degradation mechanisms have been suggested, most notably by McNeill *et al.*[77] who suggested that the ionic-based degradation mechanism does not fully account for the full range of degradation products, notably CO and CO_2 at relatively low temperatures, following isothermal volatilisation analysis. It therefore remains likely that the initial thermal degradation of PET is the result of both ionic and radical based mechanisms, with experimental evidence in support of each route. Following primary chain scission,

numerous secondary thermal decomposition processes occur to produce terephthalic acid, carbon monoxide, carbon dioxide and acetaldehyde as the main decomposition products.[77,78]

1.3 Industrial film process

PET and PEN biaxially oriented film are exclusively produced by the stenter process, a route initially developed by Imperial Chemical Industries and DuPont in the 1950s.[79] Although polymer film may be manufactured by solvent casting or blow extrusion, the stenter process offers the advantage of interchangeable polymer grades and products during manufacturing, adding significant flexibility.[21] Furthermore, the sequential nature of the process permits cast, uniaxially and biaxially oriented film to be obtained, enabling progressive analysis of the developing film. This is particularly useful with novel materials, for which an established film process does not yet exist. The annotated schematic in Figure 1.5 illustrates the process in principle, which may be separated into four primary stages: polymer preparation and handling; extrusion and casting; drawing and heat setting; winding and recovery.[80]

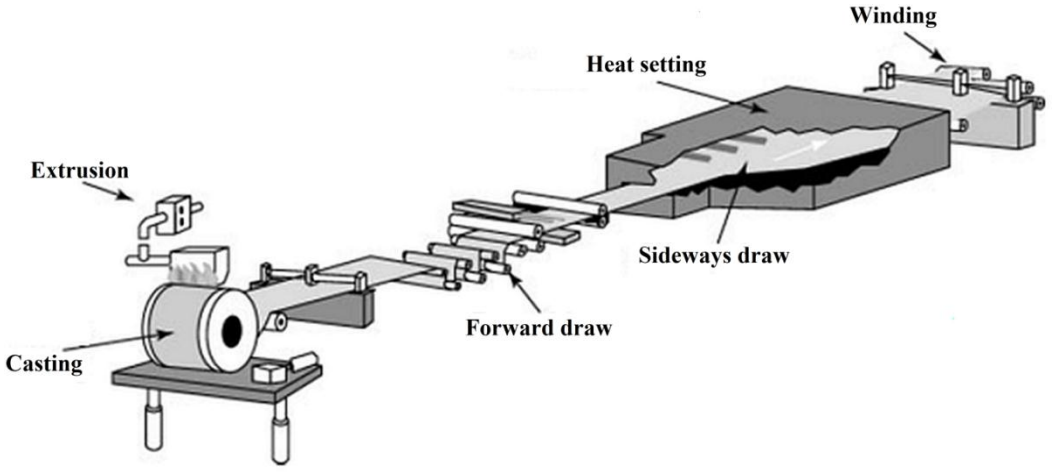

Figure 1.5 Annotated schematic of a typical extrusion fed, sequential draw stenter process for the manufacture of PET and PEN biaxially oriented film. Reproduced and edited with permission from W. A. MacDonald.[80]

The polymer chip is dried before being fed into the film process, in order to eliminate water absorbed by the carboxylic ester groups and hydroxyl chain ends. Any retention of water would significantly lower the molecular weight of the polymer through thermal hydrolytic degradation during extrusion.[68] For example, PET is typically dried at 160 °C for 4 hours under air at DTF.[31] This time period is sufficient for moisture content reduction, but short enough to avoid thermo-oxidative processes from occurring.[81,82]

Dry polymer is then melt-extruded at 270-310 °C through a horizontal slot die. There are many different extrusion systems in operation (e.g. single, twin and parallel screw), but all

exist to provide a consistent melt flow to the die. The molten polymer is consequently cast onto a chilled drum at ~ 10 °C,[83] which rapidly quenches the melt into an amorphous film.[84]

The cast film then passes through a pre-heat zone, set to ~ 15 °C above the T_g. This enables the film to be drawn in the machine direction (forward draw) at a draw ratio of ~ 3.5. As a result of the improved molecular alignment post-draw, stress-induced crystallisation is observed[85] (~ 10%) which also raises the tensile modulus and mechanical strength of the uniaxially oriented film.

In the primary stage of the stenter oven, the film edges are clipped along diverging rails and drawn in the transverse direction (sideways draw). This is performed at equivalent conditions as the forward draw, so that the developed properties in the transverse direction balance those previously observed in the machine direction (through the equal alignment of molecular chains in both directions). Further stress-induced crystallisation is observed at this stage (total of ~ 20%).

Following the sideways draw, the biaxially oriented film is heat-set in the stenter oven at temperatures above 200 °C. This process promotes thermally-induced crystallisation to give a final crystallinity of 40-50%, which reduces the tendency of the film to undergo shrinkage. As the number and size of crystallites has now increased, the molecular chains are consequently locked into an oriented state. Upon exiting the stenter oven, the film edges are trimmed and recycled back to monomer. The finished film is then quenched in air on cooled rollers and wound into rolls.

Drawn film samples may also be produced using a Long stretcher, a device designed and engineered by T. E. Long. This utilises cast film obtained from the stenter process to produce uniaxially and biaxially oriented film on a laboratory-scale. In brief, samples are attached to a vacuum-powered sample positioning arm clamped by several gas powered grips, before being held ~ 20 °C above T_g for < 1 min. The film may then be *simultaneously* drawn to achieve biaxially oriented film, in contrast to the stenter process. A more detailed description of the Long stretcher process and experimental conditions for the synthesis of oriented films in this thesis is provided in Chapter 2.

1.4 Properties of polyesters

1.4.1 Glass transition temperature

Polyester morphologies may be categorised into three main classes: amorphous; semi-crystalline and crystalline. Amorphous regions possess no long range ordering of the polyester chains but may contain embedded crystalline regions to form a semi-crystalline morphology. There has also, relatively recently, been substantial evidence for a third region denoted as the rigid amorphous phase, which will be discussed in further detail in Chapter 6.

The T_g has been operationally defined by Bicerano[86] and Bershstein *et al.*[87,88] as the temperature at which the forces holding the distinct components of an amorphous solid together are overcome by thermally induced motions. Large-scale molecular motions are enabled during the time-scale of the measured experiment, once there is sufficient freedom of motion within the chain segments to execute cooperative motions. A T_g is therefore only evident in an amorphous or semi-crystalline material.

Such restrictive forces depend on the cohesive interactions within and between chain segments and the geometric arrangement of these chain segments. Resistance to viscous flow, and consequently the value of the T_g, increases if a polymer possesses strong cohesive forces (intermolecular attractions) and high intramolecular rigidity (chain stiffness). The molecular mobility of the polymer chain and therefore the rigidity of the monomer units within the amorphous phase greatly influence the T_g. This may be manipulated by changes in the chemical structure of the repeat unit, whereby the introduction of chain stiffening groups, attractive intermolecular forces, bulky substituents or crosslinking groups all restrict rotational chain motion and thus increase the T_g.

The T_g may also described as a function of molecular weight by the Flory-Fox equation[89] (Equation 1.3):

Equation 1.3

$$\boldsymbol{T_g = T_g^* - \left(\frac{K}{M_n}\right)}$$

where T_g* is the maximum glass transition temperature that may be achieved at a theoretically infinite molecular weight, K is an empirical parameter related to the free volume present in the polymer and M_n is the number-average molecular weight of the polymer. Equation 1.3 states that the T_g increases with respect to M_n, as there is less free volume present within the polymer for molecular motion to occur. At low M_n, the molecular motion of polymer chains is dominated by that of chain-end groups and is therefore relatively low.

This concept of free volume was later modelled by Turnbull *et al.*[90] and Cohen *et al.*[91] in order to rationalise the behaviour of polymers at the T_g, where the free volume of a polymer is defined as the difference between the specific volume and the occupied volume. It was proposed that the mobility of polymer chains at a given temperature is primarily controlled by the free volume, in accordance with earlier work by Doolittle.[92] As illustrated in Figure 1.6, the occupied volume of a polymer remains relatively constant through the T_g, but the free volume which the polymer chains are able to move through increases. The sharp increase in both specific and free volume originates from conformational motions within polymer chains, which then enable molecular motions above the T_g to occur. It should be noted that the free volume model does not offer a comprehensive theoretical understanding of the T_g, with other kinetic and thermodynamic theories being proposed, most notably by Gibbs *et al.*[93]

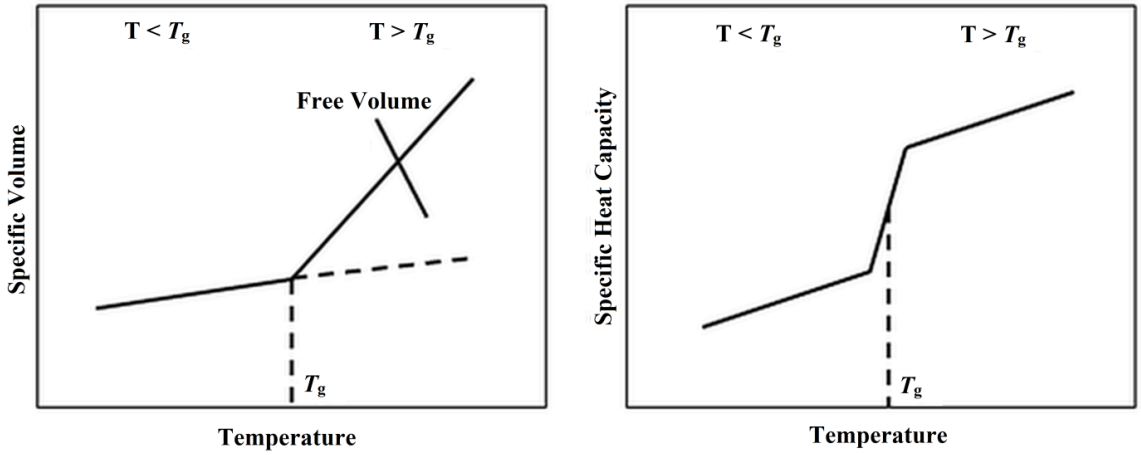

Figure 1.6 Temperature dependencies of the specific volume (left) and specific heat capacity (right) within an amorphous or semi-crystalline polymer. [86]

Although the changes in T_g may be at least partially explained and thus measured by the change in specific volume, the value is more commonly determined by a change in specific heat capacity (Figure 1.6). The increase in specific heat capacity at the T_g is discontinuous and thus characterised, most commonly by DSC, by an increased step change. This change typically occurs over a temperature range of 5-20 °C and may be influenced by the detection rate. It is therefore considered that the T_g is an experimental phenomenon and is not attributable to a first order phase transition.

In practical terms, the T_g is extremely significant as it essentially dictates many of the performance and processing characteristics of an amorphous or semi-crystalline polymer. This is most commonly illustrated by the fall in elastic modulus, E, of a polymer upon heating through the T_g with values typically ranging from 10^9-10^{10} and 10^5-10^6 Pa below and above the T_g, respectively. Such changes may be attributed to molecular relaxation of

polymer chains due to increased mobility, and in the case of oriented polymers, shrinkage or expansion associated with the relaxation of residual strain.[10] This may be qualitatively viewed as the transition from a rigid glassy state to a rubbery, pliable material.

1.4.2 Structure-property relationships

In addition to the T_g, the T_m and degree of crystallinity, χ_c, are key parameters in determining the thermomechanical performance of semi-crystalline polymers. The temperature range in which semi-crystalline polyesters exhibit improved thermal properties must also incorporate the processing temperature of the same material.[13] This is defined as the working temperature range, a phenomenon largely governed by the T_g and the T_m of a polymer. Therefore, in order to enhance the thermal properties of polyesters and ensure superior properties at a higher working temperature, the T_g must be increased. The T_m may also be increased to the maximum melt-processing temperature for polyesters (~ 300 °C), although this is not preferable as a higher melt-processing temperature promotes thermal degradation and increases manufacturing costs.

The notion of simultaneously increasing the T_g whilst maintaining the T_m for a polyester requires variation of the conventional T_g/T_m ratio found for homopolymers. Several authors[94–96] have proposed an average T_g/T_m value of 0.67 (temperature values in Kelvin) by sampling data for more than 130 different homopolymers, yet the theoretical understanding of this figure remains unknown. Lee *et al.*[96] proposed that the "two-thirds rule" may not be explained by a simple thermodynamic argument, with the energy, enthalpy, entropy and volume of a polymer system varying through the T_m yet remaining unchanged through the T_g.

It is reasonable to assume that a method to increase the T_g/T_m ratio beyond 0.67 may be designed if the T_m is considered as a function of lamellar thickness rather than a thermodynamic phenomenon.[97] This argument is based upon the knowledge that polymer crystallites are smaller than the crystals of low molecular weight compounds, which results in an extremely high surface area to volume ratio for polymer crystals. The relationship between lamellar thickness and the T_m is quantitatively described by the Thompson-Gibbs equation:[98]

Equation 1.4

$$\boldsymbol{T_m = T_m^\circ \left(1 - \left(\frac{2\sigma}{\Delta H_m^\circ \rho_c L_c}\right)\right)}$$

where T_m° is the equilibrium melting temperature and represents the T_m of a crystallite of infinite thickness, σ is the specific fold-surface free energy, ΔH_m° is the enthalpy of fusion for a crystal at the T_m°, ρ_c is the crystalline density and L_c is the lamellar thickness. Due to the T_g

being a property of the amorphous phase whereas the T_m is a property of the crystalline phase in a semi-crystalline polymer, the T_g may be conceivably manipulated without affecting the T_m assuming the lamellar thickness of the crystalline phase remains unchanged. It is noted that an increase in lamellar thickness represents the formation of more stable polymer crystals and thus leads to an increase in the T_m of the polymer.

The chemical structures of PET and PEN differ only in the aromatic moiety of the repeating unit: a terephthalate ring for PET; and a 2,6-naphthalate ring for PEN.[99] Although PET exhibits an excellent balance of overall properties in comparison to alternative thermoplastic polymers, the increased rigidity conferred upon PEN by the naphthalene rings has a significant effect on the comparative polymer properties (Figure 1.7). It is observed that heat-stabilised PEN biaxially oriented film displays superior thermal [T_g, coefficient of thermal expansion (CTE), processing temperature] and mechanical properties (moduli and shrinkage) to the PET equivalent. The main disadvantage, aside from the greater manufacturing cost, in moving from PET to PEN is the slower crystallisation rate that accompanies the addition of non-collinear carbonyl groups.[100]

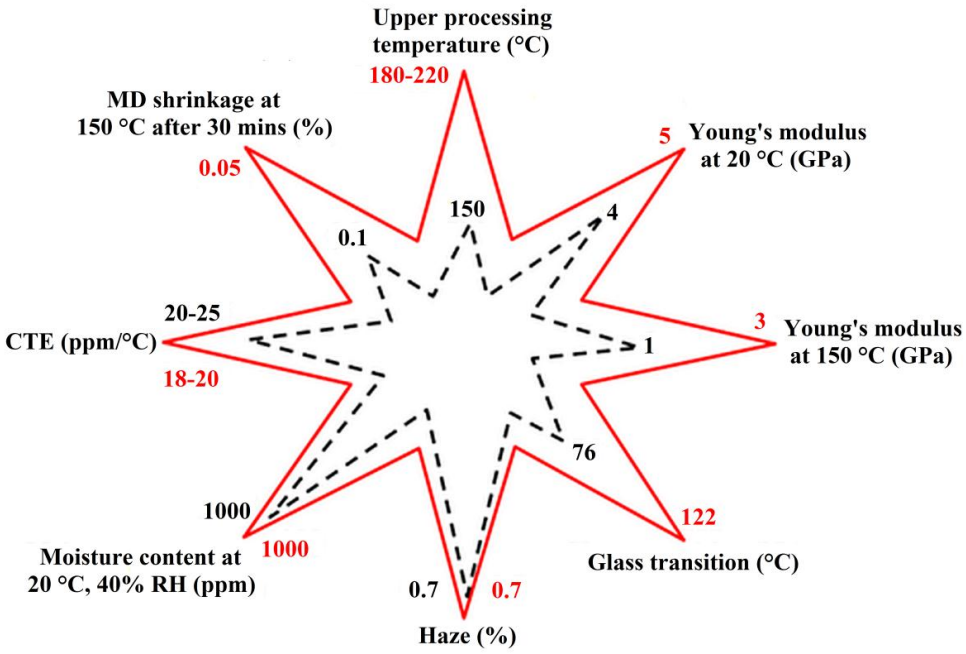

Figure 1.7 Star diagram illustrating the comparative properties of heat-stabilised PET (black) and PEN (red) biaxially oriented film.

The T_gs and T_ms of the most common semi-crystalline, semi-aromatic polyesters are illustrated in Figure 1.8, in comparison to the alternative candidate polymers for use in the applications discussed in Section 1.1. The polymers may be classified into three groups depending on their method of processing and morphology, which is determined by their

respective, increasing T_gs. These classes may be defined as: semi-crystalline thermoplastics (Nylon-6,6 to PEEK); amorphous thermoplastics [polycarbonate (PC) to polyethersulfone (PES)] and amorphous solvent cast polymers [aromatic fluorinated polyarylate (AFP) and polyimide (PI)].[10,101]

It is observed that for the semi-crystalline, semi-aromatic polyesters most relevant to this research project, a progressive reduction in chain flexibility from poly(1,4-butylene terephthalate) (PBT) to PEN results in an increasing T_g from 47 to 122 °C, respectively. However, it should be noted that with respect to PET and PEN, a 46 °C increase in T_g is accompanied by just a 16 °C increase in the T_m from 249 to 265 °C. This enables PEN to be melt-processed at temperatures below 300 °C without significant degradation occurring. In contrast, a smaller 21 °C increase in T_g from PEN to PEEK (T_g = 143 °C) affords a material that is not melt-processable (T_m = 334 °C) with conventional polyester processing equipment.

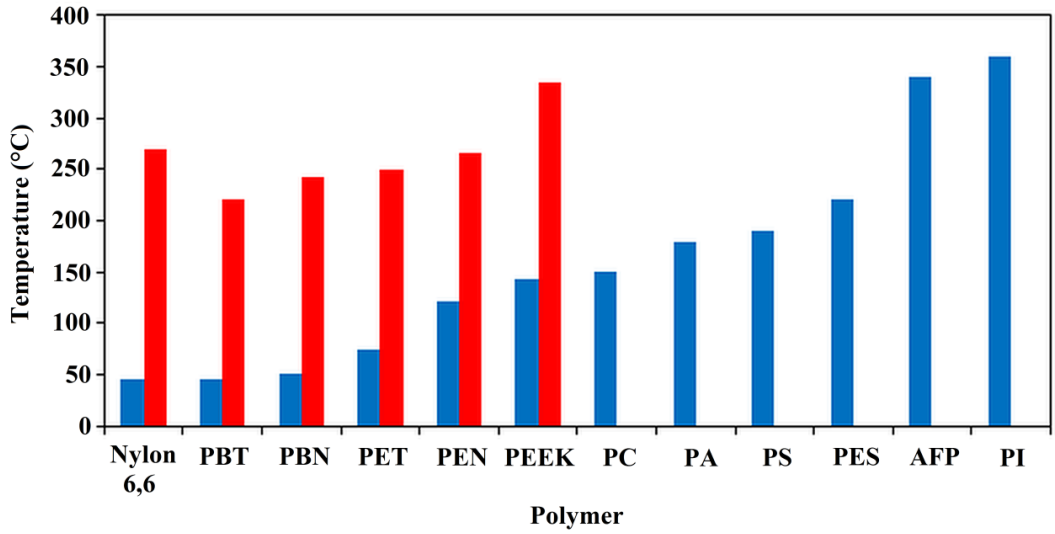

Figure 1.8 Comparative glass transition temperatures of high performance polymers where T_g = blue, T_m = red. Abbreviations: polyetheretherketone = PEEK; polycarbonate = PC; polyarylate = PA; polystyrene = PS; polyethersulfone = PES; aromatic fluorinated polyarylate = AFP; polyimide = PI. References where appropriate are given in text.

This survey revealed that amorphous morphologies are found for industrially useful thermoplastics with T_gs above 140 °C. Examples include polycarbonates and polyethersulfones which possess T_gs of ~ 150 °C and ~ 220 °C, respectively.[10] Upon increasing the T_g further to ~ 350 °C for polymers such as aromatic fluorinated polyarylates and polyimides, the ability of the polymer to be melt-processed is lost and such materials must be solvent cast to produce films. There is consequently clear scope for the production of polyester-based materials that exhibit superior performance to PEN yet *are* melt-processable.

This will be discussed and researched in more detail with reference to the comparative properties of PEN and PEEK in Chapter 3.

1.4.3 Crystallisation and morphology

Crystallinity within a polymer refers to the presence of three-dimensional order.[102] Semi-crystalline polymers contain crystalline and amorphous regions, with χ_c defined as the weight percentage of crystalline material in the total weight of the polymer. Mechanical properties such as yield stress and elastic modulus are strongly correlated to the χ_c, suggesting that the χ_c is one of the defining characteristics of a semi-crystalline polymer.[103]

The value of χ_c in a polymer is most commonly determined by DSC[104] due to the relatively low cost and ease of use, although methods based on density columns,[105] IR[106] and XRD[107,108] are also utilised. It is defined, qualitatively, as the ratio of crystalline to amorphous regions. For bulk semi-crystalline polymers, a χ_c of between 10-80% may be attained, but is commonly closer (and preferable) to 30-60% for semi-crystalline, semi-aromatic polyesters. The question as to how best determine χ_c is heavily debated[104,109] within the literature and relatively poorly understood. It is generally accepted[110] that the most accurate method to calculate the χ_c is by DSC as detailed in Equation 1.5:

Equation 1.5

$$\chi_c = \frac{(\Delta H_f - \Delta H_{cc})}{\Delta H_f^\circ}$$

where ΔH_f is the enthalpy of fusion, ΔH_{cc} is the enthalpy of cold crystallisation and ΔH_f° is the enthalpy of fusion of 100% crystalline material.

The crystallisation mechanism of semi-crystalline polymers was initially described by Herman *et al.*[111] in terms of the fringed-micelle model, based upon a polymer containing solely amorphous and crystalline regions.[112] It was proposed that the crystalline regions comprise polymer chains in parallel alignment whereas the amorphous regions contain only disordered chains. Although this model was able to explain the morphologically dependent properties of semi-crystalline polymers, the large scale morphological features that develop during crystallisation remained unaccounted for.

It is now generally understood that semi-crystalline polymers form lamellar structures upon crystallisation by the chain-folding model detailed by Storks[113] and Keller.[114] As illustrated in Figure 1.9, lamellar crystallites consist of parallel chains are connected by adjacent re-entry folds that are either uniform or non-uniform.[13] The lamellae, which are approximately 5-50 nm thick, then aggregate via amorphous regions to form spherulitic superstructures that

possess diameters on a μm-mm scale. A range of secondary crystallisation processes may succeed spherulite formation including further lamellar thickening, crystal perfection and recrystallization processes[115] but this is relatively rare for semi-crystalline, semi-aromatic polyesters which possess a fairly low χ_c.

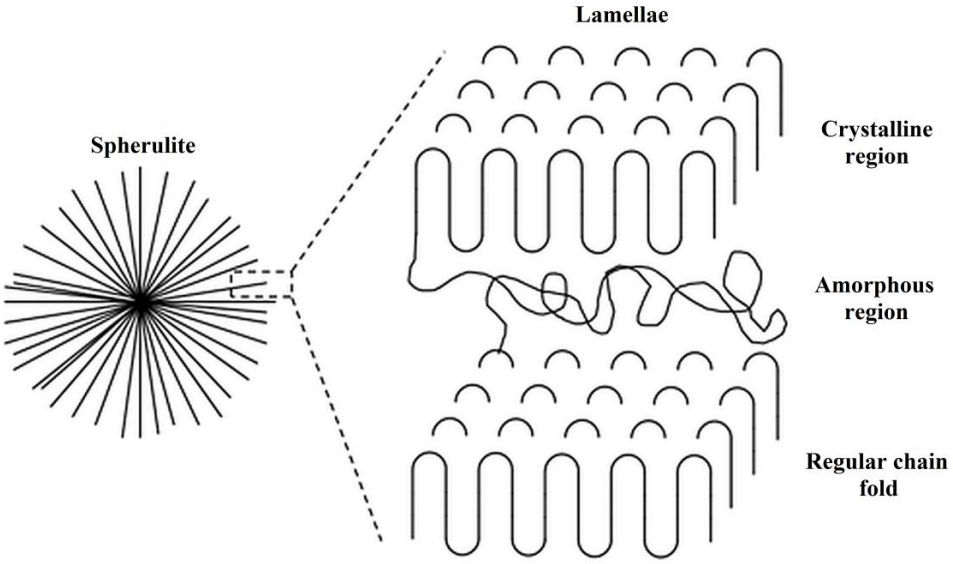

Figure 1.9 Schematic diagram of lamellae (regular adjacent-fold) and spherulite formation in a semi-crystalline polymer.[116–119]

1.4.4 Liquid crystal polymers

In addition to the morphologies previously discussed, polyesters may also adopt a mesomorphic or liquid crystalline state between the T_g and T_m. A rigid mesogenic unit within a polyester backbone is able to impart an intermediate degree of molecular order between the isotropic and crystalline states.[120] This most commonly occurs by temperature induced mesophase formation, whereby the molecules adopt an oriented conformation to afford thermotropic liquid crystal polymers because of an increase in translational entropy. The two main classes of liquid crystal polymers are illustrated in Figure 1.10.

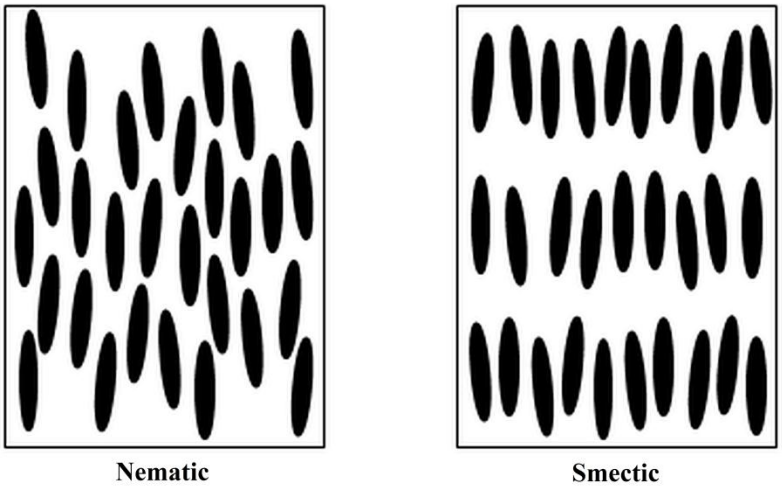

Figure 1.10 Representative classes of liquid crystal polymers.

The nematic class describes a phase with one-dimensional long range orientational order but no positional or periodic order.[121] In contrast, the smectic class of liquid crystal polymers defines a layered structure with molecules oriented normal (smectic A) or at an angle (smectic C) to the layer direction. These unique structures give rise to anisotropic chemical, thermal and mechanical behaviour, enabling liquid crystal polyesters to be utilised in several applications not accessible to conventional thermoplastic polyesters within the semiconductor packaging, aerospace and supercapacitor product markets.[122]

1.4.5 Copolymerisation

The most general approach to modifying the properties of a polymer is by copolymerisation. It is anticipated that an existing homopolymer may, to some degree, adopt the characteristics of a foreign comonomer after incorporation, to such an extent that the thermal, mechanical or chemical properties are sufficiently altered for the intended purpose.[123] The T_g of PET or PEN may therefore be expected to increase following copolymerisation with a rigid and more thermally stable monomer.

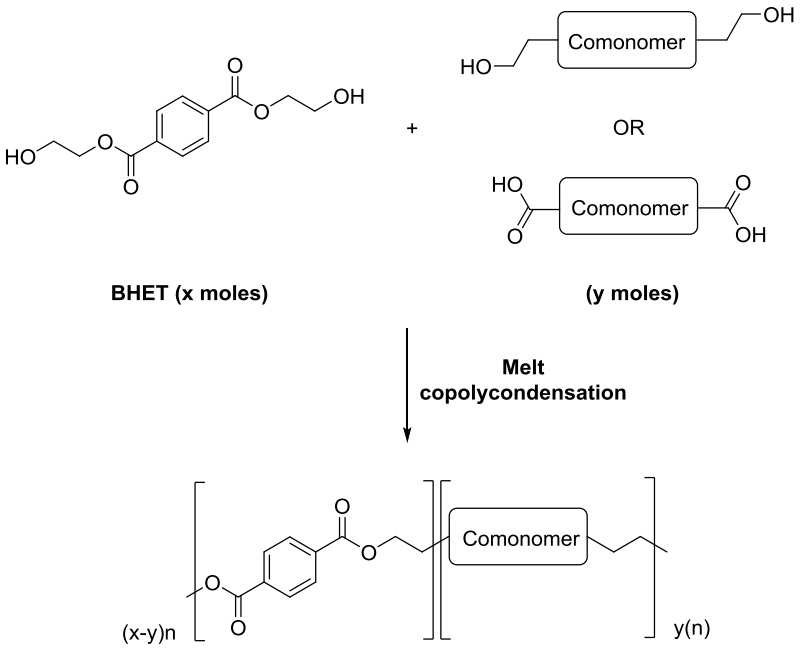

Figure 1.11 General copolymerisation scheme between a polyester monomer (bis(2-hydroxyl) terephthalate as an example) and foreign comonomer to form a statistically random copolymer.

In order to be compatible with polyester monomers during the melt-polymerisation procedure, any potential comonomer requires either the functionality of disubstituted carboxylic acid end groups (for incorporation in the direct esterification or transesterification steps) or disubstituted EG end groups (for incorporation in the polycondensation step) as illustrated in Figure 1.11 with PET. It should be noted that, despite copolymerisation, the fundamental properties of the copolymer such as its rheology and degradation temperatures must be maintained within the required specifications of the homopolyester. For polyesters, this most commonly requires that a novel copolymer must be melt-processable below 305 °C, i.e. the highest temperature at which polyesters may be extruded whilst maintaining an adequate melt viscosity with minimal degradation.

The fundamental theory for crystallisation of copolymers was established by Flory *et al.*[124,125] and later developed by Baur *et al.*[126] In both cases, an AB-type copolymer is assumed to comprise of crystallisable A units and comonomer B units that are considered to be crystal defects and therefore excluded from the crystallisable melt. Sanchez *et al.*[127,128] also provided an alternative comonomer inclusion model whereby the crystalline phase of a copolymer consists of both A and B comonomer units. Here, the B comonomer units produce defects in the crystalline A phase so that both crystalline and amorphous phases have the same copolymer composition ratio. The comonomer exclusion and inclusion models are schematically depicted in Figure 1.12.

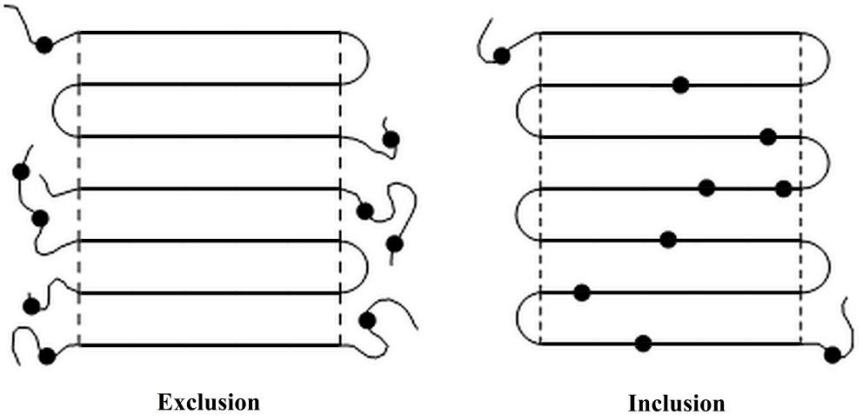

Figure 1.12 Schematic diagrams of the comonomer exclusion and inclusion models for copolymer crystallisation, adapted from Sanchez *et al.*[128] where black circles = B comonomer units and dashed line = the crystalline-amorphous phase boundary.

The effect upon the copolymer thermal properties, specifically the T_m, following the comonomer exclusion model is detailed in Equation 1.6:

Equation 1.6
$$\frac{1}{T_m} - \frac{1}{T_m^\circ} = \left(\frac{R}{\Delta H_u}\right) ln\ p$$

where ΔH_u is the heat of fusion per comonomer unit and p is the sequence propagation probability i.e. the probability that an A comonomer unit is preceded by another A comonomer unit. It is therefore predicted that the T_m is lowered with increasing p, representing the limiting sequence length.[115] This may be explained by the introduction of B comonomer units lowering the average crystallisable sequence length, which in turn results in the formation of relatively smaller crystals and thus thinner lamellae and a depressed T_m (Equation 1.4).

The observed depression in T_m upon copolymerisation may also be expressed from a thermodynamic perspective. Equation 1.7 details how the T_m relates to ΔH_m and ΔS_m, defined as the enthalpy and entropy of melting respectively when $\Delta G = 0$.

Equation 1.7
$$T_m = \frac{\Delta H_m}{\Delta S_m}$$

It is clear that in the comonomer exclusion model, copolymerisation is accompanied with increased disorder and therefore a lower T_m. In contrast, the observed depression in T_m from the comonomer inclusion model is an enthalpic effect, caused by the defect comonomer lowering the heat of fusion of the polymer crystallites.

1.4.5.1 Isomorphism and cocrystallisation

In the copolymerisation strategy previously discussed, it is envisaged that an existing homopolymer may adopt some of the characteristics of a foreign comonomer after

incorporation. However, such comonomers typically also disrupt the packing of polymer chains in the crystal lattice so that although the T_g increases, the T_m and χ_c typically decrease rapidly with respect to increasing comonomer content. Figure 1.13 illustrates the validity of this concept using the PET*co*PEN copolymer series, which has been extensively studied in the literature.[99,129–134]

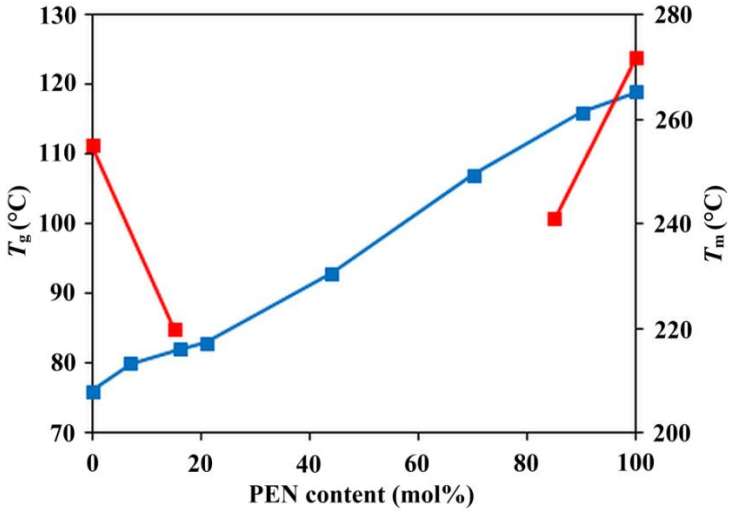

Figure 1.13 Comparative thermal properties of the PET*co*PEN copolymer series in terms of naphthalate content (data points taken from Po *et al.*[99] and Karayannidis *et al.*[129]) where T_g = blue and T_m = red.

Considering the measured T_gs of PET and PEN at 76 and 119 °C, respectively, there is an almost linear increase in the T_g across the PET*co*PEN copolymer series. However, as the terephthalate and naphthalate units are non-isomorphic, the melt-crystallisation process is inhibited leading to the generation of amorphous materials above ~ 15 mol% incorporation of foreign comonomer. This is demonstrated in Figure 1.13 by the disappearance of the T_m between 15-85 mol% content of PEN. The maximum T_g for a PET*co*PEN copolymer with retention of crystallinity is subsequently just 82 °C, emphasising the requirement for the T_g to be raised in conjunction with isomorphic behaviour.

It is therefore a requirement of this research project that a potential comonomer for PET or PEN must cocrystallise with the parent polymer in order to retain some level of crystallinity. If this is not possible, then crystallinity must be induced into a produced film by other means. As discussed previously, this may occur by the forward draw, sideways draw or heat-set during the stenter film process. A compromise may need to be ultimately reached whereby the T_g is raised to the optimum level through increasing levels of comonomer without causing a detrimental crystallinity loss in terms of the processing and performance parameters. This may prove to be irrelevant if sufficiently crystalline film is obtained through orientation and annealing of low-crystalline or even amorphous copolymer.

Cocrystallisation may occur through one of two types of phenomena in a polymer chain: isomorphism and isodimorphism.[135] Isomorphism is observed when two comonomer residues have a similar chemical structure and will occupy a similar geometric volume. Hence, the excess Gibbs free energy of cocrystallisation is relatively small so the chain conformation of either homopolymer becomes compatible with either crystal lattice.[136] A continuous change with composition in the lattice parameters between the two homopolymers is observed. Alternatively, iso*di*morphism is displayed when two crystalline phases of the respective homopolymers are both observed in the copolymer crystal structure, as one homopolymer unit is able to cocrystallise with incorporation of the other comonomer unit to some extent. As a result, a plot of T_m against the copolymer composition will reveal a minimum eutectic melting point where the crystal lattice transition occurs.[137]

There are few examples within the literature demonstrating cocrystallisation behaviour in copolyesters whose homopolymers are both crystalline. The most notable is the poly(3-hydroxybutyrate-*co*-3-hydroxyvalerate) P3HB*co*P3HV copolymer series, as illustrated in Figure 1.14.[138,139] As the monomer repeat units of 3HB and 3HV only differ by a CH_2 unit in the side-chain, it is easy to understand how the respective comonomers are isomorphic in character. These statistically random copolyesters display high levels of crystallinity (χ_c > 60%) throughout the entire copolymer series, with the eutectic T_m occurring at 30 mol% inclusion of 3HV.

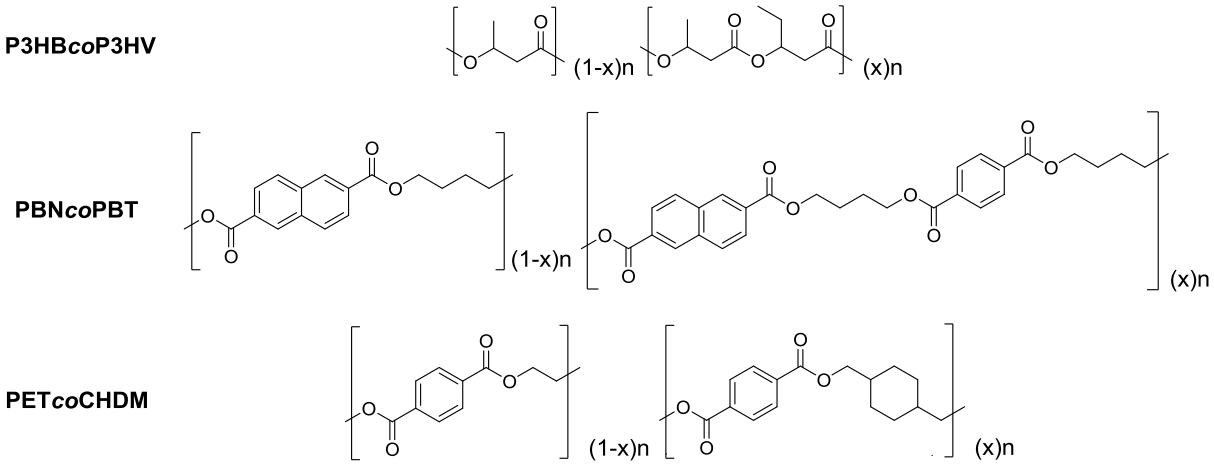

Figure 1.14 Notable molecular structures of literature[138,139] copolyesters that display isomorphism.

In the context of the current project, there are also known instances of cocrystallisation occurring in copolymers when one of the comonomers involved is a terephthalate unit: poly(butylene-2,6-naphthalate-*co*-1,4-butylene terephthalate) (PBN*co*PBT)[140] and poly(ethylene terephthalate-*co*-1,4-cyclohexylenedimethylene terephthalate)

(PET*co*CHDM).[141,142] As illustrated for the P3HB*co*P3HV copolymer series, isomorphism is made possible by the similarity in comonomer repeat unit content, geometry and dimensions. In both cases, melting point depression was observed with respect to each homopolymer to give a minimum T_m at ~ 35 mol% inclusion of PBN and CHDM content, respectively.

Jeong *et al*.[140] observed retention of semi-crystalline behaviour across the entire PBN*co*PBT copolymer series, rationalised by comonomer crystallisation affording single T_gs and T_ms because of statistically random copolymer sequence distributions. Analysis of the cocrystallisation behaviour by the comonomer inclusion model proposed by Wendling *et al*.[137] revealed that the average defect free energy was higher for the incorporation of butylene naphthalate units in the PEN crystal lattice. In practical terms, this reflects greater steric hindrance and thus isodimorphic behaviour between the two comonomers, as the difference in defect free energies suggests near isomorphism. The PET*co*CHDM copolymer series will be discussed further in Section 1.5.1, with specific reference given to the thermal properties.

1.5 High performance polymers

Previous attempts to increase the T_g, and therefore the thermal performance, of polyesters have generally relied upon the copolymerisation strategy previously discussed. In principle, many rigid comonomers have been screened for this purpose but no viable comonomer has yet been identified. From an industrial perspective, this has been due to two primary factors: (i) the high synthetic or purchasing cost of comonomers such as 2,6-naphthalene dicarboxylate (NDC); and (ii) the resultant unwarranted change in polymer properties following copolymerisation with a non-isomorphic comonomer. This section will review the previous approaches to enhancing the thermal performance of semi-crystalline polyesters, leading to the design of aims, objectives and strategies for the present research project.

1.5.1 Copolyesters

The early synthetic approaches to high performance polyester-based materials predominantly utilised more rigid ester comonomers, in an effort to functionalise PET with increasingly aromatic residues. There has been little new research within this area since the 1970s, with relevant work becoming increasingly focussed on the development of aromatic liquid crystal polyesters through incorporation of *p*-hydroxybenzoic, 4,4'-biphenol- and benzophenone-related comonomers.

Given the structural similarity to terephthalic acid, the incorporation of NDC was the most obvious route towards raising the T_g of PET. This became a commercially viable option following the opening of an industrial-scale NDC plant by the Amoco Chemical Company in 1995, as detailed by Lillwitz *et al.*[143] The thermal properties of the PET*co*PEN copolymer series have been previously discussed in Section 1.4.4.1 with reference to the lack of isomorphism displayed, and will therefore not be further detailed here. However, it should be noted that the general approach to raise the T_g of PET originated from this concept. In synthetic terms this may be conceived as the functionality change (increasing rigidity) of an aromatic diacid, as opposed to a reduction in flexibility of EG which is clearly not possible for PET or PEN.

1.5.1.1 Biphenyl-4,4'-dicarboxylic acid

The 4,4'-biphenyl unit has been extensively used to impart high rigidity to polymer chains. In the context of polyesters, copolymerisation of the rigid comonomer biphenyl-4,4'-dicarboxylic acid (BB, as illustrated in Figure 1.15) with terephthalate and naphthalate units was reported by Hu *et al.*[144,145] to impart a greater tensile moduli, improved oxygen barriers and higher thermal stability in comparison with either respective homopolyester.

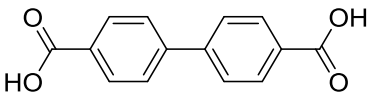

Figure 1.15 Molecular structure of biphenyl-4,4'-dicarboxylic acid.

Ma *et al.*[146] also synthesised a range of PET*co*BB copolymers which contained 5-65 mol% of BB. Amorphous copolyesters were found in the composition range between PET*co*BB-5 and 45, in partial agreement with Asrar[147] who reported amorphous behaviour between PET*co*BB-22 and 40. However, semi-crystalline copolyesters were produced for PET*co*BB-45 and 55, with T_gs of 103 and 110 ºC, respectively. The T_m for PET*co*BB-5 decreased with respect to PET as expected, but unusually increased thereafter to give values of 258 and 282 ºC for PET*co*BB45 and 55. Such copolymers therefore exhibit thermal performance within the range of PET and PEN, and could be melt-processable under similar conditions depending on the rheological properties.

Hu *et al.*[148] also studied the crystallisation kinetics of PET*co*BB-55 by Avrami analysis, from which it was concluded that the copolymer had a faster crystallisation rate than PEN. In conjunction with the retention of semi-crystalline behaviour at certain copolymer composition ratios, it was suggested that the terephthalate and bibenzoate units are able to

cocrystallise. However, this claim was not supported by any analysis of the copolymer crystal structure. The homopolymer of BB, poly(ethylene-4,4'-biphenyl carboxylate) is reported[149] to be liquid crystalline, leading Jung *et al.*[150] to infer that the enhancement in thermomechanical performance and retention of crystallinity at higher levels of BB may be attributed to pseudo-liquid crystal characteristics.

1.5.1.2 Alternative rigid ester comonomers

There have also been several examples of high performance copolyesters within the literature that contain non-isomorphic comonomers. The incorporation of cyclohexanedimethanol (CHDM) is the most notable and of greatest commercial interest, with a range of PET*co*CHDM copolyesters being marketed by Eastman Chemical Company as materials which possess enhanced hardness, heat resistance and electrical properties.[151] Zhang *et al.*[152] and Watanabe *et al.*[153] have also reported the copolymerisation of PET with bisphenol-A aryl carbonates (AR), in addition to the renowned inclusion of *p*-hydroxybenzoic acid moieties (HBA) by Jackson[154] to afford copolyesters with liquid crystalline properties. The molecular structures of these copolyesters are illustrated in Figure 1.16. It is noted that other high perfomance copolyesters containing, for example, rigid isosorbide,[155] and 2,2,4,4-tetramethyl-1,3-cyclobutanediol[156] units have been studied but contain raw materials that are not commercially available.

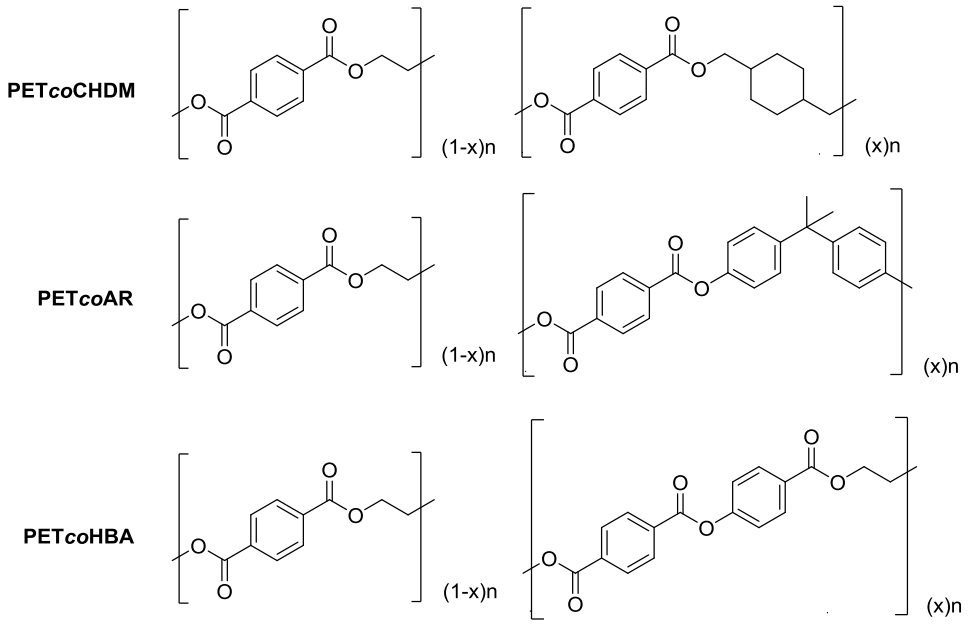

Figure 1.16 Selected molecular structures of literature high performance copolyesters.

Figure 1.17 illustrates that inclusion of AR leads to the greatest relative increase in the T_g of PET. The copolymer PET*co*AR-50 possesses a T_g of 105 °C, which is similar to that

observed for the PET*co*BB copolymer series at comparable comonomer content. However, in this (AR) case, amorphous materials were generated at all composition ratios. The increase in T_g is also fairly small at low AR content, with 30 mol% AR inclusion resulting in just a 7 °C increase.

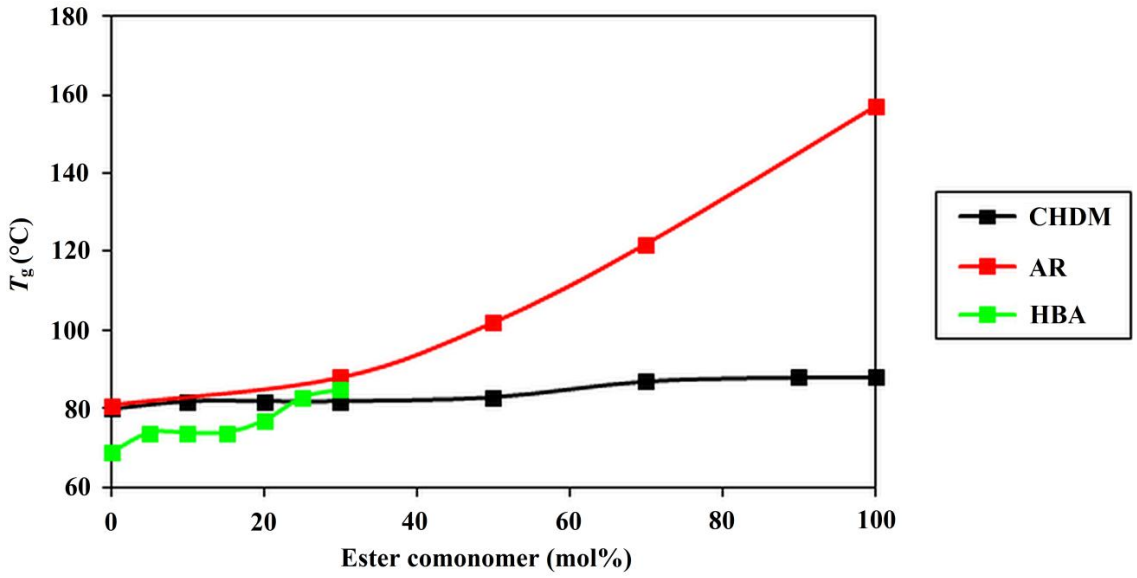

Figure 1.17 Comparison of T_gs across the PET*co*CDHM,[151,157] PET*co*AR[152,153] and PET*co*HBA[154] copolymer series.

It is observed that the increases in T_g for PET upon inclusion of CHDM and HBA are relatively much lower than for AR, with T_gs of 88 and 85 °C given for the CHDM homopolymer and PET*co*HBA-30, respectively. The T_g value determined for PET by Jackson *et al.*[154] appears anomalously low at 69 °C, thus it seems reasonable to assume that the range of T_gs across the PET*co*CHDM copolymer series is effectively 10 °C higher than stated. Greater retention of crystallinity was observed upon incorporation of the CHDM and HBA comonomers, though even here amorphous polyesters were produced at comonomer levels greater than 20 and 30 mol% content respectively. The copolymers with the largest increases in T_g that are also semi-crystalline materials are observed at 82 and 85 °C, although the values of χ_c at such compositions were not reported.

When comparing the impact of ester comonomers upon the thermal performance of PET, the greatest increase in T_g is observed for the PET*co*AR copolymer series, due to the effective removal of aliphatic EG residues and the subsequent increase in aromatic content. If such aliphatic units are present in the final copolyester, then it appears difficult to increase the T_g above ~ 85 °C. It is likely that the copolyesters in these instances are not sufficiently rigid to inhibit the molecular motions of a copolymer chain that consists of predominantly more flexible terephthalate dicarboxylate residues. Therefore, in order to raise the T_g of PET and

PEN close to that of PEEK, it may be a requirement to incorporate comonomers with greater rigidity derived from polymers that possess superior thermal performance.

1.5.2 Polyimides

Polyimides are a renowned class of high performance polymers displaying excellent mechanical, electrical and thermal properties in comparison to polyesters.[158,159] The first commercial polyimide film, Kapton® (Figure 1.18), was launched by DuPont in the 1960s. Synthesised from pyromellitic dianhydride and 4,4'-oxydiphenylamine, Kapton® has a T_g of ~ 400 ºC due to the aromatic chemical structure and intermolecular electrostatic interactions between the electron-rich diphenyl ether and electron-deficient pyromelltimide residues.[160] Kapton®, as for other polyimides, are commonly coloured in contrast to polyesters because of macromolecular chain conjugation[161] and/or intermolecular charge-transfer absorptions.

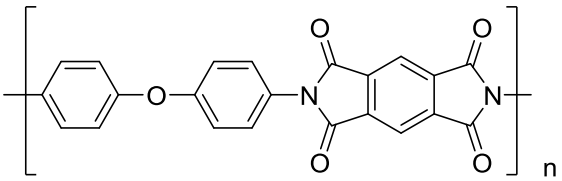

Figure 1.18 Molecular structure of Kapton®.

The synthesis of high molecular weight polyimides is most commonly achieved[162–164] as illustrated in Scheme 1.9. The first step involves the preparation of a poly(amic acid) by reaction of a dianhydride and diamine at ambient temperatures in polar, aprotic solvents e.g. DMAc or DMF. The poly(amic acid) is then isolated and processed into the desired polyimide form, before ring closure of the poly(amic acid) is achieved through imidisation under vacuum to remove water. This is typically carried out via a progressive step-wise heating method from 100 up to 350 °C,[165,166] depending on the thermal stability of the final polyimide. Dehydration may also occur upon reaction with acetic anhydride and a basic catalyst,[167] but this is less commonly used in the preparation of polyimide film.

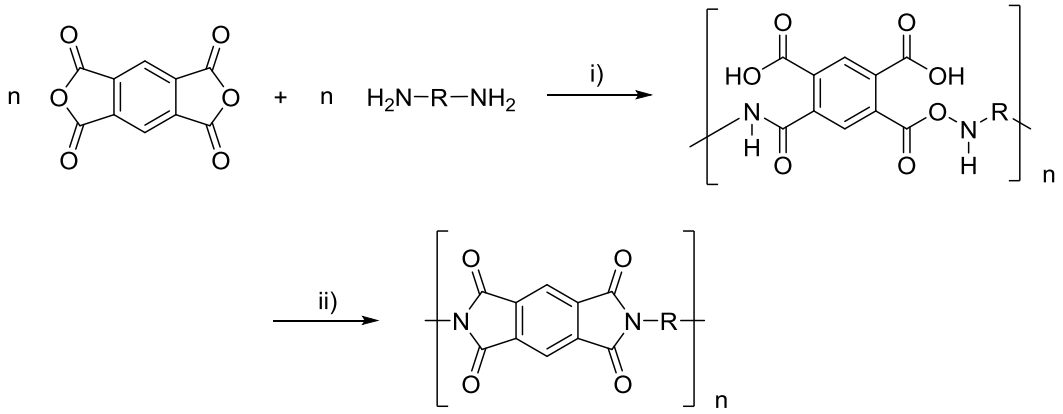

Scheme 1.9 Representative synthesis of a polyimide via the poly(amic acid) route between pyromellitic dianhydride and a diamine. Experimental conditions: i) 16 h, polar aprotic solvent, RT; ii) 100-350 °C, < 1 mbar, 2.5 h.

The synthesis of semi-aromatic polyimides (aromatic dianhydride and aliphatic diamine) is alternatively performed by direct polycondensation in *m*-cresol, as the relative increase in basicity to the aliphatic diamine results in the formation of insoluble intermediate salts with the carboxylic acid groups of the poly(amic acid).[168] This general route has been utilised[159,169,170] by several researchers in the synthesis of semi-crystalline polyimides that possess the biphenyl-3,4,3',4'-tetracarboxylic dianhydride (BPDA) unit.

Figure 1.19 illustrates the thermal properties of the BPDA polyimide series, where *m* represents the number of CH_2 groups in the α,ω-diaminoalkane reagent. It is observed that, as expected, the T_g increases with respect to decreasing *m* and thus a reduction in flexibility. The relative rigidity of the biphenyl unit in comparison to terephthalate and naphthalate units is clearly apparent, with T_gs observed between 87-158 °C when *m* = 10-5, respectively. This demonstrates a further utilisation of the biphenyl moiety to afford materials with excellent thermal performance, as observed in Section 1.5.1.1.

The BPDA polyimide series also exhibits the known odd-even effect[171] in semi-aromatic polyimides. Although a general increase in T_m with respect to decreasing *m* is observed, the T_m is lowered slightly when *m* is odd reflecting the reduction in order and ability to melt-crystallise within the polymer compared to when *m* is even. It is noted that despite the inclusion of flexible aliphatic segments where *m* = 4-6, the T_ms of such BPDA polyimides are > 330 °C, so that they would not be processable from the melt without decomposition.

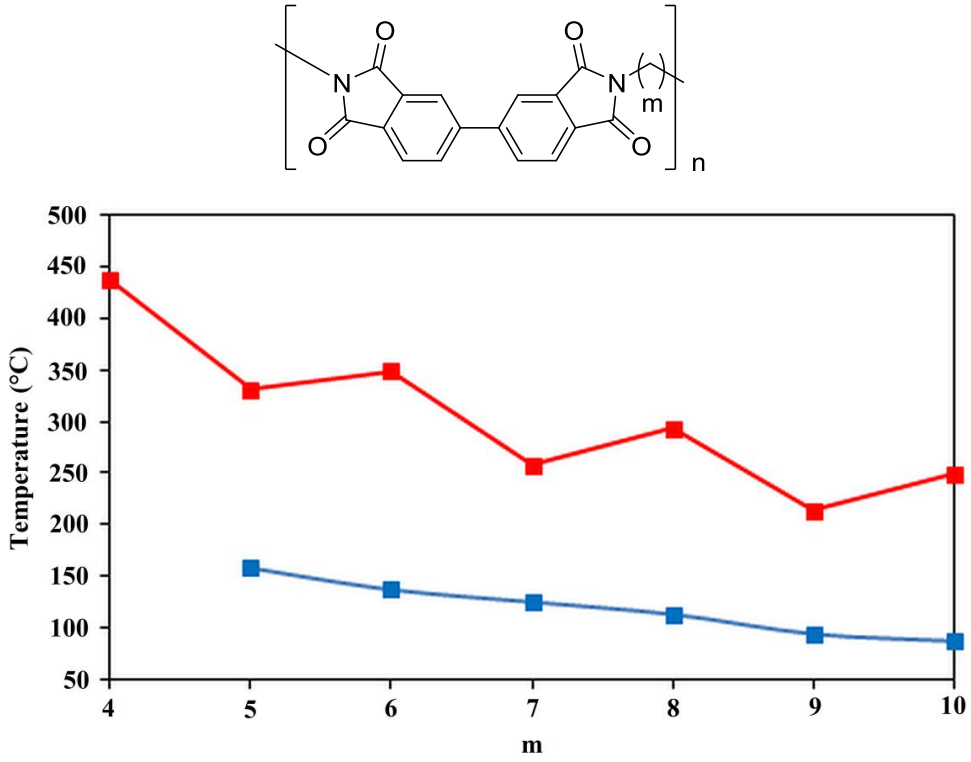

Figure 1.19 Comparative thermal properties (where blue = T_g, red = T_m, m = the number of CH_2 groups in the diamine residue in the polymer chain) across the BPDA polymer series synthesised by Koning *et al.*[170]

1.5.3 Copoly(ester-imide)s

As discussed in reference to the BPDA polyimide series, the inherent chemical characteristics of even semi-aromatic, semi-crystalline polyimides makes them difficult to fabricate as homopolymers due to their insolubility in a wide range of organic solvents and limited melt-processability. This has primarily sought to be improved in the literature through the incorporation of increasingly flexible diamide spacer groups, thus attempting to find a compromise between acceptable processing conditions and retention of the excellent thermal properties exhibited by polyimides.

The introduction of flexible ester comonomers is also theorised to improve the processing characteristics of polyimides, with the synthesis of copoly(ester-imide)s first reported in the late 1960s by Beck *et al.*[172,173] Subsequent work however, reviewed by Kricheldorf *et al.*,[159,174] primarily focussed on the synthesis of aromatic copoly(ester-imide)s and their tendency to form liquid crystal copolymers. Recent copoly(ester-imide) research within the last 20 years has shifted in approach by attempting to improve the thermal performance of polyesters through incorporation of more rigid imide comonomers, rather than to effectively reduce the thermal performance of polyimides.

Although there have been relatively few publications regarding the copolymerisation of aromatic imides with terephthalate or naphthalate ester comonomers, it is envisaged that copolymerisation of a rigid imide comonomer with PET or PEN at relatively low content will yield a copoly(ester-imide) with enhanced thermal performance that could be processable under standard polyesterification conditions. A combination of rigid aromatic imide units with flexible aliphatic glycol units may therefore produce a material that possesses the desirable properties of each respective comonomer,[175,176] The imide comonomers needed for this purpose can generally be synthesised by the imidisation of commercially available aromatic dianhydrides with an amine in a refluxing polar aprotic solvent.[177]

Xiao *et al.*[7,178–180] reported the synthesis of a PET-based copoly(ester-imide) derived from the comonomer *N*,*N*'-bis-[*p*-(2-hydroxyethoxycarbonyl)phenyl]-biphenyl-3,3',4 ,4'-tetracarboxy-diimide (BHEI, Figure 1.20) and a terephthalate unit using a melt-polycondensation method. In comparison to PET, the T_g increased by 10 and 24 ºC for PET*co*BHEI-5 and 10, respectively. Amorphous behaviour was observed at > 2 mol% BHEI inclusion, indicating that the BHEI unit inhibited the chain-packing regularity of PET. The biphenylene unit in this example does not therefore retain crystallinity with higher proportions of imide units present, in contrast to the examples described earlier by Ma *et al.*[146]

PET*co*BHEI-0.2 showed an increase in the crystallisation rate and the fastest crystallisation rate for all copolymer compositions,[179] suggesting that rigid imide comonomers incorporated at extremely low content may have nucleating properties. The mechanical properties of PET*co*BHEI-5 were also superior in comparison to control samples of PET, with the tensile modulus and tensile strength increasing by 20.2% and 38.8%, respectively.[7] This demonstrates the thermal reinforcing effect of an imide within a polyester backbone, yet it is claimed that the imide content must be limited to < 5 mol% to avoid phase separation and therefore a loss in mechanical strength. It is unknown whether the tensile measurements were performed on biaxially oriented film samples and hence would be comparable to an equivalent test performed at DTF.

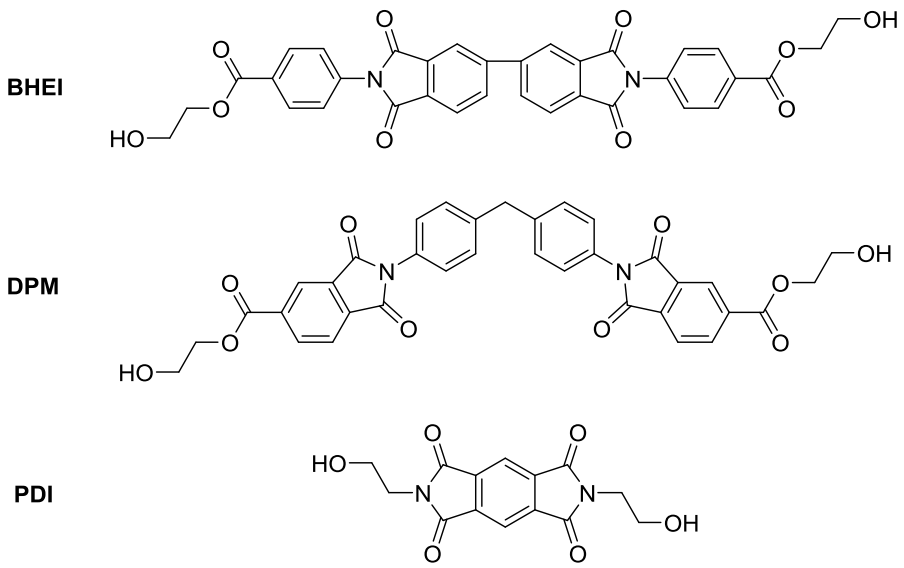

Figure 1.20 Selected chemical structures of literature rigid imide comonomers synthesised by Xiao *et al*.,[7] Park *et al*.[181] and Mary *et al*.[182]

Slightly more modest results were reported by Park *et al.*[181,183] who also synthesised a copoly(ester-imide) via melt-polycondensation to incorporate 4,4'-bis-[(4-carbo-2-hydroxyethoxy)-phthalimido]diphenylmethane (DPM) into PET up to 10 mol% content. The increase in T_g was smaller than that observed by Xiao *et al*., with 10 mol% imide resulting in a 13 ºC increase to 93 ºC. A T_m endotherm was still present at this comonomer ratio, albeit 27 ºC lower at 226 ºC and with $\chi_c < 1\%$, indicating that any further imide content would give an amorphous copolymer. It is also noted that there was little change in the decomposition temperatures despite increasing imide content. This may be due to the preferential cleavage of the more thermally labile ester units within the copolymer chain.

In conjunction with the research reported by Park *et al*.,[181] trimellitic anhydride has been utilised as a starting reagent in the production of copoly(ester-imide)s by several other researchers because of commercial availability. Selected molecular structures of these copoly(ester-imide)s are illustrated in Figure 1.21, where R and *m* represent a variety of functional and aliphatic groups respectively.

Although values of T_g are not given for the range of copoly(ester-imide)s synthesised by Babe *et al.*[184] and Kishinprasad *et al*.,[175] such polymers exhibited high decomposition temperatures between 450-480 °C in air. This was particular noticeable when R is aromatic, hence demonstrating the superior thermal stability exhibited relative to semi-aromatic polyesters. It is reasonable to assume that the T_gs of would also be increased given the correlation between the thermal parameters.

The T_gs of the copoly(ester-imide)s synthesised by Kricheldorf *et al.*[185] were lower than that of PET, and were given as 60 and 44 °C when m = 4 and 6, respectively. This may be attributed to the inclusion of octyl and dodecyl chains which were used in an attempt to induce liquid crystal properties. Interestingly, the thermal properties of these copoly(ester-imide)s are comparable to PBT and PBN yet they possess more flexible aliphatic chains. This suggests that just a slight increase in rigidity would raise the T_g of analogous structures above that of PET.

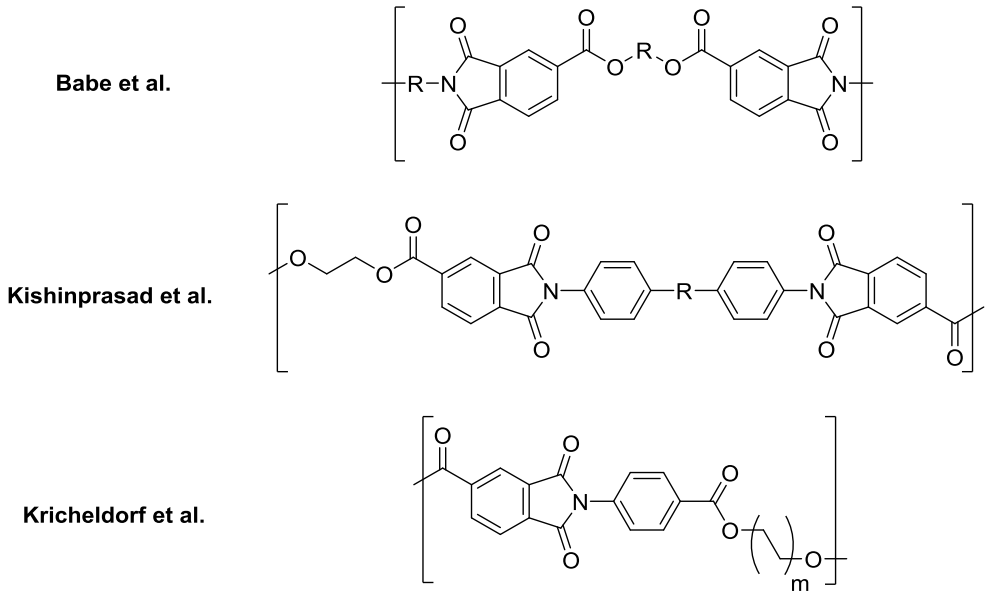

Figure 1.21 Selected literature copoly(ester-imide)s incorporating the trimellitic anhydride units synthesised by Babe *et al*., [184] Kishinprasad *et al*.[175] and Kricheldorf *et al.*[185]

Mary *et al.*[186,182] incorporated the monomer *N,N'*-bis-(2-hydroxyethyl) pyromellitimide (PDI) with terephthalic acid at a 1:1 ratio to increase the T_g relative to PET by 161 ºC. This rise in the T_g is unprecedented in the literature for a copoly(ester-imide). The inherent viscosity of PET*co*PDI-50 was recorded > 0.8 dL g^{-1} but no observable T_m endotherms were shown to confirm the claimed T_m value of 313 °C. In addition, the T_gs quoted appear to correspond to endotherms and not steps in the heat capacity baseline as conventionally seen in DSC.[187] It is therefore unlikely that this result is accurate. However, the use of an aromatic anhydride residue here again illustrates that the T_g of PET may be increased. The inclusion of a monomer such as PDI at a lower mol% may result in a thermally enhanced copoly(ester-imide) that is still melt-processable.

The incorporation of rigid amide comonomers is less common in the literature in comparison to copolyesters and copoly(ester-imide)s, from which most of the relevant research has been

published within the last 20 years. This will be separately reviewed at the start of Chapter 6 to precede the novel research presented there.

1.6 Aims and objectives

The literature discussed here has provided an overview of the synthesis and structural properties of semi-aromatic, semi-crystalline polyesters and the fundamental theories governing their properties. Previous studies have demonstrated that the thermal performance of polyesters may be increased through the copolymerisation of more rigid comonomers with terephthalate and naphthalate-based polyesters. However, this is generally accompanied by a rapid fall-off in χ_c at relatively low levels of comonomer content, typically at $\leq$ 10 mol%. In some anomalous cases however, retention of semi-crystalline behaviour is observed following copolymerisation due to the isomorphic character and thus cocrystallisation between two comonomer residues.

It is concluded that the research area of high performance copolyesters is more saturated in terms of content, and ultimately less successful in raising the T_g of PET and PEN, when compared to the inclusion of imide and amide comonomers. The utilisation of biphenyl and trimellitic anhydride units were also particularly prevalent in both the synthesis of high performance copolyesters and copoly(ester-imide)s and should therefore also be included in some capacity.

The aims and objectives of this research project may therefore be summarised as follows:

- Develop the synthetic chemistry and production of novel copoly(ester-imide)s, copoly(ester-amide)s and their respective monomers.
- Design and synthesise isomorphic PET and PEN-based copolymer series that demonstrate enhanced thermomechanical properties relative to the respective homopolyester.
- Develop a greater understanding of copolymer morphologies, through X-ray diffraction studies, computational modelling, crystallisation studies and thermal analysis.
- Optimise the industrial scale-up processes of selected copolymers, to enable the manufacture and evaluation of high performance polyester-based biaxially oriented film.

1.7 References

1 J. R. Whinfield and J. T. Dickson, *US Pat.* 2,465,319, *Polymeric linear terephthalic esters*, 1941.
2 J. R. Whinfield, *Nature*, 1946, **158**, 930–931.
3 Chem. Manuf. Assoc. India, http://cpmaindia.com/pet_about.php (accessed June 2015).

4 DuPont Teijin Films, *Internal Communication*, 2014.
5 S. Maiti and S. Das, *J. Appl. Polym. Sci.*, 1981, **26**, 957-978.
6 C. L. Mares and J. de Abajo, *Angew. Makromol. Chem.*, 1975, **55**, 65-77.
7 J. Xiao, X. Wan, D. Zhang, Q. Zhou and S. R. Turner, *J. Polym. Sci. Polym. Chem.*, 2001, **39**, 408-415.
8 P. J. Slikkerveer, *Conference Proceedings from 22nd International Display Research Conference*, 2002, 273–276.
9 P. J. Slikkerveer, *J. Soc. Inf. Disp.*, 2003, **3**, 20–24.
10 W. A. MacDonald, K. Rollins, D. MacKerron, K. Rakos, R. Eveson, K. Hashimoto and B. Rustin, *J. Soc. Inf. Disp.*, 2007, **15/12**, 1075-1083.
11 S. W. Sankey, W. A. MacDonald, D. Turner, H. Colquhoun and S. Meehan, PCT WO 2013/093446 A1, 2013.
12 T. Higashihara and M. Ueda, *Encyclopedia of Polymer Science and Technology*, Wiley, 2013, 1-27.
13 S. J. Meehan, *PhD Thesis*, *Enhancement of Polyester Properties Through Molecular Design*, University of Reading, 2012.
14 W. H. Carothers, *Trans. Faraday. Soc.*, 1936, **32**, 39–49.
15 J. K. Stille, *J. Chem. Ed*., 1981, **58**, 862–866.
16 P. J. Flory, *J. Am. Chem. Soc.*, 1939, **61**, 3334-3340.
17 J. F. Lutz, *Polym. Chem.*, 2010, **1**, 55-62.
18 K. B. Woody, B. J. Leever, M. F. Durstock and D. M. Collard, *Macromolecules*, 2011, **44**, 4690-4698.
19 T. Rieckmann and S. Volker, *Modern Polyesters: Chemistry and Technology of Polyesters and Copolyesters*, J. Scheirs and T. E. Long, British Library, 2003, 31-116.
20 K. Ravindranath and R. A. Mashelkar, *Chem. Eng. Sci.*, 1986, **41**, 2197–2214.
21 M. Hodgson, *PhD Thesis*, *Co-operative degradation in thin films of poly(methyl methacrylate) and poly(ethylene terephthalate)*, Durham University, 2000.
22 W. Sorenson, F. Sweeney and T. W. Campbell, *Preparative Methods of Polymer Chemistry*, John Wiley and Sons, New York, 2001, 181-185.
23 W. A. MacDonald, *Polym. Int.*, 2002, **51**, 923–930.
24 C. S. Wang, Y. M. Sun and L. C. Hu, *J. Polym. Res.*, 1994, **1**, 131–139.
25 K. Tomita and H. Ida, *Polymer*, 1976, **17**, 221–224.
26 F. Pillati in *Comprehensive Polymer Science*, G. Allen and J. C. Bevington, Pergamon, 1989.
27 C. M. Fontana, *J. Polym. Sci. Part A: Polym. Chem.*, 1968, **6**, 2343–2358.
28 C. C. Walker, *J. Polym. Sci. Part A: Polym. Chem.*, 1983, **21**, 623–626.
29 J. M. Besnoin, G. D. Lei and K. Y. Choi, *AIChE J.*, 1989, **35**, 1445–1456.
30 T. Rieckmann and S. Völker, *Chem. Eng. Sci.*, 2001, **56**, 945–953.
31 L. Turnbull, *PhD Thesis*, *Thermal, oxidative and hydrolytic degradation studies of poly(ethylene naphthalate)*, University of Strathclyde, 2002.
32 W. Schmidt, U. Thieloff, S. Schlauhoff and D. Yu, *US* Pat., 5,798,433, 1998.
33 D. R. Kelsey, *US* Pat., *Process for preparing polytrimethylene terephthalate*, 6,093,786, 2000.
34 A. Fradet, E. Maréchal, *Polymerisation and Polymer Properties*, Springer Berlin, 1982.
35 H. K. Reimschuessel, B. T. Debona and A. K. S. Murthy, *J. Polym. Sci. Polym. Chem. Ed.*, 1979, **17**, 3217-3239.
36 H. K. Reimschuessel and B. T. Debona, *J. Polym. Sci. Polym. Chem. Ed*., 1979, **17**, 3241–3254.
37 Z. Bashir, J. Siddiqui, V. Sampath and K. Al Luhaidan, *EU Pat*., 1,593,702 A1, 2005.

38 J. Yang, Z. Xia, F. Kong and X. Ma, *Polym. Degrad. Stab.*, 2010, **95**, 53–58.
39 F. A. El-Toufaili, G. Feix and K. H. Reichert, *J. Polym. Sci. Part A: Polym. Chem.*, 2006, **44**, 1049–1059.
40 R. W. Stevenson and H. R. Nettleton, *J. Polym. Sci Part A-1*, 1968, **6**, 889–900.
41 G. Challa, *Makromol. Chem*, 1960, **38**, 138–146.
42 E. Santacesaria, F. Trulli, L. Minervini, M. di Serio, R. Tesser and S. Contessa, 1994, **4**, 1371–1384.
43 H. Kamatani, S. Konagaya and Y. Nakamura, *Polym. J.*, 1980, **12**, 125–130.
44 D. N. Bikiaris and G. P. Karayannidis, *Polym. Degrad. Stab.*, 1999, **63**, 213–218.
45 S. M. Aharoni, C. E. Forbes, W. B. Hammond, D. M. Hindenlang, F. Mares, K. O'Brien and R. D. Sedgwick, *J. Polym. Sci. Part A: Polym. Chem.*, 1986, **24**, 1281–1296.
46 S. Al Abdulrazzak and S. A. Jabarin, *Polym. Int.*, 2002, **51**, 164–173.
47 J. Scheirs and T. E. Long, *Modern Polyesters: Chemistry and Technology of Polyesters and Copolyesters*, 2003.
48 B. Gantillon, R. Spitz and T. F. McKenna, *Macromol. Mater. Eng.*, 2004, **289**, 88-105.
49 T. Y. Kim, E. A. Lofgren and S. A. Jabarin, *J. Appl. Polym. Sci.*, 2003, **89**, 197-212.
50 B. Duh, *J. Appl. Polym. Sci.*, 2001, **81**, 1748-1761.
51 V. Hornof, *J. Macromol. Sci. Chem.*, 1981, **15**, 503-514.
52 H. Yokoyama, T. Sano, T. Chijiiwa and R. Kajiwa, *J. Jpn. Pet. Inst.*, 1978, **21**, 77-79.
53 J. Chen and L. Chen, *J. Polym. Sci. Part A: Polym. Chem.*, 1998, **36**, 3073–3080.
54 L. Chen and J. Chen, *J. Polym. Sci. Part A: Polym. Chem.*, 1999, **37**, 1797–1803.
55 L. Chen and J. Chen, *J. Appl. Polym. Sci.*, 1999, **75**, 1229–1234.
56 L. Chen and J. Chen, *J. Appl. Polym. Sci.*, 2000, **75**, 1221–1228.
57 J. Shin, Y. Lee and S. Park, *Chem. Eng. J.*, 1999, **75**, 47–55.
58 J. Otton and S. Ratton, *J. Polym. Sci. Part A: Polym. Chem.*, 1991, **29**, 377–391.
59 S. G. Hovenkamp and P. Munting, *J. Polym. Sci Part A-1*, 1970, **8**, 679–682.
60 B. J. Holland and J. N. Hay, *Polymer*, 2002, **43**, 1835–1847.
61 S. M. West, A. J. Smallridge, A. Uhlherr and S. Vo, *Macromol. Chem. Phys*, 2000, **201**, 2532–2534.
62 L. H. Peebles and C. T. Ablett, *J. Polym. Sci Part A-1*, 1969, **7**, 479–496.
63 W. S. Ha and Y. K. Choun, *J. Polym. Sci. Polym. Chem. Ed.*, 1979, **17**, 2103–2118.
64 M. T. de Freire, A. P. Damant, L. Castle and F. Reyes, *Packag. Technol. Sci.*, 1999, **12**, 29–39.
65 M. Day and D. M. Wiles, *J. Appl. Polym. Sci.*, 1972, **16**, 175–189.
66 M. Day and D. M. Wiles, *J. Appl. Polym. Sci.*, 1972, **16**, 191–202.
67 M. Day and D. M. Wiles, *J. Appl. Polym. Sci.*, 1972, **16**, 203–215.
68 H. Zimmerman and N. T. Kim, *Polym. Eng. Sci*, 1980, **20**, 680–683.
69 M. S. Ellison, L. D. Fisher, K. W. Alger and S. H. Zeronian, *J. Appl. Polym. Sci.*, 1982, **27**, 247–257.
70 N. S. Allen, M. Edge, M. Mohammadian and K. Jones, *Polym. Degrad. Stab.*, 1994, **43**, 229–237.
71 F. Samperi, C. Puglisi, R. Alicata and G. Montaudo, *Polym. Degrad. Stab.*, 2004, **83**, 3–10.
72 G. Montaudo, C. Puglisi and F. Samperi, *Polym. Degrad. Stab.*, 1993, **42**, 13–28.
73 H. A. Pohl, *Anal. Chem.*, 1954, **26**, 1614–1616.
74 L. H. Buxbaum, *Angew. Chem. Int. Ed.*, 1968, **7**, 182–190.
75 G. Grassie and N.Scott, *Polymer degradation and stabilisation*, Cambridge University Press, 1985.
76 P. Sivasamy, M. Palaniandavar, C. T. Vijayakumar and K. Lederer, *Polym. Degrad. Stab.*, 1992, **38**, 15–21.

77 I. C. McNeill, *Polym. Degrad. Stab.*, 1991, **34**, 187–204.
78 M. Dzieciol and J. Trzeszczynski, *J. Appl. Polym. Sci*., 2000, **77**, 16–19.
79 D. W. Brooks and G. A. Giles, *PET Packaging Technology*, Wiley-Blackwell, 2002.
80 W. A. MacDonald, *Encyclopedia of Polymer Science and Technology*, Wiley, 2013, 30–41.
81 G. W. Halek, *J. Polym. Sci: Polym Symp.* 1986, **92**, 83–92.
82 F. Villain, J. Coudane and M. Vert, *Polym. Degrad. Stab.*, 1994, **43**, 431–440.
83 M. R. Smith, *PhD Thesis*, Durham University, 2004.
84 S. Tan, A. Su, W. Li and E. Zhou, *Macromol. Rapid Commun.*, 1998, **19**, 11–14.
85 D. J. Blundell, R. J. Oldman, W. Fuller, A. Mahendrasingam, C. Martin, D. H. MacKerron, J. L. Harvie and C. Riekel, *Polym. Bull.*, 1999, **42**, 357–363.
86 J. Bicerano, *Encyclopedia of Polymer Science and Technology*, Wiley, 2013, 1-29.
87 V. A. Bershstein and V. M. Yegorov, *Polym. Sci. USSR*, 1985, **27**, 2743–2757.
88 V. A. Bershstein, V. M. Yegorov and Y. A. Yemelyanov, *Polym. Sci. USSR*, 1985, **27**, 2757–2764.
89 T. G. Fox and P. J. Flory, *J. Appl. Phys.*, 1950, **21**, 581–591.
90 D. Turnbull and M. H. Cohen, *J. Chem. Phys.*, 1961, **34**, 120–124.
91 M. H. Cohen and G. S. Grest, *Phys. Rev. B*, 1979, **20**, 1077–1098.
92 A. K. Doolittle, *J. Appl. Phys.*, 1951, **22**, 1471-1474.
93 J. H. Gibbs and E. A. di Marzio, *J. Chem. Phys.*, 1958, **28**, 373-383.
94 R. G. Beaman, *J. Polym. Sci*, 1952, **9**, 470–472.
95 R. F. Boyer, *J. Appl. Phys.*, 1954, **25**, 825-829.
96 W. A. Lee and G. J. Knight, *Br. Polym. J.*, 1970, **2**, 73–80.
97 H. M. Colquhoun, *Personal Communication*, 2007.
98 U. W. Gedde, *Polymer Physics*, Chapman and Hall, London, 1995.
99 R. Po, E. Occhiello, G. Giannotta, L. Pelosini and L. Abis, *Polym. Advan. Technol.*, 1995, **7**, 365-373.
100 A. E. Tonelli, *Polymer*, 2002, **43**, 637–642.
101 W. A. MacDonald, M. K. Looney, D. MacKerron, R. Eveson, R. Adam, K. Hashimoto and K. Rakos, *J. Soc. Inf. Disp.*, 2007, **15**, 1075–1083.
102 IUPAC, *Pure Appl. Chem.*, 1974, **40**, 477.
103 Z. Bashir, I. Al Aloush, I. Al Raqibah and M. Ibrahim, *Polym. Eng. Sci*., 2000, **40**, 2442-2455.
104 Y. Kong and J. N. Hay, *Polymer*, 2002, **43**, 3873–3878.
105 A. B. Thompson and D. W. Woods, *Nature*, 1955, **175**, 642–643.
106 J. Runt, *Encyclopedia of Polymer Science and Technology*, Wiley, 2003, 446–464.
107 G. Farrow and I. Ward, *Polymer*, 1960, **1**, 330–339.
108 W. O. Statton, *J. Appl. Polym. Sci.*, 1963, **7**, 803–815.
109 Y. Kong and J. N. Hay, *Eur. Polym. J.*, 2003, **39**, 1721–1727.
110 E. Kaisersberger and E. Mohler, *DSC on polymeric materials: NETZCH annual for science and industry*, Wurzburg, 1991.
111 K. Herman, O. Gerngross and W. Abitz, *Z. Phys. Chem.*, 1930, **B10**, 371.
112 P. J. Flory, *J. Chem. Phys.*, 1949, **17**, 223-240.
113 K. H. Storks, *J. Am. Chem. Soc.*, 1938, **60**, 1753-1761.
114 A. Keller, *Philos. Mag.*, 1957, **2**, 1171-1175.
115 V. Ratta, *PhD Thesis, Crystallisation, morphology, thermal stability and adhesive properties of novel high performance semicrystalline polyimides*, Virginia Polytechnic Institute and State University, 1999.
116 M. Raimo, *Prog. Polym. Sci.*, 2007, **32**, 597–622.
117 N. B. McCrum, C. P. Buckley and C. B. Bucknall, *Principles of Polymer Engineering*, Oxford University Press, 1988.

118 L. Mandelkern, *Characterisation of Materials in Research: Ceramics and Polymers*, Syracuse University Press, New York, 1975.
119 Z. Chen, *PhD Thesis, The crystallisation of poly(ethylene terephthalate) studied by thermal analysis and FTIR spectroscopy*, University of Birmingham, 2012.
120 A. Ciferri, *Liquid Crystallinity in Polymers: Principles and Fundamental Properties, VCH Publishers, New York*, 1991.
121 A. M. Donald, A. H. Windle and S. Hanna, *Liquid Crystalline Polymers*, Cambridge University Press, 1992.
122 X. Wang, J. Engel and C. Liu, *J. Micromechanics Microengineering*, 2003, **13**, 628–633.
123 D. A. Schiraldi, *Modern Polyesters: Chemistry and Technology of Polyesters and Copolyesters*, J. Scheirs and T. E. Long, British Library, 2003, 245–266.
124 P. J. Flory, *J. Chem. Phys.*, 1947, **15**, 684.
125 P. J. Flory, *Trans. Faraday. Soc.*, 1955, **51**, 848-856.
126 V. H. Baur, *Makromol. Chem.*, 1966, **98**, 297-301.
127 I. C. Sanchez and R. K. Eby, *J. Res. Natl. Bur. Stand. Sect. A Phys. Chem.*, 1973, **77A**, 353-358.
128 I. C. Sanchez and R. K. Eby, *Macromolecules*, 1975, **8**, 638–641.
129 G. P. Karayannidis, N. Papachristos, D. N. Bikiaris and G. Z. Papageorgiou, *Polymer*, 2003, **44**, 7801–7808.
130 C. Santa Cruz, F. J. Baltá Calleja, H. G. Zachmann and D. Chen, *J. Mater. Sci.*, 1992, **27**, 2161–2164.
131 D. Chen and H. G. Zachmann, *Polymer*, 1991, **32**, 1612–1621.
132 P. S. R. Cheung, C. W. Roberts and K. B. Wagener, *J. Appl. Polym. Sci*., 1979, **24**, 1809–1830.
133 X. Lu, *Polymer*, 1995, **36**, 451–459.
134 T. A. Ezquera, F. J. Baltá Calleja and H. G. Zachrnann, *Acta. Polymer*, 2000, **24**, 18–24.
135 G. Natta, G. Allegra, I. W. Bassi, D. Sianesi, G. Caporiccio and E. Torti, *J. Polym. Sci. Polym. Chem.*, 1965, **3**, 4263-4278.
136 E. Bhoje Gowd, *PhD Thesis, Effect of additives and comonomers on crystallization and solid state polymerization of polyesters*, University of Pune, 2005.
137 J. Wendling and U. W. Suter, *Macromolecules*, 1998, **31**, 2516-2520.
138 S. Bloembergen, D. A. Holden, G. K. Hamer, T. L. Bluhm and R. H. Marchessault, *Macromolecules*, 1986, **19**, 2865–2871.
139 T. L. Bluhm, G. K. Hamer, R. H. Marchessault, C. A. Fyfe and R. P. Veregin, *Macromolecules*, 1986, **19**, 2871–2876.
140 Y. G. Jeong, W. H. Jo and S. C. Lee, *Macromolecules*, 2000, **33**, 9705–9711.
141 H. Y. Yoo, S. Umemoto, T. Kikutani and N. Okui, *Polymer*, 1994, **35**, 117–122.
142 N. Yoshie and Y. Inoue, *Polymer*, 1994, **35**, 1931–1935.
143 L. D. Lillwitz, *Appl. Catal. A: Gen.*, 2001, **221**, 337–358.
144 Y. S. Hu, R. Y. F. Liu, M. Rogunova, D. A. Schiraldi, S. Nazarenko, A. Hiltner and E. Baer, *J. Polym. Sci. Part B: Polym. Phys.*, 2002, **40**, 2489–2503.
145 Y. S. Hu, R. Y. F. Liu, D. A. Schiraldi, A. Hiltner and E. Baer, *Macromolecules*, 2004, **37**, 2136-2143.
146 H. Ma, M. Hibbs, D. M. Collard, S. Kumar and D. A. Schiraldi, 2002, *Macromolecules*, **35**, 5123–5130.
147 J. Asrar, *J. Polym. Sci. Polym. Chem.*, 1999, **37**, 3139-3146.
148 Y. S. Hu, M. Rogunova, D. A. Schiraldi, A. Hiltner and E. Baer, *J. Appl. Polym. Sci.*, 2002, **86**, 98–115.

149 W. R. Krigbaum, J. Asrar, H. Toriumi, A. Ciferri and J. Preston, *J. Polym. Sci. Polym. Lett. Ed.*, 1982, **20**, 109–115.
150 H. T. Jung, S. D. Hudson and R. W. Lenz, *Macromolecules*, 1997, **38**, 67–68.
151 R. W. Seymour and R. R. Light, *US* Pat., 4,474,918, *Thermoplastic polyester compositions having improved barrier properties*, 1984.
152 G. Y. Zhang, J. W. Ma, B. X. Cui, X. L. Luo and D. Z. Ma, *Macromol. Chem. Phys*., 2001, **202**, 604–613.
153 H. Watanabe and M. Okada, *Jpn. Kokai*, 1972, **72**, 295.
154 W. J. Jackson and H. F. Kuhfuss, *J. Polym. Sci. Polym. Chem. Ed.*, 1976, **14**, 2043–2058.
155 H. R. Kricheldorf and S. M. Weidner, *Eur. Polym. J.*, 2013, **49**, 2293–2302.
156 D. R. Kelsey, B. M. Scardino, J. S. Grebowicz and H. H. Chuah, *Macromolecules*, 2000, **33**, 5810–5818.
157 N. Gonzalez-Vidal, A. Martinez de Ilarduya and S. Munoz-Guerra, *J. Polym. Sci. Part A: Polym. Chem.*, 2009, **47**, 5954-5966.
158 S. Srinivas, F. E. Caputo, M. Graham, S. Gardner, R. M. Davis, J. E. McGrath and G. L. Wilkes, *Macromolecules*, 1997, **30**, 1012–1022.
159 H. R. Kricheldorf and V. Linzer, *Polymer*, 1995, **36**, 1893–1902.
160 R. G. Bryant, *Encyclopedia of Polymer Science and Technology*, Wiley, 2003, 1-32.
161 B. R. Bikson and Y. F. Freimanis, *Polym. Sci. U.S.S.R.*, 1970, **12**, 81–85.
162. W. L. Edwards and M. L. Andrews, PCT WO2005/073272 A1, *Imide modified polyester resins and methods making the same*, 2005.
163 A. L. Endrey, *US Pat*., 3,179,635, 1965.
164 C. E. Sroog, *Prog. Polym. Sci.*, 1991, **16**, 561–694.
165 M. H. Brink, D. K. Brandom, G. L. Wilkes and J. E. McGrath, *Polymer*, 1994, **35**, 5018–5023.
166 D. K. Brandom and G. L. Wilkes, *Polymer*, 1994, **35**, 5672–5677.
167 S. V. Vinogravadova, L. I. Vorobev, V. D. Churochkina, N. A. Chudina, T. N. Sprina and V. V. Korshak, *Polym. Sci. USSR*, 1974, **A16**, 584.
168 A. E. Eichstadt, T. C. Ward, M. D. Bagwell, I. V. Farr, D. L. Dunson and J. E. McGrath, *Macromolecules*, 2002, **35**, 7561–7568.
169 J. A. Kreuz, B. S. Hsiao, C. A. Renner and D. L. Goff, *Macromolecules*, 1996, **25**, 6926–6930.
170 C. Koning, A. Delmotte, P. Larno and B. van Mele, *Polymer*, 1998, **39**, 3697–3702.
171 J. de Abajo, J. de la Campa, H. R. Kricheldorf and G. Schwarz, *Makromol. Chem.*, 2000, **547**, 537–547.
172 D. Beck. *GB Pat*., 1,043,098, *Process for the manufacture of thermohardening synthetic resins*, 1966.
173 K. Herberts, *GB Pat*., 1,093,734, *A process for the production of insulating coatings on electric conductors*, 1966.
174 H. R. Kricheldorf, V. Linzer and C. Bruhn, *J. Macromol. Sci. A*, 1994, **31**, 1315–1328.
175 V. S. Kishanprasad and P. H. Gedam, *J. Appl. Polym. Sci*., 1993, **48**, 1151-1162.
176 C. P. Yang, G. S. Liou, R. S. Chen and C. Y. Yang, *J. Polym. Sci. Part A: Polym. Chem.*, 2000, **38**, 1090–1099.
177 Q. Zheng, J. Huang, A. Sarjeant and H. E. Katz, *J. Am. Chem. Soc.*, 2008, **130**, 14410–14411.
178 J. Xiao, H. Zhang, X. Wan, D. Zhang and Q. F. Zhou, *Polymer*, 2002, **43**, 7377–7387.
179 J. Xiao, H. Zhang, X. Wan, D. Zhang, Q.-F. Zhou, E. M. Woo and S. R. Turner, *Polymer*, 2002, **43**, 3683–3690.
180 J. Xiao, X. Wan, D. Zhang, H. Zhang, Q. F. Zhou and S. R. Turner, *J. Polym. Sci. Part A: Polym. Chem.*, 2002, **40**, 852–863.

181 L. S. Park and D. C. Lee, *Polym. Eng. Sci*., 1995, **35**, 1629–1635.
182 L. J. F. Mary and P. Kannan, *Eur. Polym. J.*, 1999, **35**, 17–26.
183 L. S. Park, J. H. Do and D. C. Lee, *J. Appl. Polym. Sci*., 1996, **60**, 2059–2067.
184 S. G. Babe, J. de Abajo and J. Fontan, *Angew. Makromol. Chem.*, 1972, **21**, 65–77.
185 H. R. Kricheldorf, G. Schwarz, M. Berghahn, J. de Abajo and J. G. de la Campa, *Macromolecules*, 1994, **27**, 2540–2547.
186 L. J. F. Mary and P. Kannan, *Polym. Int.*, 1998, **47**, 317–323.
187 L. J. F. Mary and P. Kannan, *J. Polym. Sci. Part A Polym. Chem.*, 1999, **37**, 1755-1761.

Chapter 2

Experimental methods

2.1 Melt-polymerisation procedures

2.1.1 Laboratory-scale melt-polycondensation

The majority of polyester-based materials detailed in this research were initially produced on a 20-50 g scale, utilising a custom built melt-polycondensation rig (Figure 2.1) developed from previous iterations at Reading and DTF. Polycondensation occurs in a one-step synthesis with elimination of a diol from the appropriate bis(n-hydroxyalkyl) ester monomer, polymerisable rigid comonomer (if required) and polycondensation catalyst (Sb_2O_3) added in tandem prior to the start of the reaction.

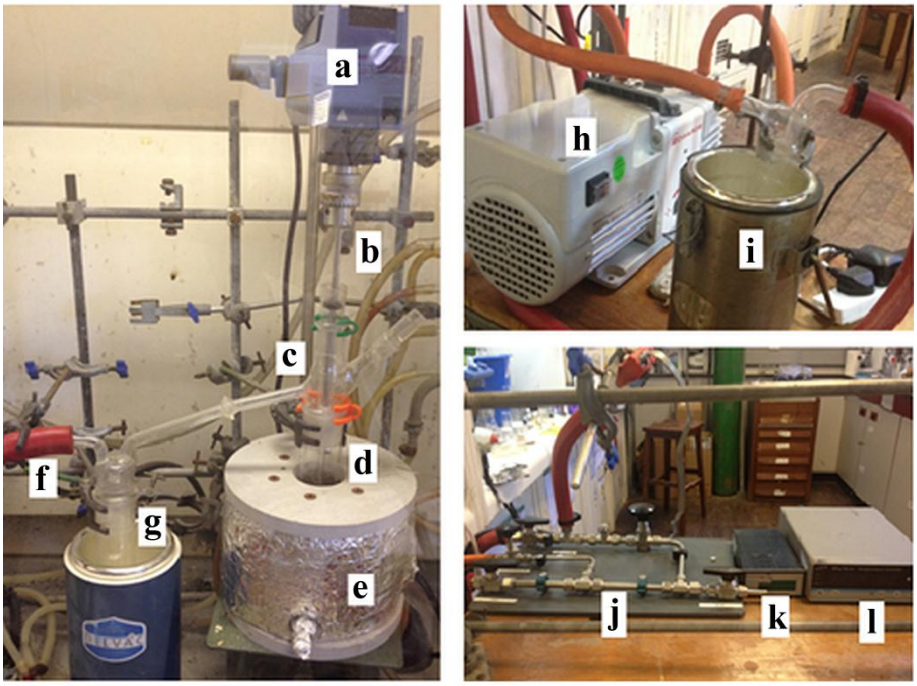

Figure 2.1 The melt-polycondensation rig constructed in the present work, with: a) mechanical stirrer; b) metal stirrer blade; c) polycondensation glass head; d) polycondensation glass tube; e) tube heater; f) rubber tubing (to gas/vacuum manifold); g) distillate trap; h) vacuum pump; i) vacuum trap; j) gas manifold; k) vacuum gauge; and l) temperature gauge.

Bespoke design of the polycondensation rig enabled successful step-growth polymerisations due to the fulfilment of three main criteria: high reaction temperatures; removal of ethylene glycol by vacuum distillation; and efficient stirring of the reaction mixture.[1] This is achieved by performing the polycondensation reaction within an aluminium-cased tube heater, which ensures the uniform heating of the polymer mixture at temperatures in excess of 300 °C if

required. The temperature is controlled and monitored by an Edwards Active Digital Controller connected to the heating unit via a Type K thermocouple. By conducting the polymerisation in a sealed, evacuated vessel, a vacuum of < 1 mbar may be generated using an Edwards RV5 rotary vacuum pump. The vacuum is monitored by an Edwards APG100-XM Active Pirani Gauge connected to a gas manifold, which in turn controls the level of nitrogen or vacuum applied to the system. Mechanical stirring of the polymer melt is achieved with spade-shaped steel stirrers inside the polycondensation glass tube, powered by an IKA RW20 overhead mechanical stirrer equipped with digital rotation readout. Hence, the progress of a polymerisation may be monitored by the drop in rpm resulting from the increase in polymer melt viscosity.

The general laboratory-scale melt-polycondensation procedure with this rig was as follows (the bracketed letters refer to those listed in Figure 2.1): a stirred mixture of bis(n-hydroxyalkyl) ester comonomer, polymerisable rigid comonomer and Sb_2O_3 (0.10 g, 0.34 mmol) was poured into a glass polycondensation tube (d). The polycondensation tube was then lightly scored to ensure safe extrusion and clamped inside the tube heater (e). After being fitted with: a polycondensation glass head (c); a metal stirrer blade (b); a mechanical stirrer (a); a delivery side arm glass tube connected to a distillate trap (g) inside a dry ice-filled Dewar® flask; thermocouples; and a gas manifold (f) connected by rubber vacuum tubing, the temperature was raised to 235 °C over a 1 h period under a nitrogen purge.

The mechanical stirrer was then run at a constant power to stir the mixture at ~ 300 rpm, with the temperature maintained at 235 °C for 30 min. The nitrogen purge was then stopped and the pressure within the system was gradually reduced to < 1 mbar as the temperature was increased to 290 °C at 1 °C min^{-1}. Once the viscosity of the polymer melt had risen sufficiently to lower the stirrer speed by ~ 20 %, the polymerisation was judged to be complete. The vacuum was then slowly replaced with a nitrogen purge.

If a "polymer lace" was required (solidified melt), the polymer melt was extruded by cracking the stem of the polycondensation tube with a hammer and chisel to quench into an ice-water bath. The formed polymer lace was then left to dry in atmospheric conditions for 24 h. If a polymer in powder form was required, the polymer melt was allowed to cool to room temperature under nitrogen before being dissolved in a mixed solvent of chloroform and TFA (2:1 v/v), reprecipitated in methanol and dried under vacuum at 100 ºC for 24 hours to afford the polymer powder.

2.1.2 Semi-technical industrial-scale melt-polymerisation

In order to manufacture polymer film on a sufficient scale for thermomechanical and optical analysis, a reaction scale-up is required from the laboratory melt-polycondensation rig. Polymers deemed to warrant further investigation following initial analysis were then synthesised in an industrial melt-polymerisation autoclave on a 7 kg scale.

The experimental design is essentially unchanged from the laboratory setup, with the polymerisation undertaken in a sealed vessel equipped with a mechanical stirrer and distillation side arm for the reasons previously outlined. However, in contrast to the one-step laboratory method, the esterification and polycondensation steps are now performed sequentially in a two-step synthesis due to the relatively high cost of the bis(n-hydroxyalkyl) ester monomer on this scale. A transesterification reaction is therefore performed first with the appropriate dimethyl ester monomer, polymerisable rigid comonomer (if required) and esterification catalyst ($Mn(OAc)_2.4H_2O$) added in tandem prior to the start. The polycondensation catalyst (Sb_2O_3) is then added to accelerate the polycondensation after the transesterification reaction.

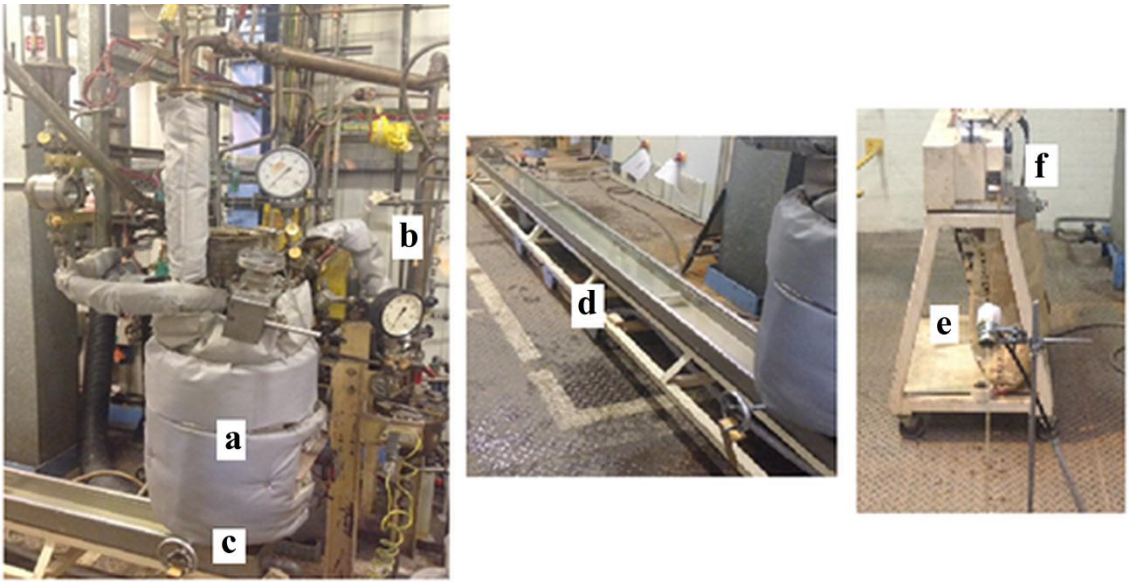

Figure 2.2 The semi-technical industrial-scale melt-polymerisation system, with: a) autoclave; b) distillation arm; c) die; d) water trough; e) air shifters; and f) mechanical cutter.

The general semi-technical melt-polymerisation procedure is as follows, with the bracketed letters referring to those illustrated in Figure 2.2: A 22 L autoclave unit (a) was loaded with dimethyl ester monomer, EG, rigid comonomer (if required) and $Mn(OAc)_2.4H_2O$ at 144 °C with stirring via an agitator. The temperature was initially increased to 184 °C and then to 196 °C in 4 °C increments held for 10 minutes each. The evolution of methanol was monitored until ~ 3 L had been removed via the distillation arm (b). Sb_2O_3 was then added to

the reaction mixture and the reaction temperature was increased to 290 °C at 1 °C min^{-1}, with a simultaneous reduction in autoclave pressure to < 1 torr. The polymerisation was monitored by the volume of EG collected over a period of 2.5 hours and the reaction was judged to be complete at a final electrical load to the agitator of 0.80 kW at 40 rpm. The agitator was then stopped and the molten polymer product was forced out of the autoclave, through a die under a nitrogen pressure of 6 psi into a water trough (d). The resulting polymer lace was then pulled through air shifters (e) into an automated mechanical cutter (f) to produce polymer chip.

2.2 Polymer film procedures

2.2.1 Semi-technical industrial-scale film line

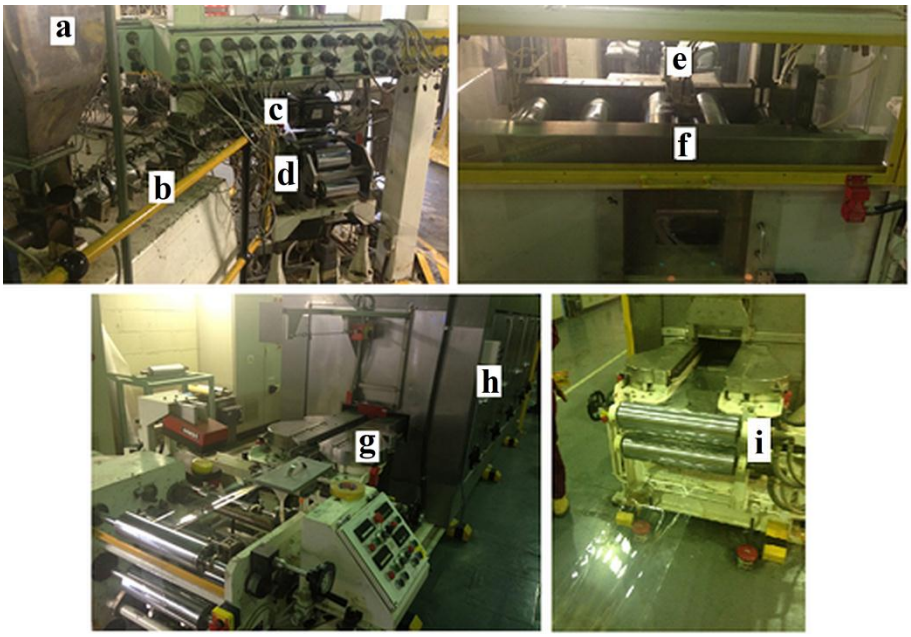

Figure 2.3 The semi-technical industrial-scale film line, with: a) hopper; b) extrusion melt pipe; c) die; d) casting drum; e) infrared heater; f) forward draw unit; g) sideways draw unit; h) stenter oven; and i) film winding unit.

Selected polymers synthesised from the semi-technical industrial-scale autoclave were processed into cast, uniaxially or biaxially oriented film on the semi-technical scale film line (Figure 2.3), via the general method detailed in Chapter 1. Experimental conditions relating to the production of specific polymers are given at the relevant points in later chapters.

2.2.2 Long stretcher

Cast polymer films produced on the semi-technical film line may be subsequently drawn to produce uniaxially or biaxially oriented film on a Long stretcher, which comprises a hydraulically operated stretching head mounted inside a heated oven with a retractable lid.

The operation of the drawing mechanism is based on the relative motion of two pairs of drawing arms, which are in turn attached to hydraulic rams that control the draw ratio and draw rate of the film.

Cut cast film samples (~ 110 x 110 mm) were loaded onto a vacuum plate before being clipped using nitrogen pressure to one or two pairs of drawing arms, for uniaxially or biaxially oriented film respectively. The drawing arms were then run into the oven at the specified temperature determined by air and plate heaters (Table 2.1). After a preheat time of 30 s, the cast film was drawn at a draw rate of 25 mm s^{-1}. Experimental conditions relating to the production of specific copolymer film are given at the relevant point in later chapters.

Table 2.1 Standard Long stretcher conditions for the production of biaxially oriented PET and PEN film.

Polymer	**Approximate draw ratio**	**Air heater temperature**	**Plate heater temperature**
	-	**°C**	**°C**
PET	3.5 x 3.5	110	110
PEN	3.5 x 3.5	150	150

2.3 Instrumental techniques

2.3.1 Nuclear magnetic resonance spectroscopy

^{1}H and ^{13}C NMR spectra were obtained on a Bruker Nanobay spectrometer at 400 and 100 MHz, respectively, and referenced to residual solvent resonances or tetramethylsilane. Samples were dissolved in various solvents at room temperature. All values representing chemical shifts, δ, quoted in the assignment of ^{1}H and ^{13}C NMR spectra are in units of ppm.

2.3.1.1 Hydroxyl end group analysis

Hydroxyl end group analysis was performed on a Jeol Eclipse +500 spectrometer at 500 MHz by ^{1}H NMR spectroscopy. Samples were dissolved in d_2-1,1,2,2-tetrachloroethane at 80 °C prior to examination.

2.3.2 Mass spectrometry

Mass spectra were obtained on a LTQ Orbitrap XL with an Accela LC autosampler. Monomer samples were analysed at a concentration of 1 mg mL^{-1} in DMSO.

2.3.3 Elemental analysis

Elemental analysis of novel monomers for scale-up were obtained by Medac Ltd., U.K.

2.3.4 Infrared spectroscopy

IR spectra were recorded on a Perkin Elmer Spectrum 100 FT-IR spectrometer with a Universal Attenuated Total Reflectance accessory. Monomer samples were analysed as powders whereas polymeric materials were analysed in powder and chip form.

2.3.5 Solution inherent viscosity

Inherent viscosities were determined at 25 °C for 0.1% wt polymer solutions in a chloroform and TFA (2:1 v/v) mixture with a Schott-Geräte CT-52 auto-viscometer, using glass capillary No. 53103 and calculated from Equation 2.1:

Equation 2.1

$$\eta_{inh} = \left(\frac{ln\left[\frac{t_2}{t_1}\right]}{c} \right)$$

where η_{inh} is inherent viscosity (dL g^{-1}), t_1 and t_2 are the flow times of the solvent and polymer solution (s) respectively and c is the concentration of the polymer solution (g dL^{-1}). Final recorded values are expressed as an average of 5 measurements per polymer solution.

2.3.6 Differential scanning calorimetry

DSC was undertaken using a TA Instruments DSC Q2000 (Chapters 3, 4 and 5) or a PerkinElmer DSC 6000 (Chapter 6) under a nitrogen atmosphere. A flow rate of 50 mL min^{-1} and aluminium pans were used. Unless otherwise stated, values of T_g, T_{cc} and T_m were obtained from 2nd heating scans whereas the T_c was calculated from the 1st cooling scan. T_{cc}, T_m and T_c values were measured as the peak exotherm or endotherm of their respective process and T_gs were determined from the initial change in the slope of the baseline (onset temperature).

Equation 2.2

$$\chi_c(\%) = \mathbf{100} * \left(\frac{\Delta H_f - \Delta H_{cc}}{\Delta H_f^{\circ}} \right)$$

Enthalpies required for determining χ_cs (Equation 2.2) were calculated[2] using the appropriate exotherm or endotherm, where ΔH_f is the enthalpy of fusion, ΔH_{cc} is the enthalpy of cold crystallisation and ΔH_f° is the enthalpy of fusion of 100% crystalline material at the equilibrium melting temperature, T_m° (all J g^{-1}). ΔH_f° values for PET (140.1 J g^{-1}) and PEN (100.3 J g^{-1}) were taken from the literature.[3]

2.3.6.1 Melting points

Monomer samples (~ 5 mg) were heated in the DSC from 0 to 450 °C at 10 °C min^{-1}.

2.3.6.2 Standard heat-cool-heat method

Polymer samples (~ 5 mg) were initially heated from 20 to 350 °C at 20 °C min^{-1} in order to erase the previous thermal history (1st heating scan). After an isothermal hold at 350 °C for 2 mins, samples were cooled to 20 °C at 5 °C min^{-1} (1st cooling scan) and isothermally held for 2 mins at 20 °C before being reheated to 350 °C at 20 °C min^{-1} (2nd heating scan).

2.3.6.3 Annealing method

Polymer samples (~ 5 mg) were initially heated from 20 to 350 °C at 20 °C min^{-1} in order to erase the previous thermal history (1st heating scan). After an isothermal hold at 350 °C for 2 mins, samples were cooled to 200 °C at 5 °C min^{-1} and isothermally held at this temperature for 2 h. Samples were then cooled to 20 °C at 5 °C min^{-1} and isothermally held for 2 mins at 20 °C before being reheated to 350 °C at 20 °C min^{-1} (2nd heating scan).

2.3.7 Hyper differential scanning calorimetry

For heating and cooling rates required above 50 °C min^{-1}, HyperDSC was undertaken using a PerkinElmer HyperDSC 8500 under a nitrogen atmosphere. A flow rate of 20 mL min^{-1} and aluminium pans (30 μL capacity) were used.

2.3.7.1 Isothermal crystallisation (Avrami) method

The kinetics of polymer crystallisation under isothermal conditions are most commonly determined using the Avrami equation[4–6] (Equation 2.3), which describes the extent of crystallisation with respect to time:

Equation 2.3
$$\mathbf{1 - V_c(t - t_0) = exp(-k(t - t_0)^n)}$$

where V_c is the relative volumetric transformed fraction, t_0 is the crystallisation onset time (s), k is the overall crystallisation rate constant (s^{-1}) and n is the Avrami exponent.

A traditional isothermal crystallisation experiment (DSC) involves heating a polymer sample above the T_m, in order to melt out any remaining crystallites. The sample is then quenched at a high cooling rate to a pre-determined isothermal temperature, T_i, between the T_g and T_m of the polymer. An isothermal hold at the T_i is then performed until crystallisation has finished, as identified by the heat flow signal equilibrating to a baseline value (Figure 2.4).

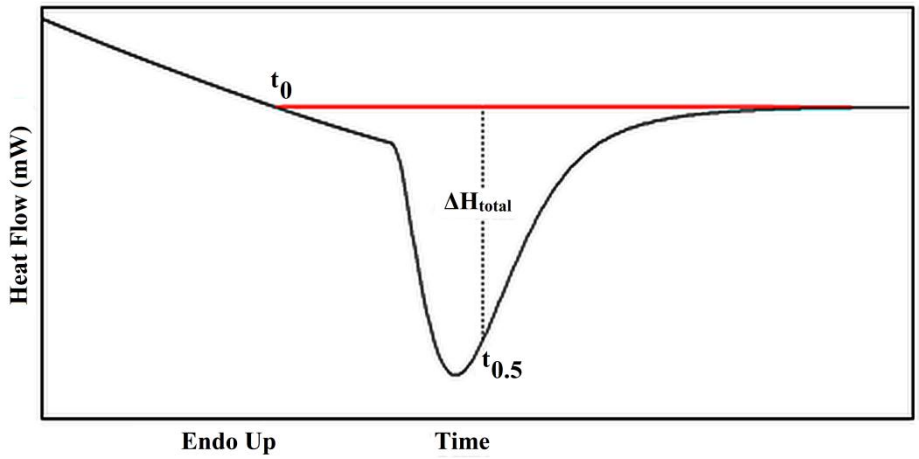

Figure 2.4 Example isothermal polymer crystallisation temperature endotherm, T_c, which is formed following the isothermal hold at T_i.

The solid horizontal red line in Figure 2.4 corresponds to the experimental baseline fitted to T_c. There is some debate in the literature as to how to best fit this, with the projection of the baseline from the finishing point on the crystallisation exotherm i.e. when there is no longer an endothermic increase in heat flow, being most commonly utilised.[7,8] The time, t_0, was therefore defined as the starting point of the experimental baseline, to minimise errors as previously reported.[9] The dashed vertical line indicates the crystallisation half-time, $t_{0.5}$, defined as the time at which the extent of crystallisation (relative to the T_c peak, not the χ_c of the polymer) has reached 50%. This may be determined experimentally by integration of the T_c endotherm, or by using calculated n and k values as described by Equation 2.4:

Equation 2.4

$$t_{0.5} = \left(\frac{ln2}{k}\right)^{\frac{1}{n}}$$

In order to calculate the Avrami parameters, the terms in Equation 2.3 may be modified to give more practically suitable variables. Assuming that a semi-crystalline polymer may be described as a two-phase model, V_c may be alternatively expressed as shown in Equation 2.5:

Equation 2.5

$$V_c = \frac{W_c}{W_c + (\rho_c/\rho_a)(1 - W_c)}$$

where ρ_a and ρ_c are the amorphous and 100% crystalline densities (g cm^{-3}) of the homopolymer, respectively[3] and W_c is the crystalline mass fraction, which may be calculated from Equation 2.6:

Equation 2.6

$$W_c = \frac{\Delta H(t)}{\Delta H_{total}}$$

where ΔH_{total} is the maximum enthalpy value (J g^{-1}) reached at the end of T_c (as illustrated in Figure 2.4) and $\Delta H(t)$ is the enthalpy variation as a function of time (J g^{-1}) at T_i. Taking

logarithms of each side of Equation 2.3 yields Equation 2.7, which is used to construct the Avrami plot:

Equation 2.7 $$Log\left[-Ln[1-V_c]\right] = Log(k) + nLog(t-t_0)$$

Polymer samples (~ 5 mg) were equilibrated at 20 °C before being heated to 300 or 350 °C (for PET and PEN respectively) at 20 °C min^{-1}. After an isothermal hold at this temperature for 5 mins, samples were cooled to x °C at 250 °C min^{-1} and held at this temperature for 60 mins, where x = 180, 190, 200, 210 and 220 °C for PET-based samples and 200, 210, 220, 230 and 240 °C for PEN-based samples.

2.3.7.2 StepScan® differential scanning calorimetry

Polymer samples (~ 5 mg) were initially heated from -30 to 350 °C at 50 °C min^{-1} in order to erase the previous thermal history (1st heating scan). After an isothermal hold at 350 °C for 2 mins, samples were cooled to -30 °C at a ballistic cooling rate (~ 900 °C min^{-1}) and isothermally held at this temperature for 2 mins. Samples were then reheated to 350 °C in 2 °C intervals at 20 °C min^{-1}, with an isothermal hold of 30 s after each interval repetition.

2.3.7.3 Rigid amorphous phase determination

Polymer samples (~ 5 mg) were initially heated from -50 to 335 °C at 175 °C min^{-1} in order to erase the previous thermal history (1st heating scan). After an isothermal hold at 335 °C for 2 mins, samples were cooled to -50 °C at 5 °C min^{-1} and held at this temperature for 2 mins. Samples were then reheated to 335 °C at 175 °C min^{-1} (semi-crystalline heating scan) and isothermally held for 2 mins at 335 °C before being cooled to -50 °C at a ballistic cooling rate (~ 900 °C min^{-1}) and isothermally held at this temperature for 2 mins. Samples were then reheated to 335 °C at 175 °C min^{-1} (amorphous heating scan).

2.3.8 Solid-state polymerisation

Polymer samples (~ 2 g) were placed in separate Schlenk tubes inside a hot block. The samples were then held under dynamic vacuum (< 0.1 mbar) at 200 °C for 16 h.

2.3.9 Thermogravimetric analysis

TGA was performed on a Mettler Toledo TGA1 in Al_2O_3 pans (40 μL capacity) under a nitrogen purge. Polymer samples (~ 5 mg) were equilibrated at 20 °C before being heated to 600 °C at 10 °C min^{-1}.

2.3.10 Dynamic mechanical analysis

DMA was performed on a TA Q800 DMA using a frequency of 10 Hz and strain of 0.1%. Polymer film and fibre samples were held in place using tensile clamps before being heated from 0 to 200 °C at 4 °C min^{-1}.

2.3.11 Gel permeation chromatography

2.3.11.1 Chapters 3, 5 and 6

GPC measurements were performed on a Malvern/Viscotek TDA 301 using an Agilent PL HFIPgel guard column plus 2 x 30 cm PL HFIPgel columns. A solution of HFIP with 25 mM NaTFAc was used as eluent, with a nominal flow rate of 0.8 mL min^{-1}. All experimental runs were conducted at 40 °C, employing a refractive index detector. Molecular weights are referenced to polymethylmethacrylate calibrants. Data capture and subsequent data analysis were carried out using Omnisec software. Samples were prepared at a concentration of 2 mg mL^{-1}, with 20 mg of sample dissolved in 10 mL eluent. These solutions were stirred for 24 h at room temperature and then warmed at 40 °C for 30 mins to fully dissolve the polymer. Each sample was filtered through a 0.45 μm polytetrafluoroethylene membrane prior to injection.

2.3.11.2 Chapter 4

GPC measurements were performed on a Viscotek GPC Max instrument using 2 x 30 cm PLgel HFIPgel columns. A solution of HFIP was used as eluent, with a flow rate of 0.7 mL min^{-1}. All experimental runs were conducted at 40 °C, employing an UV detector with sampling via automatic sample injection. Molecular weights are referenced to polystyrene standards. Data capture and subsequent data analysis were carried out using Omnisec software. Samples were prepared at a concentration of 4 mg mL^{-1}, with 20 mg of sample dissolved in 5 mL eluent. These solutions were stirred for 24 h at room temperature to fully dissolve the polymer. Each sample was filtered through a 0.2 μm polytetrafluoroethylene membrane prior to injection.

2.3.12 X-ray powder diffraction

2.3.12.1 Pellet method

X-ray powder diffraction data were obtained using an Oxford Diffraction Gemini Ultra diffractometer. Isotropic polymer samples (~ 10 mg) were produced by annealing compressed powder discs in a Mettler Toledo DSC823^{e} furnace under a nitrogen atmosphere at a flow rate of 50 mL min^{-1} inside an Al pan. Samples were heated from 20 to 350 °C at 20 °C min^{-1}

before an isothermal hold was performed at 350 °C for 5 mins. The samples were then cooled to 180 °C at 20 °C min^{-1} and held at this temperature for 2 hours, before being cooled to 20 °C at 20 °C min^{-1}. The resultant polymer pellet was mounted on Blu-Tack® and subjected to Cu Kα radiation (where λ = 1.5418 Å) at 90° φ rotations over the 2θ range 5-72°. Intensity data were merged and corrected (subtraction of amorphous regions) for absorption using CrysalisPro7 software, before the powder diffraction data was circularly integrated to give one-dimensional powder data. The four diffraction patterns corresponding to φ angles of 0°, 90°, 180°, and 270° were then summed together and underwent a Savitzky-Golay smoothing filter to improve the signal to noise ratio of the final one-dimensional powder diffraction pattern.

2.3.12.2 Capillary method

X-ray powder data for structural analysis and modelling were obtained from polymer samples (~ 50 mg) annealed under solid-state polymerisation conditions (200 °C for 16 h under dynamic vacuum). Samples were then ground to a fine powder under liquid nitrogen, sieved through a 300 mm screen, and loaded into a 0.3 mm Lindemann capillary tube. Diffraction data were collected at room temperature using a Bruker D8 powder diffractometer using Cu-Kα1 radiation (λ = 1.5406 Å) over the 2θ range 5-60° with a 0.05° step size. The amorphous scattering component was removed from the data before these were used for direct comparison with simulated powder data from the various modelled structures.

2.3.13 X-ray fibre diffraction

X-ray fibre patterns were obtained using a Rigaku/MSC FR-D X-ray source (Cu-Kα radiation, λ = 1.5418 Å) and a Saturn 92 CCD detector on an Oxford Diffraction Gemini Ultra diffractometer. Data were collected for 45 seconds with a sample-to-plate distance of 50 mm and the X-ray beam normal to the plane of the film.

2.3.13.1 Uniaxially oriented film

Cast film samples produced on the semi-technical film line were drawn at a draw ratio of ~ 4 using the Long stretcher, at 10 °C above the T_g of the sample, to give a uniaxially oriented film of ~ 50 μm thickness. Uniaxially oriented film samples were then clamped to a metal frame and annealed for 2 hours at 200 °C in a Technico laboratory oven.

2.3.13.2 Uniaxially oriented fibres

Polymer samples (~ 50 mg) were melted at 30 °C above the T_m of the sample upon a sheet of thick aluminium foil (40 x 80 mm) on a ceramic hotplate. The polymer melt was formed into

a rectangular sheet ~ 0.5 mm in thickness and then quenched rapidly in water. The aluminium foil was dissolved away from the polymer by stirring in a 30% HCl solution for 10 minutes, and the polymer sheet was cut into *ca*. 2 mm wide strips which were then manually drawn over a ceramic hotplate (draw ratio of 4) at 10 °C above the T_g of the sample.

2.3.14 Computational modelling

Model building and powder diffraction simulation were performed using Materials Studio software (v.7.0, Accelrys, San Diego, USA). Geometric and energy minimisation of chemical structures was carried out using molecular mechanics with the Accelrys Universal force field. Powder diffraction simulations and refinements (Pawley and Reitveld) were typically based upon Bragg-Brentano diffraction geometry, where Cu λ = 1.54 Å over the 2θ range 5-50° with a 0.05° step size.

2.3.14.1 Crystal structure building and refinement[10,11]

In order to determine an unknown polymer crystal structure from X-ray powder diffraction data, the monomer repeat unit of the polymer was first sketched in 3D. The monomer was then built into an "infinite" polymer crystal, aligning the polymer chain parallel to the *c*-direction of the unit cell so that the *c*-axis length was defined by the monomer repeat unit of the polymer. A nominal orthorhombic unit cell was initially assigned to the polymer crystal, with cell dimensions *a* and *b* = 10 Å, $\alpha = \beta = \gamma = 90°$. Geometric optimisation of the chain was then performed with a variable *c*-axis, with all other cell parameters fixed.

Several symmetry operations were then introduced into the crystal structure by evaluating the space group symmetry for atomic position tolerances in the range 0.01-0.50 Å and selecting the highest symmetry space group consistent with realistic molecular parameters. After geometric optimisation of the unit cell, an initial comparison between simulated and experimental X-ray powder data was determined. If a reasonable match was observed, manual adjustment of the cell parameters was performed in a further effort to improve the match between simulated and experimental data. If no good match was observed, different symmetry operations were introduced into the crystal structure until the resulting evaluation of the geometric optimisation and data comparison steps produced a reasonable preliminary crystal structure.

Pawley and Rietveld refinements were then performed on the preliminary crystal structure (refinement of lattice parameters, occupancies, crystallite sizes and lattice strains) against the

experimental powder data until a satisfactory weighted-average agreement factor, R_{wp}, was obtained, typically < 15%.

2.3.15 Polarised optical microscopy

Polarised optical microscopy was performed on a Leica DMRX compound microscope using a polarised light setup in transmitted light mode. Isotropic sample pellets were immersed in 1.600 refractive index liquid on a glass side prior to use.

2.3.16 Rotational rheology analysis

Rotational rheology analysis was performed on a Rheometrics rheometer. Polymer samples (~ 2.5 g) were dried under vacuum at 140 °C for 16 h prior to being placed between 2 x 25 mm diameter parallel plates and heated to the required temperature under a nitrogen atmosphere. Measurements were taken every 30 s.

2.3.16.1 Temperature sweep mode

Polymer samples were heated from above the T_m to 350 °C at 4 °C min^{-1} at constant frequency (100 rad s^{-1}) and strain amplitude (25%).

2.3.16.2 Frequency sweep mode

Polymer samples were subject to a change in frequency (between 0.1-100 rad s^{-1}) at constant temperature (300 °C) and strain amplitude (25%).

2.3.17 Tensile testing

2.3.17.1 Standard (fibre) method

Elastic moduli were obtained for polymer fibre samples on an Instron Model 4464 using a gauge length of 50 mm. Final recorded values are expressed as the mean of at least 4 measurements per fibre sample.

2.3.17.2 Hot-box (cast film) method

Polymer cast film samples (25 x 90 mm) were clamped inside an Instron Model 4464 equipped with a high temperature oven chamber at a gauge length of 50 mm. The oven was pre-equilibrated at the desired temperature for 30 minutes and for 5 minutes after the sample was clamped. Samples were then uniaxially drawn at 25 mm min^{-1} to a targeted draw ratio of 3 and quenched between two aluminium sheets post-draw.

2.3.18 Film crystallinity studies

2.3.18.1 Crystallisation rig

Biaxially oriented film samples measuring 150 x 100 mm were annealed in the crystallisation rig within a bespoke metal frame. Samples were held between heated platens under stated conditions before being automatically ejected and quenched into an ice-water bath.

2.3.18.2 Density column

The χ_c of biaxially oriented and heat-set biaxially oriented film samples was obtained via measurement of density. Calcium nitrate solutions (2 x 860 mL) of known densities were prepared, filtered and degassed in vacuo for 2 h before being pumped simultaneously into a graduated column tube under hydrostatic equilibrium. The two calcium nitrate solutions of known density are low and high concentration solutions which form a density gradient within the column to encompass the expected densities of the film samples. For PEN-based films, the low concentration solution (density 1.32 g cm^{-3}) comprised: 275.20 g calcium nitrate; 860 mL water; i.e. 1.95 M calcium nitrate, whereas the high concentration solution (density 1.41 g cm^{-3}) comprised: 352.60 g calcium nitrate, 860 mL water; i.e. 2.50 M calcium nitrate.

The density column was calibrated using eight standard pips of known density which were washed in calcium nitrate solution before being placed in the graduated column. For each pip placed in the column, the volume height of the column was recorded upon the pip reaching a constant level of suspension (after 4 hours) in the calcium nitrate solution. Separate measurements were taken for each pip to generate a calibration plot of volume height against density. Film samples (~ 5 x 5 mm) were placed in a calibrated calcium nitrate/water density column at 23 °C. The measurement method was repeated for each film sample with a minimum of 3 samples used to generate a mean of the measured volume height, from which the measured density was obtained from the calibration plot. The χ_c was then calculated for each sample using:

Equation 2.8

$$\chi_c(\%) = 100\left(\frac{\rho_{recorded}-\rho_{amorphous}}{\rho_{crystalline}-\rho_{amorphous}}\right)$$

where ρ_{recorded} is the recorded density of polymer (g cm^{-3}), ρ_a is the known density of amorphous homopolymer (g cm^{-3}) and ρ_c is the known density of 100% crystalline homopolymer (g cm^{-3}).[3]

2.3.19 Film thickness

Film thickness measurements of polymer film samples were obtained on a 122D Mercer Gauge by a point to point method. Final recorded values are expressed as an average of 3 measurements per sample.

2.3.20 Colour-view

Colour-view values were obtained on a BYK Gardner Colour-view box. Film samples were calibrated against a 10A cream standard tile using CIE L*a*b* colour space. Final recorded values are expressed as an average of 5 measurements per film sample.

2.3.21 Oxygen transmission rate

Oxygen transmission rates were obtained on a Mocon 10/50 Oxtran. 6 prepared film samples were purged with nitrogen before 4 cycles of recordings were taken over a period of 8-10 h. The final recorded value is expressed as an average of the final cycle from each sample.

2.3.22 Water vapour transmission rate

Water vapour transmission rates were obtained on a Lyssy L80-5000 Water Vapour Permeability Tester. The equipment was calibrated using 19 μm PET film with a known WVTR of 20 g m^{-2} day^{-1}. Measurements of prepared film samples were repeated until 5 consecutive readings had an error of < 2 % to give an average recorded value.

2.3.23 Haze/total light transmission

Haze and TLT percentage values were obtained on a M57D Spherical Hazemeter. Final recorded values are expressed as an average of 5 measurements per film sample.

2.3.24 UV-visible absorption spectroscopy

UV-Vis absorption spectra of film samples in solution were obtained on a Shimadzu UV-Visible spectrophotometer UV1800. Hellma precision quartz glass cells with a pathlength, l = 1 cm were used and a background reference spectrum of pure solvent was obtained for baseline correction.

2.4 References

1 S. J. Meehan, *PhD Thesis*, *Enhancement of Polyester Properties Through Molecular Design*, University of Reading, 2012.
2 Y. Kong and J. N. Hay, *Polymer*, 2002, **43**, 3873–3878.
3 B. Wunderlich, *Macromolecular Physics*, Academic Press, 1976.
4 M. Avrami, *J. Chem. Phys.*, 1939, **7**, 1103-1102.
5 M. Avrami, *J. Chem. Phys.*, 1940, **8**, 212-224.
6 M. Avrami, *J. Chem. Phys.*, 1941, **9**, 177-183.

7 J. Hay and P. Mills, *Polymer*, 1982, **23**, 1380–1384.
8 A. Booth and J. N. Hay, *Br. Polym. J.*, 1972, **4**, 9–17.
9 A. T. Lorenzo, M. L. Arnal, J. Albuerne and A. J. Müller, *Polym. Test.*, 2007, **26**, 222–231.
10 P. L. Aldred, *PhD Thesis*, University of Reading, *Diffraction studies and computational modelling of high-performance aromatic polymers*, 2003.
11 R. A. Young, *The Rietveld Method*, Oxford University Press, 1995.

Chapter 3

Cocrystalline copoly(ester-imide)s of poly(ethylene-2,6-naphthalate) (PEN)

The research described in this chapter has, in part, been published by the author as an article entitled "Co-crystalline copolyimides of poly(ethylene-2,6-naphthalate) (PEN)", S. J. Meehan, S. W. Sankey, **S. M. Jones**, W. A. MacDonald and H. M. Colquhoun, *ACS Macro Lett.*, 2014, **3**, 968-971.

3.1 Abstract

Copolycondensation of *N*,*N*'-bis(2-hydroxyethyl)-biphenyl-3,4,3',4'-tetracarboxylic diimide (5-50 mol%) with bis(2-hydroxyethyl)-2,6-naphthalate affords a series of cocrystalline PEN-based copoly(ester-imide)s. The glass transition temperature, T_g, rises with the level of imide comonomer, from 122 °C for PEN itself to 178 °C for the 50 mol% imide copolymer. X-ray powder and fibre diffraction studies interfaced to computational modelling illustrates that, when ≥ 5 mol% of diimide is present, the α-PEN crystal structure is replaced by a new crystalline phase arising from the isomorphic substitution of naphthalate for PEN residues in the copolymer crystal lattice. This new phase is identified as monoclinic, space group *C*2/*m*, ρ = 1.38 g cm^{-3}, two chains per unit cell with dimensions a = 10.56, b = 6.74, c = 13.25 Å, β = 143.0°. Scale-up on a semi-technical industrial-scale of this novel copoly(ester-imide) series led to the successful production of numerous thermally enhanced semi-crystalline biaxially oriented films.

3.2 Introduction

Several demanding applications that require relatively high upper operating temperatures are unattainable for poly(ethylene terephthalate) (PET) because of the relatively low T_g (76 °C) it possesses. This limitation led to the commercial introduction of poly (ethylene-2,6-naphthalate) (PEN) as a thermomechanically-enhanced semi-aromatic polyester,[1] to be then manufactured as biaxially oriented film.[2,3] Although the T_g of PEN (122 °C) is significantly greater than that of PET, the T_m is only 16 °C higher (265 °C against 249 °C) enabling PEN to be melt-processed under standard polyester conditions (< 300 °C).

Although PEN exhibits superior thermomechanical, electrical and barrier performance in comparison to PET,[4] the scale of production of PET biaxially oriented film is several orders

of magnitude greater.[5] This is mainly due to the relative scarcity and cost of the intermediate reagent NDC, which restricts the economic growth of PEN biaxially oriented film.

However, in turn, the production of PEN biaxially oriented film is still considerably cheaper than that of PEEK, which is manufactured in the high boiling solvent diphenylsulfone at 320 °C.[6] PEEK is currently the highest thermally performing semi-crystalline filmable polymer with a T_g of 143 °C, but it possesses a T_m of 334 °C.[7] From a commercial perspective, it would therefore be logical to raise the T_g of PEN to compete with PEEK as a high performing thermoplastic, in contrast to waiting for external economic factors i.e. the lowered production cost of NDC, to enable the manufacture of PEN biaxially oriented film on an equivalent scale to PET.

The T_g of PEN has been previously increased following the introduction of rigid comonomer residues, as discussed in Chapter 1, but this has always been accompanied by complete loss of the crystallinity which is essential for achieving biaxial orientation. In this chapter, the synthesis of novel PEN-based copoly(ester-imide)s incorporating rigid biphenyldiimide residues is reported. Inclusion of this unit in PET at diimide levels > 5 mol% affords only amorphous materials, but PEN-based copolymers incorporating the same diimide comonomer retain semi-crystalline behaviour across a wide composition range. This suggests that the biphenyldiimide and naphthalenedicarboxylate residues are isomorphic (Figure 3.1), enabling their random copolymers to melt-crystallise.

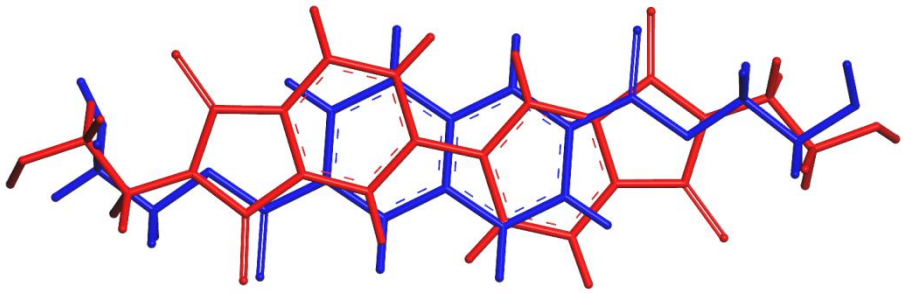

Figure 3.1 Overlaid comparison of energy-minimised coplanar models of the bis(2-hydroxyethyl)-2,6-naphthalate diester (blue) and *N*,*N*'-bis(2-hydroxyethyl)-biphenyl-3,4,3',4'-tetracarboxylic diimide (red) residues.

In this thesis, the industrial-scale synthesis, thermal characterisation and structural analysis of a novel PEN-based copoly(ester-imide) series is reported. This is followed by an investigation of the copolymer film properties in comparison to PEN and subsequent evaluation for use as a high performance polyester-based material.

3.3 Results and discussion

3.3.1 Polymer synthesis and characterisation

The novel diimide comonomer, *N*,*N*'-bis(2-hydroxyethyl)-biphenyl-3,4,3',4'-tetracarboxylic diimide, **3.1**, has been previously obtained[8] in relatively small quantities (< 15 g) from the reaction of 3,4,3',4'-biphenyltetracarboxylic dianhydride (BPDA) and 2-aminoethanol in excellent yield (96%). This synthesis was repeated on a 100 g scale, before being performed by High Force Research Ltd., U.K, to afford multiple 5 kg batches. Novel PEN-based copoly(ester-imide)s (Scheme 3.1) incorporating 5, 10, 18 and 25 mol% of **3.1** on a 7 kg industrial-scale were then produced via melt-copolymerisation of 2,6-DMN with **3.1**.

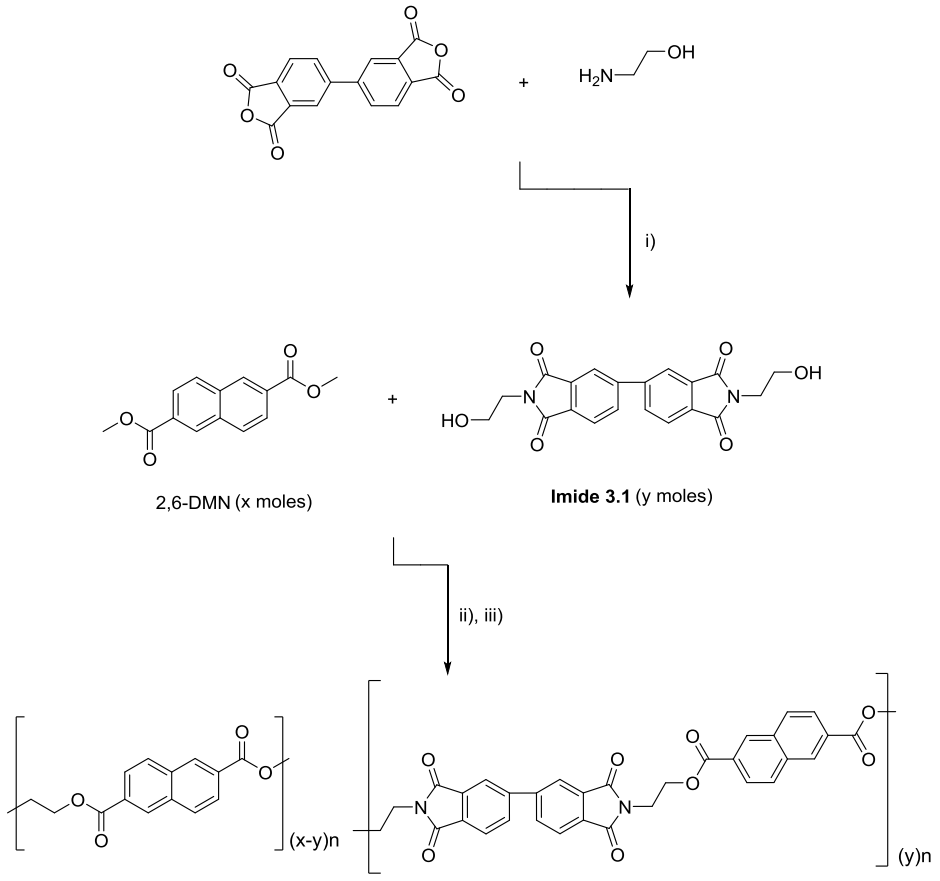

Scheme 3.1 Synthesis of PEN-based copoly(ester-imide)s via melt-copolymerisation of 2,6-dimethylnaphthalate (2,6-DMN) with **3.1**, where y ≤ x. Reaction conditions: i) DMAc/toluene, reflux, 16h. ii) EG, $Mn(OAc)_2.4H_2O$, 195 °C, 0.5 h. iii) Sb_2O_3, 290 °C, 2.5 h, < 1mbar.

Analysis of the resulting copolymers by ^{1}H NMR spectroscopy verified copolymerisation and indicated that the ratio of naphthalate to diimide residues were close to the comonomer feed ratios (Table 3.1).

Table 3.1 Comparison of the comonomer feed ratio and the copolymer composition ratio for PEN*co*(**3.1**)-5, 10, 18 and 25.

Comonomer feed ratio (mol%)		**Copolymer composition ratio[a] (mol%)**	
2,6-DMN	**3.1**	**PEN**	**3.1**
mol%	**mol%**	**mol%**	**mol%**
95	5	94	6
90	10	90	10
82	18	82	18
75	25	74	26

[a] Determined by ^{1}H NMR spectroscopy.

The extent of **3.1** incorporation in each copolymer was calculated from Equation 3.1, where H_e is the ^{1}H NMR resonance integral associated with the ethylene protons situated in between two naphthalate residues and H_f is the resonance integral associated with the ethylene protons situated next to **3.1**.

Equation 3.1

$$\mathbf{3.1}\ (\boldsymbol{mol}\%) = \mathbf{100} * \frac{\boldsymbol{H_f}}{(\boldsymbol{H_e}+\boldsymbol{H_f})}$$

The stacked ^{1}H NMR spectra of the PEN*co*(**3.1**) copolymer series are illustrated in Figure 3.2, whereby an increased feed ratio of **3.1** relative to PEN results in the continuing emergence of the H_f and H_g resonances at ~ δ_H = 4.77 and 4.34 ppm, respectively.

Slight discrepancies between the feed and actual copolymer composition ratios in the PEN*co*(**3.1**) copolymer series were accounted for upon analysis of the esterification and polycondensation distillates by ^{1}H NMR spectroscopy. The esterification distillate consisted of methanol and minor impurities as expected, but the polycondensation distillate contained both 2,6-DMN and **3.1** at ~ 0.5 mol% relative to EG and residual methanol.

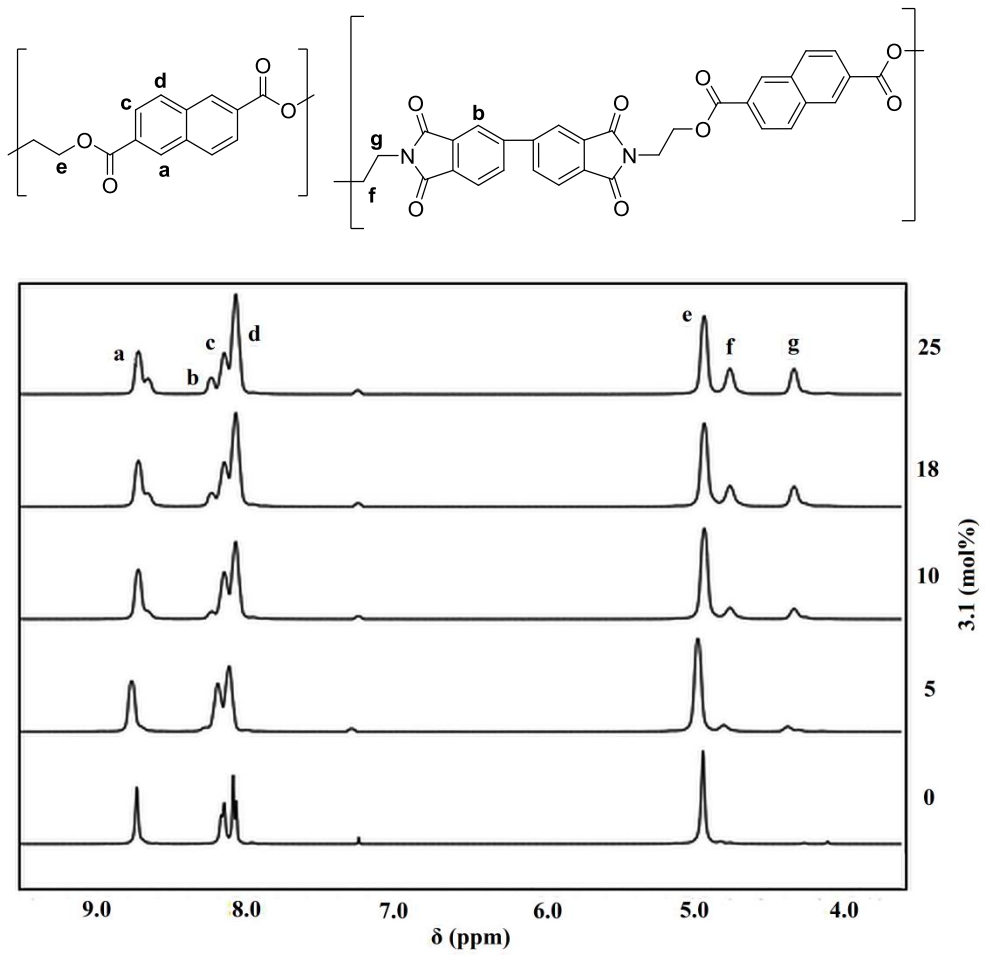

Figure 3.2 ^{1}H NMR assignment of a PEN-based copoly(ester-imide) incorporating **3.1** juxtaposed with a stacked comparison of ^{1}H NMR spectra for the PEN*co*(**3.1**) copolymer series.

During the copolycondensation step, a proportion of both ester and imide reagents are removed from the reaction autoclave. This changes the effective feed ratio of the comonomers to give a slightly different composition ratio in the final copolymer. It was observed that the carry-over of reagents is not identical for different polymerisation batches of the same intended composition, meaning that copolymer composition ratios may differ despite the same comonomer feed content.

The comonomer sequence distributions of the PEN*co*(**3.1**) copolymer series were studied by ^{13}C NMR spectroscopy via analysis of the dyad sequences about the ethylene residues within the copolymer chain. Figure 3.3 and Table 3.2 illustrate the possible dyad sequences of the PEN*co*(**3.1**) copolymer series and corresponding ^{13}C NMR ethylene resonances for PEN*co*(**3.1**)-25 (where N = naphthalate, E = ethylene and B = biphenyl). It is observed that the relative integrals of the ethylene resonances determined by ^{13}C NMR spectroscopy shown in Figure 3.3 are equivalent to the determined copolymer composition ratios listed in Table 3.1, thus allowing the ^{13}C ethylene resonances to be quantitatively compared.

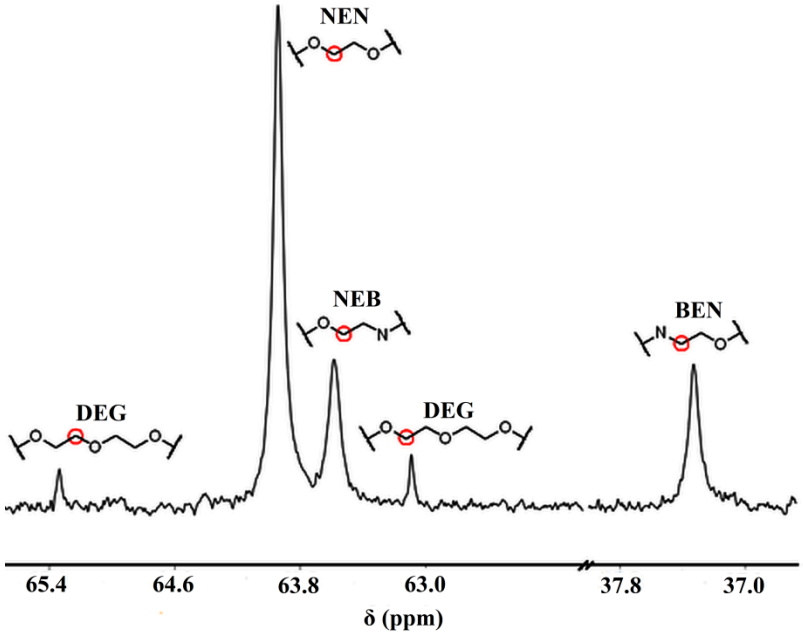

Figure 3.3 Molecular structures of the possible dyad sequences in a PEN*co*(**3.1**) copolymer overlaid with the ^{13}C NMR spectrum of the dyad sequences about the ethylene residues in PEN*co*(**3.1**)-25.

Table 3.2 Theoretical and experimental dyad ratios for PEN*co*(**3.1**)-25.

Dyad	Dyad ratios	
	Theoretical[a]	Experimental[b]
NEN	0.55	0.58
NEB	0.19	0.20
BEN	0.19	0.19
BEB	0.07	-
DEG	-	0.03

[a] Bernoullian model. [b] Determined by ^{13}C NMR spectroscopy.

The observed dyad sequences in a PEN*co*(**3.1**) copolymer differ from a simple random model, with no BEB dyad resonance being observed. This observation may be explained mechanistically, in that **3.1** is unable to form N-C-C-N residues in the copolymer chain due to the presence of the glycol functional group, as cleavage of a C-OH bond and the formation of a C-N bond during polycondensation would be required. Alternatively, DEG is observed and confirmed by the 2 resonances at δ_C = 63.0 and 65.4 ppm, and appears at consistent levels with respect to the NEN resonance despite varying **3.1** content. The average level of DEG content across the PEN*co*(**3.1**) copolymer series is also comparable to DEG levels determined for PET and PEN produced on an industrial-scale (~ 2.5%).

Calculation of the number average sequence lengths of PEN repeat units in the copolymer chain, $\overline{n}_{PEN}$, and the degree of randomness, χ, from the dyad ratios determined by ^{13}C NMR spectroscopy indicates that the PEN*co*(**3.1**) copolymers are statistically random in terms of

sequence distribution. Table 3.3 details the good agreement in experimental values for $\bar{n}_{PEN}$ and χ against the theoretical Bernoullian model for a statistically random PEN*co*(**3.1**) copolymer.[9] The slight difference between the theoretical and experimental $\bar{n}_{PEN}$ values may be explained by the lack of BEB dyad sequence units, which therefore increases the probability that a NEN dyad sequence will be present.

Table 3.3 Sequence distribution analysis of selected PEN*co*(**3.1**) copolymers.

Polymer	**Number average sequence length**		**Degree of randomness**	
	Theoretical	**Experimental**	**Theoretical**	**Experimental**
	$\bar{n}_{PEN}$		χ	
PEN*co*(**3.1**)-10	16.8	17.4	1.00	0.97
PEN*co*(**3.1**)-18	9.9	10.0	1.00	1.02
PEN*co*(**3.1**)-25	6.8	7.1	1.00	1.01

GPC analysis revealed that the PEN*co*(**3.1**) copolymer series have comparable molecular weight distributions to PEN (Figure 3.4 and Table 3.4), with M_ws of 14,000-18,000 Da and η_{inh} of 0.77-0.91 dL g^{-1}. In general, the value of M_w across the PEN*co*(**3.1**) copolymer series is observed to decrease with respect to increasing **3.1** content. This trend may be attributed to the increasing melt viscosity of the copolymer melt with respect to **3.1** content, which restricts the amount of product that may be extruded before an optimum M_w is achieved. This topic will be discussed later in the chapter, in reference to the consequence of increasing melt viscosity upon film production. A direct correlation between decreasing copolymer molecular weights and increases in the amount of hydroxyl end groups present in the final copolymer is also observed, due to increasingly incomplete polycondensation reactions.

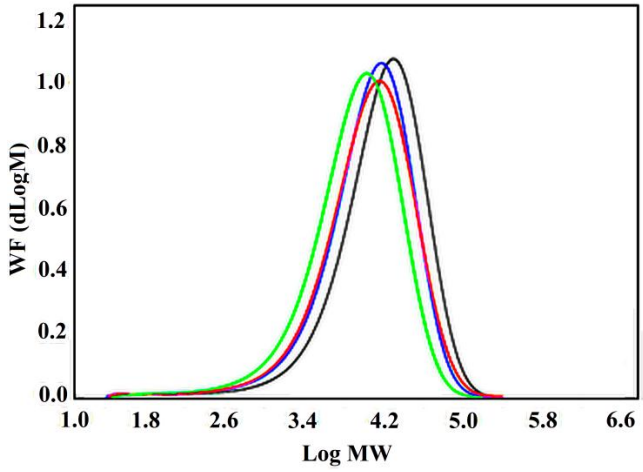

Figure 3.4 Comparative molecular weight distributions of PEN (black), PEN*co*(**3.1**)-5 (blue), PEN*co*(**3.1**)-10 (red) and PEN*co*(**3.1**)-25 (green).

Table 3.4 Molecular weight distributions, dispersities and inherent viscosities of PEN and selected PEN*co*(**3.1**) copolymers.

Polymer		M_w [a]	M_n [a]	M_z [a]	Đ	η_{inh} [b]	CH_2OH end groups [c]
		Da	**Da**	**Da**	**-**	**dL g^{-1}**	**/100 repeat units of polymer**
PEN	pre-SSP	24,000	5,200	41,000	4.6	0.98	3.18
	post-SSP	35,000	10,200	67,000	3.4		2.72
PEN*co*(**3.1**)-5		18,000	4,100	32,000	4.4	0.91	-
PEN*co*(**3.1**)-10		19,000	4,300	36,000	4.3	0.80	-
PEN*co*(**3.1**)-18	pre-SSP	16,000	3,900	31,000	4.2	0.77	4.68
	post-SSP	25,000	4,100	59,000	6.0		3.66
PEN*co*(**3.1**)-25		14,000	3,700	25,000	3.7	0.84	-

[a] Determined by GPC (HFIP eluent). [b] Determined by solution viscometry [$CHCl_3$:TFA (2:1 v/v) eluent]. [c] Determined by ^{1}H NMR spectroscopy.

Values of M_w for the PEN*co*(**3.1**) copolymer series may thus be alternatively increased via SSP. Annealing PEN and PEN*co*(**3.1**)-18 polymer chip post-polymerisation at 200 °C under dynamic vacuum raised M_ws by 45 and 55% respectively (accompanied by simultaneous decreases in hydroxyl end group values). This is illustrated by the molecular weight distributions pre- and post-SSP for PEN*co*(**3.1**)-18 in Figure 3.5. From an industrial perspective, these data indicate that the standard manufacturing approach of melt-copolymerisation followed by SSP to achieve sufficient molecular weight distributions, is applicable to this novel copoly(ester-imide) series.

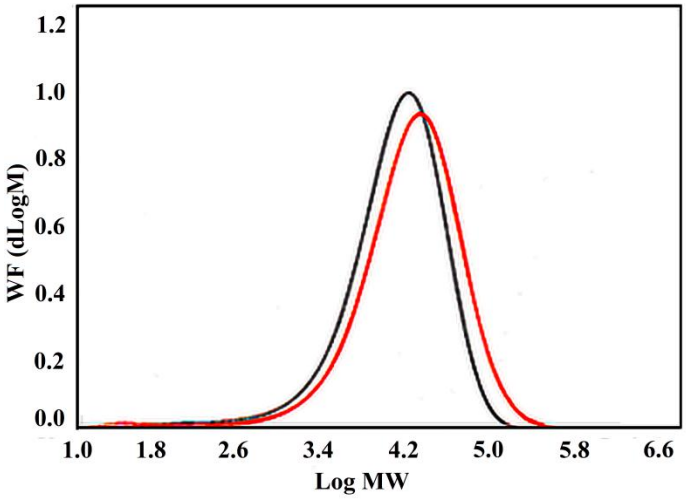

Figure 3.5 Comparative molecular weight distributions of pre- (black) and post-SSP (red) PEN*co*(**3.1**)-18.

3.3.2 Thermal properties

The incorporation of comonomer **3.1** at significant levels into PET or PEN produced copoly(ester-imide)s with markedly different thermal characteristics. Figure 3.6 illustrates that the ability of PET to melt-crystallise is destroyed following copolymerisation with **3.1** at 25 mol%, as may be expected from the previously discussed literature studies. Although the T_g of PET*co*(**3.1**)-25 has increased from 75 to 121 °C relative to PET, there is no observable T_m indicating the generation of an amorphous material. However, copolymerisation of **3.1** with PEN at 25 mol% increases the T_g relative to the homopolyester by 26 °C and y*et also* produces a copolymer that has retained substantial levels of crystallinity.

When viewing the entire PEN*co*(**3.1**) copolymer series produced by the industrial-scale melt-copolymerisation process (Figure 3.7), the T_g progressively increases as the proportion of **3.1** rises from 5 to 25 mol%. This confirms the increased rigidity imparted on the copolymer crystal lattice by the biphenyl diimide residues. Moreover, despite the T_m and χ_c initially falling for PEN*co*(**3.1**)-5 by 9 °C and 29%, respectively, both parameters then *also* increase with respect to increasing imide content, with the T_m eventually surpassing the T_m of PEN itself. All copolymers display a single T_g and T_m, further establishing the statistically random sequence distribution across the series.

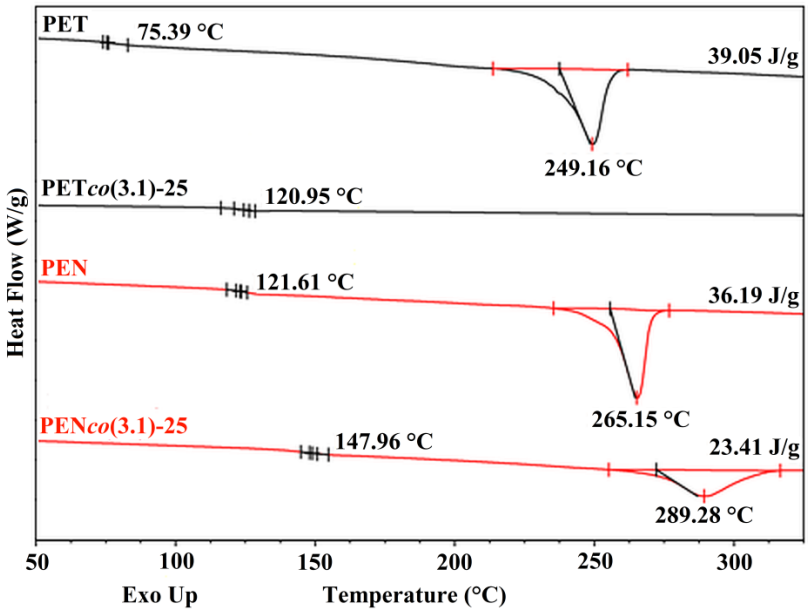

Figure 3.6 DSC 2nd heating scans (20 °C min^{-1}) of PET, PET*co*(**3.1**)-25, PEN and PEN*co*(**3.1**)-25.

This unique retention of semi-crystalline behaviour at high levels of imide incorporation supports the proposed isomorphism, and therefore cocrystallisation, of the biphenyldiimide and naphthalenedicarboxylate residues as discussed in Section 3.2. If the biphenydiimide residues were excluded from the PEN crystal lattice, then the T_m would be expected to progressively decrease as the average lamellar thickness is decreased, and eventually disappear altogether as amorphous materials were produced. In the present work, such behaviour was observed for analogous PEN-based copoly(ester-imide)s containing diphenylether and pyromellitic tetracarboxylic diimide residues, which failed to melt-crystallise once imide comonomer levels exceeded ~ 5 mol%.[8]

Incorporation of 18 mol% of comonomer **3.1** produced especially interesting thermal behaviour, with the copolymer T_g exceeding that of PEEK but crucially possessing a T_m ~ 60 °C lower. Consequently, the T_g/T_m ratio of PEN*co*(**3.1**)-18 has been raised from 0.68 to 0.76, yet affords a semi-crystalline polyester-based material that is theoretically still melt-processable. The T_g of PEN*co*(**3.1**)-25 is also greater than PEEK at 148 °C, but has a T_m that extends to ~ 310 °C which is likely too high for polyester-based melt-processing conditions. Therefore, the 18 mol% copolymer appears to be the optimum composition ratio for achieving increased thermal performance compared to PEN.

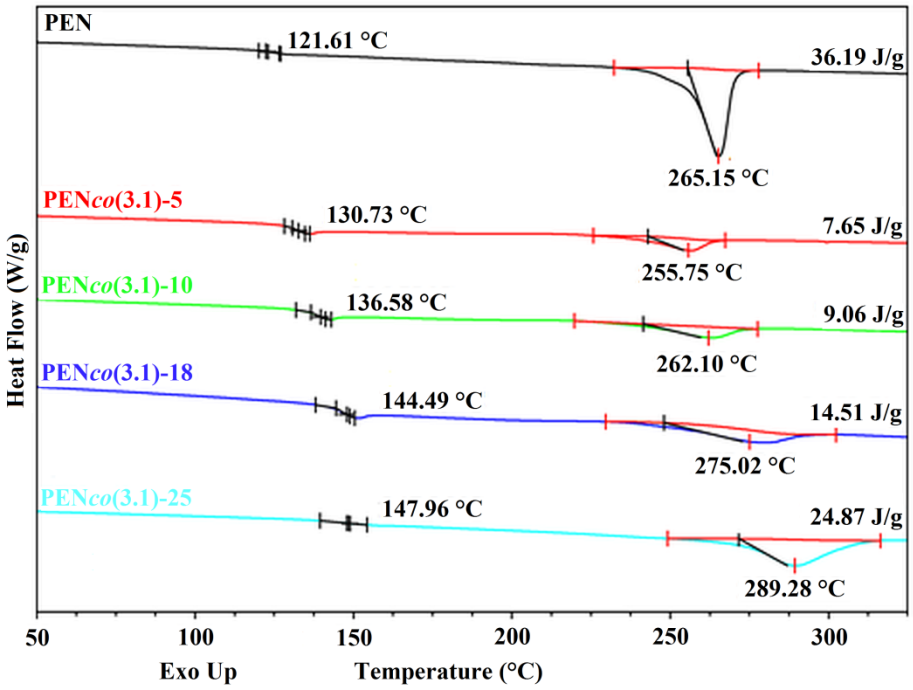

Figure 3.7 DSC 2nd heating scans (20 °C min^{-1}) of PEN and selected PEN*co*(**3.1**) copolymers.

In addition to the χ_c reaching 24% upon 25 mol% **3.1** incorporation following melt-crystallisation, significant further levels of crystallinity (33-37%) are induced across the PEN*co*(**3.1**) copolymer series following a 2 hour long anneal at 200 °C (Figure 3.8). Double melting behaviour is present for all copolymers post-annealing. This is common amongst semi-crystalline polyesters, having been previously observed for both PET and PEN[10,11] It is considered[12–14] that the multiple endotherms result from the presence of different lamellar thicknesses, as predicted by the Gibbs-Thomson equation in Chapter 1.

Within the context of the annealed PEN*co*(**3.1**) copolymer series, the lower temperature endotherms, T_{m1}, may be attributed to a melting-recrystallisation-remelting process of thinner lamellar formed at the annealing temperature of 200 °C (T_i). Hence, the lower temperature endotherms remain relatively constant (221-233 °C) with respect to increasing **3.1** content at constant T_i. In contrast, the higher temperature endotherms, T_{m2}, reflect the melting of thicker lamellae formed during the primary crystallisation stage and are therefore similar to those observed on the 2nd heating scans in Figure 3.7.

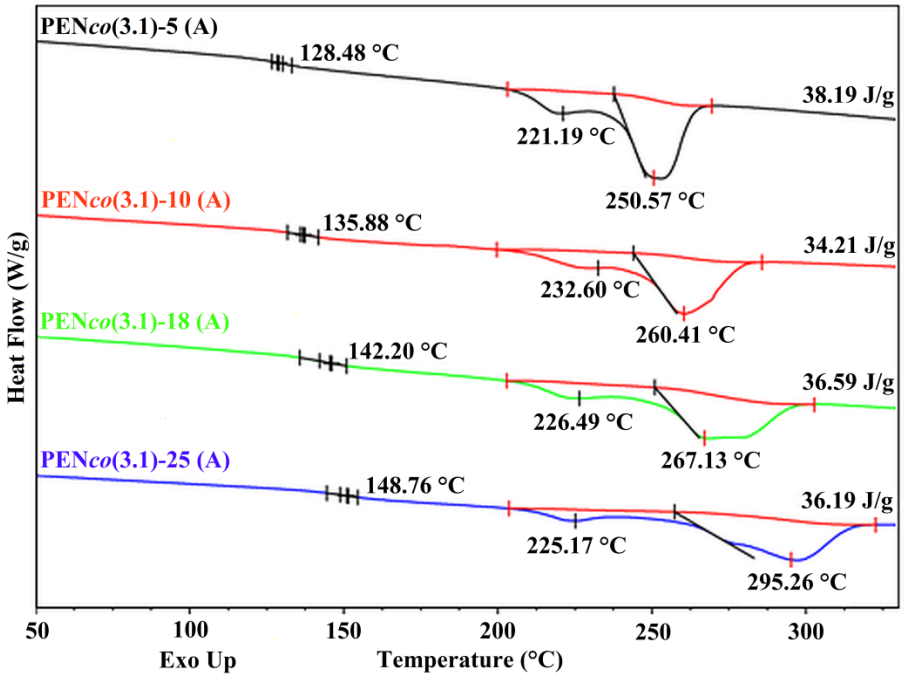

Figure 3.8 DSC 2nd heating scans (20 ºC min^{-1}) of PEN and selected PEN*co*(**3.1**) copolymers following 2 h anneal at 200 ºC.

The positive correlation between lamellar thickness and T_m is quantitatively utilised by the Hoffman-Weeks method[15] to establish the equilibrium crystalline melting temperature, $T_m°$, for a given polymer:

Equation 3.2

$$T_m = T_m° \left(1 - \frac{1}{\gamma}\right) + \frac{T_c}{\gamma}$$

where γ is the lamellar thickening factor representing the ratio of final to critical lamellar thickness. Therefore, the T_m will increase with respect to T_c under the assumption that γ is independent of T_c. The $T_m°$ is representative of a polymer crystal exhibiting infinite lamellar thickness, in contrast to the finite lamellae thickness possessed at the lower temperature T_m.[16] Based on Equation 3.2, $T_m°$ is obtained at the intercept of the T_m = T_c line with the extrapolated plot generated from experimentally obtained T_m values at set T_is.[17] PEN and selected PEN*co*(**3.1**) copolymers were cooled from the melt at 250 °C min^{-1} to various T_i (equivalent to T_c in this context) and annealed at this temperature for 1 hour. Values for T_m were acquired on the HyperDSC 2nd heating scan (20 °C min^{-1}).

At relatively high T_i, conventional double melting behaviour was observed. The T_m value used for the Hoffman-Weeks plot was therefore assigned to T_{m2} for the reasons previously outlined in reference to Figure 3.8. Triple melting behaviour was consistently obtained for all samples at relatively low T_i in accordance with literature studies,[11] whereby the medium temperature endotherm corresponds to T_{m2} at high T_i.[18] It is believed[19] that the higher

temperature endotherm, T_{m3}, can be attributed to the melting of crystallites formed in a recrystallisation process during the scan. The Hoffman-Weeks plot for the PEN*co*(**3.1**) copolymer series is illustrated in Figure 3.9, where a clear correlation between increasing T_m (lamellar thickness) and T_c is observed for each sample.

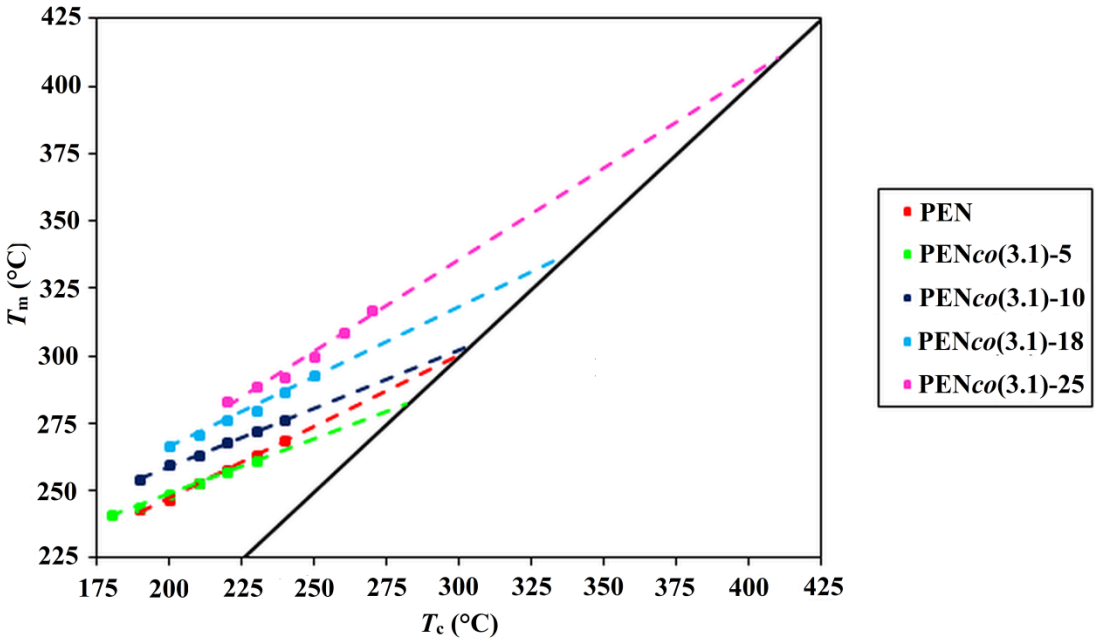

Figure 3.9 Hoffman-Weeks plot (T_m vs T_c) of PEN and selected PEN*co*(**3.1**) copolymers.

A $T_m°$ value of 301 °C was obtained for PEN, some 5 °C lower than the literature[18] value indicating a suitable test method. The slopes of the Hoffman-Weeks plots range from 0.40-0.68 implying reasonable stability (lamellar thickness) of the crystals undergoing the melting process, with values of 0 and 1 representing perfect and imperfect stability, respectively.[15]

Equilibrium melting point depression is observed across the PEN*co*(**3.1**) copolymer series (Figure 3.10) in a similar manner to the slight T_m depression exhibited previously (Figure 3.7). This is expected as the introduction of differing comonomer units should, in theory,[20,21] impose restrictions on the crystallisation process. It is therefore probable that the resulting copolymer will possess a lower, finite lamellar thickness in contrast to the homopolymer due to the reduction in long-range three-dimensional order. However, in terms of the PEN*co*(**3.1**) copolymer series, depression of T_m and $T_m°$ only occurs at 5 mol% **3.1** composition. This observation suggests that the PEN*co*(**3.1**) copolymer series forms an almost ideal crystalline structure, with near isomorphic behaviour displayed (which would be represented by a linear increase in T_m upon **3.1** inclusion).

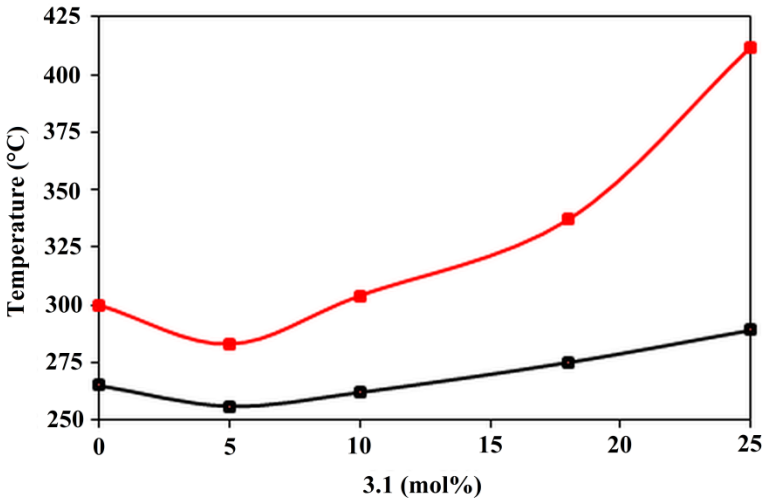

Figure 3.10 Crystalline melting temperature (black), T_m, and equilibrium crystalline melting temperature (red), $T_m°$, as a function of **3.1** content across the PEN*co*(**3.1**) copolymer series.

StepScan® (modulated) DSC was utilised in order to establish the accurate T_m of PEN*co*(**3.1**)-18 post-annealing. In comparison to conventional DSC, a non-linear heating rate is applied consisting of repetitive short heating increments followed by isothermal holds. By representing the heat flow response of this non-linear rate mathematically as in Equation 3.3,[22] it is clear that there are two contributions to the heat flow: thermodynamic and kinetic. The change in heat flow during the heating segments are attributed to thermodynamic processes, with the equilibriation in heat capacity during the isothermal holds attributed to kinetic processes.

Equation 3.3
$$\frac{dQ}{dt} = -\frac{dT}{dt}\left[C_p + f''(t,T)\right] + f(t,T)$$

where *dQ/dt* is the heat flow, *dT/dt* is the heating rate, C_p is the heat capacity, *f''(t,T)* is the thermodynamic heat flow component and *f(t,T)* is the kinetic heat flow component.

The thermodynamic and kinetic components of a DSC heating scan may be therefore separated into its reversing and non-reversing parts, as illustrated in Figure 3.11. After subjecting PEN*co*(**3.1**)-18 to a ballistic cool (~ 900 °C min^{-1}) from the melt to prevent crystallisation, a heating rate of 20 °C min^{-1} in 2 °C intervals with isothermal holds of 30 s was applied.

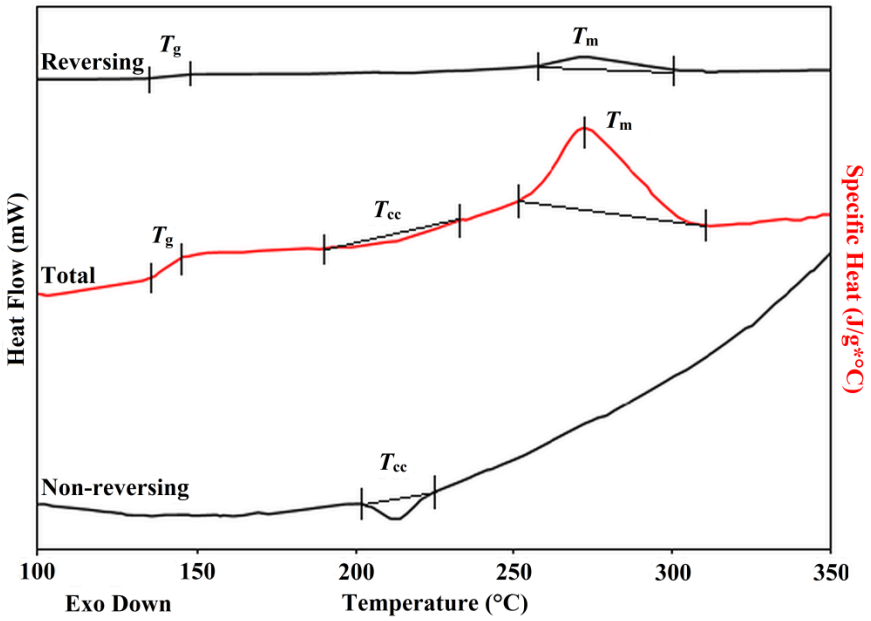

Figure 3.11 StepScan® DSC 2nd heating scan (20 °C min^{-1}, 2 °C intervals, 30 s isotherm hold) of PEN*co*(**3.1**)-18 separated into reversing and non-reversing components.

Annealing PEN*co*(**3.1**)-18 whilst heating, in comparison to a set annealing temperature, has ensured a clear T_m of 273 °C on the conventional scan. The reversing scan is similar to the total heat flow contribution, with temperature dependent thermal properties such as the T_g and T_m observed at 139 °C and 274 °C (23.97 J g^{-1}), respectively. However, the non-reversing scan reveals a T_{cc} peak at 214 °C (-23.06 J g^{-1}), which was largely hidden in the total heat flow scan because of the kinetically slow cold-crystallisation process (on the relative timescale of the experiment).[23,24] It is noted that the determined enthalpies for the T_{cc} and T_m are close to being equal. This indicates an amorphous material at the start of the 2nd heating scan and that all melted crystallites at the T_m were formed during the heating process at the T_{cc}.

The thermal crystallisation properties of the PEN*co*(**3.1**) copolymer series revealed further evidence of semi-crystalline behaviour. At a cooling rate of 5 °C min^{-1}, all such copolymers demonstrate the ability to melt-crystallise (Figure 3.12). In contrast to PEN, which shows a T_c of 209 °C, incorporation of 5 mol% **3.1** lowers the T_c to give dual exotherms at 135 and 191 °C. However, as the imide content is raised further, the T_c peak progressively rises to 236 °C thus replicating the trend observed for T_ms across the copolymer series in Figure 3.7. As the T_c of PEN*co*(**3.1**)-25 is greater than that of PEN, it would suggest that crystallisation becomes increasingly facile upon greater imide incorporation. This is supported by the supercooling temperature range ($T_m - T_c$) also decreasing from PEN to PEN*co*(**3.1**)-25 from 56 to 53 °C, respectively.

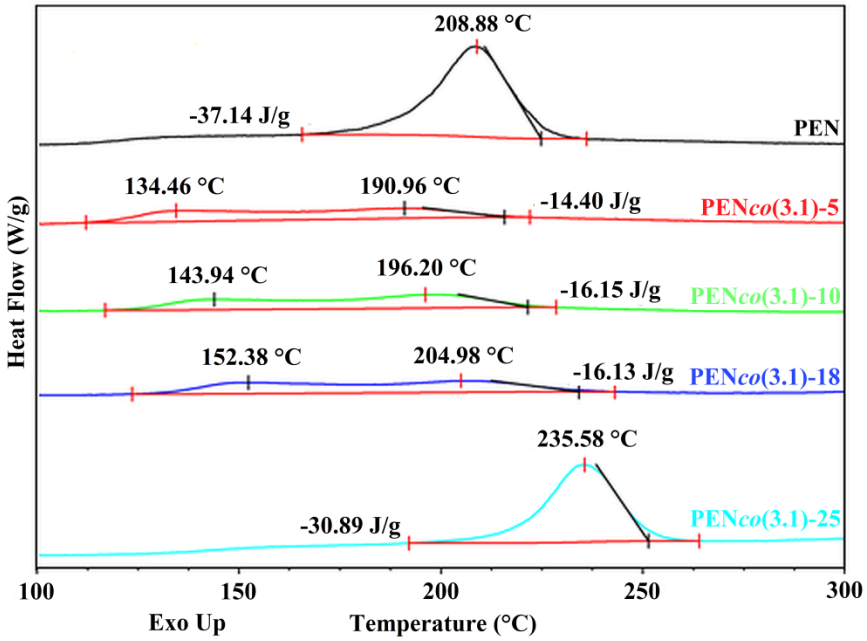

Figure 3.12 DSC 1st cooling scans (5 °C min^{-1}) of PEN and selected PEN*co*(**3.1**) copolymers.

In order to confirm the notion of comparable crystallisation rates following significant **3.1** incorporation, the isothermal crystallisation kinetics of PEN and selected PEN*co*(**3.1**) copolymers were studied by Avrami analysis,[25–27] as outlined in Chapter 2. Samples were rapidly quenched in the HyperDSC from the melt, at 250 °C min^{-1} to T_i between 200-240 °C and were annealed at this temperature until crystallisation was complete.

Figure 3.13 illustrates the extent of crystallisation, stated as the relative volumetric transformed fraction, V_c, of PEN from the onset of T_i. It is concluded that a change in T_i is not significant to the overall crystallisation profile, with a typical sigmoidal curve observed at all temperatures.[28] Initially, the rate of crystallisation is relatively slow as the formation of new spherulitic nuclei is restricted by an induction time. Once these nuclei begin to grow and crystallise (here new nuclei also continue to form), the extent of crystallisation increases rapidly until there is little untransformed material remaining. When such amorphous material does become finite, the crystallisation rate subsequently decreases.[29] However, an increase in T_i appears to affect the crystallisation rate of PEN, with a faster rate illustrated by a left-shift in Figure 3.13 at higher temperatures.

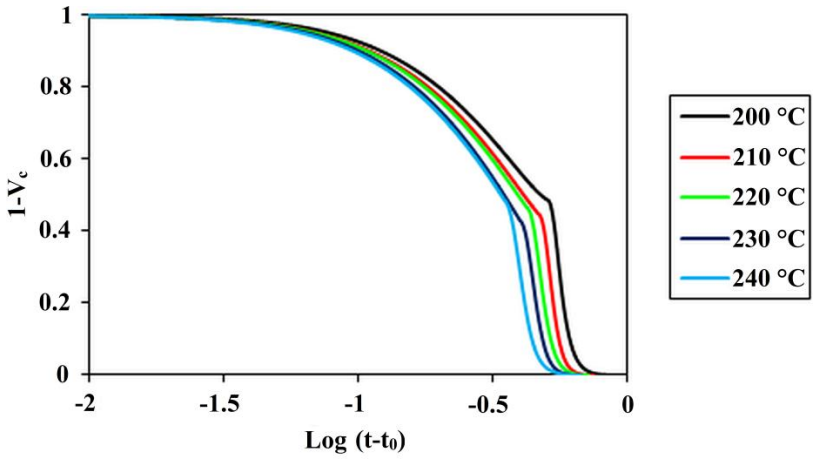

Figure 3.13 Extent of isothermal crystallisation with respect to time for PEN at T_i = 200-240 °C.

By taking logarithms of both sides of the Avrami equation (Equation 3.4), an Avrami plot may be constructed to quantitatively deduce the crystallisation kinetics, as discussed in Chapter 2:

Equation 3.4 $$\boldsymbol{1 - V_c(t - t_0) = exp(-k(t - t_0)^n)}$$

where t_0 is the crystallisation onset time, k is the crystallisation rate constant and n is the Avrami exponent.

The parameters determining the primary crystallisation mechanism of PEN are derived from Figure 3.14, with k and n representing the slope and intercept of the Avrami plot, respectively. Therefore, with respect to PEN, an upwards-shift in the curve at increasing T_i respresents a faster crystallisation rate. However, the slopes of all the plots are relatively similar and therefore will possess analogous n values and crystallisation mechanisms (as described in Figure 3.13). It is noted that all of the constructed Avrami plots are suitably linear (where $R^2 > 0.99$), which has led to a reliable fitting of the Avrami parameters and validation of the method developed here.

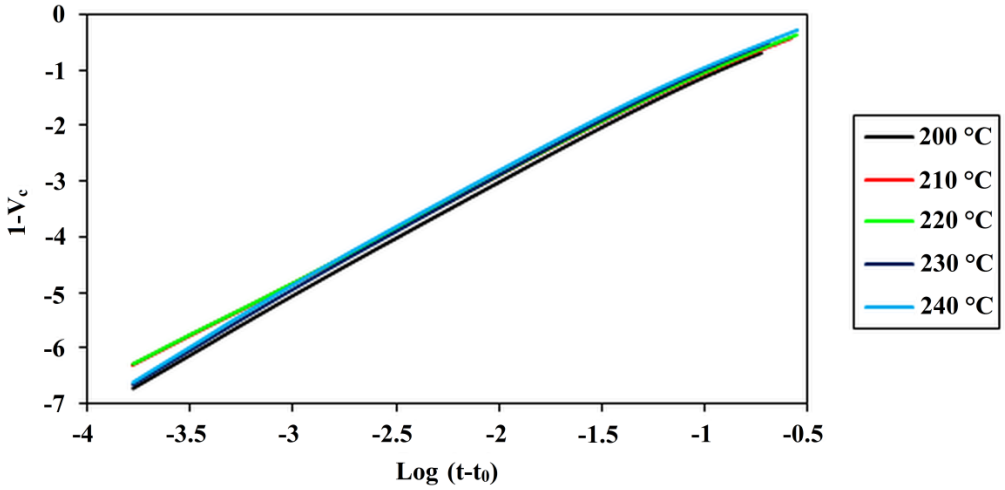

Figure 3.14 Avrami plot for PEN with respect to time at T_i = 200-240 °C.

Incorporation of **3.1** into PEN results in no significant impact on the crystallisation mechanism. Values of *n* across the PEN*co*(**3.1**) copolymer series remain between 1.65-1.77, suggesting that crystallisation proceeds via bidimensional growth with instantaneous nucleation.[30] When comparing the crystallisation half-times, $t_{0.5}$, (calculated from *k*) illustrated in Figure 3.15, there is little difference in the crystallisation rate following incorporation of **3.1**, at a constant T_i.

This observed phenomenon is in direct contrast to the accepted crystallisation kinetic theory[31,32] of copolymers which do not cocrystallise. Here, incorporation of a comonomer is expected to inhibit the chain packing arrangement following disruption of the copolymer chain, which either destroys or reduces the ability of the copolymer to melt-crystallise. However as the PEN*co*(**3.1**) copolymers are able to cocrystallise, this reduction in *k* is not observed. From an industrial perspective, PEN*co*(**3.1**) copolymers should therefore be heat-set or annealed at the same temperatures as PEN in order to maximise the χ_c obtained.

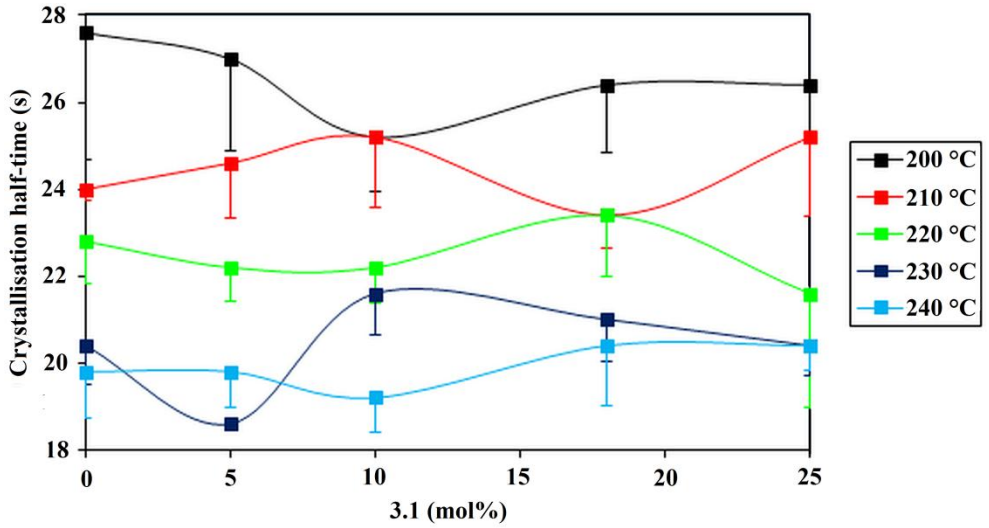

Figure 3.15 Comparative crystallisation half-times, $t_{0.5}$, of PEN and selected PEN*co*(**3.1**) copolymers as a function of isothermal temperature (where T_i = 200-240 °C). Error bars correspond to calculated $t_{0.5}$ values from experimentally obtained *n* and *k* values.

In order to deduce the maximum possible T_g for a PEN*co*(**3.1**) copolymer, the synthesis of an alternating AB-type PEN*co*(**3.1**)-50 copolymer was investigated. Synthesis via laboratory-scale melt-polycondensation was unsuccessful, due to the carryover of reagents and the tendency of the comonomers to copolymerise in a statistically random distribution. The content of **3.1** residues in the synthesised PEN*co*(**3.1**)-50 copolymer was determined at 45 mol% [herein denoted as PEN*co*(**3.1**)-45] in the final copolymer composition. The synthesis of PEN*co*(**3.1**)-50 was therefore achieved by reaction of 2,6-naphthoyldichloride and **3.1** via a solution-based method (Scheme 3.2).

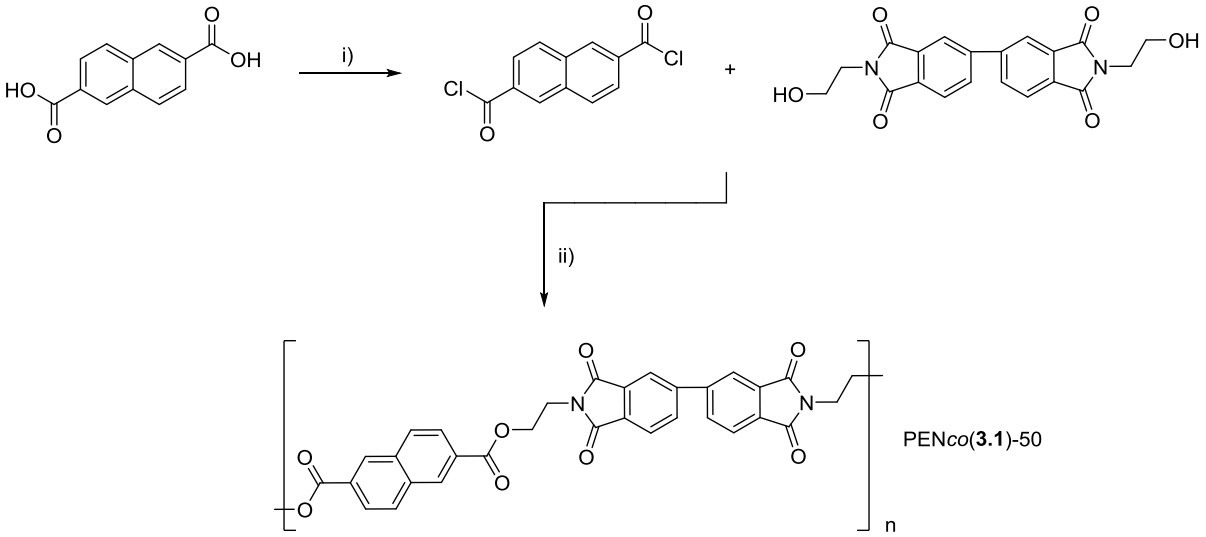

Scheme 3.2 Synthesis of PEN*co*(**3.1**)-50 via acid chloride route. Reaction conditions: i) $SOCl_2$, reflux, 4 h; ii) 1-chloronaphthalene, 210 °C, 40 h.

DSC analysis (1st heating scans at 10 °C min^{-1} as illustrated in Figure 3.16) of both the high **3.1** content PEN*co*(**3.1**) copolymers revealed semi-crystalline behaviour and large increases in T_g with respect to PEN – determined as 162 °C and 178 °C (obtained on the DSC 1st cooling scan at 5 °C min^{-1} for PEN*co*(**3.1**)-50 and therefore not observed in Figure 3.16).

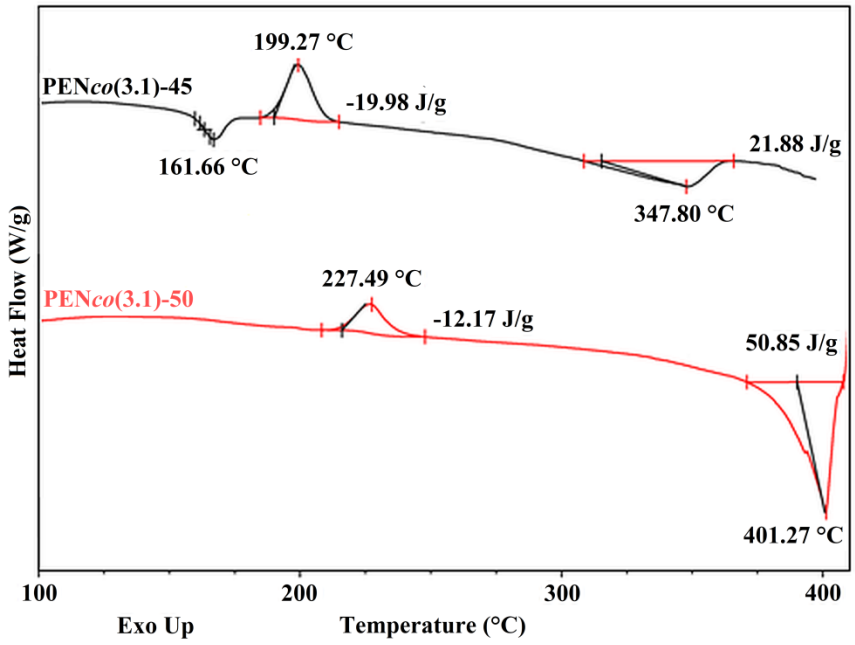

Figure 3.16 DSC 1st heating scans (20 °C min^{-1}) of PEN*co*(**3.1**)-45 and 50.

The thermal properties of PEN*co*(**3.1**)-45 and 50 are compared to those of other PEN*co*(**3.1**) copolymers in Figure 3.17. A linear increase in T_g is observed ($R^2 = 0.98$) across the PEN*co*(**3.1**) copolymer series, with a slight discrepancy noted for PEN*co*(**3.1**)-50. Overall, there is the capacity to effectively tune the T_g between 122 and 178 °C depending on the physical and application requirement of the final copolymer.

The anomalously high T_g and T_m values for PEN*co*(**3.1**)-50 may be attributed to the more ordered structure in the polymer chain, with PEN*co*(**3.1**)-50 comprising an *alternating* structure as opposed to the statistically random copolymers [PEN*co*(**3.1**)-5 to 45] synthesised by melt-copolycondensation. This higher level of sequencing order is reflected in Figure 3.16, with PEN*co*(**3.1**)-50 demonstrating a much larger ΔH_m (50.85 J g^{-1}, χ_c = 37%) in comparison to a copolymer with a similar composition ratio [PEN*co*(**3.1**)-45]. With a higher χ_c present, it is reasonable to assume that the T_g will also increase as a result of increased restrictions on chain motion in the amorphous regions, imposed by the crystallites.

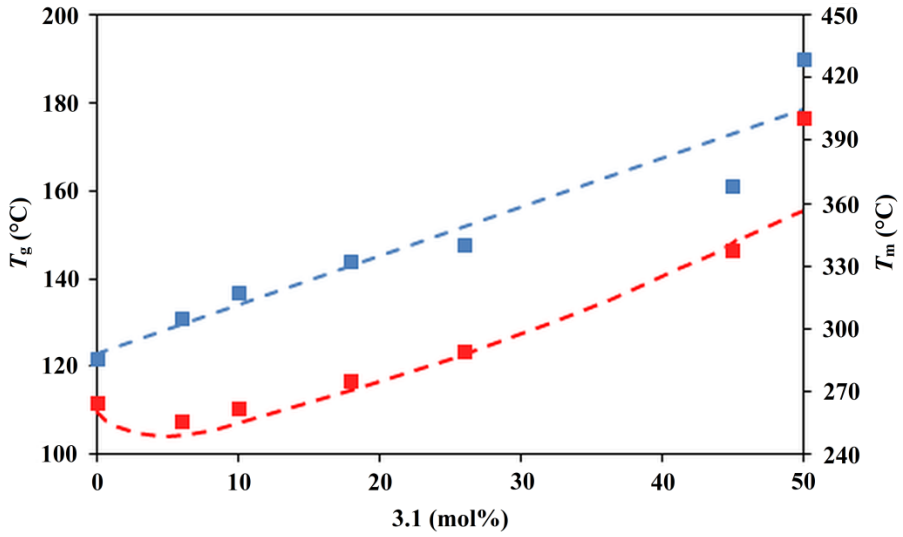

Figure 3.17 Comparative thermal properties (where blue = T_g, red = T_m) across the PEN*co*(**3.1**) copolymer series.

Degradation studies on PEN and the PEN*co*(**3.1**) copolymer series by TGA (Figure 3.18) revealed little change in T_d (415-432 °C) following inclusion of **3.1** up to 50 mol%, suggesting that the imide residues within the copolymer chain are less susceptible to thermal degradation than the ester equivalents. Therefore, PEN*co*(**3.1**) copolymers may be melt-processed and utilised in similar applications to PEN without any concern of thermal degradation occurring.

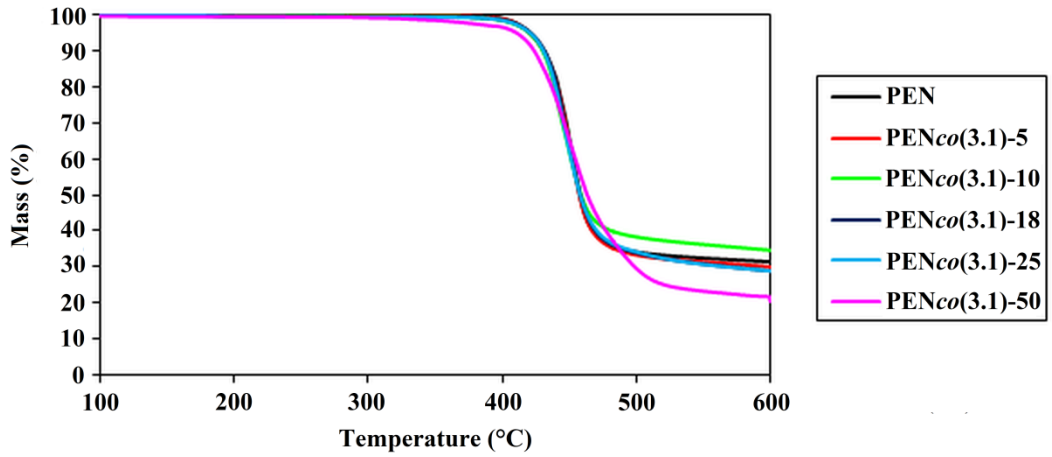

Figure 3.18 Comparative selected TGA scans (10 °C min^{-1}) for PEN and the PEN*co*(**3.1**) copolymer series.

As discussed in Chapter 1, polyimide synthesis is routinely achieved in two steps following the reaction of an aromatic dianhydride and diamine via a poly(amic acid) intermediate. For the synthesis of **3.1** homopolymer, this would require the successful reaction of BPDA and ethylenediamine. However, if a more basic aliphatic diamine is utilised, the formation of insoluble intermediate salts with the carboxylic acid groups with of the poly(amic acid) is proposed to occur.[17,33] It is consequently difficult to obtain high molecular weight semi-

aromatic polyimides by this route.[34] The homopolymer **3.1** was therefore synthesised by direct polycondensation in *m*-cresol[35] (Scheme 3.3) to avoid salt formation.

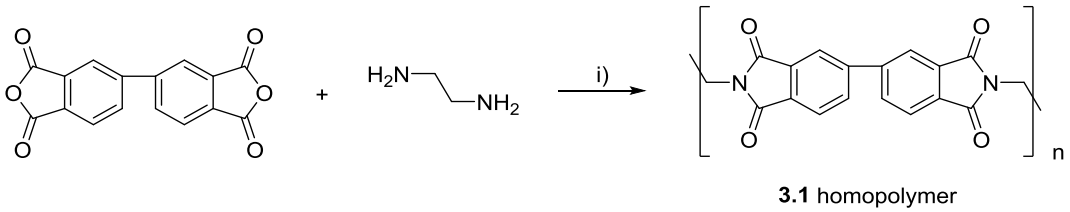

Scheme 3.3 Synthesis of **3.1** homopolymer via solution polycondensation route.[17] Reaction conditions: i) *m*-cresol, 180 °C, 3 h.

The successful conversion of BPDA to **3.1** homopolymer was monitored by IR spectroscopy (Figure 3.19). It is clear that the carbonyl absorption bands have shifted post-reaction and are in good agreement with the reported[36] absorptions for anhydrides and cyclic imides, respectively. A respectable η_{inh} of 0.36 dL g^{-1} was obtained, suggesting a comparable molecular weight distribution to PEN*co*(**3.1**)-50 (also synthesised by a solution polycondensation route).

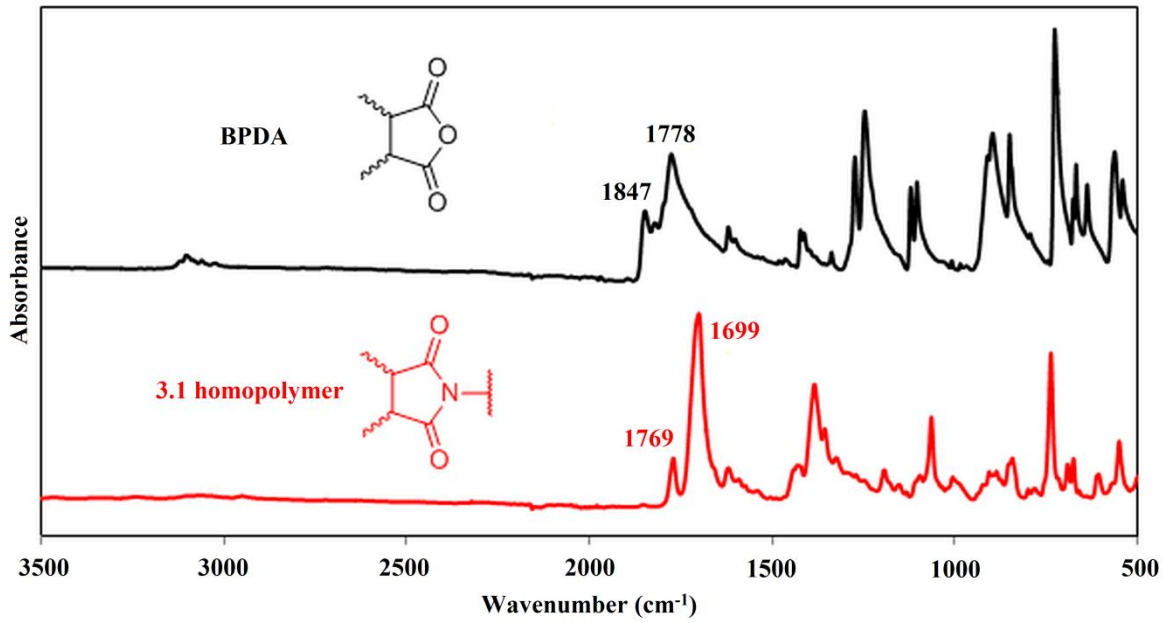

Figure 3.19 Comparative IR spectra of 3,4,3',4'-biphenyltetracarboxylic dianhydride (BPDA) and **3.1** homopolymer.

Despite the semi-aromatic nature of **3.1** homopolymer, remarkable thermal stability is observed with a T_m = 562 °C and T_d = 533 °C. The T_g of **3.1** homopolymer could not be obtained from quenched samples as a result of thermal degradation occurring above the T_m. Although not melt-processable, the outstanding thermal properties exhibited by **3.1** homopolymer reinforces the imparted characteristics of the rigid biphenyl unit upon the PEN*co*(**3.1**) copolymer series.

3.3.3 X-ray diffraction and computational modelling

There are two known polymorphs for PEN: α-form and β-form. The α-form is formed following crystallisation from the amorphous state (by cold crystallisation) or from the melt below 200 °C. This structure is well-established[37–40] as triclinic, space group $P\bar{1}$, a = 6.51, b = 5.75, c = 13.2 Å, α = 81.3, β = 144°, γ = 100°, one chain per unit cell, ρ = 1.38 g cm^{-3}. Crystallisation from the melt above 200 °C gives rise to the β-form. In contrast, this crystal structure is debated with several variations detailed[38,40,41] of a four chain per unit cell system.

X-ray powder diffraction patterns of the PEN*co*(**3.1**) copolymer series are presented in Figure 3.20, which confirm that significant levels of crystallinity are retained across all of the compositions investigated. In addition, the obtained powder diffraction pattern of α-PEN is in good agreement with those previously reported in the literature. It is observed that although the α-PEN structure is still present with 2 mol% of **3.1** incorporated, this switches to a novel crystal structure for PEN*co*(**3.1**)-5 which is retained at higher levels of **3.1** content through to the alternating copolymer, PEN*co*(**3.1**)-50. This is illustrated by the gradual disappearance of the (010) peak at 2θ = 11.4° from α-PEN to PEN*co*(**3.1**)-18 and the emergence of the (110) and (020) peaks at 2θ = 19.2 and 26.5° from PEN*co*(**3.1**)-5 to PEN*co*(**3.1**)-50. Although these peaks shift to slightly lower 2θ angles with respect to increasing imide content, the fundamental pattern remains the same.

In addition to being different from the α-form of PEN, it was established that the novel copolymer crystal structure was not the known β-form of PEN as the characteristic β-phase reflections[40] at 2θ = 16.4 and 23.3° (Table 5) are absent from the powder patterns of PEN*co*(**3.1**)-5 to 50. Incorporation of **3.1** at levels > 5 mol% does therefore not stabilise β-PEN, but results in a novel copolymer crystal structure that forms upon cocrystallisation between the naphthalene dicarboxylate and biphenyldiimide residues.

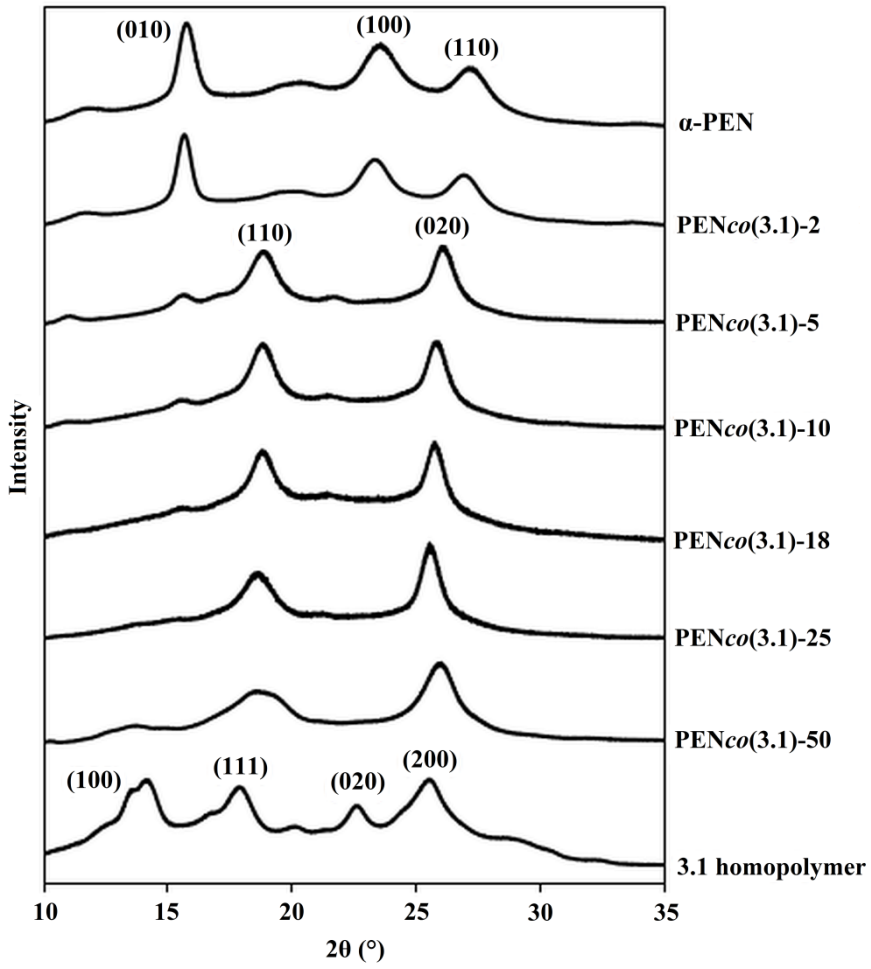

Figure 3.20 X-ray powder diffraction patterns of PEN, the PEN*co*(**3.1**) copolymer series and **3.1** homopolymer.

Table 3.5 X-ray powder diffraction data for α-PEN, β-PEN and PEN*co*(**3.1**)-5.[40]

Polymer	2θ (°)	Relative Intensity	Assignment
α-PEN	11.4	0.29	(0 0 1)
	15.7	1.00	(0 1 0)
	20.5	0.52	(1 1 $\bar{1}$)
	23.3	0.81	(1 0 0)
	27.1	0.62	(1 1 0)
β-PEN	16.4	m	($\bar{1}$ $\bar{1}$ 1)
	18.5	m	(0 2 0)
	23.3	w	($\bar{2}$ 0 2)
	25.5	s	(2 $\bar{4}$ 2)
PEN*co*(**3.1**)-5	11.1	0.23	(0 0 1)
	15.9	0.48	(1 1 $\bar{1}$)
	19.2	1.00	(1 1 0)
	22.1	0.52	(0 0 2)
	26.5	0.97	(0 2 0)

A provisional crystal structure for the PEN*co*(**3.1**) copolymer (at > 5 mol% **3.1**) has therefore been identified by X-ray powder and fibre diffraction interfaced to computational modelling.[42,43] Since the copolymer crystal structure emerges at relatively low amounts of **3.1** content (between 2-5 mol%), the copolymer model was approximated as a polymorph of α-PEN based on the assumption that any simulated diffraction pattern from the model would not be greatly affected by the presence (or absence) of comonomer residues totalling 5 mol%. The molecular structure of α-PEN was initially reproduced to give a simulated pattern matching those in the literature and obtained experimentally, hence validating the model.

Exploration of possible two-chain cells for the new copolymer crystal structure led to a C-centered monoclinic unit cell in which the chain conformation is essentially coplanar. The ester functional groups adopt the *anti*-conformation and the chain itself is therefore identical to α-PEN, as illustrated in Figure 3.21. Each chain has a mirror plane in the plane of the molecule, and a two-fold rotation axis passing through the centre of the naphthalene residue, normal to *ac*.

As demonstrated in Figure 3.1, the coplanar naphthalene dicarboxylate and biphenyldiimide residues have very similar overall dimensions and could therefore be accommodated in the same crystal lattice, requiring only that the biphenyl unit adopts a coplanar geometry. Although a torsion angle of zero at the biphenyl linkage would not represent the energy minimum in an isolated molecule,[44] this geometry is required by symmetry when an inversion center is present in the middle of the biphenyl linkage. Coplanarity is relatively common in the crystal structures of biphenyl-containing molecules,[45,46] including specifically BPDA.[47]

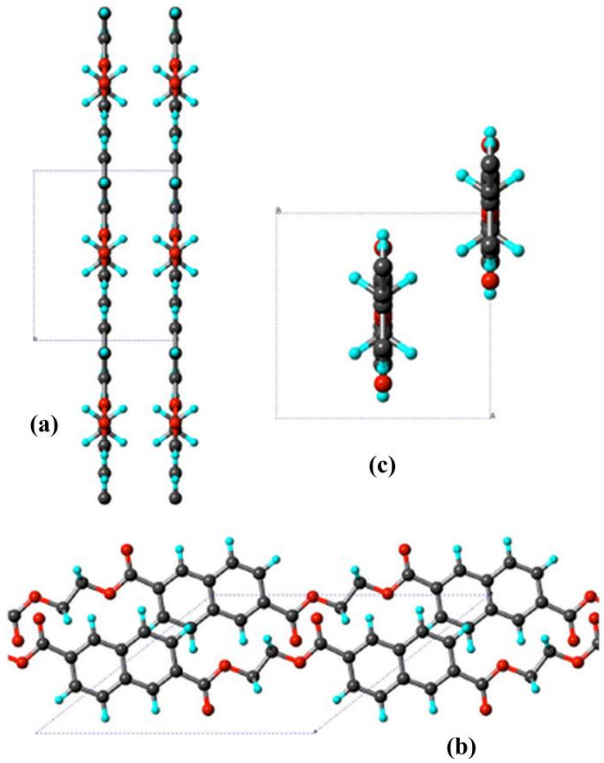

Figure 3.21 Proposed crystal structure of the PEN*co*(**3.1**) copolymer when relative **3.1** content ≥ 5 mol%. Viewed as a polymorph of α-PEN along the *a*, *b* and *c*-axes of the unit cell.

Simulation of an X-ray powder diffraction pattern from this modelled structure gave a promising initial match with the experimental X-ray powder diffraction pattern of PEN*co*(**3.1**)-5. Energy minimisation of the structure with unconstrained cell parameters gave a preliminary unit cell with dimensions a = 10.82, b = 6.75, c = 13.27 Å and β = 141.6°. Interactive, manual adjustment of the cell dimensions improved the fit between simulated and experimental X-ray powder diffraction data substantially. The structure was then reminimised with cell dimensions fixed at the derived experimental values and underwent Pawley refinement to identify the PEN*co*(**3.1**) unit cell dimensions as a = 10.56, b = 6.74, c = 13.25 Å, β = 143.0°. Examination of the resulting crystal structure showed it to be consistent with the symmetry operations of space group *C*2/*m*. Energy minimisation in this space group led to a structure giving the simulated X-ray powder diffraction pattern illustrated in Figure 3.22, superimposed on the experimental pattern for PEN*co*(**3.1**)-5 to give an excellent agreement in peak positions and relative intensities.

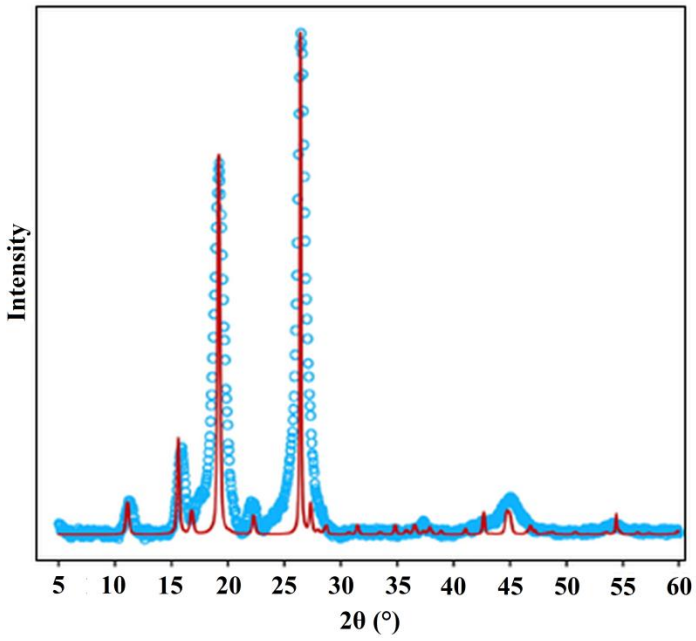

Figure 3.22 Simulated X-ray powder diffraction pattern (red) for the PEN*co*(**3.1**) copolymer series in space group *C*2/*m*, superimposed on the experimental powder diffraction pattern (blue) for PEN*co*(**3.1**)-5.

Uniaxially oriented film samples of the PEN*co*(**3.1**) copolymer series, drawn on the Long stretcher at 30 °C above T_g, afforded promising X-ray fibre diffraction patterns with the clearest image being obtained from PEN*co*(**3.1**)-18. The proposed structure, obtained by diffraction modelling of powder data, produced a simulated fibre diffraction pattern in very good agreement with the experimental data (Figure 3.23). It is, however, noticeable that the (002) reflection on the second layer line in the experimental pattern is displaced slightly above the predicted line. Non-periodic layer lines are characteristically associated with copolymer crystallites containing random sequence chains,[48,49] and Figure 3.23 is therefore also consistent with the proposed isomorphic character of the two comonomers.

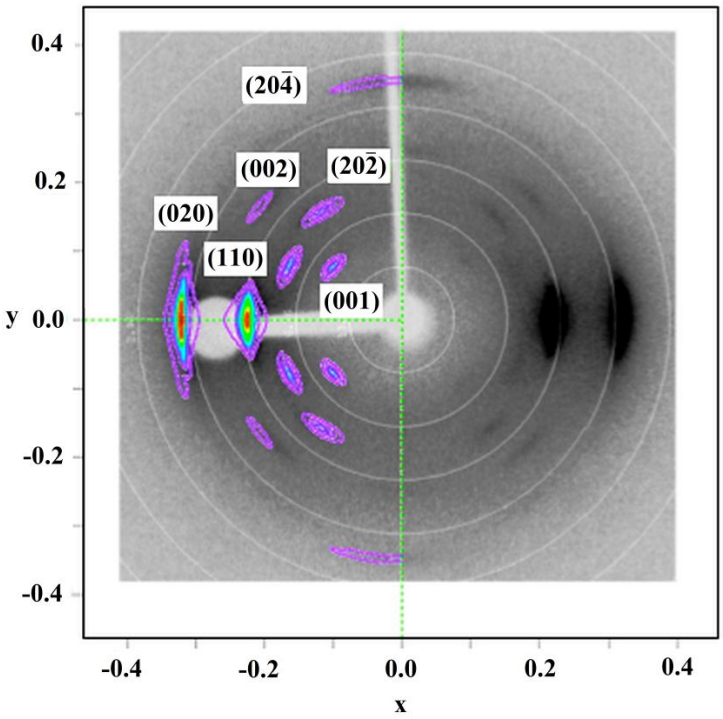

Figure 3.23 Simulated X-ray fibre pattern (coloured contour lines) overlaid on the experimental fibre pattern (grayscale) for uniaxially oriented PEN*co*(**3.1**)-18 film.

A significant change in powder diffraction pattern is observed upon transition from PEN*co*(**3.1**)-50 to **3.1** homopolymer (Figure 3.20). Although this would appear to suggest a fundamental difference in crystal structure, it is proposed that **3.1** homopolymer still adopts a centrosymmetric, monoclinic unit cell. Reitveld refinement (R_{wp} = 14%) of the **3.1** homopolymer model against the experimental powder diffraction pattern afforded a provisional crystal structure (Figure 3.24) in space group $P2_1/c$, a = 7.40, b = 7.24, c = 13.25 Å, β = 69.5°, ρ = 1.36 g cm^{-3}.

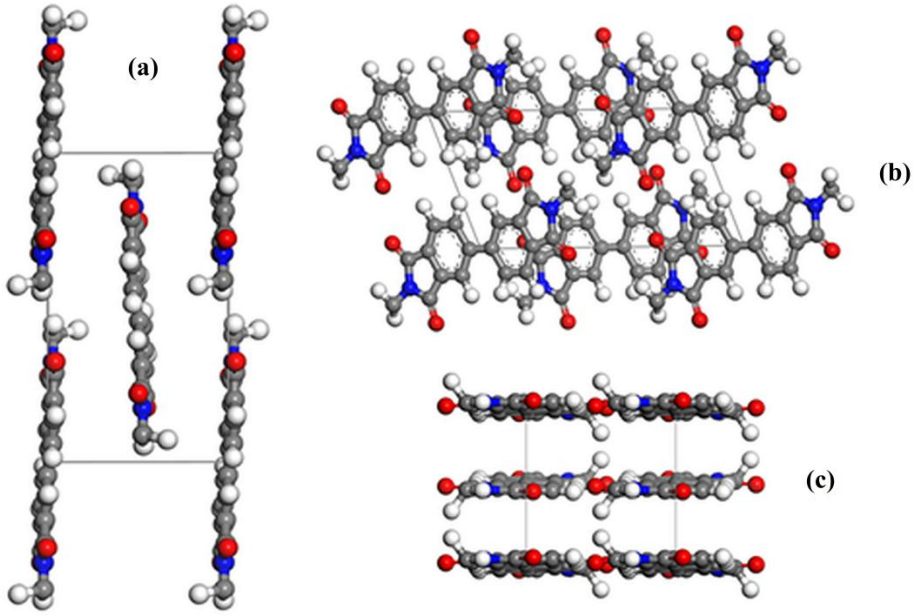

Figure 3.24 Proposed crystal structure of **3.1** homopolymer viewed along the *a*, *b* and *c*-axes of the unit cell.

3.3.4 Production of PEN-based copoly(ester-imide) biaxially oriented film

With the thermal characteristics and structural morphology of the PEN*co*(**3.1**) copolymer series now well-established, further investigation of the copolymer rheology and film properties was required in order to establish an industrial production process for PEN*co*(**3.1**) copolymer biaxially oriented film.

It was suggested previously, in reference to Figure 3.7, that PEN*co*(**3.1**)-18 may be the optimum copolymer composition for film production as it possessed the largest rise in T_g compared to PEN accompanied with a relative maintenance of the T_m. The rotational rheology analysis of selected PEN*co*(**3.1**) copolymers appears to support this proposal, implying that above 18 mol% **3.1** incorporation, it would not be possible to melt-process such copolymers under standard polyester extrusion temperatures (280-300 °C).

Table 3.6 lists the G'/G'' crossover temperatures of selected PEN*co*(**3.1**) copolymers, where applicable. The parameters G' and G'' are defined as the storage and loss moduli, representing the elastic and viscous components of a viscoelastic material, respectively. Above the G'/G'' crossover temperature, the behaviour of a polymer melt is comparable to a viscoelastic liquid i.e. the contribution from G'' is greater, therefore enabling the material to be melt-processable and readily extruded.

Table 3.6 Comparative rotational rheology analysis of selected PEN*co*(**3.1**) copolymers.

Polymer	η*[a]	G'/G'' crossover
	Pa s	°C
PEN*co*(**3.1**)-5	251	196
PEN*co*(**3.1**)-18	293	278
PEN*co*(**3.1**)-25	503	> 300

[a] Determined by rotational rheology temperature sweep mode at 290 °C.

It is observed that the G'/G'' crossover temperatures rise with respect to increasing **3.1** content, to the extent that a crossover of moduli no longer occurs for PEN*co*(**3.1**)-25 below 300 °C. The anticipated increase in viscous behaviour through copolymerisation with a rigid comonomer is transferrable to the complex viscosity, η*, of the copolymer series, which also rises with increasing levels of imide and is therefore in correlation with the higher T_m and χ_c. A η* range of 100-400 Pa s is considered[50] to be the optimum processing range on the semi-technical industrial-scale melt-polymerisation and filming extruders, so that PEN*co*(**3.1**)-18 appears to represent the limiting content of **3.1** in terms of film extrusion.

The rheological properties of PEN*co*(**3.1**)-18 are further illustrated in Figure 3.25 and Figure 3.26. If G', G'' and η* are measured as a function of increasing temperature i.e. an equivalent scenario to the reaction conditions in a typical copolycondensation reaction, large decreases in all parameters start to occur at the T_m onset of 270 °C. Upon melting by 290 °C, the η* of PEN*co*(**3.1**)-18 has fallen sufficiently to allow facile extrusion as discussed.

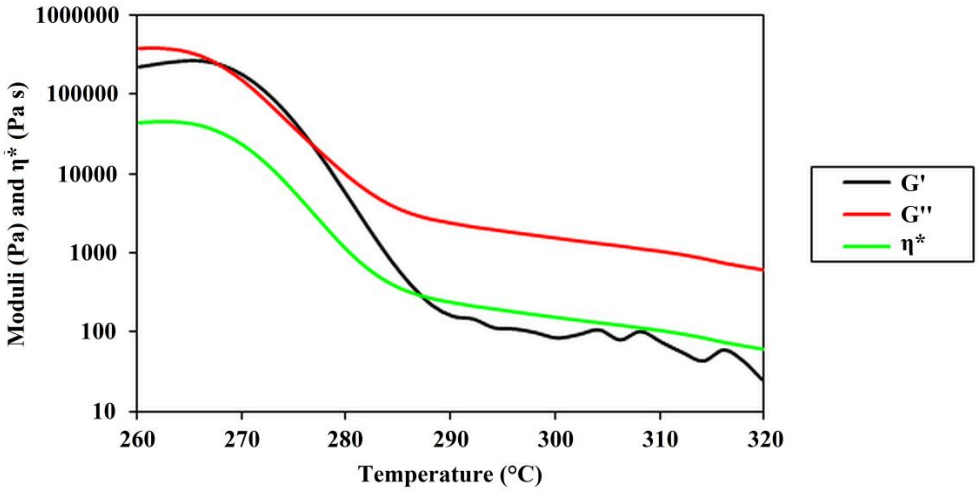

Figure 3.25 Rotational rheology analysis of PEN*co*(**3.1**)-18 performed in temperature sweep mode (heating rate of 4 °C min^{-1}, frequency of 100 rad s^{-1} and 25% strain).

Furthermore, when rotational rheology analysis is undertaken as a function of frequency rather than temperature, PEN*co*(**3.1**)-18 displays near-Newtonian behaviour[51] as a copolymer

melt at constant temperature (Figure 3.26), especially at low frequencies. Assuming the measured properties are independent of strain (constant at 25%), the values of η* and frequency may be considered equivalent to shear viscosity and shear rate. Therefore, the shear viscosity of PEN*co*(**3.1**)-18 is essentially independent of the shear rate at 300 °C and constant strain, demonstrating only slight shear thinning as a result of molecular alignments and the disentanglement of polymer chains.[52] The extrusion properties of PEN*co*(**3.1**)-18 are consequently analogous to semi-crystalline polyesters, such as PET,[53] simplifying the industrial-scale filming process.

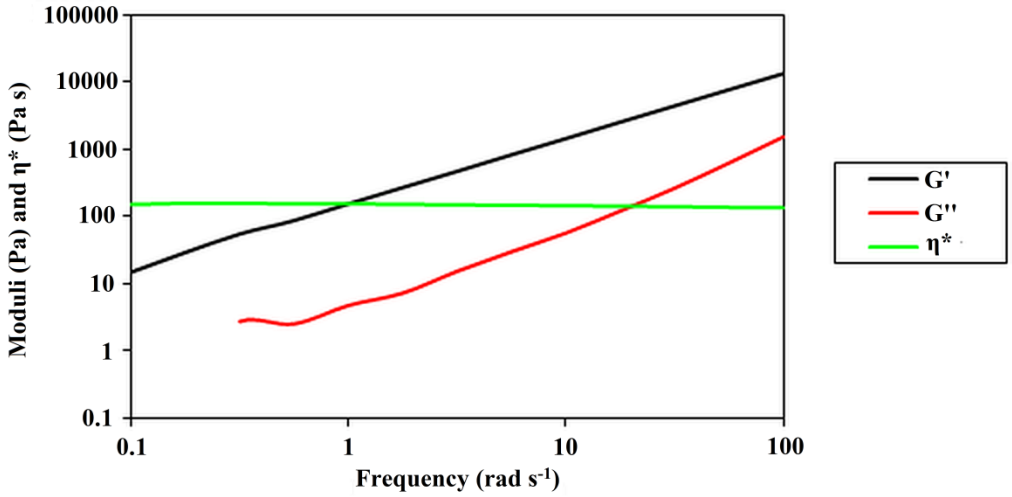

Figure 3.26 Rotational rheology analysis of PEN*co*(**3.1**)-18 performed in rate sweep mode (temperature of 300 °C and 25% strain).

PEN, PEN*co*(**3.1**)-10 and 18 cast film were produced on the DTF semi-technical industrial-scale film line at an extrusion temperature of 290 °C and line speed of 5 m min^{-1}. As PEN*co*(**3.1**)-18 possesses a T_g ~ 20 °C higher than PEN, the forward draw behaviour of PEN and PEN*co*(**3.1**)-18 cast film with respect to temperature was investigated by Instron hot box tensile analysis. In addition to providing optimum forward draw temperatures for future filming production, it was unknown whether a cocrystalline copoly(ester-imide) such as PEN*co*(**3.1**)-18 would display analogous drawing behaviour and mechanical properties to that of PEN. Cast film samples were drawn at 25 mm min^{-1} at 10 °C intervals from the T_g to a targeted forward draw ratio of 3, after being equilibrated at the drawing temperature for 5 minutes to avoid pre-crystallisation. The stress-strain relationships of the drawn films were calculated from Equation 3.5 and Equation 3.6.[54]

Equation 3.5 $$\sigma = \frac{F}{A}$$

Equation 3.6 $$\varepsilon = \frac{\Delta l}{l_0}$$

where σ is the tensile stress, F is the load, A is the cross-sectional area of film, ε is strain, Δl is the change of film length and l_o is the initial film length.

In contrast to PET, PEN shows necking behaviour when drawn from the amorphous state above the T_g. Here, tensile deformation occurs whereby large amounts of strain disproportionately localise in small regions of the film decreasing the cross-sectional area.[55] This is attributed[56] to cooperative naphthalene rings parallel to the surface of the film imparting increased chain stiffness and so affecting the mechanical properties of the polymer.

It is reported[56–58] that the stress-strain curve of PEN at 130 °C (~ 10 °C above T_g) exhibits two yield points i.e. where the film shows appreciable elongation without any increase in load. After the first yield point, the tensile stress is essentially constant as necking occurs, before the tensile stress rises again as a result of hardening associated with stress-induced crystallisation due to improved chain orientation.[57] This behaviour is typical of an isotropic to nematic structural transition which occurs in highly localised regions of the film, with the PEN mesophase present in addition to the α-form.

The stress-strain curves for PEN at 120 and 130 °C replicate those observed in the literature[56–58] (Figure 3.27), with a clear initial yield point followed by a decrease in stress that in turn gives way to a second yield point as the forward draw ratio approaches 3. As the drawing temperature is increased above the T_g, a lower tensile stress at a given draw ratio is observed, in addition to a smaller loss of tensile stress after the first yield point.

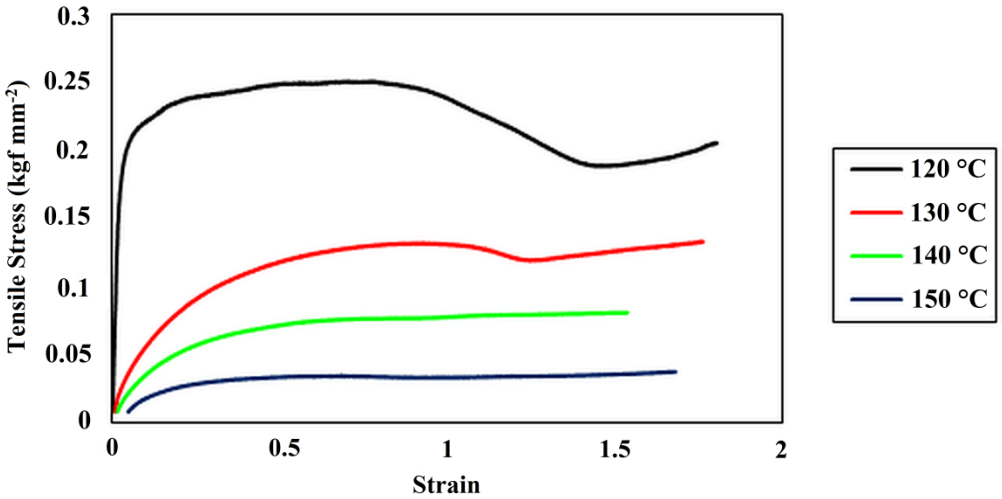

Figure 3.27 Stress-strain curves of PEN cast film drawn (targeted draw ratio of 3) at selected temperatures.

Although the two yield points are still observed for PEN at forward draw temperatures of 140 and 150 °C, there is no substantial increase in tensile stress with respect to increasing strain.

This suggests that a forward draw temperature of 140-150 °C is adequate for PEN (~ 20-30 °C above T_g) on the semi-technical film line. An increase in draw temperature from 120 °C has decreased the tensile stress due to increased molecular mobility resulting in near homogeneous deformation. However, any further increase in draw temperature is likely to cause thermally-induced crystallisation.

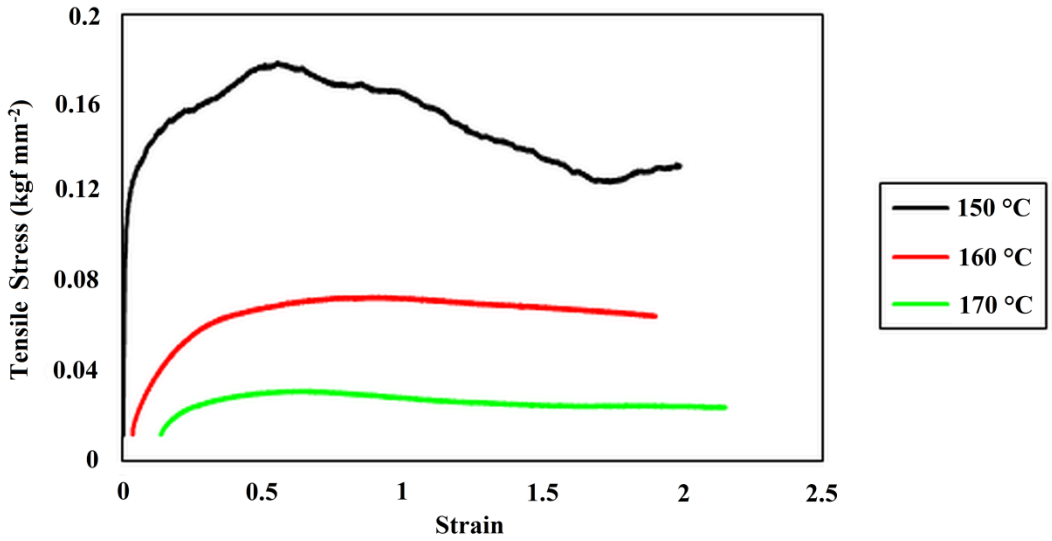

Figure 3.28 Stress-strain curves of PEN*co*(**3.1**)-18 cast film drawn (targeted draw ratio of 3) at selected temperatures.

The forward draw behaviour of PEN*co*(**3.1**)-18 cast film is analogous to that of PEN, at elevated temperatures, with the two yield point stress-strain curve also observed ~ 10 °C above T_g (150 °C). At their equivalent temperatures above T_g, the tensile stress of PEN*co*(**3.1**)-18 is ~ 70% of PEN, indicating a more facile draw due to the lower χ_c induced. However, Figure 3.28 suggests that the optimum drawing temperature for PEN*co*(**3.1**)-18 is between 160-170 °C, some 20-30 °C higher than the upper temperature limit of the forward draw unit on the industrial-scale film line. Therefore, it is not currently possible to produce PEN*co*(**3.1**)-18 oriented film on this line.

Thus, as an alternative production method, cast PEN, PEN*co*(**3.1**)-10 and 18 films were simultaneously biaxially drawn using the Long stretcher at close to the optimised drawing temperatures previously established (130 , 160 and 165 °C, respectively). The biaxially oriented film samples were then heat-set in a crystallisation rig at 240 °C for 10 s, in an attempt to replicate the effect of the stenter oven on the film line at the optimised isothermal crystallisation temperature determined from Avrami analysis (Figure 3.15). This route produced biaxially oriented heat-set film samples on an A4-scale, illustrated in Figure 3.29 as

a comparison between PEN and PEN*co*(**3.1**)-18 polymer chip and heat-set biaxially oriented film.

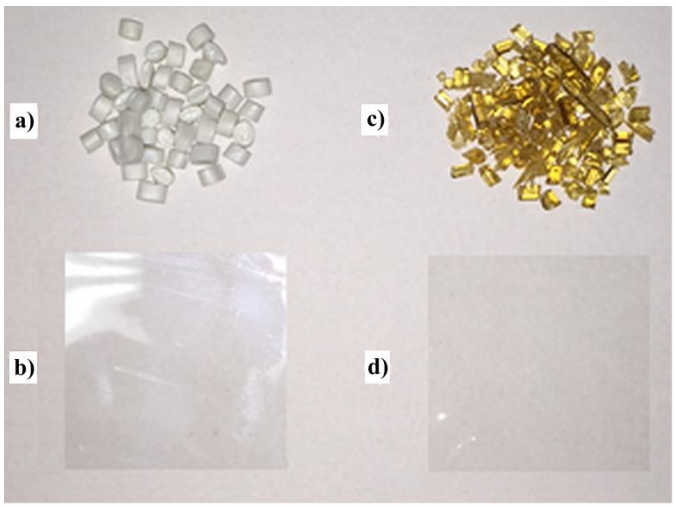

Figure 3.29 Comparison of industrial-scale polymer chip and heat-set biaxially oriented film of PEN (a) and b) respectively) and PEN*co*(**3.1**)-18 (c) and d) respectively).

DSC 1st heating scans (20 °C min^{-1}) of the respective cast and heat-set biaxially oriented films revealed that the thermal properties observed in chip form are transferrable to the films (Figure 3.30). In cast form, PEN and PEN*co*(**3.1**)-18 are essentially amorphous and display T_gs, as expected, of 118 °C and 140 °C. Cold crystallisation occurs in both systems, indicating that facile crystallisation may occur upon drawing (stress-induced) and annealing (thermally-induced). This has occurred, crucially, with χ_cs of 40 and 21% observed for PEN and PEN*co*(**3.1**)-18 heat-set biaxially oriented film confirming the production of a thermally enhanced semi-crystalline material.

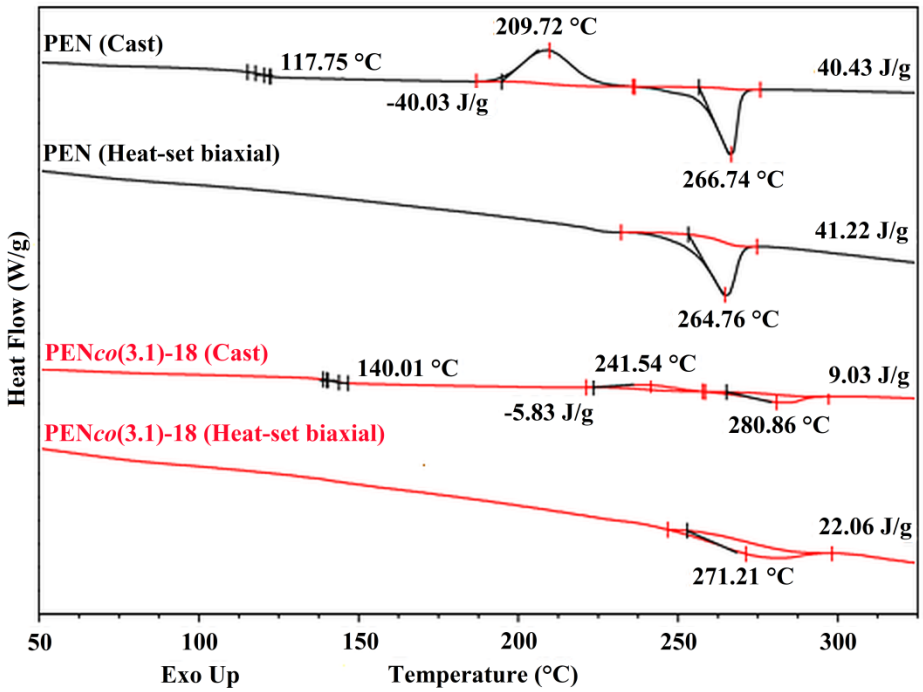

Figure 3.30 DSC 1st heating scans (20 °C min^{-1}) for cast and heat-set biaxially oriented film of PEN and PEN*co*(**3.1**)-18.

Further evidence of semi-crystalline behaviour in PEN*co*(**3.1**) copolymer biaxially and heat-set biaxially oriented film was provided by film density analysis. The density column method for determining χ_cs involves placing biaxially oriented film samples into a graduated calcium nitrate aqueous solution of a prepared density range. Recorded heights of equilibrated film samples within the column may then be compared against standard pips of known densities. Hence, the height of a film sample corresponds to a density value, which may then be used to calculate the χ_c utilising known density values for the equivalent amorphous and 100% crystalline film sample. This route is therefore dependent on the validity of the two-phase model description for semi-crystalline polymers, whereby there are strictly amorphous or crystalline regions.

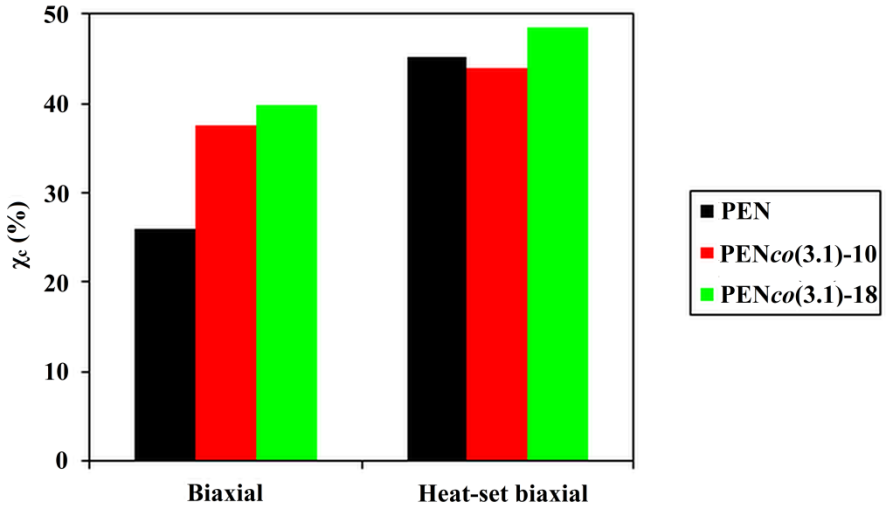

Figure 3.31 Crystallinity analysis of PEN, PEN*co*(**3.1**)-10 and 18 where biaxial = biaxially oriented film and heat-set biaxial = heat-set biaxially oriented film.

Figure 3.31 reveals that the χ_c of PEN *heat-set* biaxially oriented film determined by density is 5% greater than the DSC measurement. Comparison to the biaxially oriented film suggests that, in PEN, roughly half of the induced crystallinity originates from the simultaneous biaxial draw, followed by an additional 19% post-anneal. In contrast to DSC analysis, both PEN*co*(**3.1**)-10 and 18 have comparable χ_cs to PEN post-annealing, yet a smaller proportion of this level of crystallinity is thermally-induced (increase of 7 and 8%, respectively). This confirms the thermal behaviour demonstrated in Figure 3.7, with the PEN*co*(**3.1**) copolymer series unable to reach a final χ_c comparable to PEN after thermal treatment, albeit still at a respectable level.

It is, however, likely that using the density values for amorphous and 100% crystalline PEN[11] to calculate χ_cs for the PEN*co*(**3.1**) copolymer series has led to inaccurate values from density analysis. This is on the basis that **3.1** residues are most likely denser than PEN, which gives artificially high χ_c values for PEN*co*(**3.1**)-10 and 18 in Figure 3.31 (from Equation 2.8). Furthermore, $\Delta H°_f$ values for 100% crystalline PEN*co*(**3.1**) copolymers are unknown, thus the $\Delta H°_f$ value of PEN (which is itself disputed[59]) has been used for all χ_c calculations utilising enthalpies obtained by DSC. Since the measurement of crystallinity in semi-crystalline copolymers is heavily debated,[60–66] it is difficult to state the quantitative amount of crystallinity in this novel PEN-based copoly(ester-imide) series. However, the qualitative presence and substantial retention of semi-crystalline character following the copolymerisation of PEN with **3.1** is clear.

Initial film property analysis revealed that PEN*co*(**3.1**)-18 biaxially oriented film has comparable barrier properties to PEN, in terms of water vapour and oxygen transmission

rates (WVTR and OTR, respectively, Table 3.7). The permeation of gases through semi-crystalline polymers is inversely dependent on the degrees of orientation and crystallinity,[67,68] with transmission solely occurring through the amorphous regions. The results suggest that PEN*co*(**3.1**)-18 has slightly lower levels of crystallinity in comparison to PEN, as discussed above.

Table 3.7 Comparative barrier-property analysis of biaxially oriented and heat-set biaxially oriented PEN and PEN*co*(**3.1**)-18 film.

Polymer	WVTR		OTR	
	g m^{-2} day^{-1}		cc m^{-2} day^{-1}	
	Biaxial	Heat-set biaxial	Biaxial	Heat-set biaxial
PEN	11.13	7.53	38.87	27.69
PEN*co*(**3.1**)-18	15.59	12.95	38.58	33.34

The optical properties of PEN*co*(**3.1**) copolymer heat-set biaxially oriented film are also extremely promising. Despite the slight colouration observed upon incorporation of imide residues relative to PEN itself (Figure 3.29), as reflected in the slightly higher yellowness index (Table 3.8), the crucial optical parameters of haze and total light transmission (TLT) are superior for PEN*co*(**3.1**)-18. For current usage in flexible electronic applications as a bottom-emissive display, DTF Teonex® film meets the stringent requirements of possessing a haze value < 0.7% and TLT value > 85% over 400-800 nm.[69,70] It is evident that heat-set biaxially oriented PEN*co*(**3.1**)-18 film has the required transparency (88.1%) for such applications and a haze value (2.2%), that is low enough to be improved with iterative film production.

Table 3.8 Comparative optical analysis of PEN and PEN*co*(**3.1**)-18 heat-set biaxially oriented film.

Property	Unit	PEN	PEN*co*(3.1)-18
Brightness[a]	L*	88.77	89.27
Whiteness Index[a]	W1 E313-73	55.19	50.50
Yellowness Index[a]	Y1 E313-73	6.27	8.11
Haze[b]	%	3.5	2.2
Total Light Transmission[b]	%	86.9	88.1
UV absorption onset[c]	nm	390	400

[a] Determined by colour-view box. [b] Determined by hazemeter. [c] Determined by UV-vis absorption spectroscopy.

3.4 Conclusions

The molecular design and synthesis of an isomorphic biphenyldiimide comonomer, **3.1**, for PEN has enabled the industrial-scale production of a novel PEN-based copoly(ester-imide)

series with enhanced thermal properties in comparison to PEN. Moreover, retention of semi-crystalline character is observed across the copolymer series despite increasing imide content, attributed to cocrystallisation of the two different monomer residues. A range of semi-crystalline polyester-based materials encompassing a T_g range of 66 °C above that of PEN may therefore be manufactured. Structural analysis of the copolymer series, when **3.1** > 5 mol%, has led to the discovery of a novel copolymer crystal structure that differs from the known α- and β-polymorphs of PEN.

Aided by isothermal crystallisation, rheology and temperature dependent drawing studies, several variants of PEN-based copoly(ester-imide) heat-set biaxially oriented film were produced. Such films display analogous drawing behaviour, semi-crystalline behaviour and optical properties to that of PEN, whilst demonstrating a 22 °C rise in T_g for the case of the optimised 18 mol% copolymer.

3.5 Experimental

3.5.1 Materials

3,4,3',4'-Biphenyltetracarboxylic dianhydride was purchased from Tokyo Chemical Industries, U.K. Antimony trioxide was purchased from SICA, France. Dimethyl terephthalate, 2,6-dimethyl naphthalate, ethylene glycol and manganese acetate tetrahydrate were obtained from DuPont Teijin Films, U.K. Deuterated chloroform, dimethylsulfoxide, deuterated dimethylsulfoxide, 2,6-naphthalene dicarboxylic acid, thionyl chloride, 1-chloronaphthalene, methanol, toluene, *m*-cresol, ethylenediamine, ethanolamine and *N*,*N*'-dimethylacetamide were purchased from Sigma Aldrich, U.K. Chloroform was purchased from Fisher Scientific, U.K. Trifluoroacetic acid and 1,1,1,3,3,3-hexafluoro-2-propanol were purchased from Fluorochem, U.K. All materials were used as purchased.

3.5.2 Monomer synthetic procedures

3.5.2.1 *N*,*N*'-bis(2-hydroxyethyl)-biphenyl-3,4,3',4'-tetracarboxylic diimide (3.1)

Ethanolamine (4.24 g, 69.68 mmol) was added to a solution of 3,4,3',4'-biphenyltetracarboxylic dianhydride (10.00 g, 33.99 mmol) in DMAc (25 mL) and toluene (15 mL). The solution was heated under reflux for 16 h with Dean-Stark removal of water before being cooled to room temperature, precipitated into distilled water, filtered, washed with methanol and dried under vacuum at 100 ºC for 24 h to afford product **3.1** as an off-white powder (12.40 g, 96%). This synthesis was then reproduced multiple times on a 5 kg scale by High Force Research Ltd., U.K.

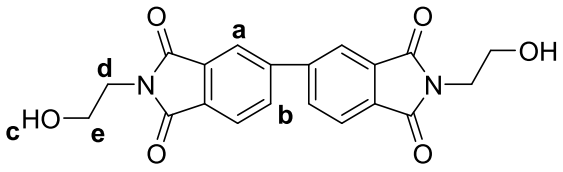

3.1

M.P. (DSC) 285 °C. Found: C, 62.9; H, 4.2; N, 7.4. Calc. for $C_{20}H_{16}N_2O_6$: C, 63.2; H, 4.2; N, 7.4. MS m/z = 381.1081 $[M+H]^+$, calculated 381.1095. ^{1}H NMR (400 MHz, d_6-DMSO) δ_H (ppm) 8.20 (4H, m, H_a), 7.92 (2H, d, J = 8.0 Hz, H_b), 4.87 (2H, t, J = 6.0 Hz, H_c), 3.65 (4H, m, H_d), 3.59 (4H, m, H_e). ^{13}C NMR (100 MHz, d_6-DMSO) δ_C (ppm) 167.5, 144.0, 133.2, 132.7, 131.4, 123.5, 121.7, 57.9, 40.4. IR (ν_{max} cm^{-1}) 3344 (νO-H), 2948 (νC-H) 1683 (νC=O), 1381 (νC-O).

3.5.3 Polymer synthetic procedures

Polymers were synthesised via the laboratory melt-polycondensation or industrial-scale melt-polymerisation procedure as described in Chapter 2, unless otherwise stated.

3.5.3.1 PET

Reagents			
(g)			
DMT	**EG**	**$Mn(OAc)_2.4H_2O$**	**Sb_2O_3**
8500	5550	3.50	2.80

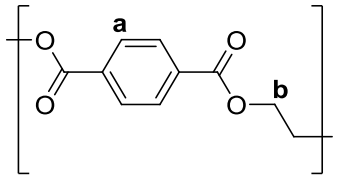

^{1}H NMR [400 MHz, $CDCl_3$:TFA (2:1)] δ_H (ppm) 8.20 (4H, s, H_a), 4.87 (4H, s, H_b). ^{13}C NMR [100 MHz, $CDCl_3$:TFA (2:1)] δ_C (ppm) 168.0, 133.3, 130.0, 66.8, 64.0. T_g = 75 °C, T_c = 198 °C, T_m = 249 °C, T_d = 420 °C. η_{inh} ($CHCl_3$:TFA) (2:1) = 0.75 dL g^{-1}. IR (ν_{max} cm^{-1}) 2996 (νC-H) 1716 (νC=O), 1246 (νC-O).

3.5.3.2 PET*co*(3.1)-25

Reagents					Comonomer feed ratio		Copolymer composition ratio	
(g)					(mol%)		(mol%)	
DMT	3.1	EG	$Mn(OAc)_2.4H_2O$	Sb_2O_3	DMT	3.1	PET	3.1
4481	2268	3774	2.81	2.10	75	25	75	25

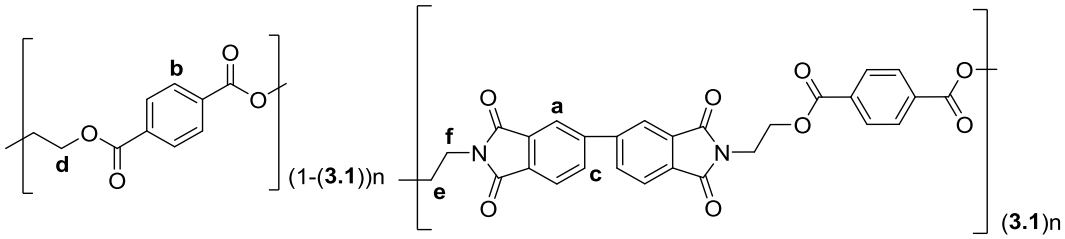

^{1}H NMR [400 MHz, $CDCl_3$:TFA (2:1)] δ_H (ppm) 8.24 (2H, s, H_a), 8.18 (10H, m, H_b), 8.09 (2H, m, H_c), 4.84 (4H, s, H_d), 4.72 (4H, s, H_e), 4.30 (4H, s, H_f). ^{13}C NMR [100 MHz, $CDCl_3$:TFA (2:1)] δ_C (ppm) 145.9, 134.1, 133.3, 132.2, 130.9, 130.0, 125.1, 123.1, 63.9, 37.3. T_g = 121 °C, T_d = 413 °C. η_{inh} ($CHCl_3$:TFA) (2:1) = 0.60 dL g^{-1}. IR (ν_{max} cm^{-1}) 2964 (νC-H) 1707 (νC=O), 1242 (νC-O).

3.5.3.3 PEN

Reagents			
(g)			
2,6-DMN	EG	$Mn(OAc)_2.4H_2O$	Sb_2O_3
7000	4620	2.81	2.10

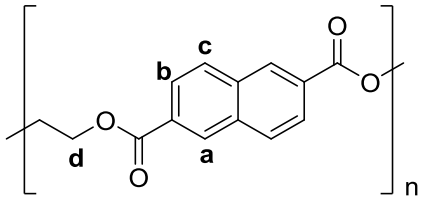

^{1}H NMR [400 MHz, $CDCl_3$/TFA (2:1)] δ_H (ppm) 8.73 (2H, s, H_a), 8.15 (2H, d, J = 8.0 Hz, H_b), 8.09 (2H, d, J = 8.6 Hz, H_c), 4.94 (4H, s, H_d). ^{13}C NMR [100 MHz, $CDCl_3$:TFA (2:1)] δ_C (ppm) 135.0, 131.6, 130.2, 128.4, 125.8, 64.0. T_g = 122 °C, T_c = 209 °C, T_m = 265 °C, T_d = 431 °C. η_{inh} ($CHCl_3$:TFA) (2:1) = 0.98 dL g^{-1}. IR (ν_{max} cm^{-1}) 2994 (νC-H) 1717 (νC=O), 1256 (νC-O).

3.5.3.4 PEN*co*(3.1) copolymer series

Reagents					Comonomer feed ratio		Copolymer composition ratio	
(g)					(mol%)		(mol%)	
2,6-DMN	3.1	EG	$Mn(OAc)_2.4H_2O$	Sb_2O_3	2,6-DMN	3.1	PEN	3.1
7000	560	4620	2.81	2.10	95	5	94	6
7000	1233	4620	2.81	2.80	90	10	90	10
5734	1740	3744	2.97	2.10	82	18	82	18
7000	2744	4620	2.81	2.80	75	25	74	26

Reagents			Comonomer feed ratio		Copolymer composition ratio	
(g)			(mol%)		(mol%)	
BHEN	3.1	Sb_2O_3	BHEN	3.1	PEN	3.1
30.00	37.37	0.10	50	50	55	45

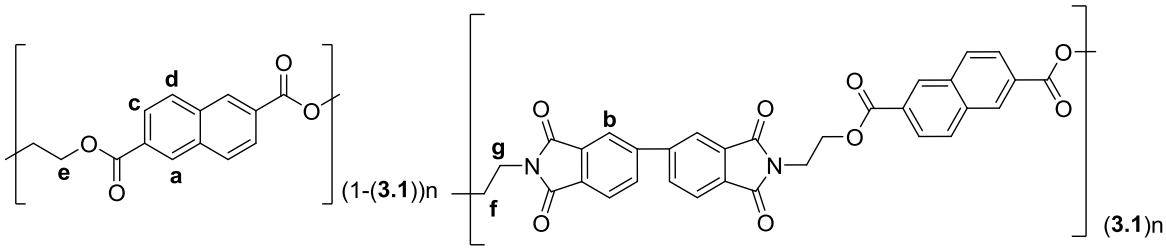

PEN*co*(3.1)-2

Synthesis and characterisation of this copolymer composition were as previously reported.[8]

PEN*co*(3.1)-5

^{1}H NMR [400 MHz, $CDCl_3$/TFA (2:1)] δ_H (ppm) 8.77 (4H, m, H_a), 8.27 (2H, m, H_b), 8.20 (2H, m, H_c), 8.12 (10H, m, H_d), 4.99 (4H, m, H_e), 4.81 (4H, s, H_f), 4.39 (4H, s, H_g). ^{13}C NMR [100 MHz, $CDCl_3$:TFA (2:1)] δ_C (ppm) 135.0, 131.6, 130.3, 128.4, 125.8, 64.0. T_g = 131 °C, T_c = 191 °C, T_m = 256 °C, T_d = 431 °C. η_{inh} ($CHCl_3$:TFA) (2:1) = 0.91 dL g^{-1}. IR (ν_{max} cm^{-1}) 2972 (νC-H) 1738 (νC=O), 1366 (νC-N), 1217 (νC-O).

PEN*co*(3.1)-10

^{1}H NMR [400 MHz, $CDCl_3$/TFA (2:1)] δ_H (ppm) 8.73 (4H, m, H_a), 8.25 (2H, m, H_b), 8.16 (2H, m, H_c), 8.09 (10H, m, H_d), 4.94 (4H, m, H_e), 4.77 (4H, s, H_f), 4.34 (4H, s, H_g). ^{13}C NMR [100 MHz, $CDCl_3$:TFA (2:1)] δ_C (ppm) 145.1, 135.0, 134.1, 131.6, 131.0, 130.3, 128.4, 127.3, 125.8, 125.1, 123.1, 64.0. T_g = 137 °C, T_c = 196 °C, T_m = 262 °C, T_d = 430 °C. η_{inh} ($CHCl_3$:TFA) (2:1) = 0.80 dL g^{-1}. IR (ν_{max} cm^{-1}) 2971 (νC-H) 1742 (νC=O), 1367 (νC-N), 1218 (νC-O).

PEN*co*(3.1)-18

^{1}H NMR [400 MHz, $CDCl_3$/TFA (2:1)] δ_H (ppm) 8.73 (4H, m, H_a), 8.24 (2H, m, H_b), 8.16 (2H, m, H_c), 8.08 (10H, m, H_d), 4.95 (4H, m, H_e), 4.77 (4H, s, H_f), 4.34 (4H, s, H_g). ^{13}C NMR [100 MHz, $CDCl_3$:TFA (2:1)] δ_C (ppm) 145.9, 135.0, 134.1, 132.3, 131.6, 131.0, 130.3, 128.4, 125.8, 125.1, 123.1. T_g = 144 °C, T_c = 205 °C, T_m = 275 °C, T_d = 432 °C. η_{inh} ($CHCl_3$:TFA) (2:1) = 0.77 dL g^{-1}. IR (ν_{max} cm^{-1}) 2991 (*ν*C-H) 1710 (*ν*C=O), 1379 (*ν*C-N), 1248 (*ν*C-O).

PEN*co*(3.1)-25

^{1}H NMR [400 MHz, $CDCl_3$/TFA (2:1)] δ_H (ppm) 8.73 (4H, m, H_a), 8.25 (2H, m, H_b), 8.16 (2H, m, H_c), 8.08 (10H, m, H_d), 4.95 (4H, m, H_e), 4.77 (4H, s, H_f), 4.35 (4H, s, H_g). ^{13}C NMR [100 MHz, $CDCl_3$:TFA (2:1)] δ_C (ppm) 145.9, 135.0, 134.1, 132.3, 131.6, 131.0, 130.3, 128.4, 128.2, 125.8, 125.1, 123.1, 64.0, 63.7, 37.4. T_g = 148 °C, T_c = 236 °C, T_m = 289 °C, T_d = 431 °C. η_{inh} ($CHCl_3$:TFA) (2:1) = 0.84 dL g^{-1}. IR (ν_{max} cm^{-1}) 2957 (*ν*C-H) 1703 (*ν*C=O), 1380 (*ν*C-N), 1250 (*ν*C-O).

3.5.3.5 PEN*co*(3.1)-45

^{1}H NMR [400 MHz, $CDCl_3$/TFA (2:1)] δ_H (ppm) 8.69 (4H, d, J = 32.0 Hz, H_a), 8.24 (2H, s, H_b), 8.15 (2H, m, H_c), 8.08 (10H, m, H_d), 4.94 (4H, s, H_e), 4.77 (4H, s, H_f), 4.34 (4H, s, H_g). ^{13}C NMR [100 MHz, $CDCl_3$:TFA (2:1)] δ_C (ppm) 170.0, 169.2, 146.1, 135.2, 134.3, 132.5, 131.8, 131.2, 130.5, 128.6, 128.4, 126.0, 125.3, 123.3, 64.2, 63.9, 63.4, 37.6. T_g = 162 °C, T_{cc} = 199 °C, T_m = 345 °C, T_d = 415 °C. η_{inh} ($CHCl_3$:TFA) (2:1) = 0.15 dL g^{-1}. IR (ν_{max} cm^{-1}) 3538 (*ν*O-H), 2957 (*ν*C-H) 1710 (*ν*C=O), 1388 (*ν*C-N), 1255 (*ν*C-O).

3.5.3.6 PEN*co*(3.1)-50[71]

A solution of 2,6-naphthalene dicarboxylic acid (2.00 g, 9.25 mmol) and thionyl chloride (81.90 g, 668.4 mmol) was heated under reflux for 4 h. The excess thionyl chloride was then removed via distillation under reduced pressure and the reaction flask was purged with nitrogen for 16 h. A solution of **3.1** (3.52 g, 9.25 mmol) and 1-chloronaphthalene (50 mL) was then added and the reaction solution was heated to 170 °C and held at this temperature for 1 h. The temperature was then increased to 210 °C over a 3 h period and held for 24 h at this temperature. The reaction mixture was then cooled to room temperature, diluted with methanol, and the product filtered off and dried under vacuum at 110 ºC for 24 h to afford the alternating polymer **PEN*co*(3.1)-50** (4.56 g).

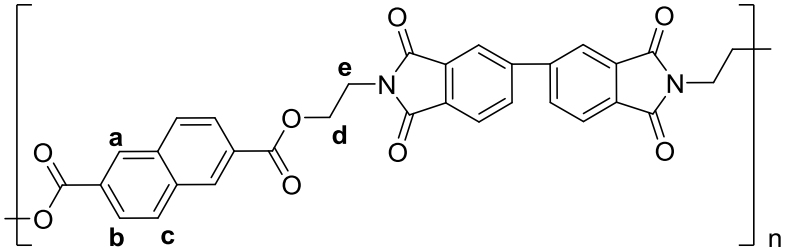

^{1}H NMR [400 MHz, $CDCl_3$:TFA (2:1)] δ_H (ppm) 8.65 (2H, s, H_a), 8.24 (2H, s, H_b), 8.07 (8H, d, H_c), 4.77 (4H, m, H_d), 4.34 (4H, m, H_e). ^{13}C NMR [100 MHz, $CDCl_3$:TFA (2:1)] δ_C (ppm) 169.6, 169.0, 145.9, 135.0, 134.1, 132.2, 131.6, 130.9, 130.2, 128.2, 125.6, 125.1, 123.1, 63.7, 37.4. T_g = 178 °C, T_{cc} = 227 °C, T_c = 309 °C, T_m = 401 °C. T_d = 424 °C. η_{inh} ($CHCl_3$:TFA) (2:1) = 0.19 dL g^{-1}. IR (ν_{max} cm^{-1}) 2970 (νC-H) 1739 (νC=O), 1365 (νC-N), 1217 (νC-O).

3.5.3.7 3.1 Homopolymer[35]

Ethylenediamine (1.01 g, 16.80 mmol) was dissolved in *m*-cresol (150 mL), to which 3,4,3',4'-biphenyltetracarboxylic dianhydride (5.00 g, 17.00 mmol) was added. The reaction solution was then heated to 180 °C over a 3 h period before being cooled to room temperature, added with stirring to ethanol (1 L), filtered and dried under vacuum at 140 °C for 24 h.

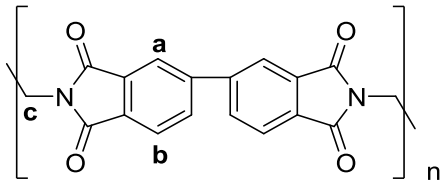

^{1}H NMR [400 MHz, $CDCl_3$:TFA (2:1)] δ_H (ppm) 8.18 (2H, m H_a), 8.06 (4H, m, H_b), 4.19 (4H, s, H_c). ^{13}C NMR [100 MHz, $CDCl_3$:TFA (2:1)] δ_C (ppm) 170.0, 169.7, 145.9, 134.1, 130.7, 130.0, 125.0, 123.0. T_m = 562 °C, T_d = 533 °C. η_{inh} ($CHCl_3$:TFA) (2:1) = 0.36 dL g^{-1}. IR (ν_{max} cm^{-1}) 1697 (νC=O), 1384 (νC-N), 1065 (νC-O).

3.6 References

1 D. D. Callandar in *Modern Polyesters: Chemistry and Technology of Polyesters and Copolyesters*, ed. J. Scheirs and T. E. Long, Wiley, Chichester, 2003, 323–333.

2 T. Tanabe, H. Aoki, H. Murakami, F. Matsumoto, *US* Pat., 3,683,060, *Method of preparing biaxially oriented polyethylene 2,6-naphthalate film*, 1972.

3 K. Song and J. L. White, *Polym. Eng. Sci.*, 2000, **40**, 1122–1131.

4 A. E. Tonelli, *Polymer*, 2002, **43**, 637–642.

5 W. A. Macdonald in *Encyclopedia of Polymer Science and Technology*, Wiley, New York, 2002, **11**, 30–41.

6 Y. Meng, A. R. Hlil and A. S. Hay, *Polymer*, 1998, **37**, 1781–1788.
7 M. B. Cinderley and J. B. Rose, *US* Pat., 4,176,222, *Production of aromatic* polyethers, 1979.
8 S. J. Meehan, *PhD Thesis*, *Enhancement of Polyester Properties Through Molecular Design*, University of Reading, 2012.
9 Y. G. Jeong, W. H. Jo and S. G. Lee, *Macromolecules*, 2000, **33**, 9705–9711.
10 Y. Kong and J. Hay, *Polymer*, 2003, **44**, 623–633.
11 S. Z. D. Cheng, M. Y. Cao and B. Wunderlich, *Macromolecules*, 1986, **19**, 1868–1876.
12 B. Wunderlich, *Macromolecular Physics*, Academic Press, 1976.
13 S. Y. Hobbs and C. F. Pratt, *Polymer*, 1975, **16**, 462–464.
14 F. J. M. Rodriguez, P. J. Phillips, J. S. Lin and R. Campos, *J. Polym. Sci. Part B Polym. Phys.*, 1997, **35**, 1757–1774.
15 J. D. Hoffman and J. J. Weeks, *J. Res. Natl. Bur. Stand. Sect. A Phys. Chem.*, 1962, **66**, 13.
16 P. Srimoaon, N. Dangseeyun and P. Supaphol, *Eur. Polym. J.*, 2004, **40**, 599-608.
17 J. A. Kreuz, B. S. Hsiao, C. A. Renner and D. L. Goff, *Macromolecules*, 1996, **28**, 6926–6930.
18 Y. U. Shi and S. A. Jabarin, *J. Appl. Polym. Sci.*, 2001, **81**, 11–22.
19 S. B. Lin and J. L. Koenig, *J. Polym. Sci. Polym. Symp.*, 1984, **71**, 121–135.
20 J. P. Flory, *J. Chem. Phys.*, 1947, **15**, 684.
21 G. Goldbeck-Wood, *Polymer*, 1992, **33**, 778–782.
22 P. S. Gill, S. R. Sauerbrunn and M. Reading, *J. Therm. Anal.*, 1993, **40**, 931–939.
23 B. Cassel, *Modulated Temperature DSC and the DSC 8500: A Step Up in Performance*, 2010.
24 J. Holubová, E. Černošková and Z. Černošek, *J. Therm. Anal. Calorim.*, 2012, **111**, 1633–1638.
25 M. Avrami, *J. Chem. Phys.*, 1939, **7**, 1103.
26 M. Avrami, *J. Chem. Phys.*, 1940, **8**, 212.
27 M. Avrami, *J. Chem. Phys.*, 1941, **9**, 177.
28 X. Lu and J. Hay, *Polymer*, 2001, **42**, 9423–9431.
29 M. Muthukumar, *Nucleation in Polymer Crystallization*, S. A. Rice, Wiley, 2004, 1-63.
30 T. W. Chan and A. Isayev, *Polym. Eng. Sci.*, 1994, **34**, 461–471.
31 J. Bicerano, *J. Macromol. Sci. Rev. Macromol. Chem. Phys*, 1998, **38**, 391.
32 J. Xiao, H. Zhang, X. Wan, D. Zhang, Q. F. Zhou, E. M. Woo and S. R. Turner, *Polymer*, 2002, **43**, 3683–3690.
33 W. Volksen, H. J. Cha, M. I. Sanchez and D. Y. Yoon, *React. Funct. Polym.*, 1996, **30**, 61–69.
34 A. E. Eichstadt, T. C. Ward, M. D. Bagwell, I. V. Farr, D. L. Dunson and J. E. McGrath, *Macromolecules*, 2002, **35**, 7561–7568.
35 C. Koning, A. Delmotte, P. Larno and B. van Mele, *Polymer*, 1998, **39**, 3697–3702.
36 R. M. Silverstein, G. C. Bassler and T. C. Morrill, *Spectrometric Identification of Organic Compounds*, John Wiley & Sons, New York, 2006.
37 Z. Mencik, *Chem. Prum.*, 1976, **17**, 78-83.
38 S. Buchner and H. G. Zachmann, *Polymer*, 1989, **30**, 480–488.
39 W. D. Lee, E. S. Yoo and S. S. Im, *Polymer*, 2003, **44**, 6617–6625.
40 C. J. M. van den Heuvel and E. A. Klop, *Polymer*, 2000, **41**, 4249–4266.
41 J. Liu, G. Sidoti, J. A. Hommema, P. H. Geil, J. C. Kim and M. Cakmak, *J. Macromol. Sci. B*, 1998, **37**, 567.
42 P. D. Coulter, S. Hanna and A. H. Windle, *Liq. Cryst.*, 1989, **5**, 1603–1618.

43 H. M. Colquhoun and D. J. Williams, *Acc. Chem. Res*, 2000, **33**, 189-198.
44 D. H. Barich, R. J. Pugmire, D. M. Grant and R. J. Iuliucci, *J. Phys. Chem. A*, 2001, **105**, 6780–6784.
45 C. P. Brock and R. P. Minton, *J. Am. Chem. Soc.*, 1989, **111**, 4586–4593.
46 H. M. Colquhoun, C. A. O'Mahoney and D. J. Williams, *Polymer*, 1993, **34**, 218-221.
47 Y. Tong, W. Huang, J. Luo and M. Ding, *J. Polym. Sci. Part A Polym. Chem.*, 1999, **37**, 1425–1433.
48 G. A. Gutierrez, J. Blackwell and R. A. Chivers, *Polymer*, 1985, **26**, 348–354.
49 Y. Sun and C. S. Wang, *J. Polym. Sci. Part A Polym. Chem.*, 1996, **34**, 1783–1792.
50 M. K. Looney, *Internal Communication*, 2014.
51 J. Aho, *PhD Thesis, Rheological Characterization of Polymer Melts in Shear and Extension: Measurement Reliability and Data for Practical Processing*, Tampere University of Technology, 2011.
52 J. Vlachopoulos and D. Strutt, *New Technologies for Extrusion Conference*, Milan, Italy, 2003, 1–26.
53 L. Incarnato, P. Scarfato, L. di Maio and D. Acierno, *Polymer*, 2000, **41**, 6825–6831.
54 B. Yang, *Stress, Strain and Structural Dynamics*, Academic Press, New York, 2005.
55 P. W. Bridgman, *Large Plastic Flow and Fracture*, Harvard University Press, 1952.
56 G. Schoukens, *Polymer*, 1999, **40**, 5637–5645.
57 S. Murakami, Y. Nishikawa, M. Tsuji, A. Kawaguchi, S. Kohjiya and M. Cakmak, *Polymer*, 1995, **36**, 291–297.
58 M. Cakmak and S. W. Lee, *Polymer*, 1995, **36**, 4039–4054.
59 W. G. Kampert and B. B. Sauer, *Polymer*, 2001, **42**, 8703–8714.
60 G. Farrow and I. Ward, *Polymer*, 1960, **1**, 330–339.
61 G. Farrow and D. Preston, *Br. J. Appl. Phys.*, 2002, **11**, 448–448.
62 W. Statton, *J. Appl. Polym. Sci.*, 1963, **7**, 803–815.
63 W. L. Lindner, *Polymer*, 1973, **14**, 9–15.
64 Z. Bashir, I. Al-Aloush, I. Al-Raqibah and M. Ibrahim, *Polym. Eng. Sci.*, 2000, **40**, 2442–2455.
65 Y. Kong and J. N. Hay, *Polymer*, 2002, **43**, 3873–3878.
66 Y. Kong and J. N. Hay, *Eur. Polym. J.*, 2003, **39**, 1721–1727.
67 A. Polyakova, R. Y. F. Liu, D. A. Schiraldi, A. Hiltner and E. Baer, *J. Polym. Sci. Part B Polym. Phys.*, 2001, **39**, 1889–1899.
68 N. Qureshi, E. V. Stepanov, D. Schiraldi, A. Hiltner and E. Baer, *J. Polym. Sci. Part B Polym. Phys.*, 2000, **38**, 1679–1686.
69 W. A MacDonald, M. K. Looney, D. MacKerron, R. Eveson, R. Adam, K. Hashimoto and K. Rakos, *J. Soc. Inf. Disp.*, 2007, **15**, 1075–1083.
70 W. S. Wong and A. Salleo, *Flexible Electronics: Materials and Applications*, Springer, Berlin, 2009.
71 S. W. Kantor, R. W. Lenz and W. J. Ward, *US Pat.*, 5,032,669, *Liquid crystalline polyesters formed by reaction of bis(hydroxyalkoxy) biphenyls with terephthaloyl chloride*, 1991.

Chapter 4

Mesomorphic behaviour in copoly(ester-imide)s of poly(butylene-2,6-naphthalate) (PBN)

The research described in this chapter has, in part, been published by the author as an article entitled "Mesomorphic behaviour in copoly(ester-imide)s of poly(butylene-2,6-naphthalate) (PBN)", **S. M. Jones**, S. J. Meehan, S. W. Sankey, W. A. MacDonald and H. M. Colquhoun, *Polymer*, 2015, **69**, 66-72.

4.1 Abstract

Copolycondensation of *N*,*N*'-bis(4-hydroxybutyl)-biphenyl-3,4,3',4'-tetracarboxylic diimide at 20 and 25 mol% with bis(4-hydroxybutyl)-2,6-naphthalate produces PBN-based copoly(ester-imide)s that not only crystallise but also form a (smectic) mesophase upon cooling from the melt. Incorporation of 25 mol% imide in PBN causes the glass transition temperature (measured by DSC) to rise from 51 to 74 °C, a significant increase relative to PBN. Furthermore, increased storage (G'), loss (G") and elastic (E) moduli are observed for both copoly(ester-imide)s when compared to PBN itself. Structural analysis of the 20 mol% copolymer by X-ray powder and fibre diffraction, interfaced to computational modelling, suggests a triclinic crystal structure related to that of α-PBN, in space group $P\bar{1}$ with cell dimensions a = 4.74, b = 6.38, c = 14.45 Å, α = 106.1, β = 122.1, γ = 97.3°, ρ = 1.37 g cm^{-3}.

4.2 Introduction

Semi-crystalline, semi-aromatic polyesters such as PET, PEN and PBT have found widespread use as engineering polymers in film and fibre form, and (for PBT) in moulding applications, due to their high mechanical strength, chemical resistance and dimensional stability.[1] Most recently, PBN has been introduced as a fast-crystallising polyester with enhanced thermomechanical characteristics relative to PBT.[2] However, the thermal performance of semi-aromatic polyesters remains relatively low in comparison to high-temperature engineering thermoplastics such as PEEK, with the T_gs of semi-aromatic, semi-crystalline polyesters being generally considered the limiting factor in terms of future product innovation in this field.[3–5]

As discussed in Chapter 1, an apparently straightforward approach to enhancing the thermomechanical properties of a polymer involves copolymerisation with a more rigid comonomer, in order to increase the T_g. This technique has been employed previously in

semi-aromatic polyester chemistry, most commonly utilising rigid biphenylene[6,7] and diimide moieties.[8,9] Modest increases in T_g were indeed obtained, but almost invariably with little or no retention of crystallinity in the resulting copolymers. Such copolymers would be inadequate for film applications requiring the mechanical strength achieved from biaxial orientation.

It would therefore be preferable to use a rigid comonomer that is also isomorphic with the homopolymer repeat unit, enabling the copolymer to crystallise from the melt at any comonomer composition ratio. In the context of PBN-based copolymers, it has been observed that the copolymers of PBN with PEN[10] and PBN with PBT[11] cocrystallise across a wide composition range. In contrast to PET,[12] PBT,[13] and PEN,[14] there have been relatively few investigations of the melt-crystallisation processes and resulting morphologies of PBN. However, it has been reported that PBN is capable of adopting two different crystal structures upon cooling from the melt, referred to as the α-form and the β-form.[15] The α-form is obtained at moderate cooling rates (20-50 °C min^{-1}) from temperatures lower than 205 °C whereas the β-form is exclusively present after very slow cooling (0.1 °C min^{-1}) from above 280 °C. Both forms may coexist after melt-crystallisation from close to the T_m of PBN (238 °C).

In addition, a mesophase has been reported for PBN upon very rapid quenching from the melt to 0 °C. The liquid crystalline phase has been characterised as smectic A, with a layer periodicity of *ca*. 14 Å, corresponding closely to the length of the molecular repeat unit.[16] This polyester thus displays the characteristics of both a semi-crystalline and a mesomorphic material, depending on the conditions of melt-processing. In this chapter, a novel series of PBN-based cocrystalline copoly(ester-imide)s that display both significantly higher T_gs than PBN itself *and* a more accessible mesophase are reported.

4.3 Results and discussion

4.3.1 Polymer synthesis and characterisation

The synthesis of a novel group of PBN-based copoly(ester-imide)s and evaluation of their potential as new high performance materials is herein reported. This research is an extension of that discussed in Chapter 3, which showed that copolycondensation of *N*,*N*'-bis(2-hydroxyethyl)-biphenyl-3,4,3',4'-tetracarboxylic diimide, **3.1**, with bis(2-hydroxyethyl)-2,6-naphthalate afforded a series of semi-crystalline PEN-based copoly(ester-imide)s.[17] Such copolymers exhibited both enhanced T_gs *and* retention of semi-crystalline behaviour, from

which it was evident that the two different comonomer residues are able to cocrystallise. It was thus envisaged that copolymerisation of bis(4-hydroxybutyl)-2,6-naphthalate (BHBN) with *N*,*N*'-bis(4-hydroxybutyl)-biphenyl-3,4,3',4'-tetracarboxylic diimide, **4.1**, might well produce cocrystalline, PBN-based copoly(ester-imide)s with significantly higher T_gs than the homopolymer.

Considering the overall dimensions of the two comonomers involved, the notion of cocrystallisation appears entirely feasible. Figure 4.1 illustrates the potentially isomorphic nature of BHBN and **4.1** by superposing their molecular structures. Comonomer **4.1** residues could thus potentially be accommodated in the crystal lattice of PBN if **4.1** adopted a coplanar geometry, resulting in minimal disruption to the α-PBN crystal. This coplanarity of the biphenyl unit ensures that the required symmetry operation for space group $P\bar{1}$ (an inversion centre) is maintained, as has often been observed in the crystal structures of biphenyl-containing small molecules.[18,19]

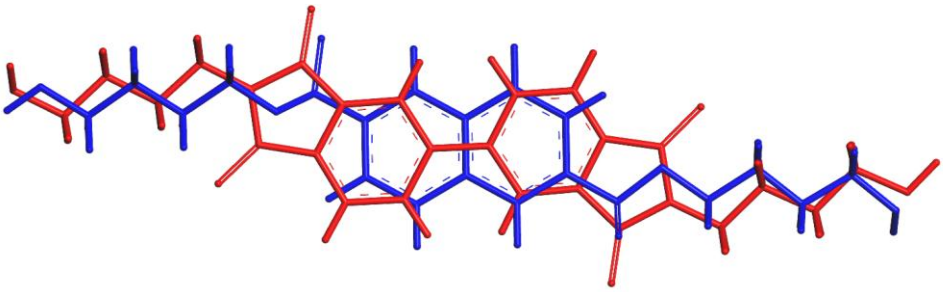

Figure 4.1. Comparison of energy-minimised coplanar models of monomer residues from bis(4-hydroxybutyl)-2,6-naphthalate (blue) and *N*,*N*'-bis(4-hydroxybutyl)-biphenyl-3,4,3',4'-tetracarboxylic diimide (red).

The novel diimide comonomer, **4.1**, was obtained in good yield (89%) from BPDA and 4-aminobutanol. The homopolyester PBN (α-form) and PBN-based copoly(ester-imide)s containing **4.1** at 20 and 25 mol% were synthesised by laboratory-scale melt-copolycondensation of **4.1** with BHBN. (Scheme 4.1).

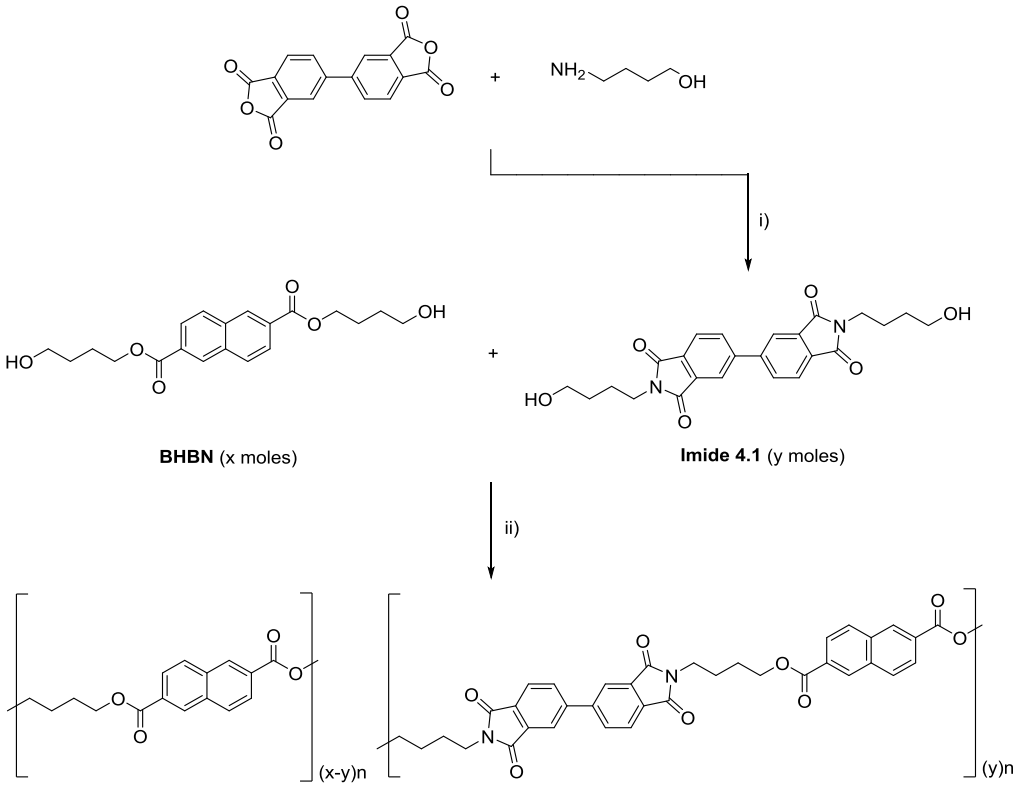

Scheme 4.1. Synthesis of PBN-based copoly(ester-imide)s via melt-copolycondensation of bis(4-hydroxybutyl)-2,6-naphthalate with **4.1**, where y ≤ x. Reaction conditions: i) DMF, reflux, 16h. ii) Sb_2O_3, 280 °C, 0.5 h, < 1mbar.

Successful copolymerisation was verified by ^{1}H NMR spectroscopy, as illustrated by the ^{1}H NMR spectrum of PBN*co*(**4.1**)-25 in Figure 4.2. Here, the aromatic and ethylene resonances associated with **4.1** are clearly distinguishable from those of PBN at the appropriate level of content. It is observed that the copolymer composition ratios of PBN and **4.1** closely match the comonomer feed ratios (19 and 24 mol% actual content of **4.1** in comparison to the feed ratios of 20 and 25 mol%, respectively).

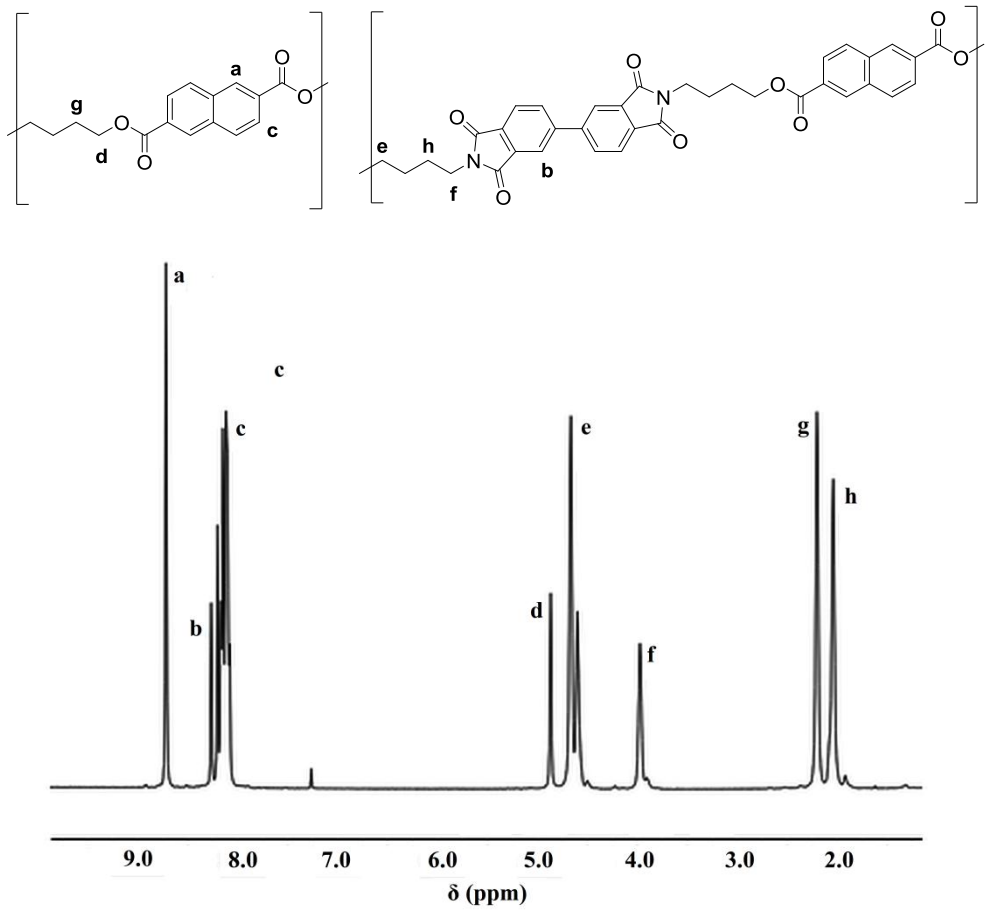

Figure 4.2 ^{1}H NMR spectrum, with assignments, of PBN*co*(**4.1**)-25.

The degrees of polymerisation achieved for PBN and the PBN*co*(**4.1**) copolymers were identified by inherent viscosity and GPC (Table 4.1), giving η_{inh} = 0.54 - 0.69 dL g^{-1} and molecular weights (M_w) in the range 13,000-16,000 Da. The molecular weight distributions of the PBN*co*(**4.1**) copolymers are thus comparable to those of PBN itself, indicating that high molecular weights may be achieved despite the substantial amount of imide present.

Table 4.1 Molecular weight distributions, dispersities and inherent viscosities for PBN, PBN*co*(**4.1**)-20 and 25.

Polymer	M_w [a]	M_n [a]	M_z [a]	**Đ**	η_{inh} [b]
	Da	**Da**	**Da**	**-**	**dL g^{-1}**
PBN	13,400	3,300	28,000	4.0	0.66
PBN*co*(**4.1**)-20	15,000	3,600	35,000	4.2	0.69
PBN*co*(**4.1**)-25	15,500	4,400	38,000	3.6	0.54

[a] Determined by GPC (HFIP eluent). [b] Determined by solution viscometry ($CHCl_3$:TFA (2:1 v/v) eluent).

Rotational rheology analysis of PBN*co*(**4.1**)-20 and 25 revealed similar extrusion behaviour to that found for PBN (Figure 4.3). Upon heating past their respective T_ms (4 °C min^{-1}, constant frequency of 10 rad s^{-1} and amplitude of 5%), all synthesised materials showed values for η* of < 40 Pa s at the extrusion temperature of 290 °C. This suggests facile melt

extrusion (which was observed following copolycondensation), in accordance with G'' > G' signifying liquid viscoelastic behaviour.

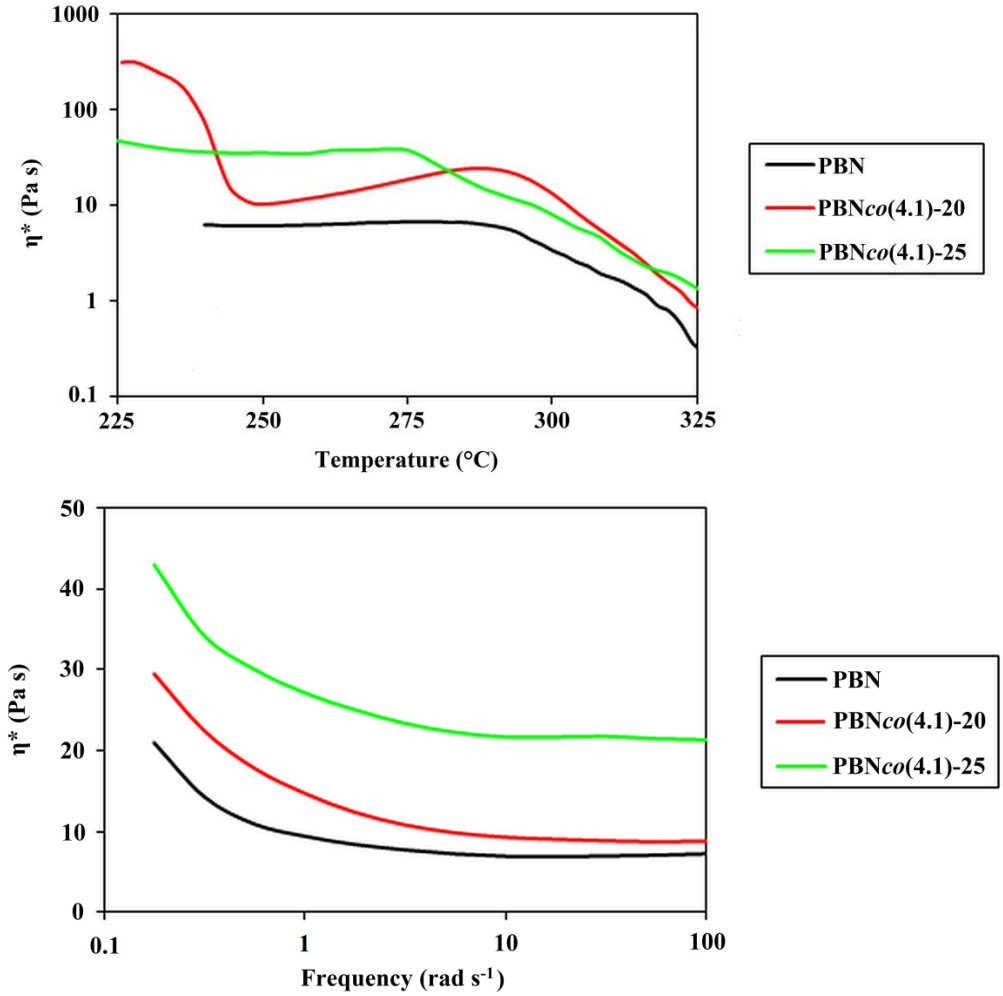

Figure 4.3 Rotational rheology analysis of PBN, PBN*co*(**4.1**)-20 and 25 performed in temperature sweep mode (above, heating rate of 4 °C min^{-1}, frequency of 10 rad s^{-1} and 5% strain) and frequency sweep mode (below, temperature of 300 °C and 25% strain).

At a constant temperature of 300 °C, shear-thinning is observed with respect to increasing frequency. This may be attributed to increased molecular alignments and the disentanglement of polymer chains. The η* of PBN is also noted to rise proportionally in the temperature and frequency sweep modes, following inclusion of **4.1**. Although this has no significant consequence on the melt-processability of the PBN*co*(**4.1**) copolymers, the incorporation of a rigid imide comonomer has clearly increased η* in comparison to PBN itself.

4.3.2 Thermomechanical properties

In the DSC, 1st cooling scans from the melt were recorded at 20 °C min^{-1} for the PBN homopolymer and for the 20 and 25 mol% copolymers, as illustrated in Figure 4.4. At this cooling rate it is observed that PBN itself has a single, well-defined T_c at 209 °C (36.7 J g^{-1}).

However, upon incorporation of **4.1** into PBN at levels of 20 and 25 mol%, two major exothermic transitions (the first sharp and the second rather broader) are now seen upon cooling at 20 °C min^{-1}. It should be noted that these two transitions are observed for both copolymers at all cooling rates between 5 and 50 °C min^{-1}.

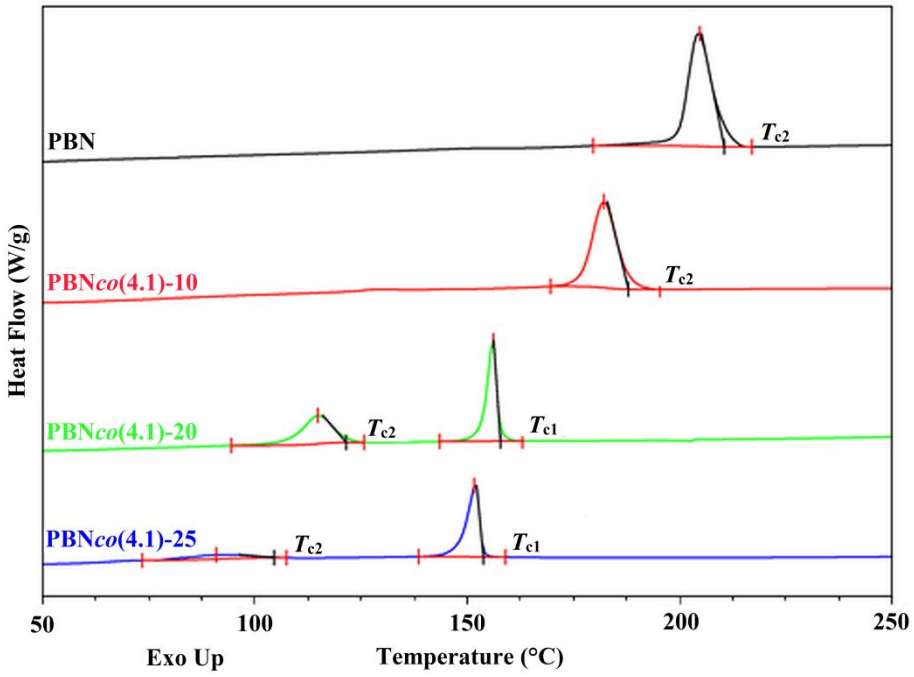

Figure 4.4. DSC 1st cooling scans (20 °C min^{-1}) of PBN, PBN*co*(**4.1**)-10, 20 and 25.

The higher temperature exotherm, T_{c1}, may be attributed to a transition from the isotropic melt to a mesophase (presumably smectic A),[16] occurring at 156 (14.4 J g^{-1}) and 152 °C (12.5 J g^{-1}) for the 20 and 25 mol% copolymers, respectively. The lower temperature exotherm, T_{c2}, is then assigned as a mesophase to crystalline transition, which is progressively depressed upon incorporation of 20 mol% (115 °C, 11.8 J g^{-1}) and 25 mol% (91 °C, 3.1 J g^{-1}) of comonomer **4.1** into PBN. For PBN*co*(**4.1**) copolymers containing < 20 mol% of **4.1**, T_{c1} is < T_{c2}, resulting in no mesophase formation as the copolymer preferentially undergoes melt-crystallisation.

This observation is illustrated by PBN*co*(**4.1**)-10 in Figure 4.4, which possesses a T_{c2} peak (182 °C, 28.2 J g^{-1}) that is greater than the theoretical T_{c1} exotherm. The DSC 1st cooling scans are thus consistent with PBN*co*(**4.1**) being a monotropic liquid crystalline system, in which the metastable mesophase is only observed when direct melt-crystallisation is bypassed by choice of a sufficiently fast cooling rate.[20]

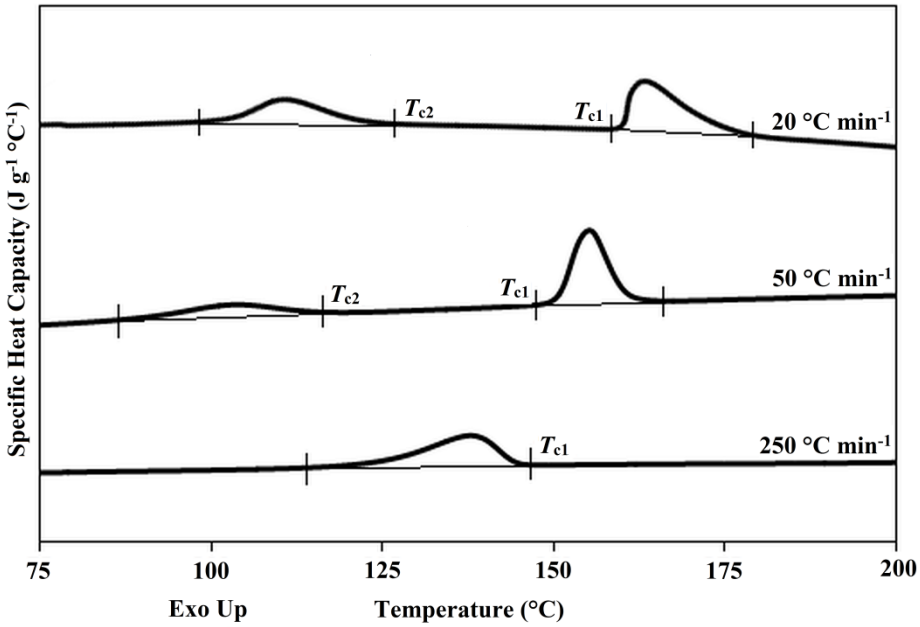

Figure 4.5. HyperDSC 1st cooling scans (20, 50 and 250 °C min^{-1}) of PBN*co*(**4.1**)-20.

For PBN*co*(**4.1**)-20, a cooling rate from the melt of 250 °C min^{-1} depresses T_{c1} to 141 °C (13.2 J g^{-1}) and T_{c2} is no longer observed (Figure 4.5). Thus, the higher cooling rate freezes the copolymer in the mesophase (as a smectic glass) because there is insufficient time for crystallisation to occur below the melt-to-mesophase transition. It is observed that the copolymer mesophase is isolated at *very* much lower rates of cooling than the mesophase of PBN itself (which typically requires cooling rates of > 20,000 °C min^{-1}),[21] indicating that the copolymer mesophase is significantly slower to crystallise. Isolation of the mesophase is also promoted by the depressed crystallisation temperature of PBN*co*(**4.1**)-20 (T_{c2} = 115 °C at a cooling rate of 20 °C min^{-1}) which allows the transition from the melt to the mesophase to occur in preference to melt-crystallisation.

Subjecting the PBNco(**4.1**) copolymers to ballistic cooling (approximate rate of 900 °C min^{-1}) from the melt at 300 °C to 0°C allowed T_gs to be calculated from subsequent heating scans at a reheating rate of 20 °C min^{-1} (Table 4.2 and Figure 4.6). Onset temperatures for T_g were 66 and 74 °C at 20 and 25 mol% incorporation of **4.1**, respectively, the latter affording a 23 °C increase in T_g when compared to PBN itself (51 °C). In addition, the cold crystallisation temperatures, T_{cc}s, for both copolymers are much lower than that of PBN, indicating a more facile crystallisation upon heating, perhaps templated by the mesophase.[22]

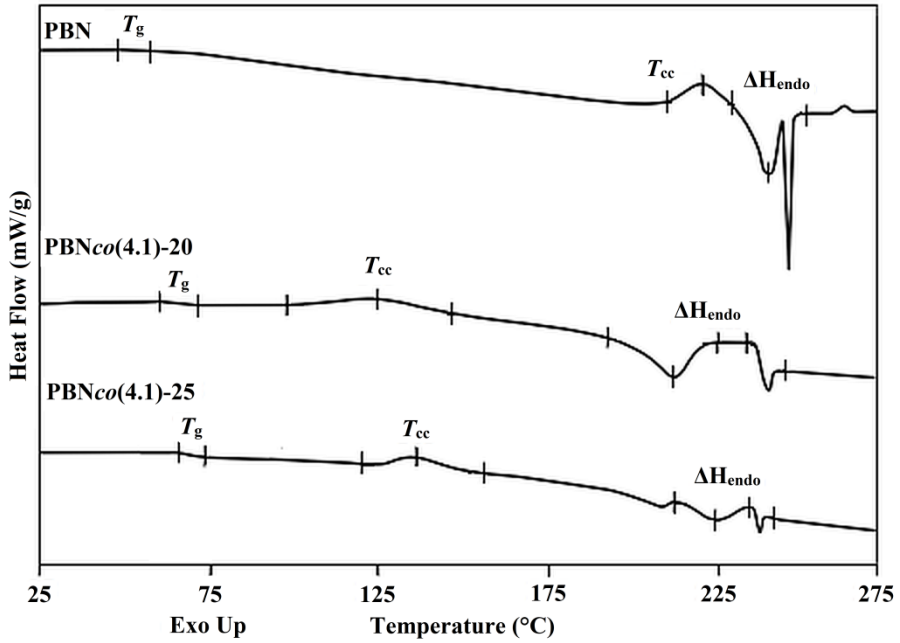

Figure 4.6. HyperDSC 2nd heating scans (20 °C min^{-1}) of PBN, PBN*co*(**4.1**)-20 and 25 following a ballistic cool (~ 900 °C min^{-1}).

Table 4.2. Thermomechanical property comparison of PBN, PBN*co*(**4.1**)-20 and 25

Polymer	T_g [a]	T_{cc} [a]	ΔH_{cc} [a]	T_{endo} [a]	ΔH_{endo} [a]	G' [b]	G'' [c]	E [d]
	°C	°C	J g^{-1}	°C	J g^{-1}	MPa	MPa	MPa
PBN	51	222	-16.09	242, 247	27.61	735	105	919
PBN*co*(4.1)-20	68	126	-12.01	214, 242	23.92	1880	225	988
PBN*co*(4.1)-25	74	138	-12.22	226, 240	12.85	2272	240	1221

[a] Determined by HyperDSC 2nd heating scan (20 °C min^{-1}). [b] At 298K, determined from DMA temperature sweep (4 °C min^{-1}). [c] Determined from DMA, G" peak value. [d] Determined by tensile analysis at 298K.

The measured T_g of PBN in the present work was 10 °C higher than the literature value of 41 °C quoted for amorphous PBN[23], which itself is disputed with claimed T_gs ranging between 41-82 °C.[24–27] It is probable that the higher value seen in the present work (and for T_g values > 41 °C in the literature) may be due to incomplete quenching of molten PBN, as ΔH_{endo}, the sum of both endotherms observed, is greater than ΔH_{cc} indicating the presence of residual crystallinity (and a consequently raised T_g) at the start of the 2nd heating scan.

Dual endotherms are observed on reheating PBN and both PBN*co*(**4.1**) copolymers, indicating the presence of semi-crystalline regions in all quenched polymers. It was originally believed that the lower temperature endotherm corresponded to the crystalline-to-mesophase transition and the higher temperature endotherm to the transition from the mesophase to the isotropic melt, due to the higher temperature peak resembling the mesophase transition observed in Figure 4.4. However, this would imply enantiotropic behaviour considering the proposed mesophase transitions are ~ 90 °C apart for PBN*co*(**4.1**)-20 and 25. It is therefore

more likely that the multiple melting peaks arise from the presence of different crystallite lamellar thicknesses, as discussed in Chapter 3.

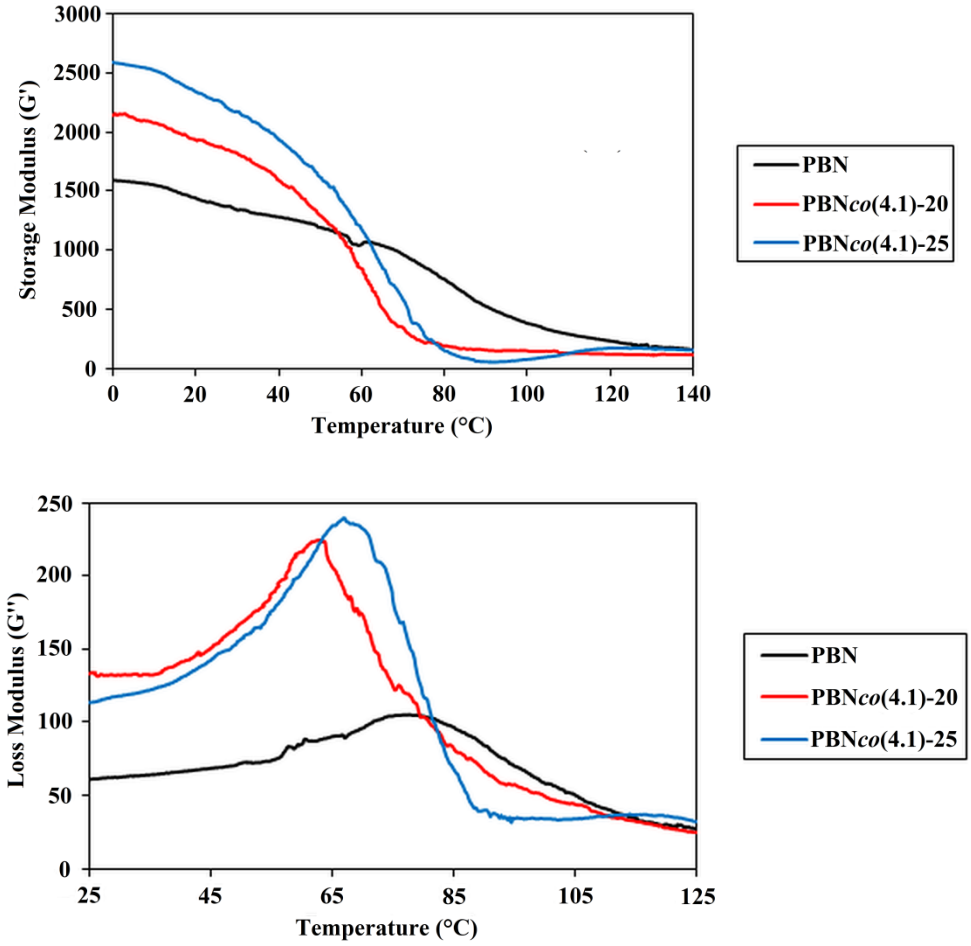

Figure 4.7 DMA heating scans (4 °C min^{-1}) at constant frequency (10 Hz) and strain (0.1%) of PBN, PBN*co*(**4.1**)-20 and 25 fibres illustrating storage (above) and loss modulus (below) against temperature.

As observed in Table 4.2 and Figure 4.7, incorporation of **4.1** has also increased the chain-stiffness relative to PBN, as would be expected from the rigid nature of the biphenyl-based comonomer. DMA performed in a temperature sweep mode (heating rate of 4 °C min^{-1}) and Instron tensile tests of PBN*co*(**4.1**)-20 and 25 revealed large increases in the raised storage (G') and loss (G'') moduli and a modest increase in the elastic moduli (E). This suggests that the selection of **4.1** as a prospective comonomer with PBN has been successful, in terms of both raising the T_g and mechanical properties relative to PBN whilst remaining melt-processable, despite significant amounts of imide incorporated. It is probable that the enhanced moduli primarily originate from inclusion of the more rigid biphenyl comonomer.

There are, however, discrepancies between the T_g onset values of PBN determined by HyperDSC (51 °C, Figure 4.6) and DMA (69 °C, Figure 4.7). Observed differences in T_gs

between DSC and DMA measurements of the same material have been previously reported,[28] with DSC values being highly dependent on the thermal history of the material, and DMA values being greatly affected by the operating frequency. In this case, a higher operating frequency leads to an increased T_g because of delayed temperature-dependent molecular relaxations.[29] It is likely that the higher T_g determined by DMA in this instance may be attributed to the presence of crystallinity that has not been fully erased from the fibre sample, by thermal quenching. This is evident in Figure 4.7, as PBN retains a higher fraction of the storage modulus post-T_g indicating higher crystallinity compared to PBN*co*(**4.1**)-20 and 25.

4.3.3 Mesophase characterisation

Confirmation of a frozen mesophase in the PBN*co*(**4.1**) copolymer series was achieved by X-ray powder diffraction analysis of PBN*co*(**4.1**)-20 after cooling at rates between 20 and 500 °C min^{-1}. The change from a semi-crystalline copolymer to a liquid crystalline material as the cooling rate increases is evident in Figure 4.8. The clear diffraction peaks at 2θ = 15.3 and 23.2°, observed upon cooling at 20 °C min^{-1}, merge into an amorphous halo on cooling at 250 °C min^{-1}, in agreement with the HyperDSC traces shown in Figure 4.5 where the copolymer mesophase is quenched at cooling rates > 50 ºC min^{-1}. Conversely, a very sharp diffraction peak at low angle (2θ = 6.2°) begins to emerge at a cooling rate of 50 °C min^{-1}, and becomes more prominent at faster cooling rates. This peak may be attributed to the smectic layers of the copolymer mesophase, corresponding to a layer spacing of ~ 14.1 Å.

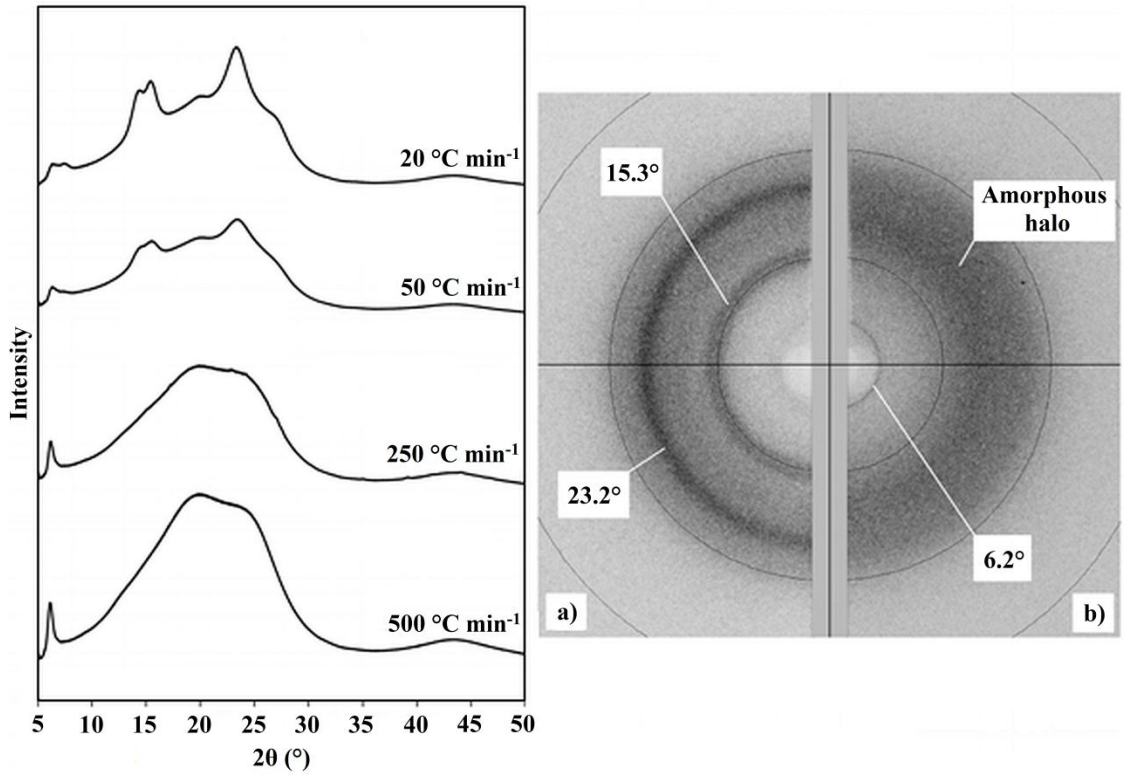

Figure 4.8 Comparative X-ray powder diffraction patterns of PBN*co*(**4.1**)-20 after cooling at 20-500 °C min^{-1} (left), together with comparative X-ray powder diffraction images (right) of PBN*co*(**4.1**)-20 after cooling at (a) 20 °C min^{-1} and (b) 500 °C min^{-1}. Diffraction angles (2θ) are shown for the main observed rings, and the two inner calibration circles represent *d*-spacings of 6.10 and 3.25 Å.

Polarised optical microscopy on ballistic-cooled samples of PBN*co*(**4.1**)-20 provided further evidence for a copolymer mesophase.[30] Birefringence, together with some indication of a Schlieren texture, is evident for PBN*co*(**4.1**)-20 cooled at 500 °C min^{-1} and at 250 °C min^{-1} (Figure 4.9a and b). In contrast, when the same copolymer is cooled at 50 °C min^{-1} and therefore allowed to melt-crystallise after mesophase formation (Figure 4.5), the sample is largely opaque (Figure 4.9c), denoting a semi-crystalline material. For comparison, PBN itself is crystalline and opaque when cooled at 500 °C min^{-1} (Figure 4.9d), because the PBN mesophase is inaccessible even at this cooling rate.

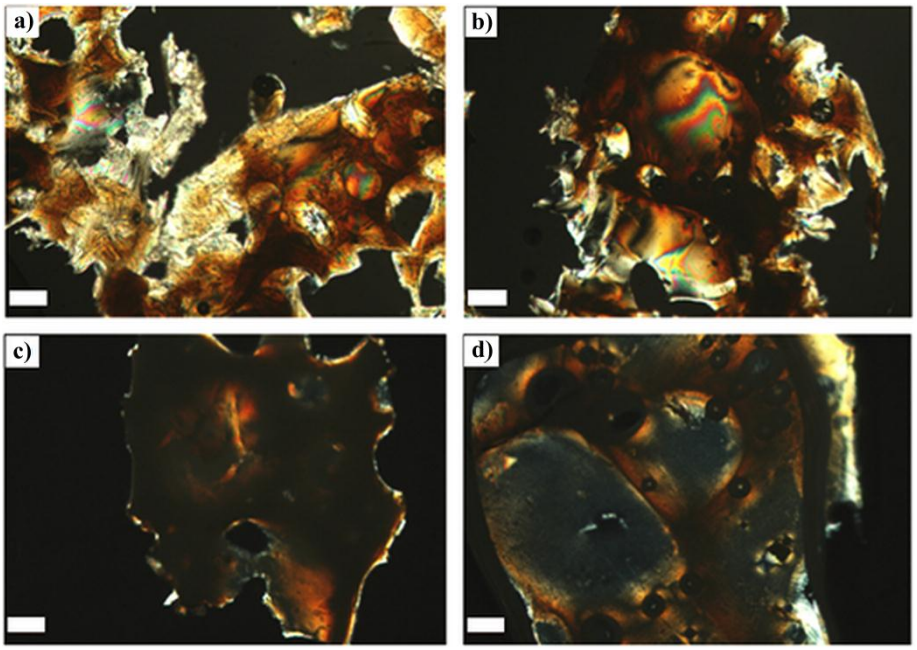

Figure 4.9 Polarised optical microscopy images of PBN*co*(**4.1**)-20 at room temperature following cooling rates from the melt of: a) 500 °C min^{-1}; b) 250 °C min^{-1}; c) 50 °C min^{-1}; and of PBN: d) 500 °C min^{-1}. White scale bar is 25 μm.

4.3.4 X-ray diffraction and computational modelling

Both crystal forms of PBN were synthesised via melt-copolycondensation of BHBN (α-form) and the slow cooling (0.1 °C min^{-1}) anneal of α-PBN from 280 °C (β-form), respectively, with the corresponding X-ray powder diffraction patterns matching those reported in the literature.[15,31]

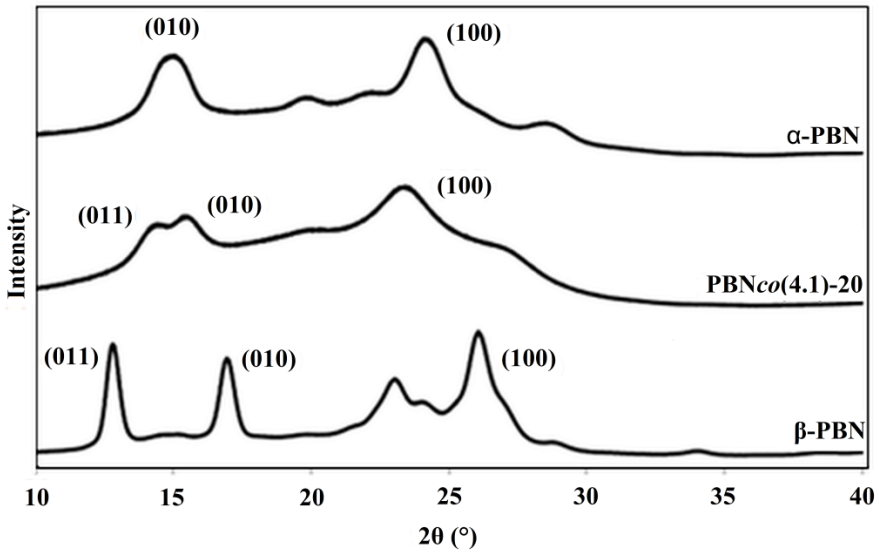

Figure 4.10 Comparative X-ray powder diffraction patterns of α-PBN, PBN*co*(**4.1**)-20 and β-PBN.

Although the X-ray powder diffraction pattern for PBN*co*(**4.1**)-20 after melt-crystallisation differs in detail from those reported for α- and β-PBN (Figure 4.10), the copolymer pattern

has broadly similar features to that of the α-phase. In particular, the 2θ peaks associated with the (010) and (100) lattice planes have only shifted slightly from 2θ = 15.3 and 24.1° to 15.4 and 23.6° respectively. The retention of thermal crystallisability, even with 20 and 25 mol% incorporation of **4.1** suggests that cocrystallisation is indeed occurring in the copolymers. However, in contrast to the analogous *PEN*-based copoly(ester-imide) series detailed in Chapter 3, it seems that no radical change in structure occurs. The copolymer crystal structure is here provisionally identified as a variant of the α-phase (with small changes to the unit cell parameters but no change in space group) by X-ray powder and fibre diffraction, interfaced to computational modelling and diffraction simulation.

The crystal structure of the PBN*co*(**4.1**) copolymer was initially modelled as a polymorph of α-PBN, assuming that the diffraction pattern of the model would not be drastically affected by the absence of comonomer residues. As a control experiment, the powder diffraction pattern for α-PBN was simulated using literature unit cell dimensions and atomic coordinates,[32] and was found to be in very good agreement with an experimental powder pattern obtained from the α-PBN synthesised in the present work. Adjustment of the α-PBN unit cell within boundary limits defined by both α- and β-PBN crystal structures lead to an extremely promising initial match between the simulated diffraction pattern and experimental pattern of PBN*co*(**4.1**)-20. On this basis, the unit cell dimensions of PBN*co*(**4.1**)-20 were provisionally set at a = 4.74, b = 6.37, c = 14.47 Å, α = 105.8, β = 122.3, γ = 98.5°.

Pawley and Rietveld refinement (R_{wp} = 9% and 12%, respectively) of the preliminary unit cell and crystal structure of the PBN*co*(**4.1**) copolymer with respect to the experimental powder diffraction pattern of PBN*co*(**4.1**)-20 (Figure 4.11) gave a final model in space group $P\bar{1}$, a = 4.74, b = 6.38, c = 14.45 Å, α = 106.1, β = 122.1, γ = 97.3°, ρ = 1.37 g cm^{-3}. The proposed crystal structure, viewed as a polymorph of α-PBN, is illustrated in Figure 4.12, projected along the *a*, *b* and *c*-axes.

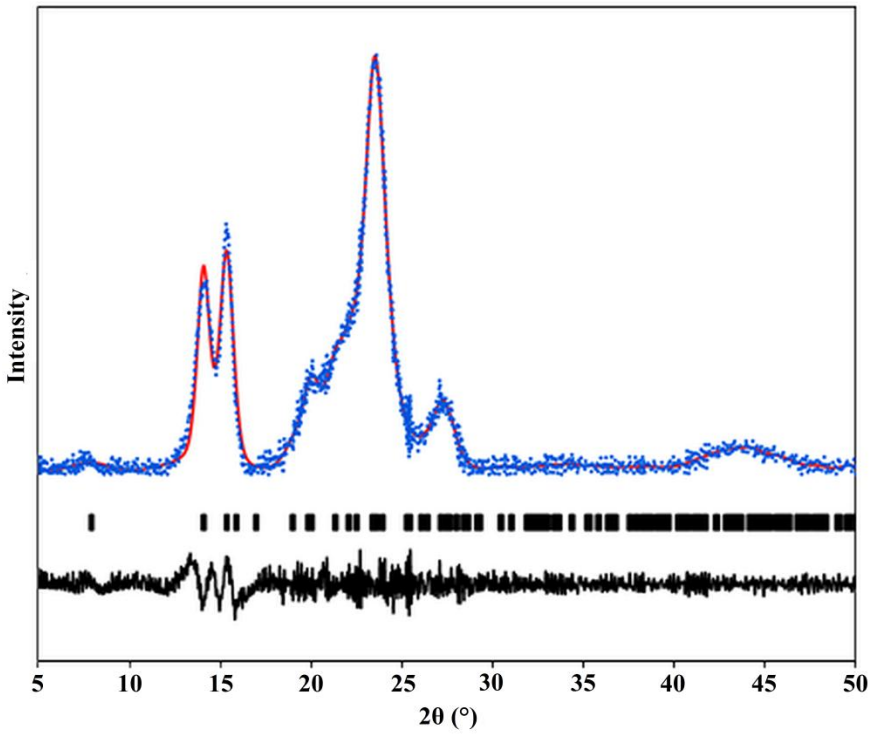

Figure 4.11 Rietveld refinement plot for PBN*co*(**4.1**)-20 (R_{wp} = 12%), where blue dots = experimental X-ray powder diffraction pattern, red line = simulated X-ray powder diffraction pattern, black rectangles = observed ticks (reflections indicated by the model) and black line = difference.

It is noted that the proposed cell parameters of PBN*co*(**4.1**)-20 (with the exception of γ) all possess values within the range of the cell parameters that define the α and β-forms of PBN (Table 4.3). This suggests that the PBN*co*(**4.1**) copolymer crystal structure may be a hybrid of α and β-PBN, whereby the presence of biphenyldiimide residues in the copolymer chain partially stabilises the β-form i.e. the more thermodynamically stable crystal phase rather than the kinetically stable α-form.

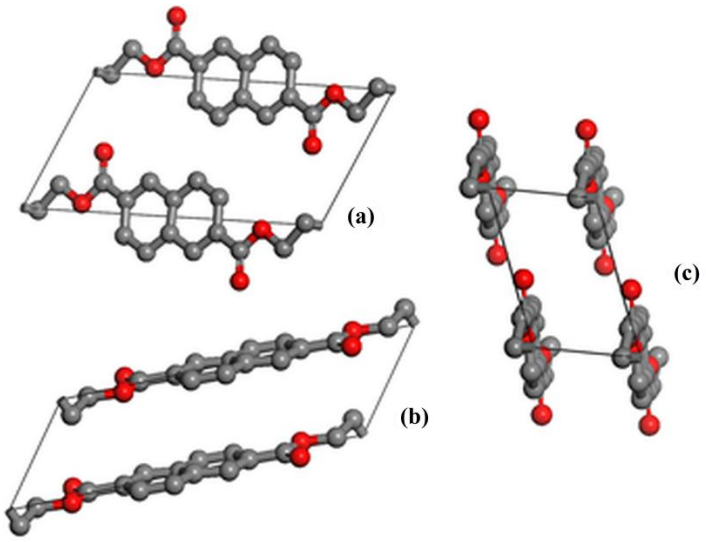

Figure 4.12 Proposed crystal structure of the PBN*co*(**4.1**) copolymer series viewed as a polymorph of α-PBN along the *a*, *b* and *c*-axes.

In addition, the similarity of the PBN*co*(**4.1**) crystal structure compared to those of α and β-PBN, in terms of crystal system, space group and cell parameters further illustrates the isodimorphism between BHBN and **4.1**, as the introduction of 20 mol% diimide has relatively little effect on the crystal morphology of α-PBN.

Table 4.3 Comparative crystal structure data for α-PBN, PBN*co*(**4.1**)-20 and β-PBN.

Parameter		**α-PBN**	**PBN*co*(4.1)-20**	**β-PBN**
Crystal system		Triclinic	Triclinic	Triclinic
Space group		$P\bar{1}$	$P\bar{1}$	$P\bar{1}$
a	**Å**	4.87	4.73	4.55
b	**Å**	6.22	6.38	6.43
c	**Å**	14.36	14.45	15.31
α	°	100.8	106.4	110.1
β	°	126.9	122.0	121.1
γ	°	97.9	97.3	100.6
Repeat units		1	1	1
Density	**g cm^{-3}**	1.36	1.37	1.39

A fibre pattern simulated from this proposed copolymer crystal structure is in good agreement with the experimental fibre pattern of a drawn PBN*co*(**4.1**)-20 fibre (Figure 4.13), thus further demonstrating the validity of the computational model. As also observed in the fibre diffraction pattern of the analogous PEN-based copolymer (Chapter 3), experimental reflections for PBN*co*(**4.1**)-20 [specifically (001), (01$\bar{1}$) and (1$\bar{1}$1)] are displaced above and below the layer lines, a characteristic feature of diffraction from crystallites containing random-sequence chains.[33,34]

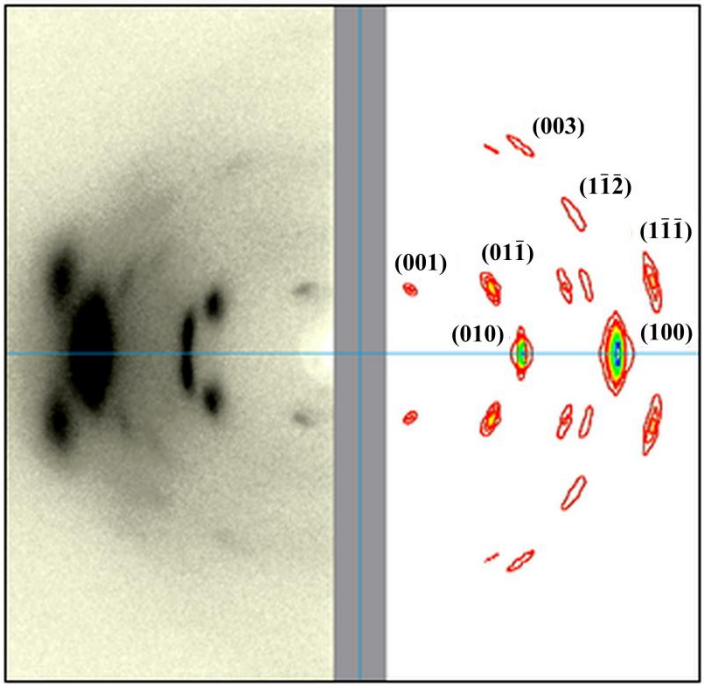

Figure 4.13 Simulated X-ray fibre pattern (coloured contour lines, right) juxtaposed with the experimental fibre pattern (grayscale, left) for a drawn fibre of PBN*co*(**4.1**)-20.

4.4 Conclusions

The synthesis of a novel biphenyldiimide comonomer, **4.1**, in excellent yield from commercially available starting reagents, and the subsequent production of PBN-based copoly(ester-imide)s with PBN is reported. Incorporation of 20 and 25 mol% of **4.1** results in increased T_gs, unusually high retention of semi-crystalline character, and facile access to a liquid crystalline phase, depending on processing conditions. Structural analysis by X-ray powder diffraction interfaced to computational modelling has enabled a provisional crystal structure for the PBN*co*(**4.1**) copolymer to be identified and rationalised in terms of isomorphism between the naphthalate-diester and biphenyldiimide comonomers.

4.5 Experimental

4.5.1 Materials

3,4,3',4'-Biphenyltetracarboxylic dianhydride was purchased from Tokyo Chemical Industries, U.K. 4-Amino-1-butanol was purchased from Alfa Aesar, U.K. Antimony trioxide was purchased from SICA, France. 2,6-Dimethyl naphthalate and titanium isopropoxide were obtained from DuPont Teijin Films, U.K. Deuterated chloroform, methanol, dimethyl sulfoxide, deuterated dimethyl sulfoxide, 1,4-butanediol and *N*,*N*'-dimethylformamide were purchased from Sigma Aldrich, U.K. Chloroform was purchased from Fisher Scientific, U.K.

Trifluoroacetic acid and 1,1,1,3,3,3-hexafluoro-2-propanol were purchased from Fluorochem, U.K. All materials were used as purchased.

4.5.2 Monomer synthetic procedures

4.5.2.1 Bis(4-hydroxybutyl)-2,6-naphthalate (BHBN)

A mixture of 2,6-dimethylnaphthalate (242 g, 0.99 mol), 1,4-butanediol (267 g, 2.96 mol) and titanium isopropoxide (0.04 g, 0.14 mmol) was heated to 230 °C over 2 h and held at this temperature for 230 °C for a further 2 h. The reaction solution was then cooled to room temperature, poured into deionised water to form a precipitate, which was filtered and dried under vacuum at 80 °C for 24 h to afford the product **BHBN** as a white powder (321 g, 90%).

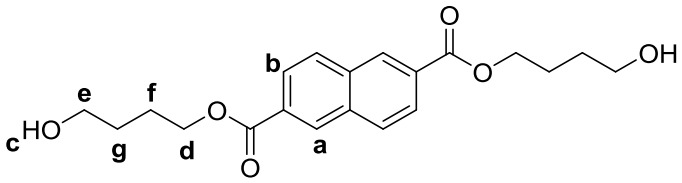

M.P. (DSC) 237 °C. ^{1}H NMR [400 MHz, $CDCl_3$/TFA (2:1)] δ_H (ppm) 8.69 (2H, s, H_a), 8.13 (4H, m, H_b), 4.64 (2H, s, H_c), 4.56 (4H, m, H_d), 3.98 (4H, m, H_e), 2.06 (4H, m, H_f), 1.91 (4H, m, H_f). ^{13}C NMR [100 MHz, $CDCl_3$/TFA (2:1)] δ_C (ppm) 169.4, 134.9, 131.3, 130.1, 128.7, 125.7, 68.1, 66.1, 37.4, 25.0, 24.6. IR (ν_{max} cm^{-1}) 3435 (νO-H), 2962 (νC-H), 1717 (νC=O), 1244 (νC-O).

4.5.2.2 *N,N*'-Bis(4-hydroxybutyl)biphenyl-3,4,3',4'-tetracarboxylic diimide (4.1)

4-Amino-1-butanol (9.92 g, 0.111 mol) was added dropwise to a solution of biphenyl-3,4,3',4'-tetracarboxylic anhydride (15.82 g, 0.054 mol) in DMF (250 mL). The reaction solution was heated to reflux for 16 h. After cooling to room temperature, the reaction solution was poured into deionised water to give a precipitate, which was filtered and dried under vacuum at 80 °C for 24 h to afford the product **4.1** as a white powder (20.54 g. 89%).

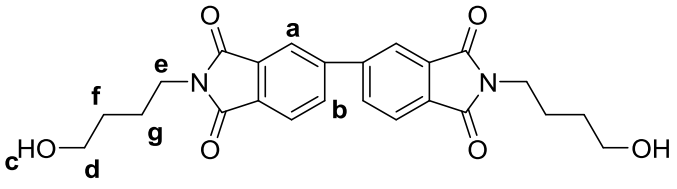

4.1

M.P. (DSC) 179 °C. MS *m/z* = 437.1706 $[M+H]^+$, calculated 437.1723. ^{1}H NMR (400 MHz, DMSO-d_6) δ_H (ppm) 8.19 (4H, m, H_a), 8.12 (4H, d, J = 8.0 Hz, H_b), 4.42 (2H, t, J = 4.0 Hz, H_c), 3.58 (4H, t, J = 8.0 Hz, H_d), 3.41 (4H, m, H_e), 1.63 (4H, q, J = 8.0, 16.0 Hz, H_f), 1.42

(4H, q, J = 8.0, 16.0 Hz, H_g). ^{13}C NMR (100 MHz, DMSO-d_6) δ_C (ppm) 167.4, 144.0, 133.2, 132.5, 131.2, 123.5, 121.7, 60.1, 37.5, 29.7, 24.7. IR (ν_{max} cm^{-1}) 3366 (νO-H), 2956 (νC-H), 1701 (νC=O), 1379 (νC-O).

4.5.3 Polymer synthetic procedures

Polymers were synthesised via the laboratory-scale melt-polycondensation procedure as described in Chapter 2, unless otherwise stated.

4.5.3.1 PBN (α-form)

Reagents	
(g)	
BHBN	Sb_2O_3
50.00	0.10

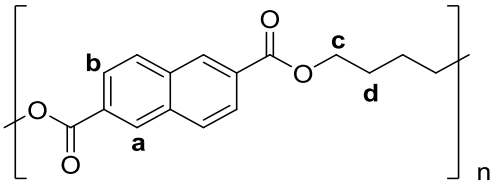

^{1}H NMR [400 MHz, $CDCl_3$/TFA (2:1)] δ_H (ppm) 8.72 (2H, s, H_a), 8.13 (4H, d, J = 8.6 Hz, H_b), 4.67 (4H, s, H_c), 2.20 (4H, s, H_d). ^{13}C NMR [100 MHz, $CDCl_3$/TFA (2:1)] δ (ppm) 169.6, 168.1, 135.0, 133.3, 131.3, 130.1, 128.7, 125.7, 66.5, 64.0, 25.0. T_g = 51 °C, T_{cc} = 222 °C, T_c = 205 °C, T_{m1} = 242 °C, T_{m2} = 247 °C, T_d = 387 °C. M_w (GPC/HFIP) = 13,400 Da, M_n (GPC/HFIP) = 3,300 Da. IR (ν_{max} cm^{-1}) 3530 (νC-H), 2941 (νC-H), 1707 (νC=O), 1259 (νC-O).

4.5.3.2 PBN (β-form)

The β-form of PBN was obtained by thermal treatment of the α-form[15] in a TA Instruments DSC Q2000 under a nitrogen atmosphere. A flow rate of 50 mL min^{-1} and a Tzero Al pan was used. A sample of α-PBN (~5 mg) was equilibrated at 25 ºC and then heated to 280 ºC at 20 ºC min^{-1}. After an isothermal hold at 280 ºC for 5 mins, the sample was cooled to 25 ºC at 0.1 ºC min^{-1} and then annealed at 220 ºC for 12 h.

4.5.3.3 PBN*co*(4.1) copolymer series

Reagents			Comonomer feed ratio		Copolymer composition ratio	
(g)			(mol%)		(mol%)	
BHBN	4.1	Sb_2O_3	BHBN	4.1	PBN	4.1
33.33	10.09	0.10	80	20	81	19
33.33	13.46	0.10	75	25	76	24

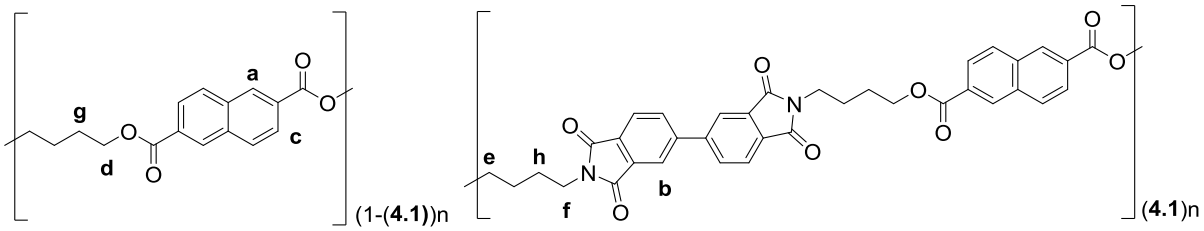

PBN*co*(4.1)-10

Synthesis and characterisation of this copolymer composition were as previously reported.[35]

PBN*co*(4.1)-20

^{1}H NMR [400 MHz, $CDCl_3$/TFA (2:1)] δ_H (ppm) 8.71 (4H, s, H_a), 8.26 (2H, s, H_b), 8.10 (12H, m, H_c), 4.66 (8H, s, H_d), 3.96 (4H, s, H_e), 2.19 (4H, s, H_f), 2.03 (8H, s, H_g). ^{13}C NMR [100 MHz, $CDCl_3$/TFA (2:1)] δ_C (ppm) 170.2, 169.6, 145.9, 134.9, 134.0, 132.3, 131.3, 131.0, 130.1, 128.7, 125.6, 124.9, 123.0, 66.5, 38.2, 25.6, 25.0. T_g = 68 °C, T_{cc} = 126 °C, T_{c1} = 156 °C, T_{c2} = 114 °C, T_{m1} = 214 °C, T_{m1} = 242 °C, T_d = 393 °C. M_w (GPC/HFIP) = 15,000 Da, M_n (GPC/HFIP) = 3,600 Da. IR (ν_{max} cm^{-1}) 2945 (νC-H), 1703 (νC=O), 1256 (νC-O).

PBN*co*(4.1)-25

^{1}H NMR [400 MHz, $CDCl_3$/TFA (2:1)] δ_H (ppm) 8.72 (4H, s, H_a), 8.27 (2H, s, H_b), 8.12 (12H, m, H_c), 4.67 (8H, s, H_d), 3.97 (4H, s, H_e), 2.20 (4H, s, H_f), 2.04 (8H, s, H_g). ^{13}C NMR [100 MHz, $CDCl_3$/TFA (2:1)] δ_C (ppm) 170.2, 169.6, 168.1, 145.9, 134.9, 134.0, 133.3, 132.3, 131.3, 131.0, 130.1, 128.7, 125.7, 124.9, 123.0, 66.5, 38.2, 25.6, 25.0. T_g = 74 °C, T_{cc} = 138 °C, T_{c1} = 152 °C, T_{c2} = 91 °C, T_{m1} = 226 °C, T_{m1} = 240 °C, T_d = 393 °C. M_w (GPC/HFIP) = 15,500 Da, M_n (GPC/HFIP) = 4,400 Da. IR (ν_{max} cm^{-1}) 2977 (νC-H), 1705 (νC=O), 1257 (νC-O).

4.6 References

1 W. A. MacDonald, *Polym. Int.*, 2002, **51**, 923–930.
2 H. Soichiro, *Jap. Pat*., JP2010013599 (A), 2010.
3 J. U. N. Xiao, X. Wan, D. Zhang, Q. Zhou and S. R. Turner, *J. Polym. Sci. Polym. Chem.*, 2001, **39**, 408-415.
4 C. L. Mares and J. de Abajo, *Angew. Makromol. Chem.*, 1975, **55**, 73-83.
5 S. Maiti and S. Das, *J. Appl. Polym. Sci*., 1981, **26**, 957–978.
6 H. Ma, M. Hibbs, D. M. Collard and D. A. Schiraldi, *Macromolecules*, 2002, **35**, 5123–5130.
7 Y. S. Hu, R. Y. F. Liu, M. Rogunova, D. A. Schiraldi, S. Nazarenko, A. Hiltner and E. Baer, *J. Polym. Sci. Part B Polym. Phys.*, 2002, **40**, 2489–2503.
8 L. E. E. S. Park and D. C. Lee, *Polym. Eng. Sci*., 1995, **35**, 1629–1635.
9 L. J. F. Mary and P. Kannan, *Polym. Int.*, 1998, **47**, 317–323.
10 G. Z. Papageorgiou and G. P. Karayannidis, *Polymer*, 2001, **42**, 8197–8205.
11 Y. G. Jeong, W. H. Jo and S. G. Lee, *Macromolecules*, 2000, **33**, 9705–9711.
12 D. A. Schiraldi, *Modern Polyesters: Chemistry and Technology of Polyesters and Copolyesters*, J. Scheirs and T. E. Long, Wiley, Chichester 2003, 245–266.
13 R. R. Gallucci and B. R. Patel, *Modern Polyesters: Chemistry and Technology of Polyesters and Copolyesters*, J. Scheirs and T. E. Long, Wiley, Chichester, 2003, 293–332.
14 D. D. Callandar, *Modern Polyesters: Chemistry and Technology of Polyesters and Copolyesters*, J. Scheirs and T. E. Long, Wiley, Chichester, 2003, 323–333.
15 M. Ju, J. Huang and F. Chang, *Polymer*, 2002, **43**, 2065–2074.
16 T. Konishi, K. Nishida, G. Matsuba and T. Kanaya, *Macromolecules*, 2008, **41**, 3157–3161.
17 S. J. Meehan, S. W. Sankey, S. M. Jones, W. A. MacDonald and H. M. Colquhoun, *ACS Macro Lett.*, 2014, **3**, 968-971.
18 H. M. Colquhoun, C. A. O'Mahoney, D. J. Williams, *Polymer*, 1993, **34**, 7–10.
19 C. P. Brock and R. P. Minton, *J. Am. Chem. Soc.*, 1989, **111**, 4586–4593.
20 S. O. Kim, C. M. Koo, I. J. Chung and H. Jung, *Macromolecules*, 2001, **34**, 8961–8967.
21 D. Cavallo, D. Mileva, G. Portale, L. Zhang, L. Balzano, G. C. Alfonso and R. Androsch, *ACS Macro Lett*., 2012, **1**, 1051-1055.
22 A. J. Jing, O. Taikum, C. Y. Li, F. W. Harris and S. Z. D. Cheng, *Polymer*, 2002, **43**, 3431–3440.
23 T. Yamanobe, H. Matsuda, K. Imai, A. Hirata, S. Mori and T. Komoto, *Polym. J*., 1996, **28**, 177-181.
24 S. C. Lee, K. H. Yoon and J. H. Kim, *Polym. J*., 1997, **29**, 1-6.
25 G. Z. Papageorgiou and G. P. Karayannidis, *Polymer*, 1999, **40**, 5325–5332.
26 R. Jakeways, I. M. Ward, M. A. Wilding, I. H. Hall, I. J. Desborough and M. G. Pass, *J. Polym. Sci. Polym. Phys.*, 1975, **13**, 799–813.
27 Y. M. Sun and C. S. Wang, *J. Polym. Sci. Polym. Chem*., 1996, **34**, 1783–1792.
28 R. J. Seyler, *Assignment of the Glass Transition*, Philadelphia, American Society for Testing and Materials, 1994, 108.
29 E. A. Turi, *Thermal Characterisation of Polymeric Materials: Second Edition, Academic Press, Brooklyn, New York*, 1997.
30 S. T. Wu, *Phys. Rev. A*, 1986, **33**, 1270–1274.
31 T. Chiba, S. Asai, W. Xu and M. Sumita, *J. Polym. Sci. Polym. Phys*., 1998, **37**, 561–574.
32 H. Koyano, Y. Yamamoto, Y. Saito, T. Yamanobe and T. Komoto, *Polymer*, 1998, **39**, 4385–4391.

33 G. A. Gutierrez, J. Blackwell and R. A. Chivers, *Polymer*, 1985, **26**, 348–354.
34 Z. Sun, H. M. Cheng and J. Blackwell, *Macromolecules*, 1991, **24**, 4162–4167.
35 S. J. Meehan, *PhD Thesis*, *Enhancement of Polyester Properties Through Molecular* Design, University of Reading, 2012.

Chapter 5

Poly(ethylene terephthalate) (PET)-based copoly(ester-imide)s

The research described in this chapter has, in part, been published by the author as Patent Cooperation Treaty (PCT) applications that are currently being progressed worldwide and a filed UK patent application due for publication in December 2015. These applications are:

a) S. W. Sankey, D. Turner, H. Colquhoun and **S. Jones**, *Copolyesterimides derived from N,N'-bis-(hydroxyalkyl)-3,4,3',4'-diphenylsulfonetetracarboxylic diimide and films made therefrom*, PCT/GB2014/051852, 2014.

b) S. W. Sankey, D. Turner, H. Colquhoun and **S. Jones**, *Copolyesterimides derived from N,N'-bis-(hydroxyalkyl)-benzophenone-3,4,3',4'-tetracarboxylic diimide and films made therefrom*, PCT/GB2014/051853, 2014.

c) S. W. Sankey, D. Turner, H. Colquhoun and **S. Jones**, *Copolyesterimides derived from aromatic dicarboxylic acids and aliphatic glycols and films made therefrom*, PCT/GB2014/052995, 2015.

d) S. W. Sankey, D. Turner, H. Colquhoun and **S. Jones**, *Copolyesterimides and films made therefrom*, GB 1411044.9, 2014.

5.1 Abstract

Melt-copolycondensation of the diimide-diester bis(2-hydroxyethyl)-2,2'-(1,4-phenylene)bis(1,3-dioxoisoindoline-5-carboxylate) with bis(2-hydroxyethyl) terephthalate at 0-30 mol% imide comonomer affords a series of poly(ethylene terephthalate) (PET)-based copoly(ester-imide)s that display enhanced glass transition temperatures, T_gs, in comparison to PET. In contrast to PET-based copoly(ester-imide)s containing alternative nitrogen-linked phthalimides, all such copolymers retain semi-crystalline behaviour. This trend is attributed to isomorphic substitution of diimide for terephthalate residues in the copolymer crystal lattice, and confirmed by X-ray powder diffraction analysis interfaced to computational modelling. The subsequent synthesis of copolymers incorporating the novel diimide at 50 and 100 mol% via an acid chloride route, affords a copoly(ester-imide) series where the T_g ranges from 75 to 163 °C depending on the copolymer composition ratio.

Furthermore, the synthesis of novel PET-based copoly(ester-imide)s incorporating rigid benzophenone, diphenylsulfone and bicyclooctene diimide residues is discussed. An increase in T_g of ~ 25 °C in comparison to PET was observed for all respective 10 mol% copolymers.

Although semi-crystalline behaviour was not observed above 15 mol% content upon cooling from the melt for each system, crystallinity may be induced by thermal annealing at 200 °C for 2 hours. The production of PET-based heat-set biaxially oriented film incorporating 10 mol% benzophenone diimide was subsequently achieved, having a T_g of 101 °C and a degree of crystallinity above 15%.

5.2 Introduction

The T_g, T_m, and χ_c are key parameters in determining the thermomechanical performance of semi-crystalline polyester-based materials. Although poly(ethylene terephthalate) (PET) is utilised extensively in polymer, fibre and film form due to its high mechanical strength, dimensional stability and electrical resistance,[1–3] several potential applications that require greater operating temperatures are currently excluded because of the relatively low T_g (75 °C) it possesses.[4–6] As discussed in Chapter 1, previous attempts to raise the thermomechanical performance of PET have mainly focussed upon the introduction of rigid biphenyl and imide moieties via copolymerisation.[7–10] Although this has led to increases in the T_g, it is also accompanied by complete loss of crystallinity at relatively low levels of comonomer content (< 10 mol%), thereby destroying the ability of the copolymer to achieve biaxial orientation.

For crystallinity to be present throughout the entire range of a copolymer series, cocrystallisation between the two comonomers must occur within the crystal lattice of either homopolymer via isomorphism.[11] This phenomenon is rarely observed when one of the comonomers incorporates a terephthalate unit, with just the poly(butylene naphthalate-*co*-butylene terephthalate)[12] and poly(ethylene terephthalate-*co*-1,4-cyclohexylene dimethylene terephthalate)[13,14] copolymer series known.

Herein, the synthesis of a novel copoly(ester-imide) series, in which diimide-diester units containing a rigid *p*-phenylene component are incorporated into PET, is detailed. Retention of semi-crystalline behaviour has been previously observed following copolycondensation of biphenyl-3,4,3',4'-tetracarboxylic diimide residues, with PEN and PBN, at significant levels of imide (> 25 mol%) as presented in Chapters 3 and 4, respectively. It was subsequently proposed that by applying the same rationale of isomorphic copolymerisations to PET, the production of analogous thermomechanically enhanced polyester-based materials might be achieved. However, in the case of PET, the design of a sufficiently rigid comonomer that was *also* isomorphic with BHET, was not found possible. Therefore, an imide comonomer, **5.1**, which could theoretically cocrystallise with the dimer of BHET was designed. Figure 5.1 illustrates the overlaid energy minimised chemical structures of the BHET dimer and **5.1**,

whereby the similarity in comonomer chain length is facilitated by the increased chain length of the BHET dimer relative to BHET.

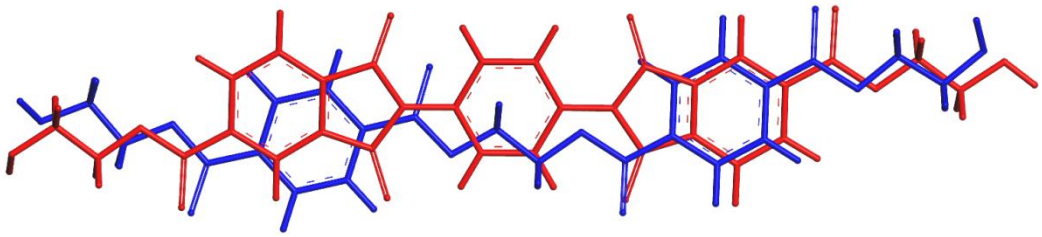

Figure 5.1 Overlaid energy minimised chemical structures of the bis(2-hydroxyethyl)terephthalate dimer (blue) and bis(2-hydroxyethyl)-2,2'-(1,4-phenylene)bis(1,3-dioxoisoindoline-5-carboxylate), **5.1** (red)

The synthesis, thermal behaviour and structural morphology of PET-based copoly(ester-imide)s incorporating **5.1** is discussed in this chapter, which details the approach to increasing the T_g of PET via copolymerisation with a rigid isomorphic comonomer (as observed in Chapters 3 and 4). In addition, an alternative strategy of increasing the thermal performance of PET via copolymerisation with rigid *non*-isomorphic diimide comonomers is detailed. Here, crystallinity may be induced post-polymerisation to produce a semi-crystalline copoly(ester-imide). A comparison of both copolymerisation routes is discussed, after which the initial production of thermally enhanced PET-based heat-set biaxially oriented film is evaluated.

5.3 Results and discussion

5.3.1 Investigation of PET-based copoly(ester-imide)s containing nitrogen-linked phthalimides

5.3.1.1 Polymer synthesis and characterisation

In addition to the synthesis of comonomer **5.1**, several other nitrogen-linked phthalimide comonomers (**5.2**-**5.4**) were produced via a two-step synthesis. The imidisation of 1,2,4-benzenetricarboxylic anhydride with selected difunctional primary amines, was followed by the glycolisation of the intermediate dicarboxylic acid utilising 2-bromoethanol and triethylamine [steps (i) and (ii) in Scheme 5.1, respectively].

Comonomers **5.2**-**5.4** were selected as control comonomers for **5.1**, in order to investigate the effect of diamine structure within the phthalimide unit on potential isomorphism with the BHET dimer. It was assumed that the presence of *m*-xylylenediamine (**5.3**) and ethylenediamine (**5.4**) residues would prevent cocrystallisation with BHET from occurring because of the significant extension in imide comonomer chain length when compared to the

p-phenylenediamine unit in **5.1**.[9,15] The isomeric *m*-phenylenediamine unit was also incorporated into the synthesis of comonomer **5.2** for comparison to **5.1**. However, it was still envisaged that cocrystallisation would not occur due to the introduction of a meta-kink to the copolymer chain, which would inhibit chain-packing and subsequent melt-crystallisation.

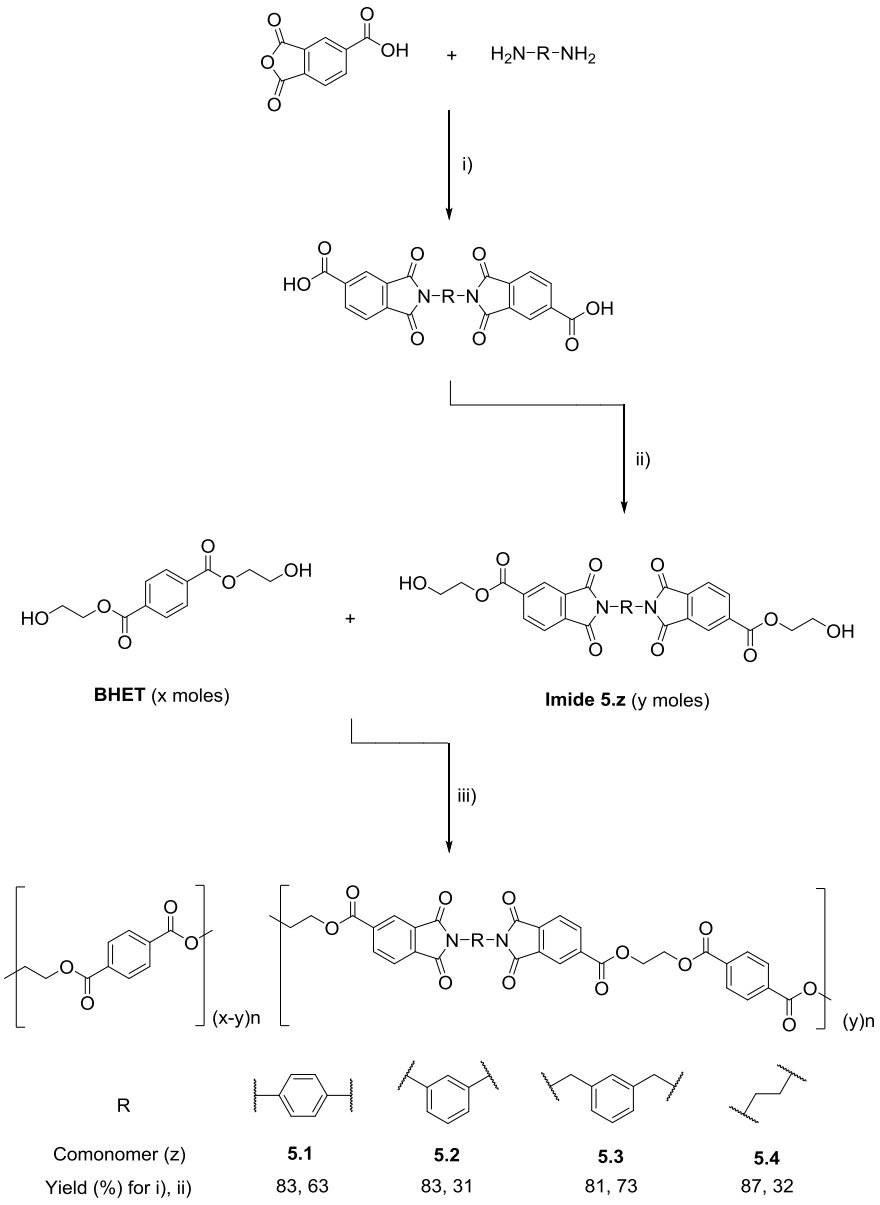

Scheme 5.1 Synthesis of PET-based copoly(ester-imide)s via melt-copolymerisation of bis(2-hydroxyethyl) terephthalate (BHET) with selected nitrogen-linked phthalimide comonomers (**5.1 – 5.4**), where $y \leq x$. Reaction conditions: i) DMF, reflux, 1.5 h for **5.1**, **5.2**, **5.3** and acetic acid, reflux, 3 h for **5.4**; ii) DMF, 2-bromoethanol, TEA, 80 °C, 16 h; iii) Sb_2O_3, 290-310 °C, 2.5 h, < 1mbar.

Good yields were achieved for all diacid intermediates (> 80%) with moderate yields observed for the following glycolisation step (31-75%). It is probable that the reduced glycolisation yields are a result of the slow and loss-making filtrations with water and methanol. PET-based copoly(ester-imide)s were synthesised by laboratory-scale

melt-copolycondensation, as described in Chapter 2. Comonomers **5.1** and **5.2**-**5.4** were incorporated into PET at levels of 5-30 and 5-10 mol% respectively.

Analysis of the resultant copolymers by ^{1}H NMR spectroscopy verified successful copolymerisation for all comonomers with BHET and indicated that the copolymer composition ratios matched the comonomer feed ratios for PET-based copolymers incorporating **5.2** and **5.4**. However, PET-based copolymers incorporating **5.1** and **5.3** always contained less imide in the final copolymer compared to the initial feed ratios (at an average of 85%), as illustrated by the measured PET*co*(**5.1**) copolymer composition ratios in Table 5.1. In addition to the carry-over of comonomer reagents in the polycondensation distillate causing discrepancies between feed and composition ratios (as discussed in Chapter 3), it is likely that **5.1** and **5.3** both exhibit low solubility in BHET due to having T_ms > 330 °C, which therefore limits the amount of comonomer that is able to react in the melt.

Table 5.1 Comparison of the comonomer feed ratio and the copolymer composition ratio for selected PET*co*(**5.1**) copolymers.

Comonomer feed ratio (mol%)		**Copolymer composition ratio[a] (mol%)**	
BHET	**5.1**	**PET**	**5.1**
95	5	96	4
90	10	93	7
85	15	87	13
80	20	82	18
75	25	77	23
70	30	74	26

[a] Determined by ^{1}H NMR spectroscopy.

The relative insolubility of **5.1** in BHET was particularly noticeable when attempting to synthesise PET*co*(**5.1**) copolymers at above 20 mol% incorporation of **5.1**, as the mechanical stirrer was unable to stir the comonomer mixture at temperatures < 300 °C. The melt-copolycondensations of PET*co*(**5.1**)-25 and 30 were therefore performed at 310 °C. As a result, higher levels of DEG are observed for the 25 and 30 mol% copolymers (~ 11 mol% relative to ~ 2.5 mol%) compared with PET*co*(**5.1**)-5 to 20. This finding is illustrated in Figure 5.2, with the DEG ^{1}H NMR resonances at δ_H = 4.2 and 4.7 ppm being clearly apparent in the ^{1}H NMR spectrum of PET*co*(**5.1**)-30.

The extent of incorporation of **5.1** within each copolymer was calculated from Equation 5.1, where H_c is the integral associated with the aromatic terephthalate protons in PET and H_d is the resonance integral associated with the aromatic *p*-phenylenediamine protons in **5.1**.

Equation 5.1

$$\mathbf{5.1}\ (\boldsymbol{mol}\%) = \mathbf{100} * \frac{\boldsymbol{H_d}}{(\boldsymbol{H_c}+\boldsymbol{H_d})}$$

The continuing emergence of **5.1** resonances assigned as H_a, H_b and H_d in accordance with an increasing feed ratio of **5.1** in Figure 5.2 confirmed the successful copolymerisation with PET.

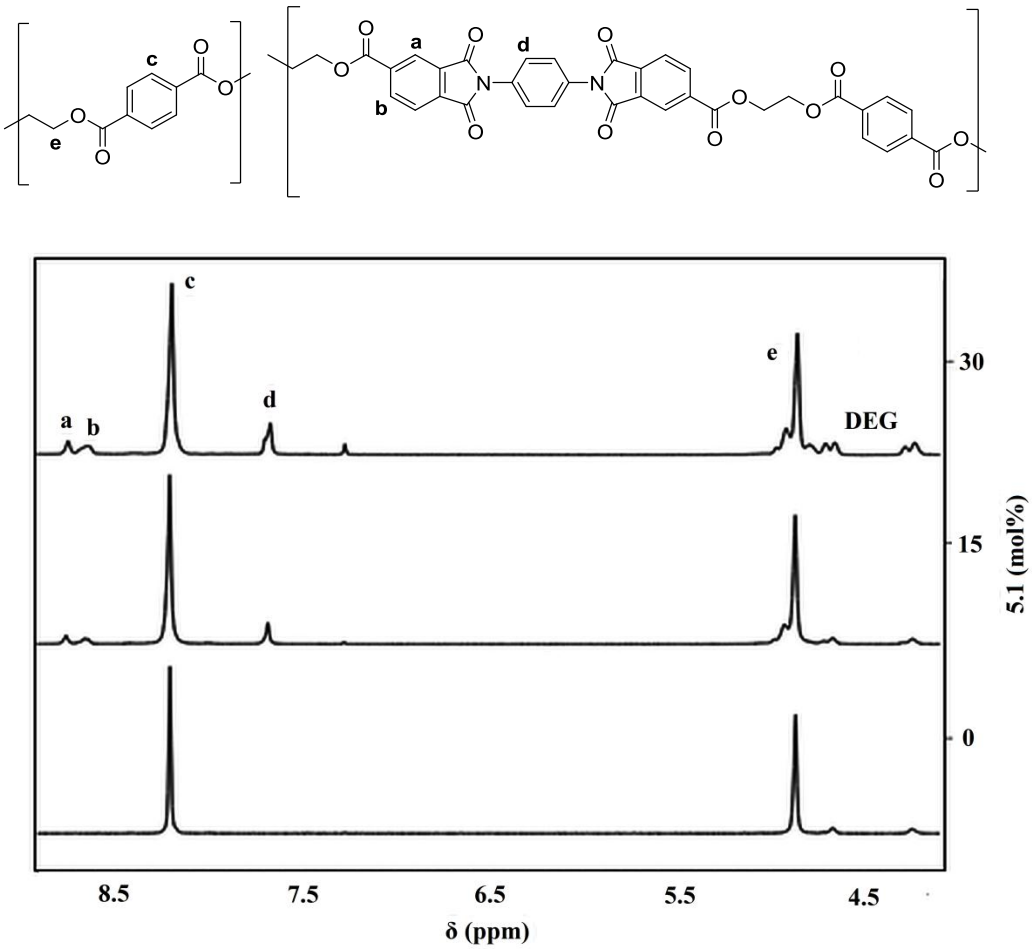

Figure 5.2 ^{1}H NMR assignments of a PET-based copoly(ester-imide) incorporating 30 mol% of **5.1**, juxtaposed with of ^{1}H NMR spectra for the PET*co*(**5.1**) copolymer and for PET itself.

Analysis of selected PET-based copoly(ester-imide)s by GPC revealed comparable molecular weight distributions relative to PET. With reference to the PET*co*(**5.1**) copolymer series, incorporation of 5 and 10 mol% **5.1** afforded M_ws of 15,800 and 18,300 Da, respectively. The presence of a weak shoulder-peak on the GPC traces of PET and PET*co*(**5.1**)-10 is observed in Figure 5.3, suggesting the presence of low molecular weight oligomers contributing to Đ values of > 3.

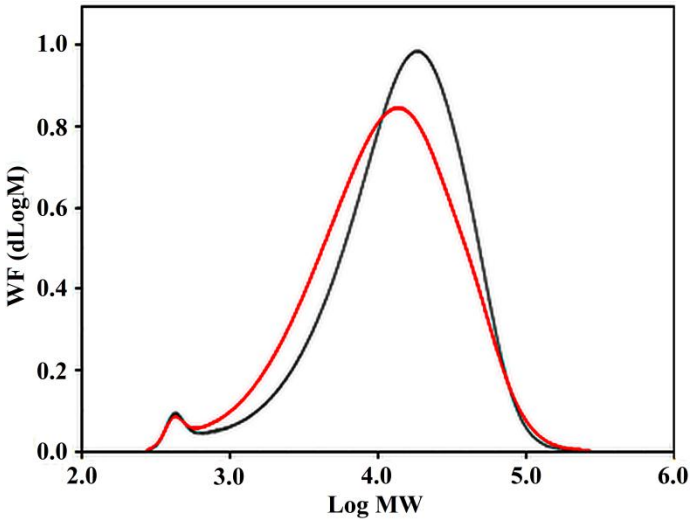

Figure 5.3 Comparative molecular weight distributions of PET (black) and PET*co*(**5.1**)-10 (red).

GPC analysis of PET*co*(**5.1**) copolymers containing > 10 mol% imide content was not possible due to copolymer insolubility in HFIP. However, the η_{inh} of PET*co*(**5.1**)-5 to 30 ranged from 0.32-0.67 dL g^{-1} indicating a sufficient degree of copolymerisation had occurred at higher levels of **5.1** content. Similar molecular weight distributions are also observed for PET-based copoly(ester-imide)s containing the control nitrogen-linked phthalimides (**5.2**-**5.4**) at 10 mol%, with observed M_ws of 21,600-26,500 Da (Table 5.2). It is noted that the solution of PET*co*(**5.2**)-10 in HFIP also contained considerable insoluble material (η_{inh} = 0.58 dL g^{-1}), thus PET*co*(**5.2**)-5 is listed for comparison in Table 5.2.

Table 5.2 Molecular weight distributions, dispersities and inherent viscosities of PET and selected PET-based copoly(ester-imide)s.

Polymer	M_w [a]	M_n [a]	M_z [a]	**Đ**	η_{inh} [b]
	Da	**Da**	**Da**	**-**	**dL g^{-1}**
PET	20,600	6,360	37,500	3.2	0.75
PET*co*(**5.1**)-10	18,300	5,160	40,000	3.5	0.37
PET*co*(**5.2**)-5	26,500	4,700	79,000	5.6	0.46
PET*co*(**5.3**)-10	21,600	6,020	42,100	3.6	0.55
PET*co*(**5.4**)-10	23,700	6,600	47,000	3.6	0.40

[a] Determined by GPC (HFIP eluent). [b] Determined by solution viscometry [$CHCl_3$:TFA (2:1 v/v) eluent].

5.3.1.2 Thermal properties

Investigation of the PET*co*(**5.1**) copolymer series by DSC demonstrated that semi-crystalline behaviour is retained at significant levels of imide content, with all copolymers possessing the ability to crystallise upon cooling from the melt. This retention of crystallinity is anomalous in behaviour when compared to the control nitrogen-linked phthalimides (**5.2**-**5.4**) incorporated into PET at 10 mol%. By replacing the *p*-phenylenediamine unit in **5.1** with

either *m*-phenylenediamine (**5.2**), *m*-xylylenediamine (**5.3**) or ethylenediamine (**5.4**) residues at 10 mol% with respect to PET, the ability of the copolymer to melt-crystallise is destroyed, emphasising the requirement for comparable comonomer chain-dimensions for isomorphism to occur (Table 5.3).

Table 5.3 Comparative thermal properties of PET and selected PET-based copoly(ester-imide)s incorporating 10 mol% of a nitrogen-linked phthalimide comonomer.

Polymer	T_g [a]	T_c [b]	ΔH_c [b]	T_{cc} [a]	ΔH_{cc} [a]	T_m [a]	ΔH_m [a]	χ_c
	°C	°C	J g^{-1}	°C	J g^{-1}	°C	J g^{-1}	%
PET	75	208	-41.50	-	-	249	39.05	28
PET*co*(**5.1**)-10	89	163	-13.23	156	-1.68	236	28.72	20
PET*co*(**5.2**)-10	99	-	-	-	-	-	-	-
PET*co*(**5.3**)-10	100	-	-	-	-	229	3.06	2
PET*co*(**5.4**)-10	99	-	-	-	-	228	1.96	1

[a] Determined by DSC (2nd heating scan, 20 °C min^{-1}). [b] Determined by DSC (1st cooling scan, 5 °C min^{-1}).

In a similar manner to PEN and the PEN*co*(**3.1**) copolymer series described in Chapter 3, inclusion of 10 mol% **5.1** has depressed the T_m in comparison to PET (249 to 236 °C). A substantial level of crystallinity is still observed, however, for PET*co*(**5.1**)-10 (ΔH_m = 28.72 J g^{-1}, χ_c = 20%). Although larger increases in T_g are obtained following copolymerisation with equivalent levels of **5.2**-**5.4**, no T_c exotherms are detected upon cooling from the melt. Therefore, amorphous material [PET*co*(**5.2**)-10] or depressed T_ms with extremely low χ_cs [PET*co*(**5.3**) and (**5.4**)-10] are observed upon DSC 2nd heating scans.

Figure 5.4 illustrates the expected, yet continued rise in T_g compared to PET following the progressive copolymerisation with comonomer **5.1**. A maximum increase in T_g of 32 °C is observed at 25 mol% **5.1** content for copolymers synthesised via the melt-copolycondensation route. The jump in T_g of 10 °C between PET*co*(**5.1**)-15 and 20 may be assigned to the crystal lattice transition,[16] whereby the copolymer may crystallise in either homopolymer crystal structure. At this point, the crystal lattice transition manifests itself at a certain composition (minimum point) for properties as a function of the composition. Moreover, it is probable that the T_g fails to increase from the 10 to 15 mol% copolymers because of the reduction in χ_c (19 to 10%). Despite the greater imide content observed upon transitioning from PET*co*(**5.1**)-10 to 15, the increase in free volume effectively counters the greater rigidity imposed on the copolymer chain.

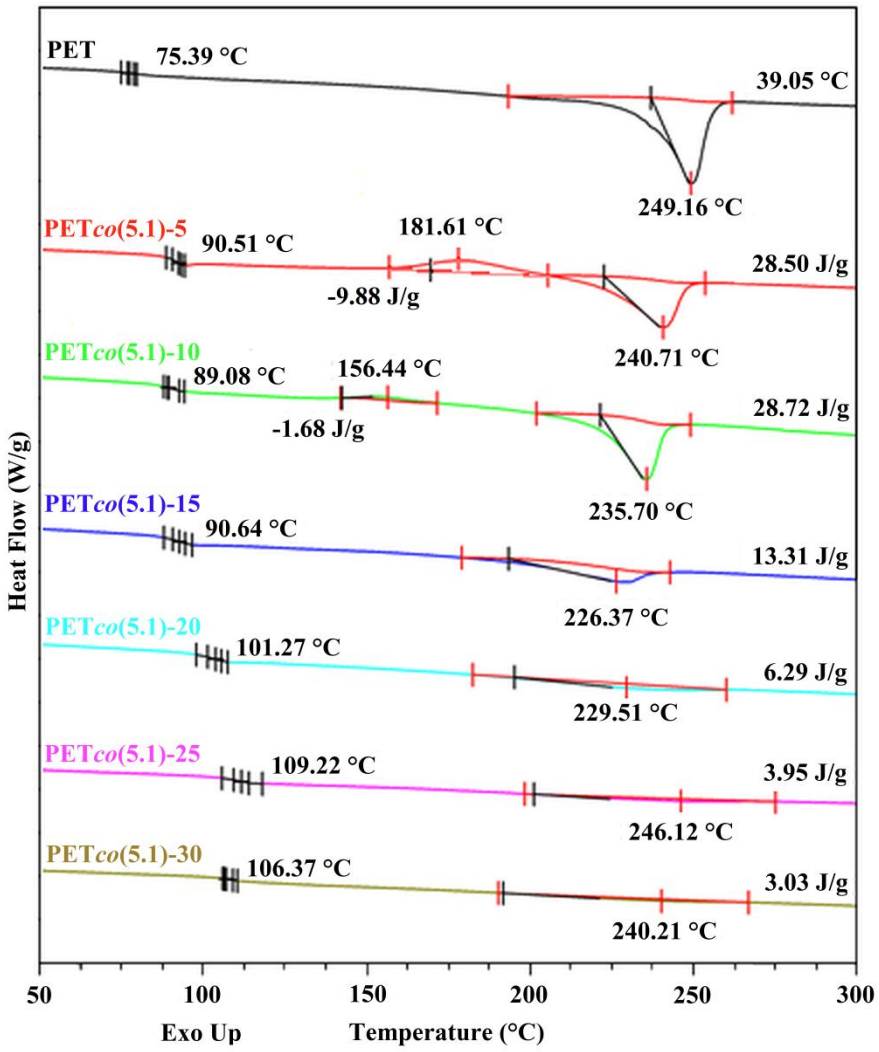

Figure 5.4 DSC 2nd heating scans (20 °C min^{-1}) of PET and selected PET*co*(**5.1**) copolymers.

Although the χ_c progressively decreases with respect to increasing levels of **5.1**, T_ms are still observed over the entire PET*co*(**5.1**) copolymer series indicating facile melt-crystallisation and semi-crystalline behaviour. It is noted that all of the copolymer T_ms are lower than that of PET, with the eutectic point for the copolymer series appearing to occur at PET*co*(**5.1**)-15 (226 °C). This evidence suggests cocrystallisation is occurring between the ester and imide residues, as previously proposed in reference to Figure 5.1. The ease of **5.1** incorporation within the PET crystal lattice is further supported by the presence of the T_{cc} peaks on the DSC reheat scans for PET*co*(**5.1**)-5 and 10.

The fall in T_m relative to PET for the PET*co*(**5.1**) copolymer series is an expected result of copolymerisation, yet the accompanied slow rise in T_m at compositions above PET*co*(**5.1**)-15 results in a copolymer series that, in theory, should still be melt-processable at an extrusion temperature of 290 °C. The validity of this statement is based upon the assumption that the

relatively high content of **5.1** does not increase the complex viscosity excessively, and that the copolymer melt is able to be mechanically stirred upon industrial scale-up.

Upon annealing the PET*co*(**5.1**) copolymer series at 200 °C for 2 hours, significant increases in ΔH_m and therefore χ_c are achieved, particularly between 5-15 mol% **5.1** incorporation (χ_c = 37 to 20%). Small increases in T_g for the majority of PET*co*(**5.1**) copolymers are observed post-anneal, most notably for PET*co*(**5.1**)-5 which has a 16 °C rise in T_g yet just a 7 °C fall in the T_m. Dual melting behaviour is observed for PET*co*(**5.1**)-5 to 15, and is again attributed to the melting of crystals formed at the annealing temperature as discussed in Chapter 3.

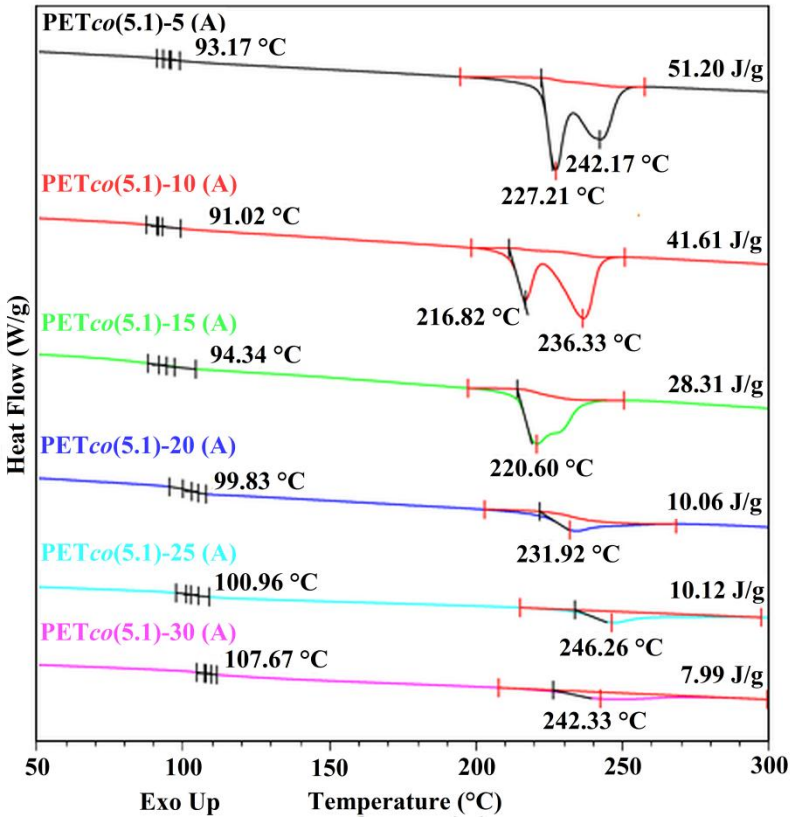

Figure 5.5 DSC 2nd heating scans (20 °C min^{-1}) of selected PET*co*(**5.1**) copolymers after annealing at 200 °C for 2 h.

DSC 1st cooling scans (5 °C min^{-1}) of the PET*co*(**5.1**) copolymer series illustrated in Figure 5.6 confirmed that all copolymers possess the ability to melt-crystallise. When compared to the T_c of PET (198 °C, 43.0 J g^{-1}) under the same conditions, addition of 5 and 10 mol% **5.1** progressively lowers the T_c to 167 and 163 °C, respectively. However, upon incorporation of > 10 mol% imide, the T_c shifts to increasingly higher temperatures, surpassing that of PET, indicating a faster crystallisation rate. This is seen for PET*co*(**5.1**)-25 in particular, whereby the supercooling temperature range has decreased from 41 to 27 °C. As was observed for the

trend in T_m (Figure 5.4), T_c exotherms are observed for the entire copolymer series emphasising the compatibility of the two comonomers within the copolymer crystal lattice. This displayed isomorphism then facilitates the appeared increase in melt-crystallisation rate, although the measured ΔH_c enthalpies progressively decrease with respect to **5.1** content.

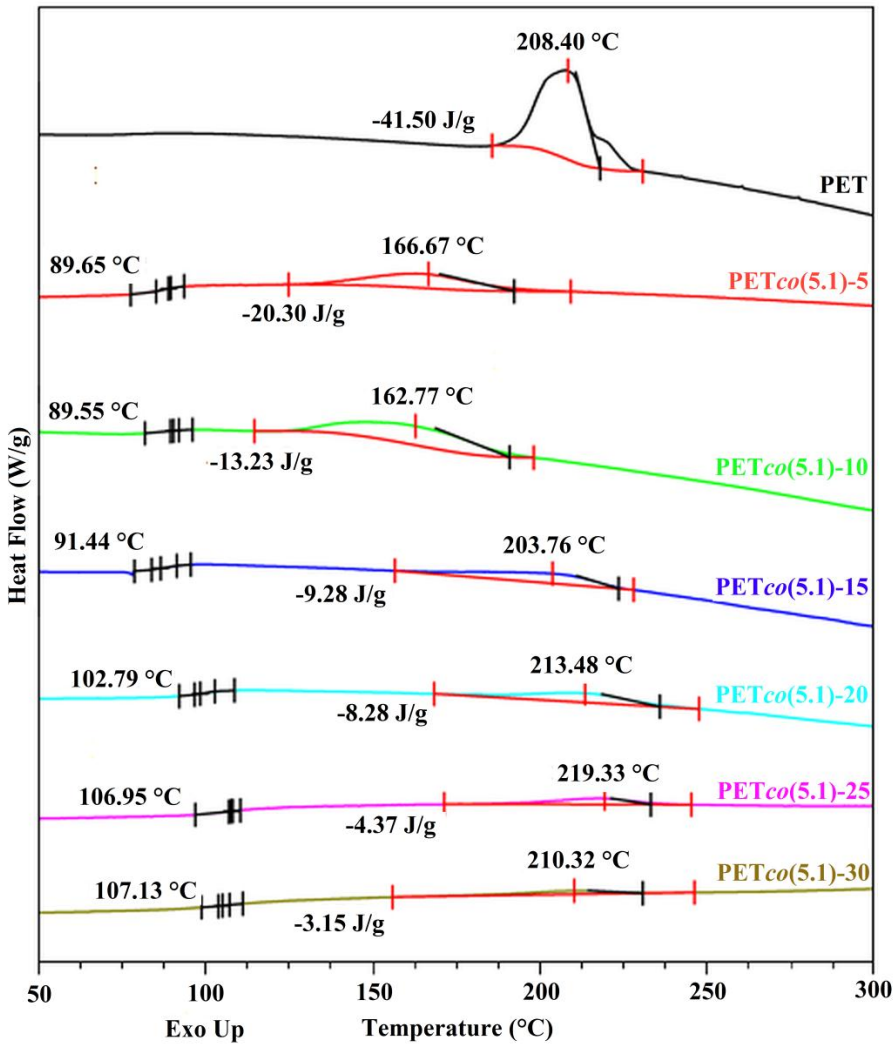

Figure 5.6 DSC 1st cooling scans (5 °C min^{-1}) of PET and selected PET*co*(**5.1**) copolymers.

The isothermal crystallisation kinetics of selected PET*co*(**5.1**) copolymers were studied by Avrami analysis,[17–20] following isothermal crystallisation at, T_i = 180-220 °C after cooling from the melt at 250 °C min^{-1} to avoid pre-crystallisation. As detailed in Chapters 2 and 3, integration of the crystallisation endotherm at T_i enabled calculation of the crystallisation half-time, $t_{0.5}$, Avrami exponent, n, and overall crystallisation rate constant, k, for each sample via construction of the Avrami plot. R^2 values > 0.99 are observed for all plots indicating a reliable method and subsequent fit of n and k values and prediction of $t_{0.5}$.

Values of *n* were determined to be in the range 1.8-2.1 for the entire copolymer series, indicating no real change in the crystallisation mechanism with respect to increasing **5.1** content or T_i. It is probable that a value of $n = 2$ represents the formation of bidimensional crystals by instantaneous nucleation, consistent with previous isothermal studies on PET.[21–23] Figure 5.7 illustrates that PET and the PET*co*(**5.1**) copolymer series (≤ 15 mol%) crystallise most rapidly at 190 °C as proposed[24] for PET, hence validating the isothermal crystallisation method developed here.

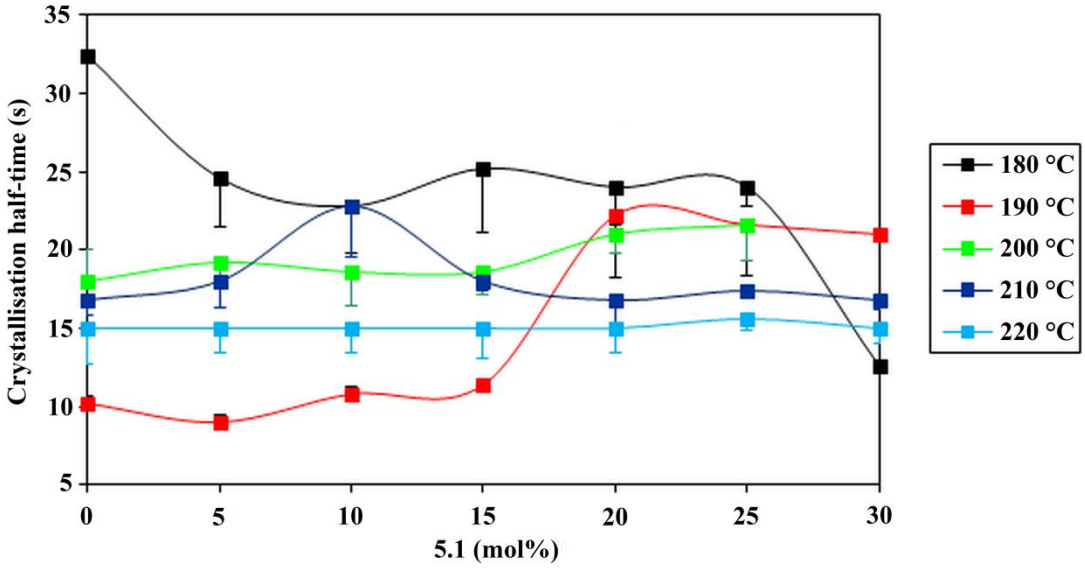

Figure 5.7 Comparative crystallisation half-times, $t_{0.5}$, of PET and selected PET*co*(**5.1**) copolymers as a function of isothermal temperature (where T_i = 180-220 °C). Error bars correspond to calculated $t_{0.5}$ values from experimentally obtained *n* and *k* values.

Incorporation of **5.1** across the range of T_i has resulted in little change in $t_{0.5}$ in comparison to PET. One of the few anomalies is that *k* is even observed to decrease when T_i = 180 °C upon increasing **5.1** content, implying that **5.1** is able to cocrystallise in a facile manner. This is supported by the $t_{0.5}$ only significantly rising at T_i = 190 °C when **5.1** content > 15 mol%. Therefore, the optimum annealing conditions used for the production of PET heat-set biaxially oriented film may be transferrable to the PET*co*(**5.1**) copolymer series.

It has been observed that the crystallisation rate of PET decreases[23] upon copolymerisation with a non-isomorphic diimide comonomer. This is due to the disruption of the regular chain structure, which in turn inhibits the chain packing arrangement of the copolymer. The $t_{0.5}$s of PET*co*(**5.2**)-5 would therefore be expected to increase relative to PET and PET*co*(**5.1**)-5, due to the introduction of a meta-kink in the copolymer chain. Although this is confirmed, as detailed in Table 5.4, the crystallisation rate of PET*co*(**5.2**)-5 is not significantly slower than that of PET. It is probable that the uninterrupted PET segments are still sufficiently flexible to

rearrange into lamellae and crystallise. This process, however, occurs on a slower time-scale in comparison to the homopolyester (PET) or to the cocrystalline copoly(ester-imide) [PET*co*(**5.1**)-5] which have no chain disruptions.

Table 5.4 Comparative crystallisation half-times (s), $t_{0.5}$, of PET, PET*co*(**5.1**)-5 and PET*co*(**5.2**)-5 as a function of isothermal temperature (where T_i = 180-220 °C).

Polymer	T_i **(°C)**				
	180	**190**	**200**	**210**	**220**
PET	32.4	10.2	18.0	16.8	15.0
PET*co*(5.1)-5	24.6	9.0	18.0	18.0	15.0
PET*co*(5.2)-5	26.4	24.0	21.0	18.0	15.6

As described previously, the synthesis of PET*co*(**5.1**) copolymers containing > 30 mol% **5.1** was not possible via the melt-polycondensation route, because of the inability to mechanically stir the comonomer mixture at temperatures below 300 °C. In order to investigate copolymers incorporating even greater **5.1** content, a solution polycondensation route was therefore utilised to synthesise PET*co*(**5.1**)-50 and **5.1** homopolymer. Scheme 5.2 shows the syntheses of these two polymers.

The degree of polymerisation was lower than commonly observed for polymers produced by the melt-polycondensation route, with η_{inh} = 0.27 dL g^{-1} observed for the **5.1** homopolymer. Analysis by DSC of PET*co*(**5.1**)-50 and **5.1** homopolymer yielded T_gs of 123 and 163 °C, respectively (Figure 5.8). All thermal properties (excluding T_c) were determined from the 1st heating scans at 20 °C min^{-1} to prevent thermal degradation at temperatures close to 400 °C.

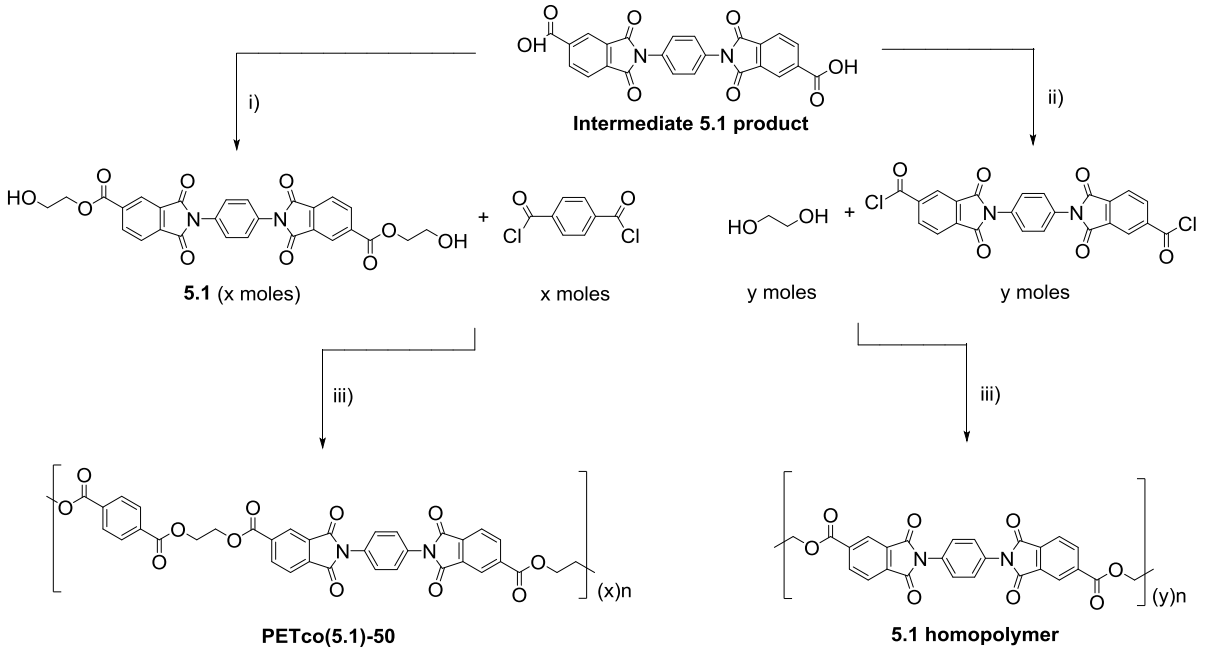

Scheme 5.2 Synthesis of PET*co*(**5.1**)-50 and **5.1** homopolymer via acid chloride route from the intermediate **5.1** product. Reaction conditions: i) 2-Bromoethanol, triethylamine, DMF, 80 ºC, 16 h; ii) $SOCl_2$, reflux, 4 h; iii) 1-Chloronaphthalene, 210 ºC, 40 h.

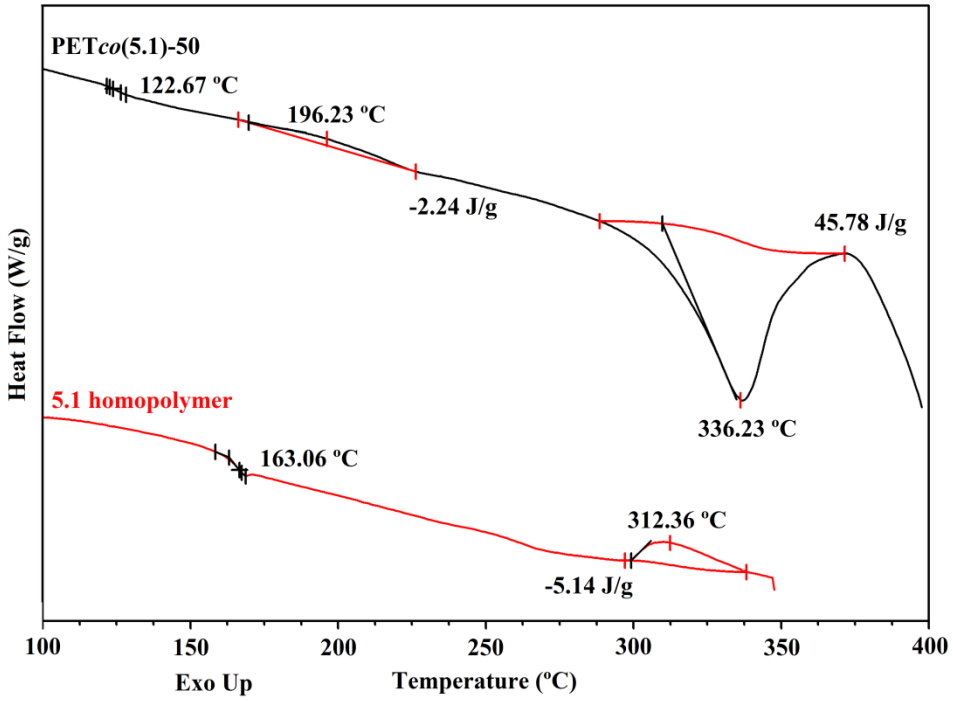

Figure 5.8 DSC 1st heating scans (20 °C min^{-1}) of PET*co*(**5.1**)-50 and **5.1** homopolymer.

A maximum rise of 88 °C in T_g across the entire PET*co*(**5.1**) copolymer series is obtained, with retention of crystallinity present at all copolymer composition ratios. Figure 5.9 illustrates this linear increase in T_g (R^2 = 0.98). The thermal properties of the PET*co*(**5.1**) copolymer series are therefore in good agreement with the Fox equation,[25] which predicts a T_g of 115 °C for PET*co*(**5.1**)-50 (against 123 °C) based upon the experimentally determined

homopolymer T_gs. Due to thermal degradation occurring from ~ 350 °C on the DSC 1st heating scan (20 °C min^{-1}), the value of T_m could not be obtained for **5.1** homopolymer, and is therefore assumed to be present at temperatures approaching 400-500 °C as observed for **3.1** homopolymer. The slight discrepancy between the theoretical and experimental T_gs is again attributed to the increased order of an alternating copolymer structure for PET*co*(**5.1**)-50 (ΔH_m = 45.78 J g^{-1}, χ_c = 31%), as discussed in Chapter 3.

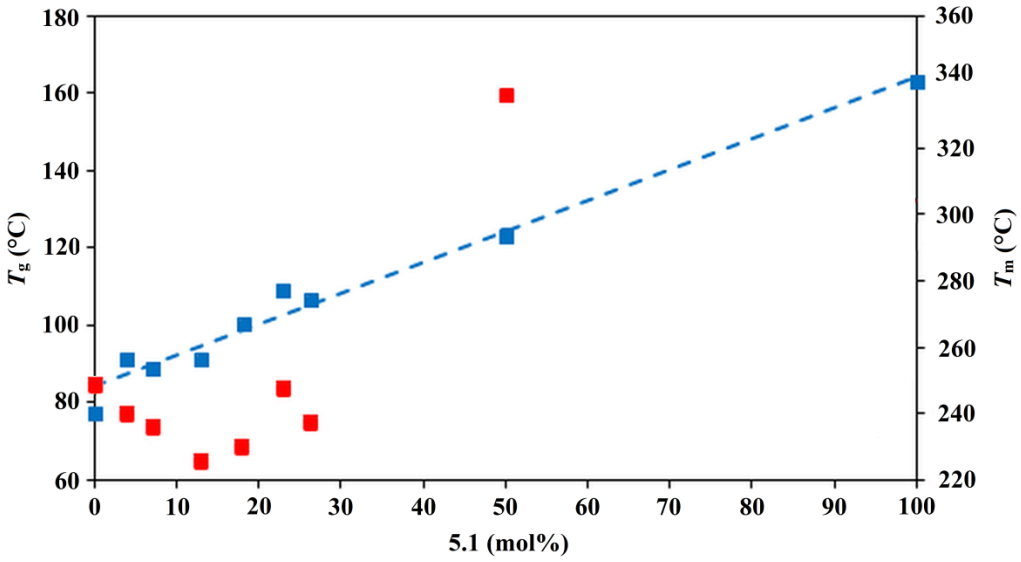

Figure 5.9 Comparative thermal properties (where T_g = blue, T_m = red) across the PET*co*(**5.1**) copolymer series.

TGA heating scans (10 °C min^{-1}) of the PET*co*(**5.1**) copolymer series revealed that the onset degradation temperatures, T_d, are only slightly lowered in comparison to PET (399-414 °C to 420 °C). This data suggests disagreement with the accepted premise[26,27] that imide residues are more thermally stable than polyesters, yet minor changes in the T_d are likely attributable to the more thermally labile ester residues. An increase in char yield (relative mass remaining at 600 °C) is observed upon increasing imide content, but this would be expected considering the relative increase in aromatic content. The melt-processing of PET*co*(**5.1**) copolymers (with < 25 mol% of **5.1** content) may therefore be undertaken at temperatures comparable to PET without significant thermal degradation occurring.

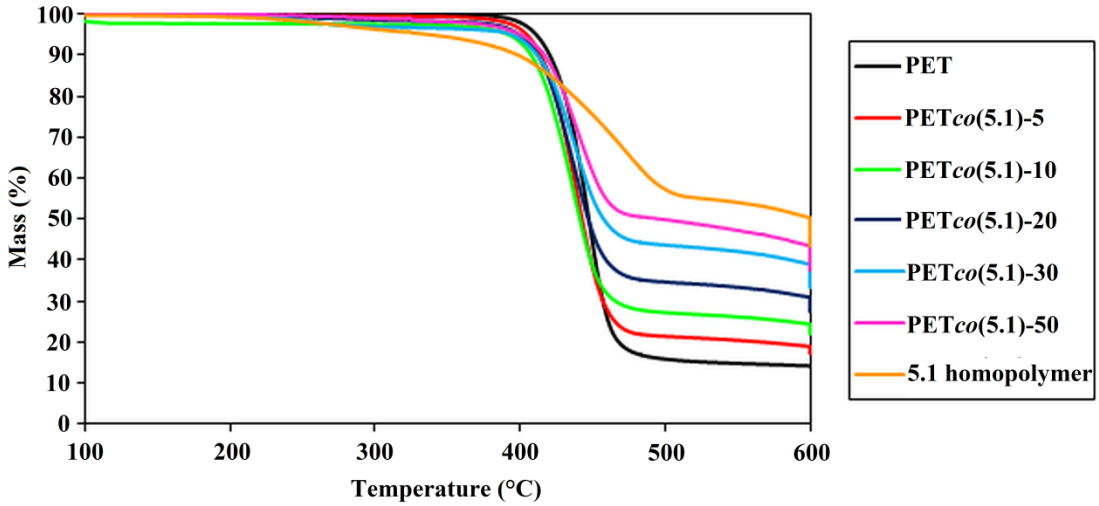

Figure 5.10 Comparative selected TGA scans (10 °C min^{-1}) across the PET*co*(**5.1**) copolymer series.

5.3.1.3 X-ray diffraction and computational modelling

Analysis of the PET*co*(**5.1**) copolymer series by X-ray powder diffraction provided further evidence of semi-crystalline behaviour, and isomorphism occurring between BHET and **5.1**. The crystal structure of PET is well-established,[28–30] as triclinic, space group $P\bar{1}$, a = 4.56, b = 5.94, c =10.75 Å, α = 98.5, β = 118, γ = 112°, ρ = 1.46 g cm^{-3}. For PET, the experimentally obtained X-ray powder diffraction pattern is in good agreement with those observed in the literature. Major peaks are observed at 2θ = 16.5 ($01\bar{1}$), 17.4 (010), 22.7 (011) and 25.7° (100).

Incorporation of 5 and 10 mol% **5.1** results in X-ray powder diffraction patterns consistent with that obtained for PET. It is established that because **5.1** is accommodated into the PET crystal lattice with ease, PET*co*(**5.1**)-10 is able to essentially crystallise as a PET analogue. However, between PET*co*(**5.1**)-15 and 25, an intermediate powder pattern emerges that appears to result from a hybrid of the PET and **5.1** homopolymer crystal phases. This intermediate PET*co*(**5.1**) crystal structure is characterised by the development of the (010) peak at 2θ = 19.2 °. This progressive change in crystal structure supports the trend in thermal properties observed previously, with the stabilisation in T_g and T_m eutectic point (Figure 5.4) both occurring at 15 mol% **5.1** content i.e. the crystal lattice transition point. The powder patterns for PET*co*(**5.1**)-30 and 50 both then clearly start to resemble that of **5.1** homopolymer, exhibited by the gradual disappearance of the ($01\bar{1}$) and (010) peaks at 2θ = 16.5 and 17.4°.

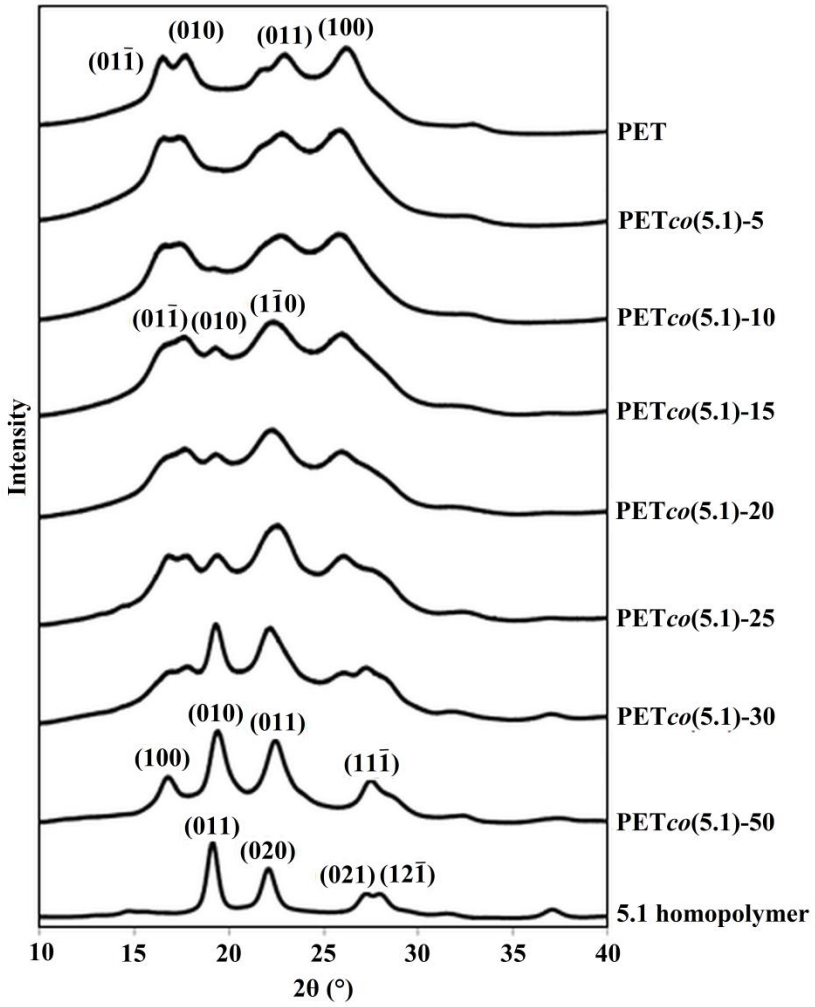

Figure 5.11 X-ray powder diffraction patterns of PET, the PET*co*(**5.1**) copolymer series and **5.1** homopolymer.

The X-ray fibre diffraction pattern for PET*co*(**5.1**)-5 provided further confirmation of the similarity in crystal morphology compared to PET. As illustrated in Figure 5.12, there is little change upon incorporation of 5 mol% **5.1**, emphasising the compatibility of the two comonomers in terms of crystallisation. Although a fibre pattern was obtained for PET*co*(**5.1**)-10, drawn fibres could not be obtained for copolymers with > 10 mol% **5.1** content. This is most probably due to insufficient molecular weights in conjunction with the limited processability of such copolymers.

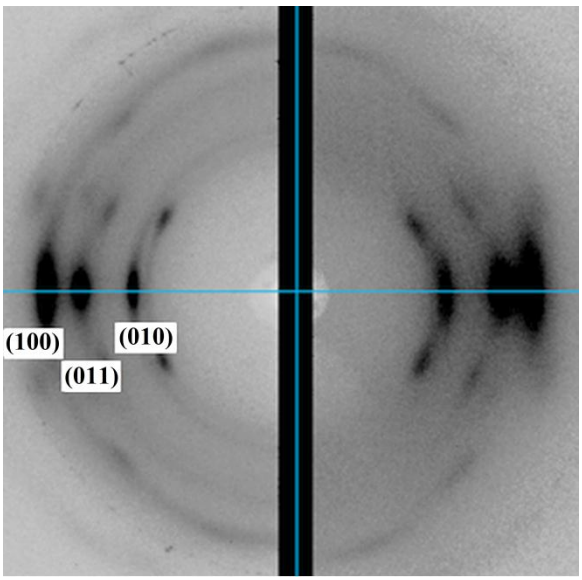

Figure 5.12 Comparative X-ray fibre diffraction patterns of PET (left) and PET*co*(**5.1**)-5 (right) drawn fibres.

The intermediate PET*co*(**5.1**) copolymer crystal structure (when **5.1** content is between 15-30 mol%) was modelled as a polymorph of PET in space group $P\bar{1}$, with the assumption that the absence of comonomer residues from the model would not have a significant effect on the powder pattern.

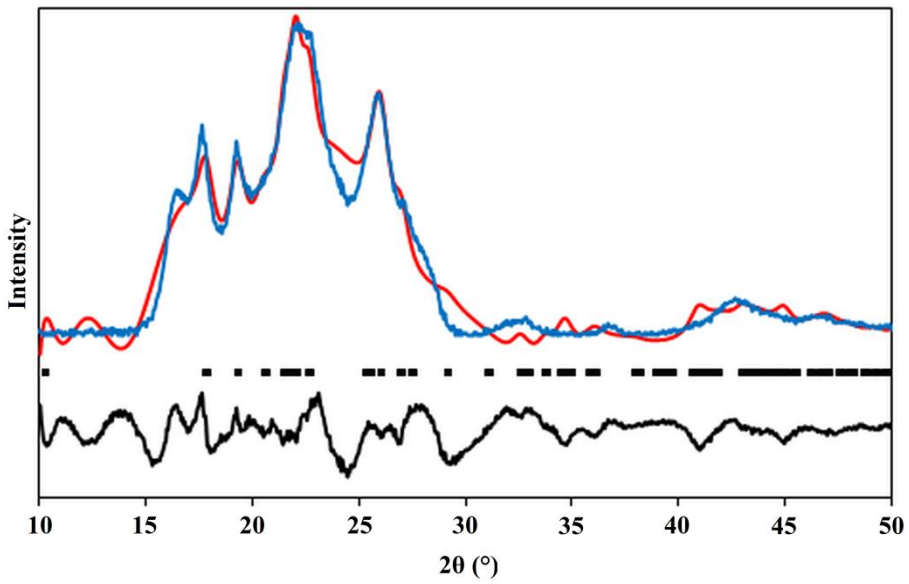

Figure 5.13 Reitveld refinement plot for PET*co*(**5.1**)-15 (R_{wp} = 13%), where blue = simulated X-ray powder diffraction pattern, red = experimental X-ray powder diffraction pattern, black rectangles = observed ticks and black = difference.

Manual adjustment of the PET unit cell parameters was then performed, after confirming that the experimental powder pattern for PET was in reasonably good agreement with the simulated powder pattern constructed from the fractional atomic coordinates and cell parameters stated in the literature.[30]

Reitveld refinement (R_{wp} = 13%) of the adjusted, simulated intermediate PET*co*(**5.1**) model against the experimental powder pattern of PET*co*(**5.1**)-15 (Figure 5.13) gave a crystal structure in space group $P\bar{1}$, cell parameters a = 4.56, b = 5.61, c = 10.44 Å, α = 98.3, β = 115.0, γ = 116.1°, ρ = 1.42 g cm^{-3}. In comparison to the cell parameters of PET, there is a small observable difference (maximum of ± 6%) upon incorporation of 15 mol% **5.1**. However, as illustrated in Figure 5.14, this intermediate PET*co*(**5.1**)-15 crystal phase may just be considered as a distorted PET crystal lattice in a similar manner to α-PBN and PBN*co*(**4.1**)-20 in Chapter 4.

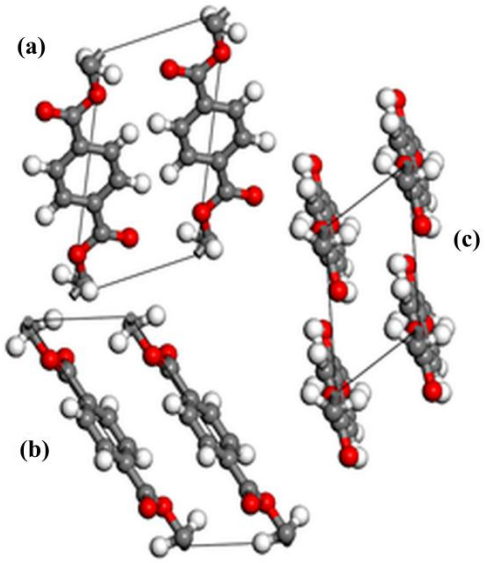

Figure 5.14 Proposed crystal structure of the PET*co*(**5.1**) copolymer series (modelled as a polymorph of PET) when relative **5.1** content is between 15-30 mol%. Viewed along the *a*, *b* and *c*-axes of the unit cell.

Studies of the PET*co*(**5.1**)-50 and **5.1** homopolymer crystal structures were also undertaken via computational modelling,[31,32] but these could not be simply regarded as a polymorphs of PET due to their obvious differences in terms of X-ray powder diffraction patterns (Figure 5.11). Instead, the molecular structures and unit cells of PET*co*(**5.1**)-50 (alternating copolymer) and **5.1** homopolymer were explicitly constructed in Materials Studio. Symmetry operations corresponding to various possible space groups were introduced, until geometric optimisation of all cell parameters afforded a reasonable qualitative match between the simulated and experimental powder patterns (as detailed in Chapter 2). Refinement methods (Pawley and Reitveld) were then used to improve the respective simulated crystal structures.

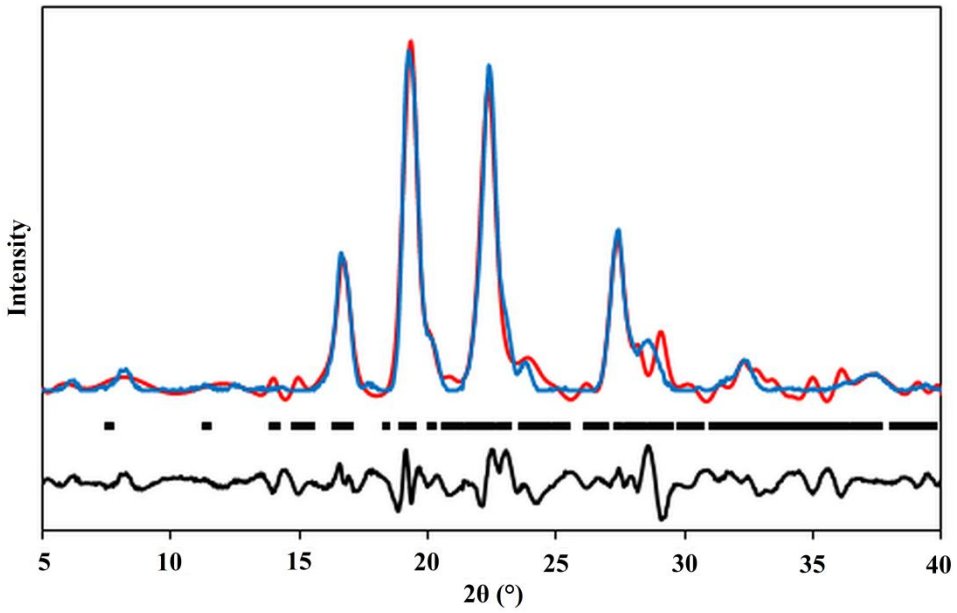

Figure 5.15 Reitveld refinement plot for PET*co*(**5.1**)-50 (R_{wp} = 15%), where red = simulated X-ray powder diffraction pattern, blue = experimental X-ray powder diffraction pattern, black rectangles = observed ticks and black line = difference.

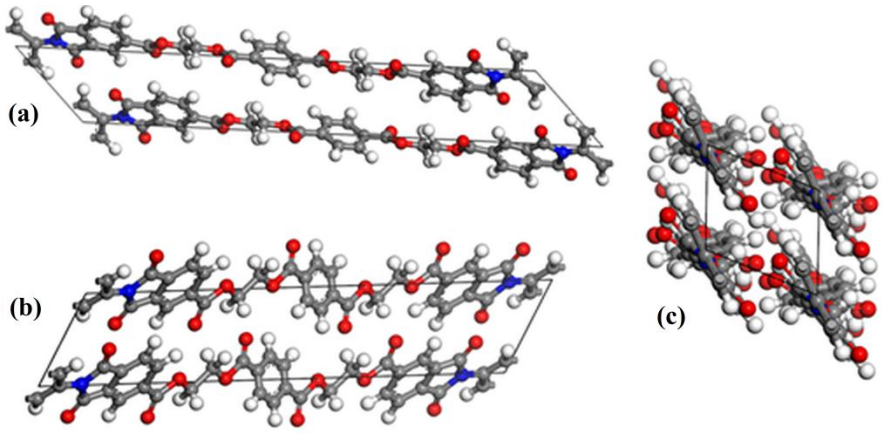

Figure 5.16 Proposed crystal structure of PET*co*(**5.1**)-50 viewed along the *a*, *b* and *c*-axes of the unit cell.

Following Reitveld refinement (R_{wp} = 15%) of the constructed model for PET*co*(**5.1**)-50 against the experimental powder pattern, it is observed that the crystal structure of PET*co*(**5.1**)-50 also adopts the same symmetry as PET in space group $P\bar{1}$ (Figure 5.16) but with an extended *c*-axis due to the increase in the chain repeat length. Cell parameters for the PET*co*(**5.1**)-50 crystal structure are proposed as a = 6.00, b = 6.04, c = 34.85 Å, α = 129.9, β = 110.5, γ = 91.7°, ρ = 1.56 g cm^{-3}.

However, the **5.1** homopolymer was found to adopt a very different though still centrosymmetric structure, in the monoclinic space group $P2_1/c$. As illustrated in Figure 5.17, one polymer chain is surrounded by four adjacent chains, one at each corner of the cell and so each contributing ¼ of a chain to the cell, which therefore contains two chains in total.

Despite the symmetry operations being considerably different from the PET, PET*co*(**5.1**)-15 and PET*co*(**5.1**)-50 crystal structures in the triclinic space group $P\bar{1}$, the structure is consistent with those of several polyimides, oligomeric poly(*p*-phenylene)s and the **3.1** homopolymer discussed in Chapter 3.[33,34]

The molecular chain within the **5.1** homopolymer crystal structure is not coplanar, with the *p*-phenylene unit adopting a ring twist with respect to the phthalimide and ethylene units. Although intermolecular forces and ring conjugation restrict poly(*p*-phenylene) to adopt a planar conformation, non-planar conformations are observed for isolated polyphenyls.[35] As the *p*-phenylene unit in **5.1** homopolymer is essentially isolated, it appears that the repulsive forces of the adjacent *o*-hydrogens forces the *p*-phenylene unit to twist.

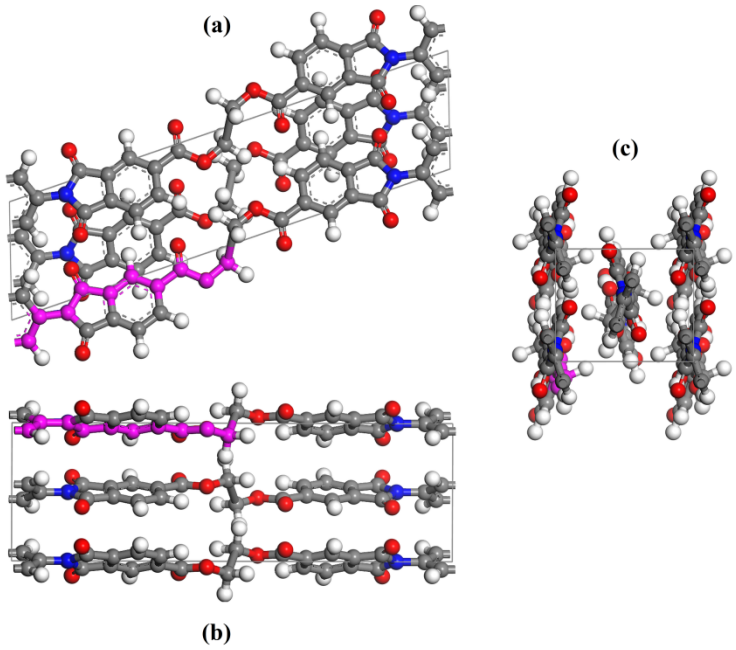

Figure 5.17 Proposed crystal structure of **5.1** homopolymer viewed along the *a*, *b* and *c*-axes of the unit cell, with the asymmetric unit highlighted in pink.

The plausibility of the proposed **5.1** homopolymer crystal structure is reflected in the extremely good match between the experimental and simulated powder patterns, following Reitveld refinement (R_{wp} = 10%, Figure 5.18). The cell parameters of this novel system are proposed as a = 5.78, b = 8.05, c = 21.32 Å, β = 79.3°, ρ = 1.51 g cm^{-3}.

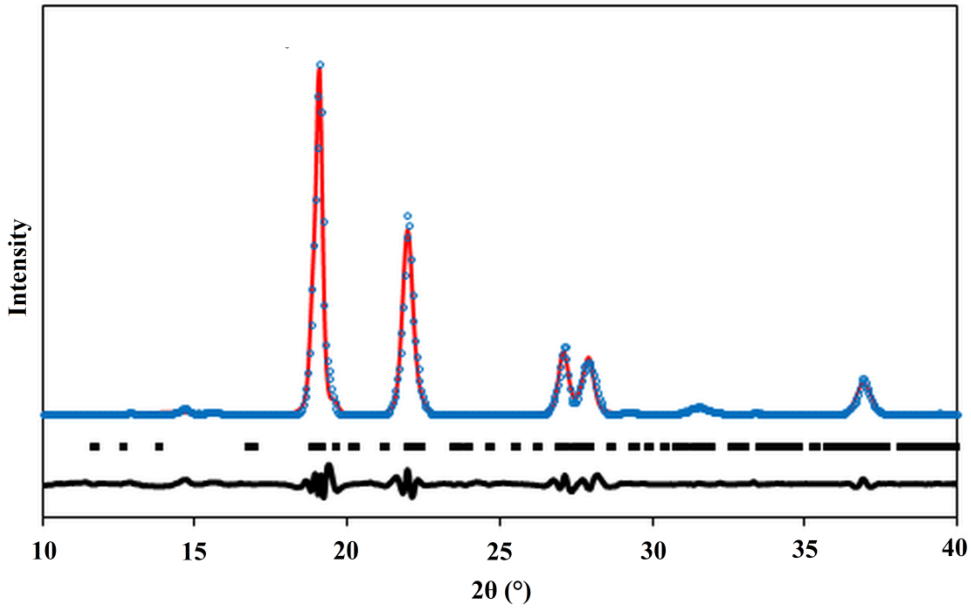

Figure 5.18 Reitveld refinement plot for **5.1** homopolymer (R_{wp} = 10%), where red = simulated X-ray powder diffraction pattern, blue = experimental X-ray powder diffraction pattern, black rectangles = observed ticks and black line = difference.

5.3.2 Investigation of PET-based copoly(ester-imide)s containing rigid diimide units

5.3.2.1 Introduction

It has been established that the T_g of PET may be raised via copolymerisation with a rigid isomorphic comonomer (**5.1**), which in turn has enabled the anomalous retention of semi-crystalline behaviour. The rise in T_g relative to imide content following copolymerisation is relatively low however. For example, the T_g of PET*co*(**5.1**)-15 is 91 °C, which approximates to a 1 °C rise in T_g per **5.1** mol%. It was therefore speculated whether the inclusion of a rigid non-isomorphic tetracarboxylic diimide comonomer would yield a greater rise in T_g, as observed for PET*co*(**3.1**)-25 (increase of 46 °C) in Chapter 3.

The notion of incorporating a structurally similar diimide comonomer to **3.1** appeared achievable, but was clearly required to be included at significantly lower content than 25 mol% to avoid the formation of amorphous materials. A targeted copolymer composition ratio of 10 mol% would therefore aim to sufficiently increase the T_g relative to PET, without disrupting the melt-crystallisation process required for retention of crystallinity. The χ_c may then be proposed to increase via thermal or stress-induced crystallisation post-polymerisation.

5.3.2.2 Polymer synthesis and characterisation

The novel rigid diimide comonomers *N*,*N*'-bis-(2-hydroxyalkyl)-benzophenone-3,4,3',4'-tetracarboxylic diimide (**5.5**), *N*,*N*'-bis-(2-hydroxyalkyl)-diphenylsulfone-3,4,3',4'-

tetracarboxylic diimide (**5.6**) and *N*,*N*'-bis-(2-hydroxyalkyl)-bicyclo-[2,2,2]-oct-7-ene-2,3,5,6-tetracarboxylic diimide (**5.7**) were readily synthesised from the respective tetracarboxylic dianhydride and 2-aminoethanol in moderate to good yields (59-81%).

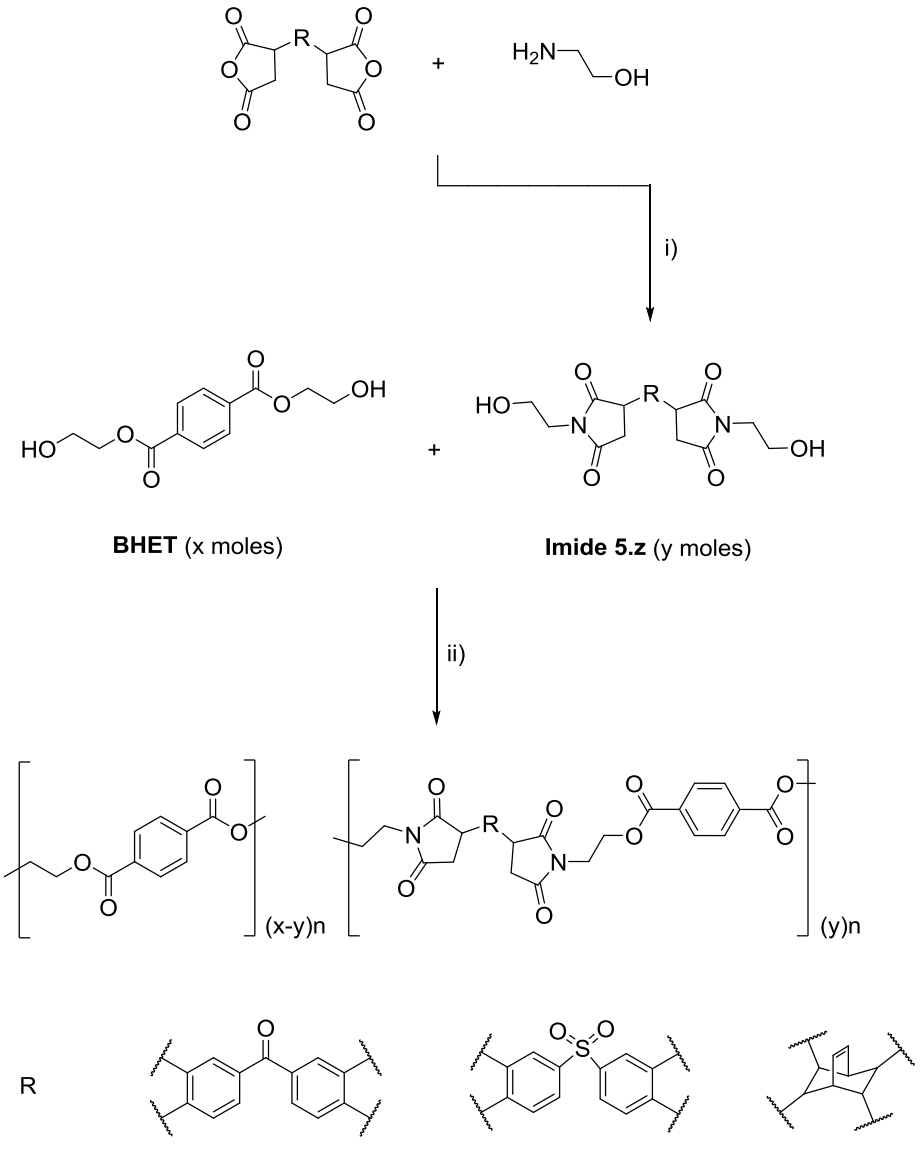

Comonomer (z)	**5.5**	**5.6**	**5.7**
Yield (%) for i)	59	59	81

Scheme 5.3 Synthesis of PET-based copoly(ester-imide)s via melt-copolymerisation of bis(2-hydroxyethyl) terephthalate (BHET) with selected diimide comonomers (**5.5 – 5.7**), where y ≤ x. Reaction conditions: i) DMF, reflux, 16 h and ii) Sb_2O_3, 290 °C, 2.5 h, < 1mbar.

Copolycondensation of **5.5**-**5.7** at 10 mol% with respect to BHET via the laboratory-scale melt-polycondensation rig afforded a range of copoly(ester-imide)s (Scheme 5.3), that exhibited comparable molecular weight distributions (Table 5.5) in comparison to PET (M_w = 17,800-27,500 Da and η_{inh} = 0.35-0.45 dL g^{-1}). Furthermore, analysis by ^{1}H NMR

spectroscopy revealed that the copolymer composition ratios matched the initial comonomer feed ratios, for all copolymers, indicating successful copolymerisations.

Table 5.5 Molecular weight distributions, dispersities and inherent viscosities of PET and selected PET-based copoly(ester-imide)s.

Polymer	M_w [a]	M_n [a]	M_z [a]	Đ	η_{inh} [b]
	Da	Da	Da	-	dL g^{-1}
PET	20,600	6,360	37,500	3.2	0.75
PET*co*(**5.5**)-10	19,900	5,550	44,700	3.6	0.35
PET*co*(**5.6**)-10	17,800	5,030	38,500	3.5	0.39
PET*co*(**5.7**)-10	27,500	5,190	15,100	2.9	0.45

[a] Determined by GPC (HFIP eluent). [b] Determined by solution viscometry ($CHCl_3$:TFA (2:1 v/v) eluent).

5.3.2.3 Thermal properties

DSC analysis (2nd heating scans, 20 °C min^{-1}) of the 10 mol% copolymers revealed significant increases in T_g relative to PET, with a minimum increase of 23 °C observed for PET*co*(**5.5**)-10 (Figure 5.19). This observation indicates that the choice of imide substrates has been successful in terms of increased thermal performance. However, there is no observable T_c or T_m peak for PET*co*(**5.5**)-10 and PET*co*(**5.6**)-10 signifying amorphous materials. Incorporation of **5.5** and **5.6** is therefore representative of the discussed literature in Chapter 1, whereby the inclusion of relatively small amounts of foreign comonomer inhibits the melt-crystallisation of PET.

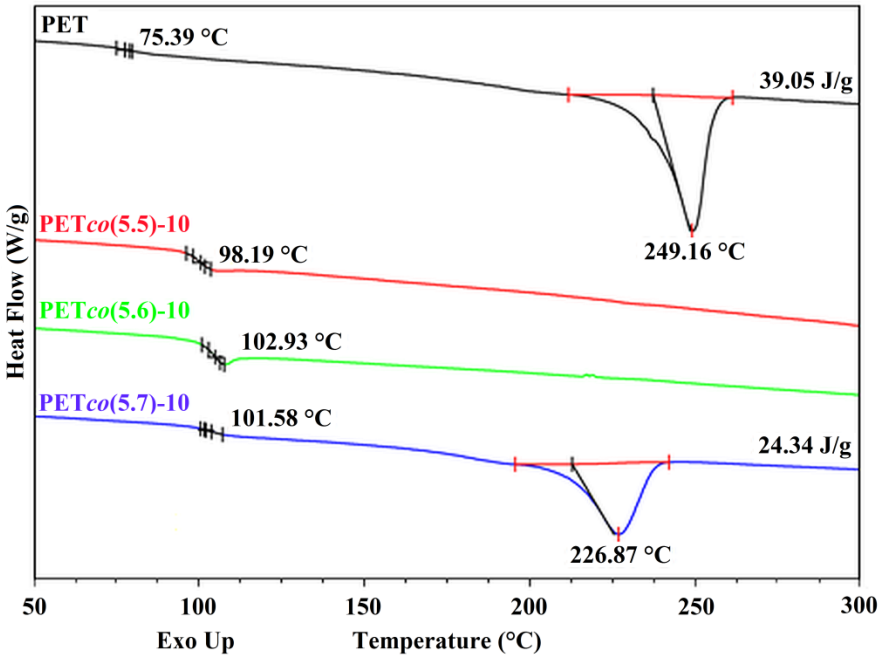

Figure 5.19 DSC 2nd heating scans (20 °C min^{-1}) of selected copoly(ester-imides).

Incorporation of 10 mol% **5.7** with PET, in contrast, affords a copoly(ester-imide) with a T_g of 102 °C *and* a T_m of 227 °C. It is noted that although PET*co*(**5.7**)-10 exhibits a reasonable χ_c (17%), semi-crystalline behaviour disappears entirely upon inclusion of **5.7** at 15 mol%. As the onset of crystallinity loss is encountered at a higher level of imide content, this suggests that the chain length of **5.7** is more compatible with PET than **5.5** and **5.6**.

Although PET*co*(**5.5**)-10 and PET*co*(**5.6**)-10 lack the ability to melt-crystallise and thus exhibit semi-crystalline behaviour upon reheat, Figure 5.20 illustrates that significant levels of crystallinity may be thermally induced following a 2 h anneal at 200 °C. In addition to possessing χ_cs > 25%, the T_gs of PET*co*(**5.5**)-10 and PET*co*(**5.6**)-10 have also increased by at least 10 °C post-anneal. It is probable that such rises in T_g originate from the introduction of crystallinity into the copolymer, which consequently reduces the amount of free volume available.[36]

For a semi-crystalline copolymer that has been subject to the same annealing conditions such as PET*co*(**5.1**)-10 or PET*co*(**5.7**)-10, the rise in T_g is much smaller post-anneal (2 and 4 °C respectively) as the relative change in χ_c is smaller. As PET*co*(**5.5**)-10 is the cheapest copolymer to manufacture yet possesses a comparable T_g to PET*co*(**5.6**)-10 and PET*co*(**5.7**)-10, it was selected as the preferred choice for industrial scale-up and subsequent film production.

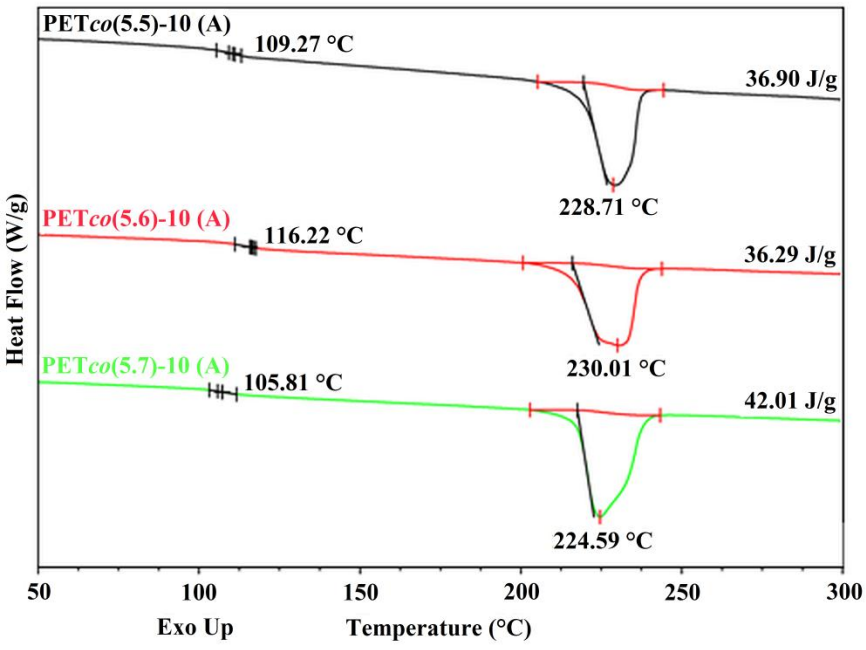

Figure 5.20 DSC 2nd heating scans (20 °C min^{-1}) of selected PET-based copoly(ester-imides) following 2 h anneal at 200 °C.

5.3.3 Production of PET-based copoly(ester-imide) biaxially oriented film

The synthesis of several PET-based novel copoly(ester-imide)s has been discussed thus far, whereby such copolymers all display enhanced T_gs in relation to PET. This has been achieved via two separate routes: copolymerisation with an isomorphic comonomer (**5.1**); and copolymerisation with non-isomorphic comonomers (**5.5**-**5.7**). Despite the retention of semi-crystalline behaviour, the increase in T_g is relatively smaller upon 10 mol% incorporation of **5.1** compared to **5.5** post-anneal (rises of 16 and 34 °C respectively).

Figure 5.21 illustrates the rheological properties of PET*co*(**5.5**)-10 against various PET*co*(**5.1**) copolymers. It is observed that upon the increasing addition of **5.1** content, accompanied with retention of semi-crystalline behaviour and maintenance of the T_m, η* rises from 374 to 1134 Pa s (290 °C) at 5 and 15 mol% **5.1**, respectively. Therefore, despite the stabilisation of the T_m below 300 °C for the entire PET*co*(**5.1**) copolymer series, incorporation of the rigid comonomer **5.1** at levels > 10 mol% results in a unprocessable copolymer melt. In contrast, PET*co*(**5.5**)-10 displays shear thinning behaviour with respect to temperature. This is expected considering the amorphous nature of PET*co*(**5.5**)-10 pre-anneal (Figure 5.19), which renders it melt-processable at 290 °C.

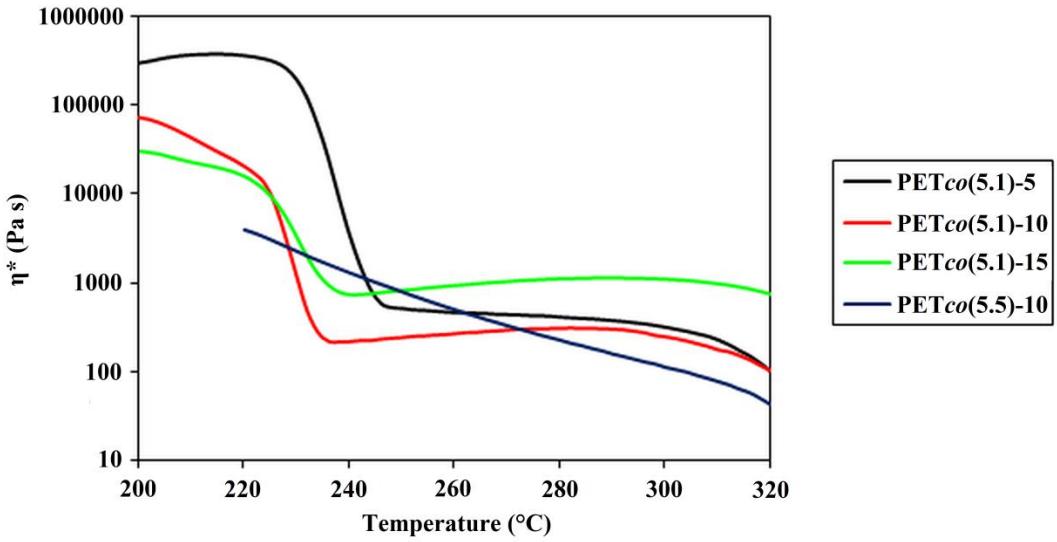

Figure 5.21 Comparative rotational rheology analysis of PET*co*(**5.1**)-5, 10, 15 and PET*co*(**5.5**)-10 performed in temperature sweep mode (heating rate of 4 °C min^{-1}, frequency of 10 rad s^{-1} and 5% strain).

In the relative time-scale of this research project, the production of PET*co*(**5.5**)-10 biaxially oriented film was therefore prioritised over any PET*co*(**5.1**) copolymer variant. This decision was aided by the facile one-step synthesis of **5.5**, which resulted in lowered scale-up costs in comparison to the two-step synthesis of **5.1**. Moreover, it was envisaged that the annealing studies performed on PET*co*(**5.5**)-10 in chip form would be transferrable to film.

Semi-crystalline behaviour could therefore be introduced via stress (forward and/or sideways draw) or thermal-induced crystallisation (annealing) during the film production process. This process was observed during the production of PEN*co*(**3.1**) heat-set biaxially oriented film in Chapter 3, which exhibited comparable χ_cs to those observed in chip form.

PET*co*(**5.5**)-10 was synthesised on an industrial-scale by melt-copolymerisation of DMT, **5.1** and EG, as detailed in Chapters 2 and 3. SSP performed on PET*co*(**5.5**)-10 (200 °C for 16 hours under dynamic vacuum) demonstrates how thermal-induced crystallisation may be utilised to raise the χ_c of PET*co*(**5.5**)-10 within an industrial context (Table 5.6), in the same manner as the previous DSC annealing studies (Figure 5.20). It is observed that PET*co*(**5.5**)-10 possesses a χ_c of 24% post-SSP, with a T_m of 232 °C. Although this represents an obvious improvement in the χ_c compared to an amorphous material pre-SSP, it is still ~ 50% of PET indicating that the melt-crystallisation process has been significantly hindered.

Table 5.6 Comparative thermal properties and molecular weight distributions of PET and PET*co*(**5.5**)-10 pre- and post-SSP.

Property	**Unit**	**PET**		**PET*co*(5.5)-10**	
		Pre-SSP	**Post-SSP**	**Pre-SSP**	**Post-SSP**
T_m [a/b]	**°C**	249	252	-	232
ΔH_m [a/b]	**J g^{-1}**	39.05	67.58	-	33.52
χ_c	**(%)**	28	48	-	24
M_w [c]	**Da**	29,500	38,400	26,100	86,200
M_n [c]	**Da**	5,230	7,870	4,930	6,620
M_z [c]	**Da**	52,700	69,400	68,500	481,000
Đ	**-**	5.6	4.9	5.3	13.0
CH_2OH end groups [d]	**/100 repeat units**	1.32	1.12	1.50	1.16

[a] Determined by DSC 2nd heating scan (20 °C min^{-1}). [b] Determined by DSC 1st heating scan (20 °C min^{-1}). [c] Determined by GPC (HFIP eluent). [d] Determined by ^{1}H NMR spectroscopy.

GPC analysis of the industrially produced PET*co*(**5.5**)-10 pre-SSP revealed a comparable molecular weight distribution in comparison to PET, with M_ws of 26,100 and 29,500 Da observed, respectively. In both cases, the molecular weights (determined by all parameters) were significantly increased post-SSP indicating successful transesterification and esterification reactions in the solid state.[37–39] This is supported by the observed reduction in hydroxyl end groups for PET and PET*co*(**5.5**)-10 of ~ 25%, highlighting how SSP may be used as an additional post-polymerisation route to enhance the performance of such copoly(ester-imide)s. For PET, M_w, M_w and M_z all increase at the same ratio post-SSP to give a comparable Đ value of 4.9. In contrast, the M_w and M_z dramatically increase for

PET*co*(**5.5**)-10 to 86,200 and 481,100 Da, respectively. This substantial rise in M_z is credited to the formation of a small quantity of very high molecular weight material, as observed in the molecular weight distributions of PET*co*(**5.5**)-10 pre- and post-SSP (Figure 5.22).

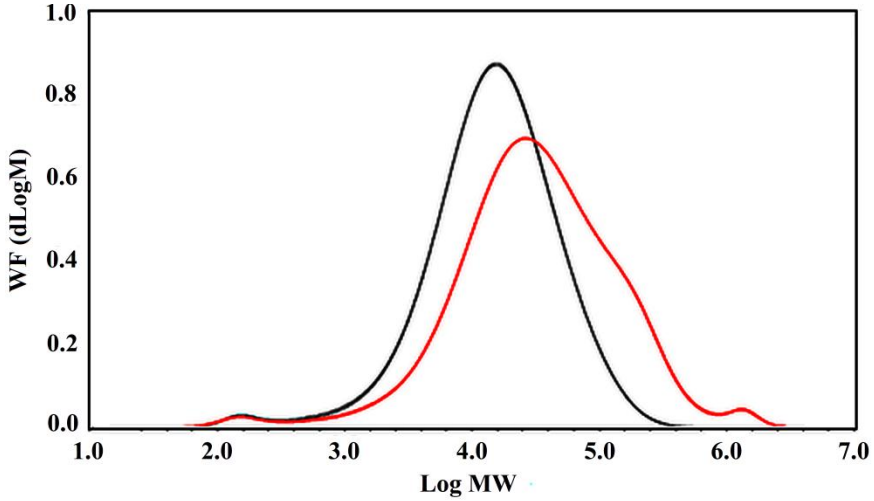

Figure 5.22 Comparative molecular weight distributions of PET*co*(**5.5**)-10 pre- (black) and post-SSP (red).

The anomalously high rise in M_w and M_z for PET*co*(**5.5**)-10 post-SSP may be explained by inter-molecular crosslinking, facilitated by the benzophenone residue in **5.5** and the susceptible β-methylene unit in linear PET (Scheme 5.4).[40,41] This process is established[42] to occur photochemically in PET-based copolymers containing benzophenone units via hydrogen atom abstraction from the benzophenone excited triplet state.

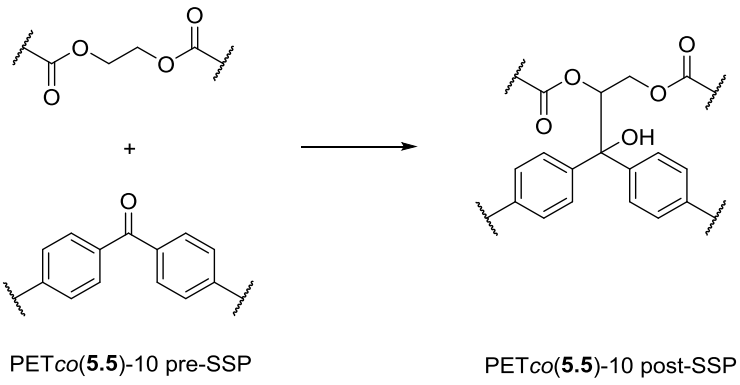

Scheme 5.4 Discussed intermolecular crosslinking mechanism for PET*co*(**5.5**)-10.

However, it is questionable whether this process would have occurred under SSP conditions with no accelerated UV irradiation present. The greater variation in M_z may therefore be attributed to the formation of high molecular weight PET*co*(**5.5**)-10 from a melting-recrystallisation-remelting process.[43] As the T_m onset for PET*co*(**5.5**)-10 post-anneal is ~ 200 °C, the chosen SSP temperature of 200 °C was likely correct for PET yet too high for PET*co*(**5.5**)-10.

Cast PET and PET*co*(**5.5**)-10 film were simultaneously biaxially drawn at 110 and 130 °C, respectively on the Long stretcher. The biaxially oriented samples were then heat-set in a crystallisation rig at 220 and 170 °C for 10 s, to afford heat-set biaxially oriented films as illustrated in Figure 5.23. The inclusion of **5.5** has clearly discoloured PET*co*(**5.5**)-10 relative to PET, as commonly observed in aromatic polyimides due to macromolecular chain conjugation.[44]

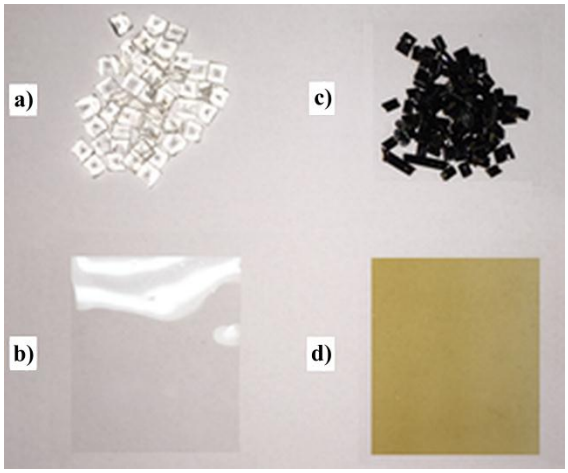

Figure 5.23 Comparison of industrial-scale polymer chip and heat-set biaxially oriented film of PET [a) and b), resepectively] and PET*co*(**5.5**)-10 [c) and d) respectively].

The successful induction of semi-crystalline behaviour in PET*co*(**5.5**)-10 was confirmed by DSC and film density analysis. In comparison to the amorphous cast film, PET*co*(**5.5**)-10 heat-set biaxially oriented film possesses a T_g of 102 °C and T_m of 214 °C (1st heating scan, 20 °C min^{-1}, χ_c = 15%). Figure 5.24 further illustrates that the final χ_c obtained post-anneal for PET*co*(**5.5**)-10 is lower than PET (52 and 38%, respectively).

Although the film densities are not strictly comparable due to the difference in annealing temperatures, it is further evidence (Table 5.6) that a sufficient χ_c may not be solely induced by post-polymerisation methods for a non-isomorphic copoly(ester-imide). This observation may be explained by just 10% of the total χ_c in PET*co*(**5.5**)-10 originating from thermal-induced crystallisation. Annealing temperatures above 170 °C were trialled in an effort to increase the χ_c gained, but only afforded film failure due to the partial melting of PET*co*(**5.5**)-10.

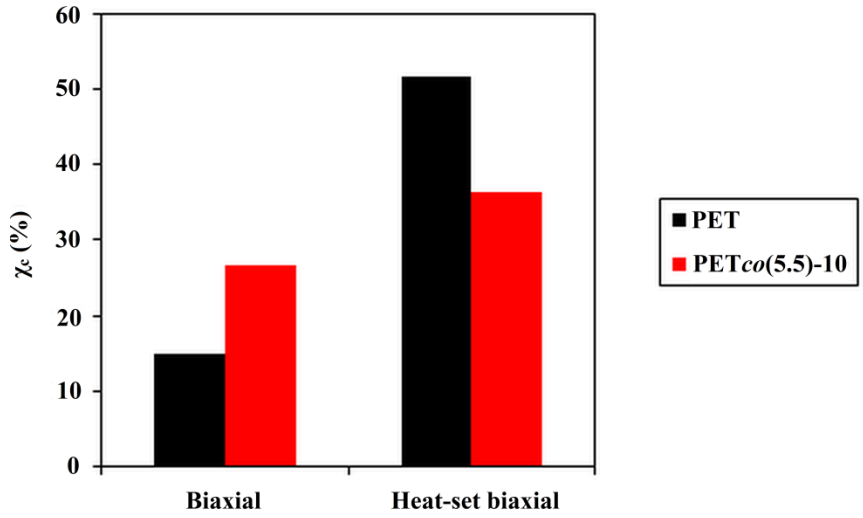

Figure 5.24 Crystallinity analysis of PET and PET*co*(**5.5**)-10 where biaxial = biaxially oriented film and heat-set biaxial = heat-set biaxially oriented film (PET annealed at 220 °C for 10 s, PET*co*(**5.5**)-10 annealed at 170 °C for 10 s).

Following the production of thermally enhanced PET-based film on a laboratory-scale, PET*co*(**5.5**)-10 heat-set biaxially oriented film was manufactured on the industrial-scale film line. Table 5.7 details the drawing and annealing conditions used for this process.

Table 5.7 Industrial-scale film line conditions for the production of PET and PET*co*(**5.5**) heat-set biaxially oriented film.

Film line component	**PET**	**PET*co*(5.5)-10**
	Temperature (°C)	
Extruder	280	270
Forward draw	85	110
Sideways draw	90	125
Stenter pre-heat	110	115
Stenter crystallisation	220	170

DMA (1st heating scan, 4 °C min^{-1}) of the obtained heat-set biaxially oriented films demonstrates the superior thermal properties of PET*co*(**5.5**)-10 in comparison to PET (Figure 5.25). Evaluation of the G' onset temperatures afforded T_gs of 84 and 101 °C, respectively, which is in agreement with the DSC measurement of PET*co*(**5.5**)-10 biaxially heat-set oriented film produced on the Long stretcher.

However, at 25 °C, the G' of PET*co*(**5.5**)-10 is ~ 60% of the PET value. This reduction in mechanical stiffness is due to the lowered χ_c in PET*co*(**5.5**)-10 as previously determined by DSC and film density analysis. Another consequence of lowered crystallinity is that the residual G' observed, above the T_g, decreases to zero indicating an amorphous material.[45,46] The thermomechanical performance of PET*co*(**5.5**)-10 may therefore be considered inferior

to PET, as the film is essentially unusable above the T_g. To obtain satisfactory thermomechanical properties for a PET-based copoly(ester-imide), it is probable that an isomorphic comonomer such as **5.1** must be included. Although PET*co*(**5.1**)-5 has a T_g ~ 10 °C lower than PET*co*(**5.5**)-10, it would likely possess a sufficient χ_c for improved thermomechanical performance. This is inferred following comparative tensile analysis of PET and PET*co*(**5.1**)-5 fibres, with E values of 413 and 1191 MPa observed, respectively.

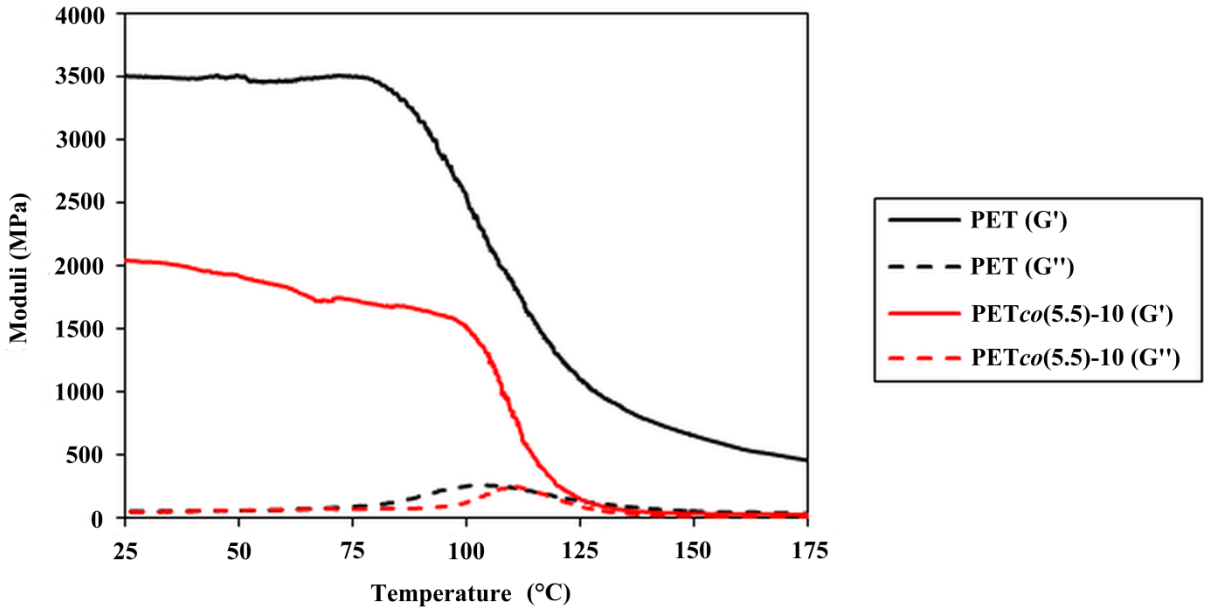

Figure 5.25 DMA heating scan (4 °C min^{-1}) at constant frequency (10 Hz) and strain (0.1%) of PET and PET*co*(**5.5**)-10 heat-set biaxially oriented film.

5.4 Conclusions

The thermal performance of PET has been increased following the separate copolymerisations with an isomorphic nitrogen-linked phthalimide imide comonomer, **5.1**, and several non-isomorphic diimide comonomers, **5.5**-**5.7**. Retention of semi-crystalline behaviour was obtained via cocrystallisation and thermal-induced crystallisation post-polymerisation, respectively.

Copolymerisation of PET with **5.1** afforded a novel copoly(ester-imide) series where the T_g may be tuned between 75-163 °C, depending on the copolymer composition ratio. Facile incorporation of **5.1** in the PET crystal lattice enabled relatively high χ_cs upon melt-crystallisation and annealing. Furthermore, the isomorphic behaviour of BHET and **5.1** ensures that there is no adverse effect upon the crystallisation rate or mechanism in comparison to PET, despite significant **5.1** inclusion. Although the T_ms of the PET*co*(**5.1**) copolymer series all occur below 300 °C, addition of > 10 mol% **5.1** raises η* sufficiently to render any copolymer unprocessable in melt form at 290 °C. Therefore, PET*co*(**5.1**)-5

(T_g = 91 °C, T_m = 241 °C) was identified as the priority copolymer for future industrial scale-up and film production. The structural morphology of the PET*co*(**5.1**) copolymer series were also studied by X-ray powder and fibre diffraction interfaced to computational modelling, which led to the proposal of three novel copolymer crystal structures, based upon the level of **5.1** present.

The incorporation of **5.5**-**5.7** at 10 mol% with respect to PET resulted in raised T_gs (98-103 °C) compared to PET*co*(**5.1**)-10 (89 °C). However, due to the non-isomorphic nature of BHET with **5.5**-**5.7**, satisfactory levels of crystallinity could only be obtained post-anneal. PET*co*(**5.5**)-10 (T_g = 98 °C) was selected for film production because of the relative raw material and scale-up synthesis cost for **5.5**. The production of PET*co*(**5.5**)-10 heat-set biaxially oriented film was successful, thus creating a novel semi-crystalline PET-based film that possessed a T_g above 100 °C. Although the thermal performance relative to PET was improved upon, the reduction in crystallinity from PET to PET*co*(**5.5**)-10 in film form resulted in relatively poor thermomechanical performance.

5.5 Experimental

5.5.1 Materials

Bis(2-hydroxyethyl) terephthalate and ethylene glycol were obtained from DuPont Teijin Films, U.K. Antimony trioxide was purchased from SICA, France. *p*-Phenylenediamine, *m*-phenylenediamine, *m*-xylylenediamine, ethylenediamine, ethanolamine, benzophenone-3,4,3',4'-tetracarboxylic dianhydride, bicyclo-[2,2,2]-oct-7-ene-2,3,5,6-tetracarboxylic dianhydride, acetic acid, *N*,*N*'-dimethylformamide, 1,2,4-benzenetricarboxylic anhydride, 2-bromoethanol, triethylamine, methanol, terephthaloyl chloride, 1-chloronaphthalene, thionyl chloride, chloroform, deuterated chloroform, dimethyl sulfoxide and deuterated dimethyl sulfoxide were purchased from Sigma Aldrich, U.K. 3,4,3',4'-Diphenylsulfonetetracarboxylic dianhydride was purchased from TCI, U.K. Chloroform was purchased from Fisher Scientific, U.K. Trifluoroacetic acid and 1,1,1,3,3,3-hexafluoro-2-propanol were purchased from Fluorochem, U.K. All materials were used as purchased.

5.5.2 Monomer synthetic procedures

5.5.2.1 Bis(2-hydroxyethyl)-2,2'-(1,4-phenylene)bis(1,3-dioxoisoindoline-5-carboxylate) (5.1)

A solution of *p*-phenylenediamine (5.40 g, 50.00 mmol) in DMF (250 mL) was added dropwise to a refluxing solution of 1,2,4-benzenetricarboxylic anhydride (19.20 g,

100.00 mmol) in DMF (50 mL) over 30 mins. The solution was refluxed for a further 1 h, cooled to room temperature, filtered, washed with deionised water and dried under vacuum at 110 °C for 24 h to afford the intermediate **5.1** product as a yellow-green powder (19.04 g, 83%).

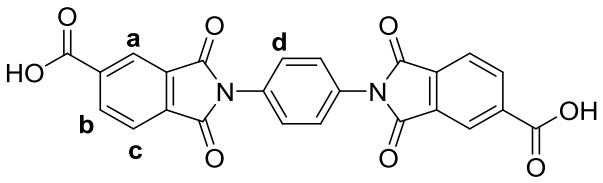

M.P. (DSC) = 449 °C. MS m/z = 455.0489 $[M-H]^+$, calculated 455.0516. ^{1}H NMR (400 MHz, d_6-DMSO) δ_H (ppm) 8.42 (2H, m, H_a), 8.33 (2H, m, H_b), 8.11 (2H, d, J = 4.0 Hz, H_c), 7.64 (4H, s, H_d). ^{13}C NMR [100 MHz, $CDCl_3$:TFA (2:1)] δ_C (ppm) 171.4, 137.3, 133.0, 129.1, 128.7, 128.6. IR (ν_{max} cm^{-1}) 2842 (νC-H), 1676 (νC=O), 1299 (νC-O), 1092 (νC-N).

A sample of the intermediate **5.1** product (5.00 g, 10.96 mmol) was dissolved in DMF (100 mL). 2-Bromoethanol (4.11 g, 32.87 mmol) and triethylamine (3.33 g, 32.87 mmol) were then added to the solution and the reaction was held at 80 °C for 16 h. The solution was cooled to room temperature and precipitated into deionised water, filtered, washed with methanol and dried under vacuum at 110 °C for 24 h to afford the product **5.1** as an off-white powder (3.78g, 63%).

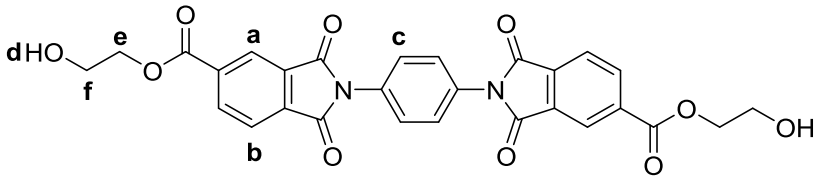

5.1

M.P. (DSC) = 341 °C. Found: C, 61.0; H, 3.7; N, 5.3. Calc. for $C_{28}H_{20}N_2O_{10}$: C, 61.8; H, 3.7; N, 5.1. MS m/z = 545.1187 $[M+H]^+$, calculated 545.1196. ^{1}H NMR (400 MHz, d_6-DMSO) δ_H (ppm) 8.46 (4H, m, H_a), 8.16 (2H, m, H_b), 7.65 (4H, s, H_c), 5.08 (2H, s, H_d), 4.36 (4H, s, H_e), 3.76 (4H, s, H_f). ^{13}C NMR [100 MHz, $CDCl_3$:TFA (2:1)] δ_C (ppm) 166.1, 164.4, 135.5, 135.3, 132.1, 131.3, 127.8, 123.9, 123.6, 67.6, 58.9. IR (ν_{max} cm^{-1}) 3468 (νO-H), 2931 (νC-H), 1706 (νC=O), 1214 (νC-O), 1066 (νC-N).

5.5.2.2 Bis(2-hydroxyethyl)-2,2'-(1,3-phenylene)bis(1,3-dioxoisoindoline-5-carboxylate) (5.2)

Intermediate synthesis as described for **5.1**. *m*-Phenylenediamine (5.41 g, 50.00 mmol) in DMF (50 mL), 1,2,4-benzenetricarboxylic anhydride (19.21 g, 100.00 mmol) in DMF (90 mL) to afford intermediate **5.2** product as an off-white powder (18.89 g, 83%).

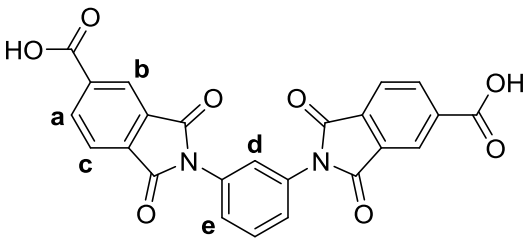

M.P. (DSC) = 288 °C. MS *m/z* = 479.0484 $[M+Na]^+$, calculated 479.0492. ^{1}H NMR (400 MHz, d_6-DMSO) δ_H (ppm) 8.39 (2H, d, J = 8.0 Hz, H_a), 8.31 (2H, s, H_b), 8.02 (2H, d, J = 8.0 Hz, H_c), 7.72 (1H, m, H_d), 7.60 (3H, t, J = 10.0 Hz, H_e). ^{13}C NMR [100 MHz, $CDCl_3$:TFA (2:1)] δ_C (ppm) 166.6, 166.4, 140.8, 135.3, 133.5, 132.2, 131.6, 129.2, 127.0, 126.0, 123.4. IR (ν_{max} cm^{-1}) 2750 (νC-H), 1692 (νC=O), 1363 (νC-O), 1101 (νC-N).

Product synthesis as described for **5.1**. Intermediate **5.2** product (22.00 g, 40.41 mmol) in DMF (250 mL), 2-bromoethanol (15.15 g, 121.22 mmol), triethylamine (12.26 g, 121.22 mmol) to afford product **5.2** as a yellow powder (6.86 g, 31%).

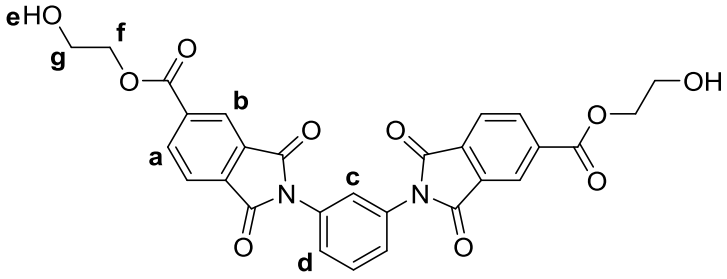

5.2

M.P. (DSC) = 190 °C. MS *m/z* = 567.1007 $[M+Na]^+$, calculated 567.1016. ^{1}H NMR (400 MHz, d_6-DMSO) δ_H (ppm) 8.48 (4H, m, H_a), 8.15 (2H, d, J = 8.0 Hz, H_b), 7.74 (1H, t, J = 8.0 Hz, H_c), 7.62 (3H, t, J = 8.0 Hz, H_d), 5.09 (2H, t, J = 6.0 Hz, H_e), 4.38 (4H, s, H_f), 3.77 (4H, s, H_g). ^{13}C NMR [100 MHz, $CDCl_3$:TFA (2:1)] δ_C (ppm) 167.5, 144.1, 133.3, 132.6, 131.3, 123.7, 121.8, 60.4, 37.6, 32.0. IR (ν_{max} cm^{-1}) 3250 (νO-H), 2943 (νC-H), 1714 (νC=O), 1250 (νC-O), 1071 (νC-N).

5.5.2.3 Bis(2-hydroxyethyl)-2,2'-(1,3-phenylenebis(methylene))bis(1,3-dioxoisoindoline-5-carboxylate) (5.3)

A solution of 1,2,4-benzenetricarboxylic anhydride (14.11 g, 73.42 mmol) and *m*-xylyenediamine (5.00 g, 36.71 mmol) in DMF (100 mL) was heated to 130 °C over a 2.5 h period. The reaction solution was cooled to room temperature before being precipitated into deionised water, filtered and dried under vacuum at 100 °C for 24 h to afford the intermediate **5.3** product as a white powder (14.45 g, 81%).

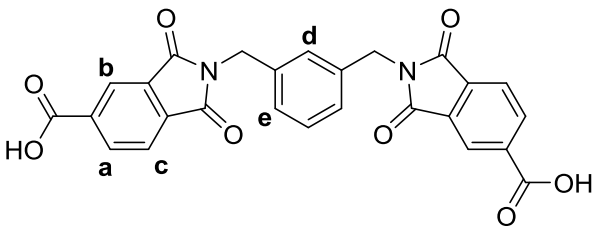

M.P. (DSC) = 335 °C. MS *m/z* = 485.0978 $[M+H]^+$, calculated 485.0985. ^{1}H NMR (400 MHz, d_6-DMSO) δ_H (ppm) 8.34 (2H, d, J = 4.0 Hz, H_a), 8.20 (2H, s, H_b), 7.96 (2H, t, J = 4.0 Hz, H_c), 7.21 (4H, m, H_d), 4.75 (4H, m, H_e). ^{13}C NMR (100 MHz, d_6-DMSO) δ_C (ppm) 166.9, 165.8, 136.7, 136.6, 135.3, 134.6, 131.9, 128.9, 126.4, 126.2, 123.5, 123.1, 40.9. IR (ν_{max} cm^{-1}) 3517 (νO-H), 2952 (νC-H), 1703 (νC=O), 1391 (νC-O), 1111 (νC-N).

Product synthesis as described for **5.1**. Intermediate **5.3** product (14.00 g, 28.90 mmol) in DMF (200 mL), 2-bromoethanol (10.83 g, 86.70 mmol), triethylamine (8.77 g, 86.70 mmol) to afford product **5.3** as a white powder (12.10 g, 73%).

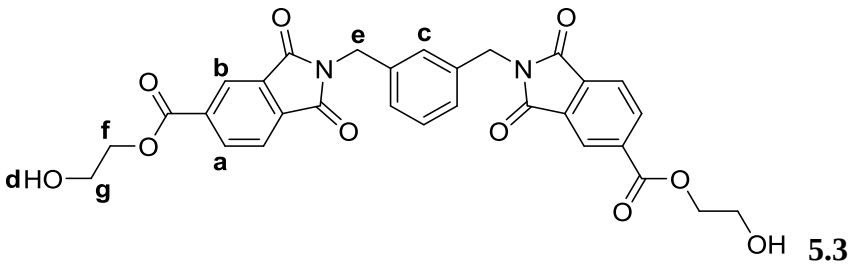

5.3

M.P. (DSC) = 153 °C. MS *m/z* = 595.1323 $[M+Na]^+$, calculated 595.1329. ^{1}H NMR (400 MHz, d_6-DMSO) δ_H (ppm) 8.30 (4H, m, H_a), 8.00 (2H, m, H_b), 7.22 (4H, m, H_c), 5.09 (2H, s, H_d), 4.76 (4H, s, H_e), 4.34 (4H, s, H_f), 3.75 (4H, s, H_g). ^{13}C NMR (100 MHz, d_6-DMSO) δ_C (ppm) 166.8, 164.2, 136.7, 135.4, 134.7, 131.9, 128.9, 126.3, 125.9, 123.6, 123.1, 67.5, 63.5, 58.9, 40.9. IR (ν_{max} cm^{-1}) 3362 (νO-H), 2928 (νC-H), 1706 (νC=O), 1251 (νC-O), 1065 (νC-N).

5.5.2.4 Bis(2-hydroxyethyl)-2,2'-(1,2-diaminoethane)bis(1,3-dioxoisoindoline-5-carboxylate) (5.4)

Ethylenediamine (2.80 g, 46.67 mmol) was added to a stirred solution of 1,2,4-benzenetricarboxylic anhydride (18.25 g, 95.00 mmol) in acetic acid (100 mL) and heated under reflux for 3 h before being cooled to room temperature, diluted with deionised water, filtered, washed with methanol and dried under vacuum at 80 °C for 24 h afford the intermediate **5.4** product as a white powder (16.64 g, 87%).

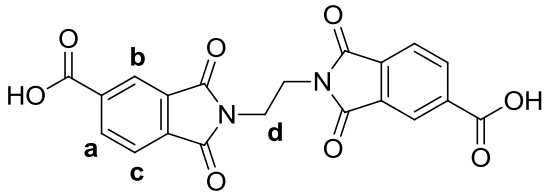

M.P. (DSC) = 358 °C. MS *m/z* = 409.0666 $[M+H]^+$, calculated 409.0672. ^{1}H NMR (400 MHz, d_6-DMSO) δ_H (ppm) 8.34 (2H, d, J = 4.0 Hz, H_a), 8.17 (2H, s, H_b), 7.96 (2H, d, J = 4.0 Hz, H_c), 3.89 (4H, s, H_d). ^{13}C NMR (100 MHz, d_6-DMSO) δ_C (ppm) 167.0, 165.7, 136.5, 135.4, 134.5, 131.7, 123.5, 123.0, 78.9, 36.4. IR (ν_{max} cm^{-1}) 2844 (νC-H), 1685 (νC=O), 1302 (νC-O), 1060 (νC-N).

Product synthesis as described for **5.1**. Intermediate **5.4** product (7.50 g, 18.37 mmol) in DMF (200 mL), 2-bromoethanol (6.89 g, 55.10 mmol), triethylamine (5.58 g, 55.10 mmol) to afford product **5.4** as a white powder (7.49 g, 82%).

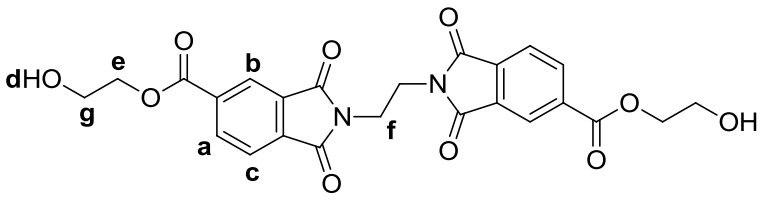

5.4

M.P. (DSC) = 201 °C. MS *m/z* = 519.1006 $[M+Na]^+$, calculated 519.1016. ^{1}H NMR (400 MHz, d_6-DMSO) δ_H (ppm) 8.39 (2H, d, J = 4.0 Hz, H_a), 8.29 (2H, s, H_b), 7.98 (2H, d, J = 4.0 Hz, H_c), 5.05 (2H, s, H_d), 4.32 (4H, s, H_e), 3.89 (4H, s, H_f), 3.72 (4H, s, H_g). ^{13}C NMR (100 MHz, d_6-DMSO) δ_C (ppm) 167.0, 164.3, 135.5, 135.3, 134.8, 131.8, 123.6, 123.2, 67.5, 58.9, 36.5. IR (ν_{max} cm^{-1}) 3410 (νO-H), 2942 (νC-H), 1706 (νC=O), 1288 (νC-O), 1084 (νC-N).

5.5.2.5 *N,N'*-bis-(hydroxyalkyl)-benzophenone-3,4,3',4'-tetracarboxylic diimide (5.5)

Ethanolamine (2.87 g, 47.00 mmol) was added dropwise to a stirred solution of benzophenone-3, 4, 3', 4'-tetracarboxylic dianhydride (7.50 g, 23.28 mmol) in DMF (100 mL). The solution was heated under reflux for 16 h, before being cooled to room temperature and precipitated into deionised water, filtered and then dried under vacuum at 100 °C for 24 h to afford product **5.5** as a brick-red powder (5.61 g, 59%).

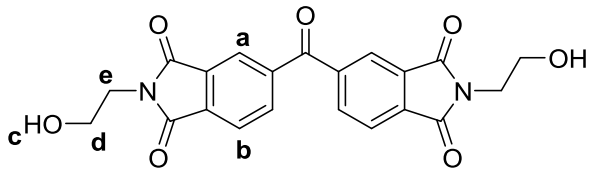

5.5

M.P. (DSC) = 213 °C. Found: C, 61.6; H, 3.9; N, 5.9. Calc. for $C_{21}H_{16}N_2O_7$: C, 61.8; H, 4.0; N, 5.9. MS *m*/*z* = 409.1030 $[M+H]^+$, calculated 409.1036. ^{1}H NMR (400 MHz, d_6-DMSO) δ_H (ppm) 8.16 (2H, d, *J* = 4.0 Hz, H_a), 8.06 (2H, m, H_b), 4.86 (2H, t, *J* = 5.0 Hz, H_c), 3.67 (4H, m, H_d), 3.60 (4H, m, H_e). ^{13}C NMR (100 MHz, d_6-DMSO) δ_C (ppm) 193.4, 167.1, 141.3, 135.5, 134.8, 132.0, 123.3, 57.8, 40.6. IR (ν_{max} cm^{-1}) 3506 (*v*O-H), 2981 (*v*C-H), 1694 (*v*C=O), 1387 (*v*C-O), 1057 (*v*C-N).

5.5.2.6 *N,N'*-bis-(hydroxyalkyl)-3,4,3',4'-diphenylsulfonetetracarboxylic diimide (5.6)

Product synthesis as described for **5.5.** Ethanolamine (0.70 g, 11.50 mmol), 3,4,3',4'-diphenylsulfonetetracarboxylic dianhydride (2.00 g, 5.58 mmol) in DMF (100 mL) to afford product **5.6** as a yellow powder (1.47 g, 59%).

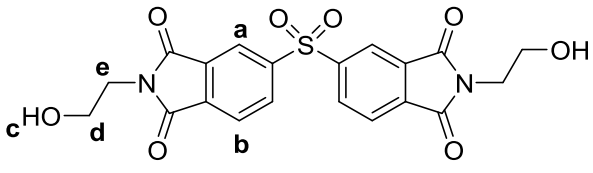

5.6

M.P. (DSC) = 219 °C. Found: C, 54.1; H, 3.5; N, 6.4; S, 7.5. Calc. for $C_{20}H_{16}N_2O_8S$: C, 54.1; H, 3.6; N, 6.3; S, 7.2. MS *m*/*z* = 467.0502 $[M+Na]^+$, calculated 467.0525. ^{1}H NMR (400 MHz, d_6-DMSO) δ_H (ppm) 8.54 (4H, m, H_a), 8.09 (2H, m, H_b), 4.39 (2H, br, H_c), 3.64 (4H, t, *J* = 6.0 Hz, H_d), 3.55 (4H, t, *J* = 6.0 Hz, H_e). ^{13}C NMR (100 MHz, d_6-DMSO) δ_C (ppm) 166.3, 145.0, 136.3, 134.0, 133.2, 124.3, 122.2, 57.7, 40.8. IR (ν_{max} cm^{-1}) 3431 (*v*O-H), 2945 (*v*C-H), 1675 (*v*C=O), 1330 (*v*S=O).

5.5.2.7 *N*,*N*'-bis-(2-hydroxyalkyl)-bicyclo-[2,2,2]-oct-7-ene-2,3,5,6-tetracarboxylic diimide (5.7)

Product synthesis as described for **5.5**. Ethanolamine (11.76 g, 204.0 mmol), bicyclo-[2,2,2]-oct-7-ene-2,3,5,6-tetracarboxylic dianhydride (24.00 g, 96.72 mmol) in DMF (250 mL), precipitated in methanol to afford product **5.7** as a white powder (29.25 g, 91%) in both *exo*- and *endo*-configurations.

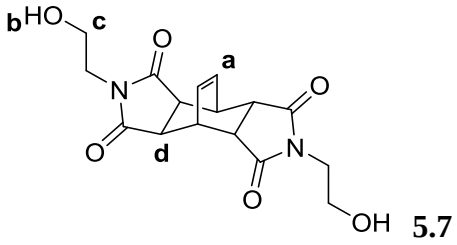

5.7

M.P. (DSC) = 287 °C. Found: C, 57.5; H, 5.4; N, 8.5. Calc. for $C_{16}H_{18}N_2O_6$: C, 57.5; H, 5.4; N, 8.4. MS *m*/*z* = 357.1050 $[M+Na]^+$, calculated 357.1063. ^{1}H NMR (400 MHz, d_6-DMSO) δ_H (ppm) 5.98 (2H, m, H_a), 4.74 (2H, t, J = 4.0 Hz, H_b), 3.34 (10H, m, H_c), 3.16 (4H, m, H_d). ^{13}C NMR (100 MHz, d_6-DMSO) δ_C (ppm) 177.4, 130.5, 57.1, 42.1, 40.4, 33.2. IR (ν_{max} cm^{-1}) 3431 (*v*O-H), 2959 (*v*C-H), 1677 (*v*C=O), 1331 (*v*C-O).

5.5.3 Polymer synthetic procedures

Polymers were synthesised via the laboratory-scale melt-polycondensation procedure as described in Chapter 2, unless otherwise stated.

5.5.3.1 PET

Reagents	
(g)	
BHET	**Sb_2O_3**
40.00	0.10

Characterisation detailed in Chapter 3.

5.5.3.2 PET*co*(5.1) copolymer series

Reagents			Comonomer feed ratio		Copolymer composition ratio	
(g)			(mol%)		(mol%)	
BHET	5.1	Sb_2O_3	BHET	5.1	PET	5.1
40.00	4.27	0.10	95	5	96	4
40.00	8.55	0.10	90	10	93	7
20.00	7.56	0.10	85	15	87	13
24.00	12.84	0.10	80	20	82	18
22.00	15.66	0.10	75	25	77	23
20.00	18.32	0.10	70	30	74	26

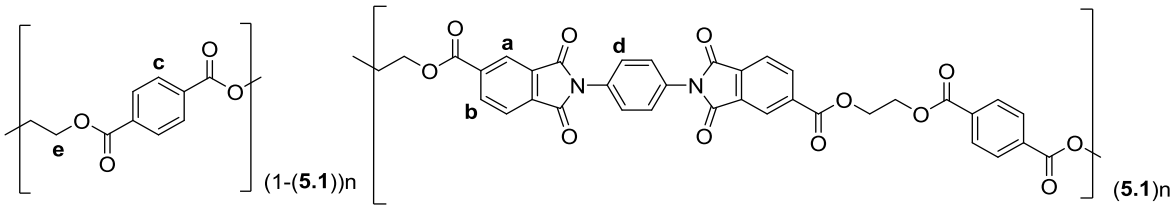

PET*co*(5.1)-5

^{1}H NMR [400 MHz, $CDCl_3$/TFA (2:1)] δ_H (ppm) 8.74 (2H, s, H_a), 8.62 (2H, m, H_b), 8.19 (10H, s, H_c), 7.67 (4H, s, H_d), 4.85 (12H, s, H_e). ^{13}C NMR [100 MHz, $CDCl_3$/TFA (2:1)] δ_C (ppm) 168.0, 136.9, 135.5, 134.9, 133.3, 131.4, 130.9, 130.0, 127.6, 125.6, 124.8, 64.0. T_g = 91 °C, T_{cc} = 182 °C, T_c = 167 °C, T_m = 240 °C, T_d = 420 °C. η_{inh} ($CHCl_3$/TFA) (2:1) = 0.67 dL g^{-1}. IR (ν_{max} cm^{-1}) 2983 (*ν*C-H), 1712 (*ν*C=O), 1242 (*ν*C-O), 1092 (*ν*C-N).

PET*co*(5.1)-10

^{1}H NMR [400 MHz, $CDCl_3$/TFA (2:1)] δ_H (ppm) 8.74 (2H, s, H_a), 8.63 (2H, s, H_b), 8.19 (10H, s, H_c), 7.67 (4H, s, H_d), 4.86 (12H, s, H_e). ^{13}C NMR [100 MHz, $CDCl_3$/TFA (2:1)] δ_C (ppm) 168.0, 136.9, 135.5, 134.9, 133.3, 131.4, 130.9, 130.0, 127.6, 125.6, 124.8, 64.0. T_g = 89 °C, T_{cc} = 156 °C, T_c = 163 °C, T_m = 236 °C, T_d = 414 °C. η_{inh} ($CHCl_3$/TFA) (2:1) = 0.37 dL g^{-1}. IR (ν_{max} cm^{-1}) 3007 (*ν*C-H), 1719 (*ν*C=O), 1249 (*ν*C-O), 1099 (*ν*C-N).

PET*co*(5.1)-15

^{1}H NMR [400 MHz, $CDCl_3$/TFA (2:1)] δ_H (ppm) 8.76 (2H, s, H_a), 8.65 (2H, s, H_b), 8.20 (10H, s, H_c), 7.68 (4H, s, H_d), 4.87 (12H, s, H_e). ^{13}C NMR [100 MHz, $CDCl_3$/TFA (2:1)] δ_C (ppm) 168.1, 137.0, 135.5, 134.9, 133.3, 131.4, 130.9, 130.0, 127.6, 125.6, 124.8, 65.1, 64.4, 64.0, 63.3. T_g = 91 °C, T_c = 204 °C, T_m = 226 °C, T_d = 408 °C. η_{inh} ($CHCl_3$/TFA) (2:1) = 0.49 dL g^{-1}. IR (ν_{max} cm^{-1}) 3007 (*ν*C-H), 1719 (*ν*C=O), 1248 (*ν*C-O), 1100 (*ν*C-N).

PET*co*(5.1)-20

^{1}H NMR [400 MHz, $CDCl_3$/TFA (2:1)] δ_H (ppm) 8.75 (2H, s, H_a), 8.65 (2H, s, H_b), 8.19 (10H, s, H_c), 7.67 (4H, s, H_d), 4.86 (12H, s, H_e). ^{13}C NMR [100 MHz, $CDCl_3$/TFA (2:1)] δ_C (ppm) 168.1, 137.0, 135.5, 135.0, 133.3, 131.4, 130.9, 130.0, 127.6, 125.6, 124.8, 65.1, 64.0, 63.3. T_g = 101 °C, T_c = 213 °C, T_m = 230 °C, T_d = 412 °C. η_{inh} ($CHCl_3$/TFA) (2:1) = 0.37 dL g^{-1}. IR (ν_{max} cm^{-1}) 2973 (*ν*C-H), 1715 (*ν*C=O), 1248 (*ν*C-O), 1096 (*ν*C-N).

PET*co*(5.1)-25

^{1}H NMR [400 MHz, $CDCl_3$/TFA (2:1)] δ_H (ppm) 8.76 (2H, s, H_a), 8.66 (2H, s, H_b), 8.21 (10H, s, H_c), 7.69 (4H, s, H_d), 4.88 (12H, s, H_e). ^{13}C NMR [100 MHz, $CDCl_3$/TFA (2:1)] δ_C (ppm) 167.9, 137.0, 135.5, 135.0, 133.3, 131.4, 130.9, 130.0, 127.6, 125.6, 124.8, 65.1, 64.0, 63.7, 63.3. T_g = 109 °C, T_c = 219 °C, T_m = 246 °C, T_d = 410 °C. η_{inh} ($CHCl_3$/TFA) (2:1) = 0.32 dL g^{-1}. IR (ν_{max} cm^{-1}) 3007 (*ν*C-H), 1718 (*ν*C=O), 1248 (*ν*C-O), 1096 (*ν*C-N).

PET*co*(5.1)-30

^{1}H NMR [400 MHz, $CDCl_3$/TFA (2:1)] δ_H (ppm) 8.74 (2H, s, H_a), 8.64 (2H, s, H_b), 8.19 (10H, s, H_c), 7.67 (4H, s, H_d), 4.86 (12H, s, H_e). ^{13}C NMR [100 MHz, $CDCl_3$/TFA (2:1)] δ_C (ppm) 168.1, 137.0, 135.5, 134.9, 133.3, 131.4, 130.9, 130.0, 127.6, 125.6, 124.8, 65.1, 64.0, 63.3. T_g = 107 °C, T_c = 210 °C, T_m = 238 °C, T_d = 410 °C. η_{inh} ($CHCl_3$/TFA) (2:1) = 0.34 dL g^{-1}. IR (ν_{max} cm^{-1}) IR (ν_{max} cm^{-1}) 2971 (*ν*C-H), 1705 (*ν*C=O), 1251 (*ν*C-O), 1099 (*ν*C-N).

5.5.3.3 PET*co*(5.1)-50[47]

A solution of terephthaloyl chloride (0.50 g, 2.46 mmol), comonomer **5.1** (1.34 g, 2.46 mmol) and 1-chloronaphthalene (50 mL) was heated to 170 °C and held at this temperature for 1 h. The temperature was then increased to 210 °C over a 3 h period and then held at this temperature for 40 h. The reaction mixture was then cooled to room temperature, precipitated in methanol, filtered and dried under vacuum for at 110 °C for 24 h to afford the polymer product **PET*co*(5.1)-50** (1.20 g).

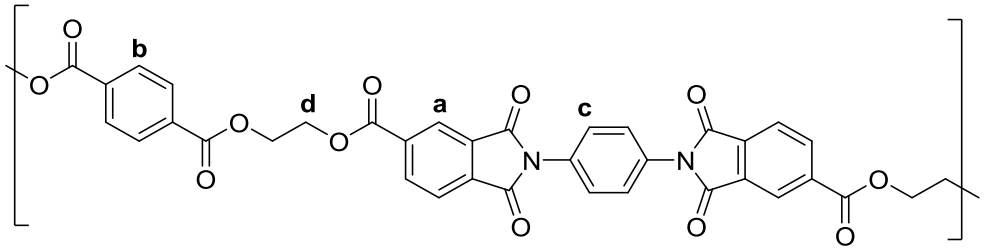

^{1}H NMR [400 MHz, $CDCl_3$/TFA (2:1)] δ_H (ppm) 8.80 (4H, s, H_a), 8.23 (6H, s, H_b), 7.71 (4H, s, H_c), 4.90 (8H, s, H_d). ^{13}C NMR [100 MHz, $CDCl_3$/TFA (2:1)] δ_C (ppm) 168.2, 137.0, 135.5, 135.0, 133.3, 131.4, 130.9, 130.5, 130.0, 127.6, 125.6, 124.8, 64.0. T_g = 123 °C, T_{cc} = 196 °C, T_c = 303 °C, T_m = 336 °C, T_d = 412 °C. IR (ν_{max} cm^{-1}) 2969 (νC-H), 1716 (νC=O), 1249 (νC-O), 1096 (νC-N).

5.5.3.4 5.1 homopolymer[47]

A solution of the intermediate **5.1** product (1.03 g, 2.26 mmol) and thionyl chloride (122.85 g, 1.03 mol) was heated under reflux for 4 h. The excess thionyl chloride was then removed via distillation under reduced pressure and the reaction flask was purged with nitrogen for 16 h. A solution of 1-chloronaphthalene (50 mL) and ethylene glycol (0.14 g, 2.09 mmol) was then added and the reaction solution was heated to 170 °C and held at this temperature for 1 h. The temperature was then increased to 210 °C over a 3 h period and held for 40 h at this temperature. The reaction was then cooled to room temperature, precipitated in methanol, filtered and dried under vacuum at 110 °C for 24 h to afford the polymer product **5.1 homopolymer** (0.60 g).

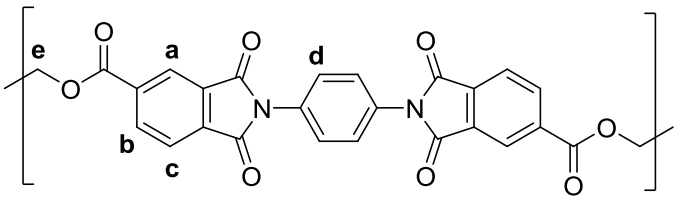

^{1}H NMR [400 MHz, $CDCl_3$/TFA (2:1)] δ_H (ppm) 8.45 (2H, m, H_a), 8.36 (2H, m, H_b), 8.13 (2H, m, H_c), 7.64 (4H, s, H_d), 3.96 (4H, s, H_e). ^{13}C NMR [100 MHz, $CDCl_3$/TFA (2:1)] δ_C (ppm) 168.0, 167.5, 136.9, 135.9, 134.7, 133.3, 131.3, 130.9, 130.0, 127.7, 125.6, 124.7, 53.7, 37.1. T_g = 163 °C, T_{cc} = 313 °C, T_d = 399 °C. η_{inh} ($CHCl_3$/TFA) (2:1) = 0.27 dL g^{-1}. IR (ν_{max} cm^{-1}) 3008 (νC-H), 1720 (νC=O), 1390 (νC-O), 1098 (νC-N).

5.5.3.5 PET*co*(5.2) copolymer series

Reagents			Comonomer feed ratio		Copolymer composition ratio	
(g)			(mol%)		(mol%)	
BHET	5.2	Sb_2O_3	BHET	5.2	PET	5.2
28.57	3.21	0.10	95	5	95	5
23.53	5.57	0.10	90	10	90	10

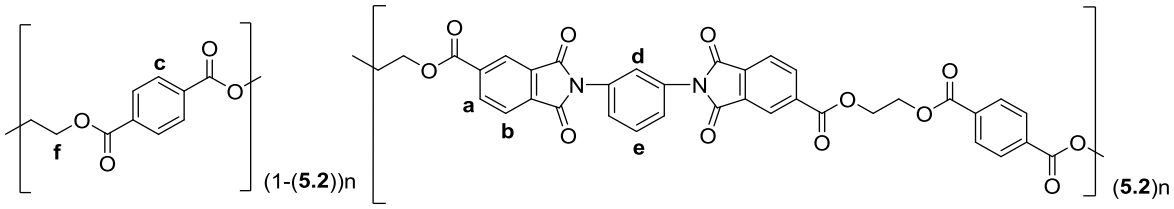

PET*co*(5.2)-5

^{1}H NMR [400 MHz, $CDCl_3$:TFA (2:1)] δ_H (ppm) 8.70 (2H, s, H_a), 8.59 (2H, m, H_b), 8.17 (10H, s, H_c), 7.74 (1H, m, H_d), 7.60 (3H, m, H_e), 4.83 (12H, s, H_f). ^{13}C NMR [100 MHz, $CDCl_3$:TFA (2:1)] δ_C (ppm) 168.0, 136.9, 135.0, 133.3, 131.3, 131.2, 130.0, 127.2, 125.6, 124.8, 63.9, 63.2. T_g = 92 °C, T_c = 161 °C, T_m = 238 °C, T_d = 400 °C. η_{inh} [$CHCl_3$:TFA (2:1)] = 0.46 dL g^{-1}. IR (ν_{max} cm^{-1}) 2960 (*ν*C-H), 1711 (*ν*C=O), 1237 (*ν*C-O), 1089 (*ν*C-N).

PET*co*(5.2)-10

^{1}H NMR [400 MHz, $CDCl_3$:TFA (2:1)] δ_H (ppm) 8.70 (2H, s, H_a), 8.59 (2H, m, H_b), 8.16 (10H, s, H_c), 7.74 (1H, m, H_d), 7.60 (3H, m, H_e), 4.83 (12H, s, H_f). ^{13}C NMR [100 MHz, $CDCl_3$:TFA (2:1)] δ_C (ppm) 135.5, 134.9, 133.3, 131.3, 131.2, 130.0, 127.1, 125.6, 124.8, 100.0, 66.6, 65.1, 63.9. T_g = 99 °C, T_d = 395 °C. η_{inh} [$CHCl_3$:TFA(2:1)] = 0.58 dL g^{-1}. IR (ν_{max} cm^{-1}) 2960 (*ν*C-H), 1711 (*ν*C=O), 1240 (*ν*C-O), 1092 (*ν*C-N).

5.5.3.6 PET*co*(5.3)-10

Reagents			Comonomer feed ratio		Copolymer composition ratio	
(g)			(mol%)		(mol%)	
BHET	5.3	Sb_2O_3	BHET	5.3	PET	5.3
29.63	7.40	0.10	90	10	92	8

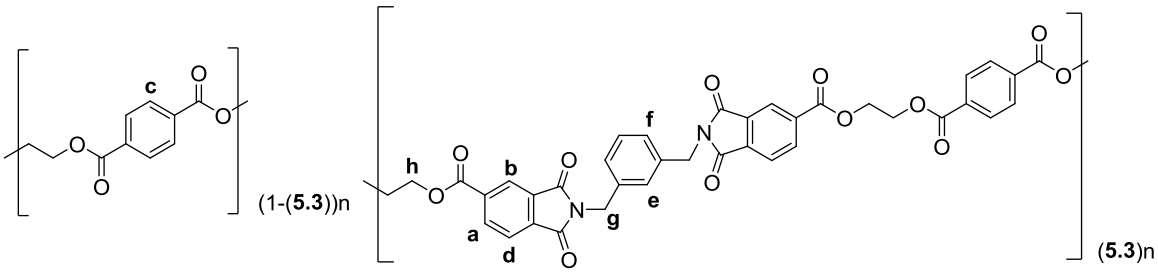

^{1}H NMR [400 MHz, $CDCl_3$:TFA (2:1)] δ_H (ppm) 8.60 (2H, s, H_a), 8.51 (2H, s, H_b), 8.17 (8H, s, H_c), 8.03 (2H, s, H_d), 7.50 (1H, s, H_e), 7.33 (3H, s, H_f), 4.84 (8H, s, H_g), 4.20 (8H, s, H_h). ^{13}C NMR [100 MHz, $CDCl_3$:TFA (2:1)] δ_C (ppm) 168.0, 136.6, 135.5, 135.2, 135.0, 133.3, 131.6, 130.0, 129.6, 128.7, 128.3, 125.2, 124.4, 63.9, 42.0. T_g = 100 °C, T_m = 232 °C, T_d = 404 °C. η_{inh} [$CHCl_3$:TFA (2:1)] = 0.55 dL g^{-1}. IR (ν_{max} cm^{-1}) 2956 (νC-H), 1714 (νC=O), 1240 (νC-O), 1093 (νC-N).

5.5.3.7 PET*co*(5.4)-10

Reagents			Comonomer feed ratio		Copolymer composition ratio	
(g)			(mol%)		(mol%)	
BHET	**5.4**	**Sb_2O_3**	**BHET**	**5.4**	**PET**	**5.4**
34.78	7.51	0.10	90	10	90	10

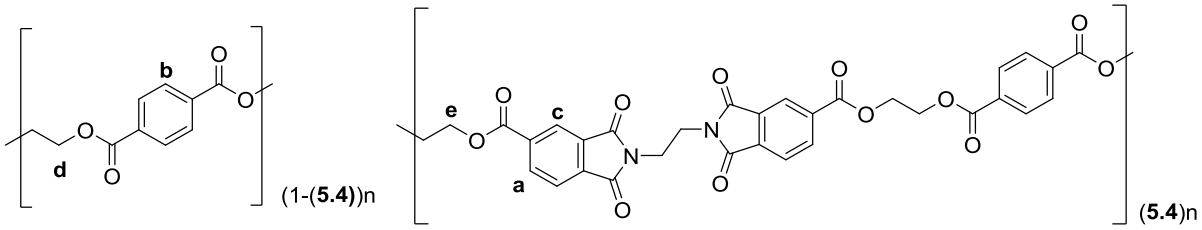

^{1}H NMR [400 MHz, $CDCl_3$:TFA (2:1)] δ_H (ppm) 8.55 (4H, m, H_a), 8.17 (8H, s, H_b), 7.96 (2H, s, H_c), 4.84 (8H, s, H_d), 4.14 (8H, s, H_e). ^{13}C NMR [100 MHz, $CDCl_3$:TFA (2:1)] δ_C (ppm) 168.0, 136.7, 135.2, 135.9, 133.3, 131.3, 130.0, 125.3, 124.4, 63.9, 37.1. T_g = 99 °C, T_m = 228 °C, T_d = 403 °C. η_{inh} [$CHCl_3$:TFA (2:1)] = 0.40 dL g^{-1}. IR (ν_{max} cm^{-1}) 2956 (νC-H), 1712 (νC=O), 1239 (νC-O), 1093 (νC-N).

5.5.3.8 PET*co*(5.5)-10

Reagents			Comonomer feed ratio		Copolymer composition ratio	
(g)			(mol%)		(mol%)	
BHET	5.5	Sb_2O_3	BHET	5.5	PET	5.5
32.00	5.11	0.10	90	10	91	9

Reagents					Comonomer feed ratio		Copolymer composition ratio	
(g)					(mol%)		(mol%)	
DMT	5.5	EG	$Mn(OAc)_2.4H_2O$	Sb_2O_3	DMT	5.5	PET	3.1
6290	1555	4318	2.81	2.10	90	10	90	10

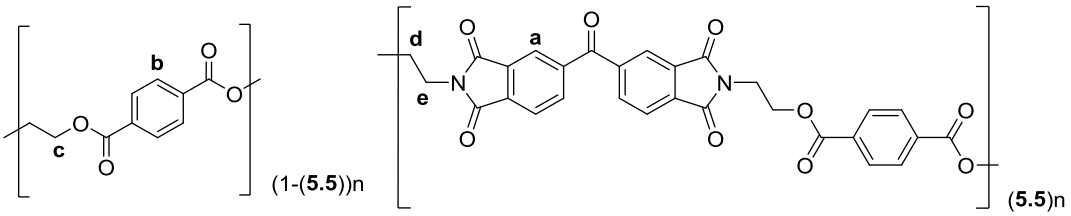

^{1}H NMR [400 MHz, $CDCl_3$:TFA (2:1)] δ_H (ppm) 8.33 (2H, s, H_a), 8.18 (12H, s, H_b), 4.85 (4H, s, H_c), 4.72 (4H, s, H_d), 4.31 (4H, s, H_e). ^{13}C NMR [100 MHz, $CDCl_3$:TFA (2:1)] δ_C (ppm) 168.1, 141.5, 136.7, 134.9, 131.7, 130.0, 125.4, 124.7, 63.9, 37.4. T_g = 98 °C, T_d = 419 °C. η_{inh} ($CHCl_3$:TFA) (2:1) = 0.35/0.77 dL g^{-1}. IR (ν_{max} cm^{-1}) 2987 (νC-H), 1712 (νC=O), 1241 (νC-O), 1092 (νC-N).

5.5.3.9 PET*co*(5.6)-10

Reagents			Comonomer feed ratio		Copolymer composition ratio	
(g)			(mol%)		(mol%)	
BHET	5.6	Sb_2O_3	BHET	5.6	PET	5.6
35.00	6.11	0.10	90	10	90	10

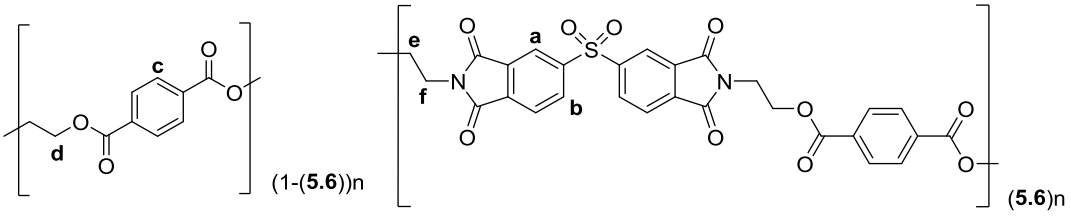

^{1}H NMR [400 MHz, $CDCl_3$:TFA (2:1)] δ_H (ppm) 8.53 (2H, s, H_a), 8.48 (2H, d, J = 8.0 Hz, H_b), 8.18 (10H, s, H_c), 4.84 (4H, s, H_d), 4.67 (4H, d, J = 6.81 Hz, H_e), 4.26 (4H, s, H_f). ^{13}C NMR [100 MHz, $CDCl_3$:TFA (2:1)] δ_C (ppm) 167.8, 145.7, 135.8, 134.7,

133.3, 132.6, 130.0, 125.4, 63.9, 37.5. T_g = 403 °C, T_d = 411 °C. η_{inh} ($CHCl_3$:TFA) (2:1) = 0.39 dL g^{-1}. IR (ν_{max} cm^{-1}) 2982 (*ν*C-H), 1708 (*ν*C=O), 1243 (*ν*C-O), 1087 (*ν*C-N).

5.5.3.10 PET*co*(5.7)-10

Reagents			Comonomer feed ratio		Copolymer composition ratio	
(g)			(mol%)		(mol%)	
BHET	**5.7**	**Sb_2O_3**	**BHET**	**5.7**	**PET**	**5.7**
35.00	4.59	0.10	90	10	90	10

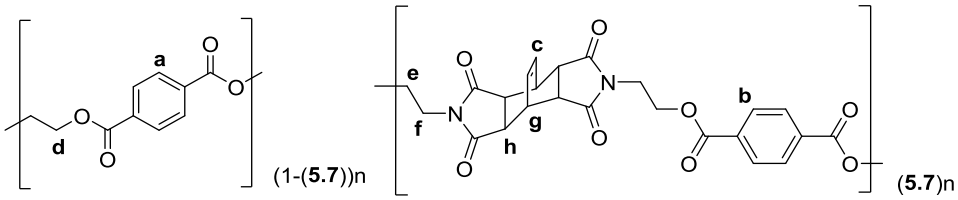

^{1}H NMR [400 MHz, $CDCl_3$:TFA (2:1)] δ_H (ppm) 8.17 (4H, s, H_a), 8.07 (4H, d, J = 8.0 Hz, H_b), 6.07 (2H, s, H_c), 4.84 (4H, s, H_d), 4.51 (4H, s, H_e), 3.98 (4H, s, H_f), 3.82 (2H, s, H_g), 3.34 (4H, s, H_h). ^{13}C NMR [100 MHz, $CDCl_3$:TFA (2:1)] δ_C (ppm) 168.0, 133.3, 130.8, 130.0, 129.9, 63.9, 42.7, 38.1, 33.3. T_g = 101 °C, T_c = 188 °C, T_m = 227 °C, T_d = 410 °C. η_{inh} ($CHCl_3$:TFA) (2:1) = 0.45 dL g^{-1}. IR (ν_{max} cm^{-1}) 2983 (*ν*C-H), 1714 (*ν*C=O), 1236 (*ν*C-O), 1095 (*ν*C-N).

5.6 References

1 J. R. Whinfield and J. T. Dickson, *US Pat*., 2,465,319, *Polymeric linear terephthalic esters*, 1949.
2 J. R. Whinfield, *Nature*, 1946, **158**, 930–931.
3 L. Turnbull, J. J. Liggat and W. A. Macdonald, 2011, **124**, 4517-4529.
4 S. Maiti and S. Das, *J. Appl. Polym. Sci.*, 1981, **26**, 957–978.
5 C. L. Mares and J. de Abajo, *Angew. Makromol. Chem.*, 1975, **55**, 73-83.
6 J. U. N. Xiao, X. Wan, D. Zhang, Q. Zhou and S. R. Turner, *J. Polym. Sci. Polym. Chem.*, 2001, **39**, 408-415.
7 H. Ma, M. Hibbs, D. M. Collard and D. A. Schiraldi, *Macromolecules*, 2002, **35**, 5123–5130.
8 Y. S. Hu, R. Y. F. Liu, M. Rogunova, D. A. Schiraldi, S. Nazarenko, A. Hiltner and E. Baer, *J. Polym. Sci. Part B Polym. Phys.*, 2002, **40**, 2489–2503.
9 L. S. Park, J. H. Do and D. C. Lee, *J. Appl. Polym. Sci*., 1996, **60**, 2059–2067.
10 L. J. F. Mary and P. Kannan, *Polym. Int.*, 1998, **47**, 317–323.
11 G. Natta, G. Allegra, I. W. Bassi, D. Sianesi, G. Caporiccio and E. Torti, *J. Polym. Sci. Polym. Chem.*, 1965, **3**, 4263-4278.
12 Y. G. Jeong, W. H. Jo and S. G. Lee, *Macromolecules*, 2000, **33**, 9705–9711.
13 H. Y. Yoo, S. Umemoto, T. Kikutani and N. Okui and P. Materials, *Polymer*, 1994, **35**, 117–122.
14 N. Yoshie and Y. Inoue, H. Y. Yoo and N. Okui, *Polymer*, 1994, **35**, 1931–1935.
15 W. L. Edwards and M. L. Andrews, *WO 2005/073272 A1*, 2005.

16 W. Messiri, J. Menczel, U. Gaur and B. Wunderlich, *J. Polym. Sci. Polym. Phys*, 1982, **20**, 719–728.
17 M. Avrami, *J. Chem. Phys.*, 1939, **7**, 1103.
18 M. Avrami, *J. Chem. Phys.*, 1940, **8**, 212.
19 M. Avrami, *J. Chem. Phys.*, 1941, **9**, 177.
20 A. T. Lorenzo, M. L. Arnal, J. Albuerne and A. J. Müller, *Polym. Test.*, 2007, **26**, 222–231.
21 Z. Chen, *PhD Thesis*, University of Birmingham, *The Crystallisation of Poly* (*ethylene terephthalate*) *Studied by Thermal Analysis and FTIR Spectroscopy*, 2012.
22 T. W. Chan and A. I. Isayev, *Polym. Eng. Sci.*, 1994, **34**, 461–471.
23 J. Xiao, H. Zhang, X. Wan, D. Zhang, Q. F. Zhou, E. M. Woo and S. R. Turner, *Polymer*, 2002, **43**, 3683–3690.
24 W. H. Cobbs Jr and R. L. Burton, *J. Polym. Sci.*, 1953, **10**, 275–290.
25 T. G. Fox, *Bull. Am. Phys. Soc.*, 1965, **1**, 123.
26 H. R. Kricheldorf and V. Linzer, *Polymer*, 1995, **36**, 1893–1902.
27 S. Srinivas, F. E. Caputo, M. Graham, S. Gardner, R. M. Davis, J. E. Mcgrath and G. L. Wilkes, *Macromolecules*, 1997, **9297**, 1012–1022.
28 R. de P. Daubeny and C. W. Bunn, *P. Roy. Soc. Lond. A. Mat.*, 1954, **7**, 531.
29 J. S. Tse and T. C. W. Mak, *J. Cryst. Mol. Struct.*, 1975, **5**, 75.
30 Y. Fu, R. B. Yimin, K. A. Affholter and B. Wunderlich, *Macromolecules*, 1993, **26**, 2187–2193.
31 P. D. Coulter, S. Hanna and A. H. Windle, *Liq. Cryst.*, 1989, **5**, 1603–1618.
32 H. M. Colquhoun and D. J. Williams, *Acc. Chem. Res*, 2000, **33**, 189-198.
33 K. Okuyama, H. Sakaitani and H. Arikawa, *Macromolecules*, 1992, **25**, 7261–7267.
34 Y. Li, H. Xu, X. Tao, K. Qian, S. Fu, Y. Shen and S. Ding, *J. Mater. Chem.*, 2011, **21**, 1810.
35 K. N. Baker, A. V. Fratini, T. Resch, H. C. Knachel, W. W. Adams, E. P. Socci and B. L. Farmer, *Polymer*, 1993, **34**, 1571–1587.
36 J. E. Mark, *Physical Properties of Polymers Handbook*, Springer, 2007, 196.
37 B. Duh, *J. Appl. Polym. Sci.*, 2001, **81**, 1748.
38 T. Y. Kim, E. A. Lofgren and S. A. Jabarin, *J. Appl. Polym. Sci.*, 2003, **89**, 197.
39 B. Gantillon, R. Spitz and T. F. McKenna, *Macromol. Mater. Eng.*, 2004, **289**, 88.
40 H. A. Pohl, *Anal. Chem.*, 1954, **26**, 1614–1616.
41 L. H. Buxbaum, *Angew. Chem. Internat. Ed.*, 1968, **7**, 182–190.
42 J. Wang, B. R. Nayak, D. Creed, C. E. Hoyle and L. J. Mathias, *Polymer*, 2005, **46**, 6897–6909.
43 P. J. Holdsworth and A. Turner-Jones, *Polymer*, 1971, **12**, 195–208.
44 B. R. Bikson and Y. F. Freimanis, *Polym. Sci. U.S.S.R.*, 1970, **12**, 81–85.
45 E. R. Dixon and J. B. Jackson, *J. Mater. Sci.*, 1968, **3**, 464-470.
46 Y. P. Khanna, *J. Appl. Polym. Sci.*, 1989, **37**, 2719–2726.
47 S. W. Kantor, R. W. Lenz and W. J. Ward, *US Pat.*, 5,032,669, 1991.

Chapter 6

Poly(ethylene terephthalate) (PET)-based copoly(ester-amide)s and their analogues

6.1 Abstract

The synthesis of poly(ethylene terephthalate) (PET)-based copoly(ester-amide)s incorporating *N*,*N*'-bis(2-hydroxyethyl) terephthalamide at 0-50 mol%, confirms that the replacement of ester functional groups by amide in PET may increase the glass transition temperature, T_g, up to 176 °C. Copolycondensation of *N*,*N*'-bis(2-hydroxyethyl)-4,4'-[terephthaloyl bis(azanediyl)] dibenzoate and *N*,*N*'-bis(4-(2-hydroxyethyl)phenyl) terephthalamide at 4 mol% affords novel enhanced PET-based copoly(ester-amide)s with T_gs of 92 and 94 °C, respectively. Both 4 mol% copolymers also exhibit significant retention of semi-crystalline behaviour, with above 35% crystallinity observed in each case post-annealing at 200 °C. The thermomechanical properties of such copoly(ester-amide)s are also improved with respect to PET. In particular, following 2 mol% incorporation, the elastic modulus (E) is increased to 1100 and 1103 MPa from 458 MPa, respectively.

6.2 Introduction

Aromatic polyamides are an established[1–4] class of high performance polymers, exhibiting superior thermal stability and mechanical performance in comparison to semi-crystalline, semi-aromatic polyesters such as PET. In addition to the increased rigidity of the amide bond relative to an ester analogue, polyamides may form hydrogen bonded networks to produce highly oriented polymer chains. The T_g may therefore be increased following the chemical modification of a polymer, in terms of intermolecular attractions.

Polyamide characteristics are typified by poly(*p*-phenylene terephthalamide), Kevlar®, which is formed by solution polycondensation between terephthaloyl chloride and *p*-phenylenediamine.[5] A T_g of ~ 450 °C is observed[6] for commercial Kevlar®, rendering the polymer unprocessable from the melt. Kevlar® is therefore spun into fibres from a liquid crystalline solution in 100% sulfuric acid, to afford materials possessing tensile moduli in excess of 100,000 MPa.[7] In the context of this thesis, the thermomechanical properties of PET may be increased by the incorporation of amide residues. Figure 6.1 illustrates this notion in the simplest form, i.e. as poly(ethylene terephthalamide), following the replacement of ester for amide functional groups in PET.

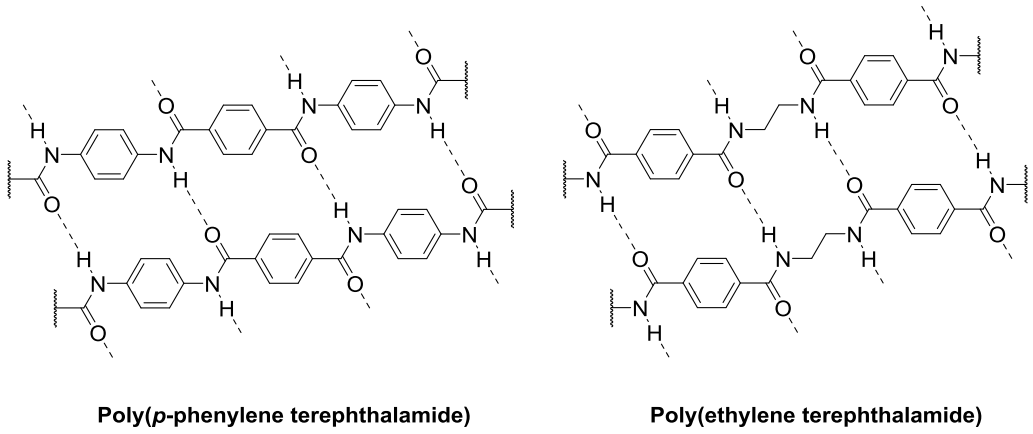

Figure 6.1 Comparison of the intermolecular hydrogen bonded networks in poly(*p*-phenylene terephthalamide) and poly(ethylene terephthalamide).

Although relatively less documented than copoly(ester-imide)s, the synthesis of copoly(ester-amide)s via a melt-copolymerisation route follows the rationale detailed in previous chapters for copolyesters and copoly(ester-imide)s. The T_g of terephthalate-based semi-crystalline polyesters may therefore be increased following copolymerisation with rigid amide comonomers.

Gaymans *et al*. have studied the incorporation of bisester diamide comonomers into PET[8–10] and PBT[11–13], illustrated as *N*,*N*'-bis(*p*-carbomethoxybenzoyl)ethanediamine (T2T) and *N*,*N*'-bis(*p*-carbomethoxybenzoyl)butanediamine (T4T) in Figure 6.2, respectively.

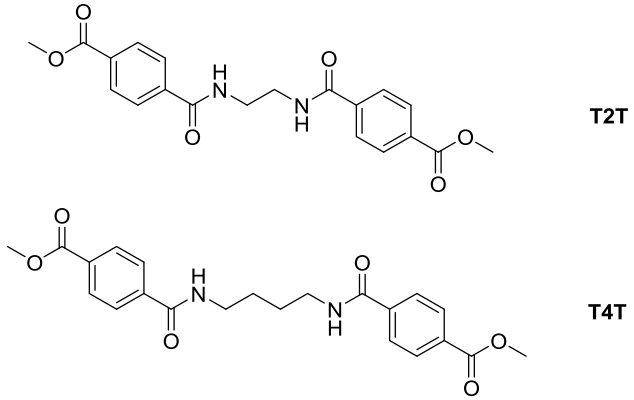

Figure 6.2 Molecular structures of the bisester diamide comonomers T2T and T4T synthesised by Gaymans *et al*.[8,12]

It was observed that inclusion of T2T at 30 mol% with respect to PET linearly increased the T_g from 88 to 112 °C, with the T_m rising by 21 °C from 254 °C. As T2T provides a comonomer residue that has a similar unit length as the chain-repeat in PET, it is confirmed that incorporation of amide bonds into PET is sufficient to increase the T_g. Furthermore, the

undercooling temperature ($\Delta T = T_m - T_g$) decreased from 76 to 58 °C for PET*co*(T2T)-2, indicating an increased crystallisation rate.

Despite the PET*co*(T2T) copolymer series displaying some retention of semi-crystalline behaviour, the value of ΔH_m decreases from 53 to 8 J g^{-1} for PET*co*(T2T)-30. This trend suggests that PET and T2T are not completely isomorphic as comonomers. The synthesis of a T2T equivalent that, in theory, *is* able to cocrystallise with PET was provided by Harashina *et al.*[14] *N*,*N*'-Bis(2-hydroxyethyl)terephthalamide (BHTA) was synthesised by reaction of DMT with ethanolamine as detailed in earlier literature,[15,16] enabling the subsequent copolymerisation with DMT and EG at 0-50 mol% imide content.

Figure 6.3 illustrates the similarity in comonomer chain length between BHET and BHTA, as expected considering BHTA is the analogous monomer for poly(ethylene terephthalamide). The substitution of amide for ester bonds therefore results in little geometric change, which might well therefore produce a semi-crystalline copoly(ester-amide) series. This was observed[14] up to 40 mol% BHTA content, to give a T_m of 256 °C. However, neither the ΔH_m value nor DSC trace for any PET*co*(BHTA) copolymer above 3 mol% are given in the literature, so the quantitative extent of semi-crystalline behaviour in this system is unknown.

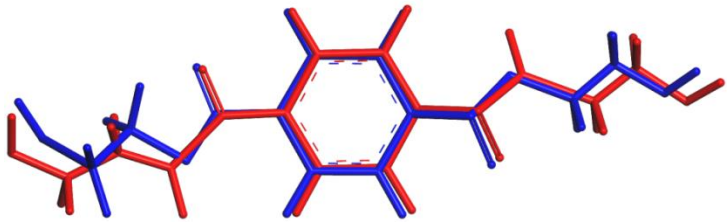

Figure 6.3 Overlaid energy minimised chemical structures of bis(2-hydroxyethyl) terephthalate, BHET, (blue) and *N*,*N*'-bis(2-hydroxyethyl)terephthalamide, BHTA, (red).

Incorporation of T4T with PBT yielded similar results to those seen in the PET*co*(T2T) copolymer series, with increased T_gs, T_ms and crystallisation rates exhibited by PBT*co*(T4T) copolymers relative to PBT. In particular, the T_g was observed to rise from 47 (PBT) to 160 °C (T4T homopolymer). The non-linear rise in T_m across the PBT*co*(T4T) copolymer series indicated a lack of structural isomorphism between PBT and T4T.

Melt-crystallisation in a statistically random copoly(ester-amide) containing two non-isomorphic comonomers i.e. that are unable to cocrystallise is therefore proposed[11] to occur via an "amide-adjacent" mechanism (Figure 6.4). The amide comonomer units are initally believed to self-associate through a hydrogen bonding mechanism, upon which the ester comonomer units order into lamellae. As the amide units crystallise fastest, they serve

as nucleation sites for the subsequent crystallisation of ester units. This leads to an enhanced crystallisation rate upon amide incorporation in polyesters, as observed for the PET*co*(T2T) and PBT*co*(T4T) copolymer series.

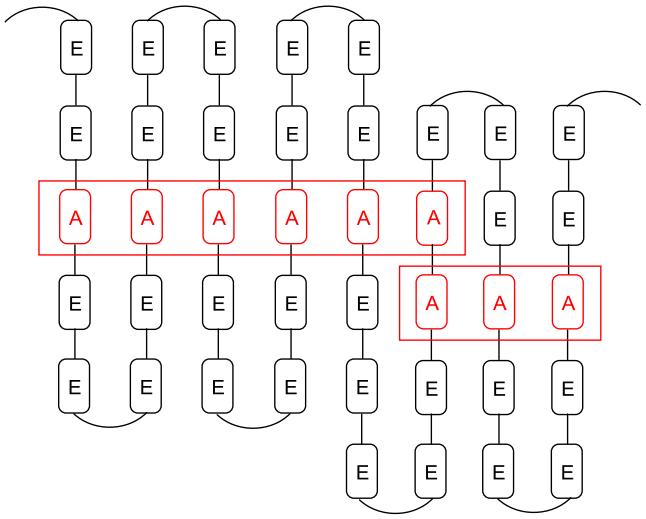

Figure 6.4 Amide-adjacent crystallisation schematic in a statistically random copoly(ester-amide) proposed by Gaymans *et al.*[11] where E = ester, A = amide.

For an amide comonomer that displays non-uniform chain length, the plane of hydrogen bonding in a lamellar is disrupted leading to the depression of a copoly(ester-amide) $T_{m.}$ It therefore seems probable, that an amide-adjacent crystallisation mechanism will not occur in a copoly(ester-amide) if the ester and amide comonomers possess different chain lengths and dimensions. However, if cocrystallisation occurs between two comonomers of a similar chain length, then an increased crystallisation rate should be facilitated.

The inclusion of predominantly aromatic amide comonomers in PET has also been considered by both Hibbs *et al.*[17] and Yamada *et al.*[18] Unlike the T2T and T4T comonomers discussed previously, the comonomers MIM, TPT and PTA (Figure 6.5) aimed to increase the T_g as a result of increased intramolecular chain stiffness *in addition* to the replacement of ester for amide functional groups.

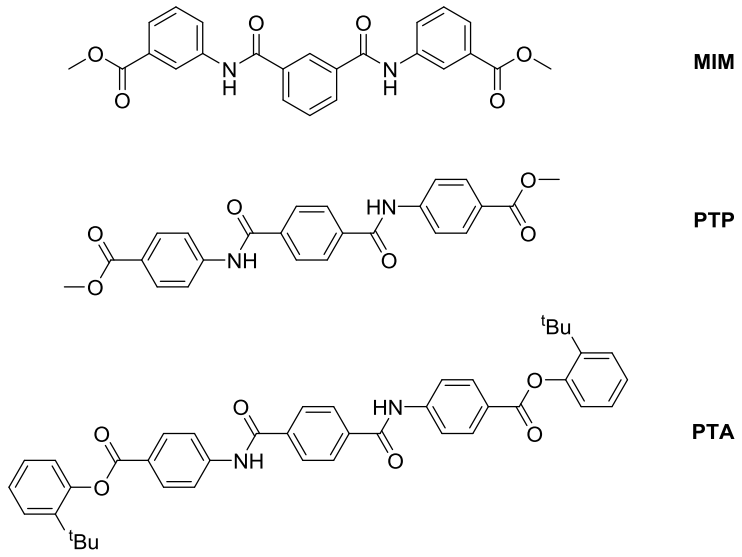

Figure 6.5 Molecular structures of the rigid amide comonomers MIM, PTP and PTA synthesised by Hibbs *et al*.[17]and Yamada *et al*.[18]

Copolymerisation of PET with MIM at 5 and 20 mol% by Hibbs *et al*. afforded copoly(ester-amide)s possessing T_gs of 85 and 90 °C, an increase of 5 and 10 °C, respectively over PET. Although PET*co*(MIM)-5 retains semi-crystalline behaviour (T_m = 237 °C, ΔH_m = 32 J g^{-1}), PET*co*(MIM)-10 is an amorphous material. It is probable that the introduction of a *meta*-kink into the copolymer has disrupted the chain packing and ability to melt-crystallise, as observed for PET*co*(**5.2**)-10 in Chapter 5. However, a similar rise in T_g (to 86 °C) was observed following just 2 mol% incorporation of PTP, accompanied by a significant χ_c (24%). The synthesis of PET*co*(PTP) copolymers containing > 2 mol% PTP was not possible via a melt-polymerisation route. This was attributed to the limited of solubility of PTP in BHET and the incomplete transesterification of PTP before the polycondensation stage (as the polymerisation was performed in two steps).

In contrast, Yamada *et al*. prepared oligomers of PTA with a X_n of 4.5. Upon copolymerisation with PET at 6 wt%, the rigid PTA segments were exclusively found in the amorphous PET segments. The level of crystallinity was therefore reduced (39 to 31% post-anneal) with respect to PET, but with a rise in T_g of 5 °C. In uniaxially oriented film form, PET*co*(PTA)-6 exhibited superior mechanical properties with both E and the yield stress, σ_y, increasing due to improved orientation of the copolymer amorphous chains. This suggests that the introduction of rigid amide comonomers, modelled on Kevlar, may be successful in improving the thermomechanical properties of PET.

The literature on terephthalate-based copoly(ester-amide)s is thus promising, but not extensive. It is clear that incorporation of rigid amide comonomers that possess a similar

chain-repeat length to either BHET or the BHET dimer, would be successful in raising the T_g of PET as detailed in Chapter 5. However, it is unknown whether copolymerisation with a BHET amide analogue (such as BHTA) or a novel comonomer modelled on Kevlar® is more appropriate for this task. Therefore, in this chapter, the copolymerisation of several rigid amide comonomers and their ester analogues with PET is described and evaluated.

6.3 Results and discussion

6.3.1 Proof of concept studies

6.3.1.1 Polymer synthesis and characterisation

Previous studies by Gaymans *et al*.[8] and Harashina *et al*.[14] have shown that the introduction of an amide facilitated hydrogen bonded network in PET, will increase the T_g. However, the incorporation of T2T with PET at 30 mol% resulted in a near amorphous material. This is in addition to there being no available quantitative thermal data for PET*co*BHTA containing > 3 mol% amide. Therefore, in order to investigate the extent of T_g enhancement in PET after copolymerisation with a structurally analogous BHET amide comonomer, the initial research by Harashina *et al*. was developed further here. This work may then decide whether an increased T_g *and* significant retention of semi-crystalline behaviour is achievable for a control copoly(ester-amide) series, as observed in Chapters 3, 4 and 5.

Synthesis of *N*,*N*'-bis(2-hydroxyethyl) terephthalamide, comonomer **6.1**, was achieved in excellent yield (85%) from the reaction of DMT and 2-aminoethanol as previously reported.[16] Melt-copolycondensation of BHET with **6.1** was performed on a laboratory-scale, as described in Chapter 2, with **6.1** incorporated at 5, 10 and 20 mol% (Scheme 6.1). The alternating PET*co*(**6.1**) copolymer, PET*co*(**6.1**)-50, was synthesised by reaction of terephthaloyl chloride with **6.1** in 1-chloronaphthalene as utilised for the synthesis of PEN*co*(**3.1**)-50 and PET*co*(**5.1**)-50 in Chapters 3 and 5, respectively.

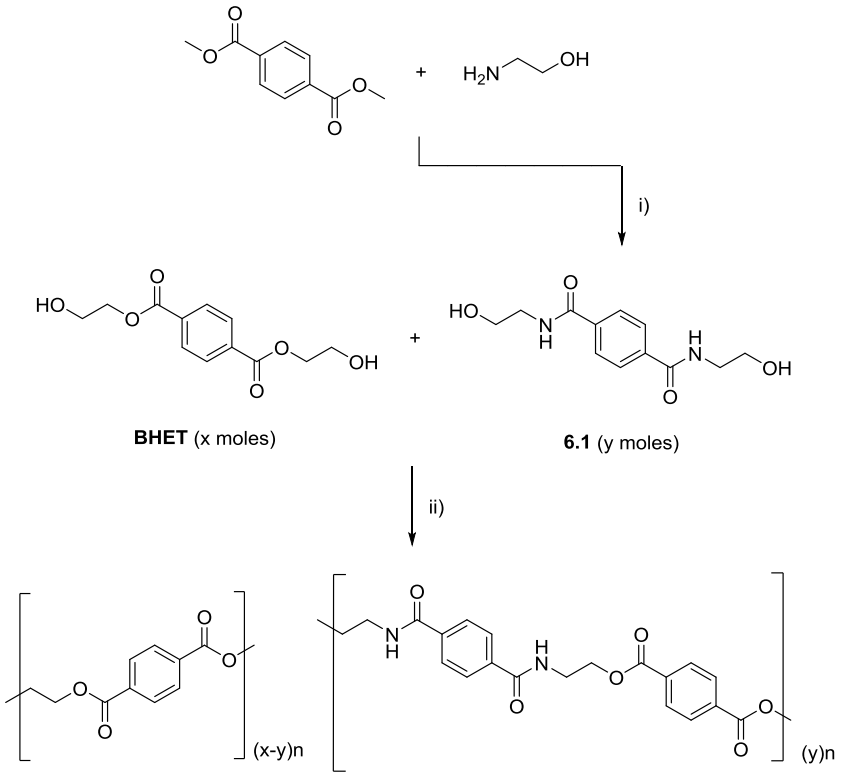

Scheme 6.1 Synthesis of PET-based copoly(ester-amide)s via melt-copolycondensation of bis(2-hydroxyethyl) terephthalate (BHET) and bis(2-hydroxyethyl) terephthalamide (**6.1**), where y ≤ x. Reaction conditions: i) 120 °C, 16 h; ii) Sb_2O_3, 280 °C, 2.5 h, < 1mbar.

Analysis by ^{1}H NMR spectroscopy confirmed the successful copolymerisation of BHET with **6.1**. The final copolymer composition ratios were in good agreement with the comonomer feed ratios, determined to be at least 90% of the feed ratios for all copolymers. This incorporation of amide residues is observed in Figure 6.6, illustrated by the emergence of terephthalamide and ethylene resonances denoted as H_b, H_e and H_f, respectively.

Following copolymerisation, an increasing **6.1** content resulted in progressively darker PET*co*(**6.1**) copolymer laces (reactor extrudates), ranging from light yellow for PET*co*(**6.1**)-5 to brown for PET*co*(**6.1**)-20. GPC analysis (HFIP) gave M_ns between 3,600-4,600 Da, indicating reasonable molecular weights in comparison to PET (M_n = 6,300 Da). It is therefore unlikely that the dark colour originates from degraded copolymer. TGA 1st heating scans (10 °C min^{-1}) of the PET*co*(**6.1**) copolymer series revealed a progressive decrease in T_d upon increasing amide content, with T_d = 420, 390 and 330 °C for PET, PET*co*(**6.1**)-5 and 50 respectively (Figure 6.7). The melt-copolycondensation extrusion temperature of 280 °C is therefore too low to cause thermal degradation to any PET*co*(**6.1**) copolymer. It is probable that the change in colour may be attributed to macromolecular chain conjugation or thermal degradation of the **6.1** comonomer, which will be discussed later in more detail.

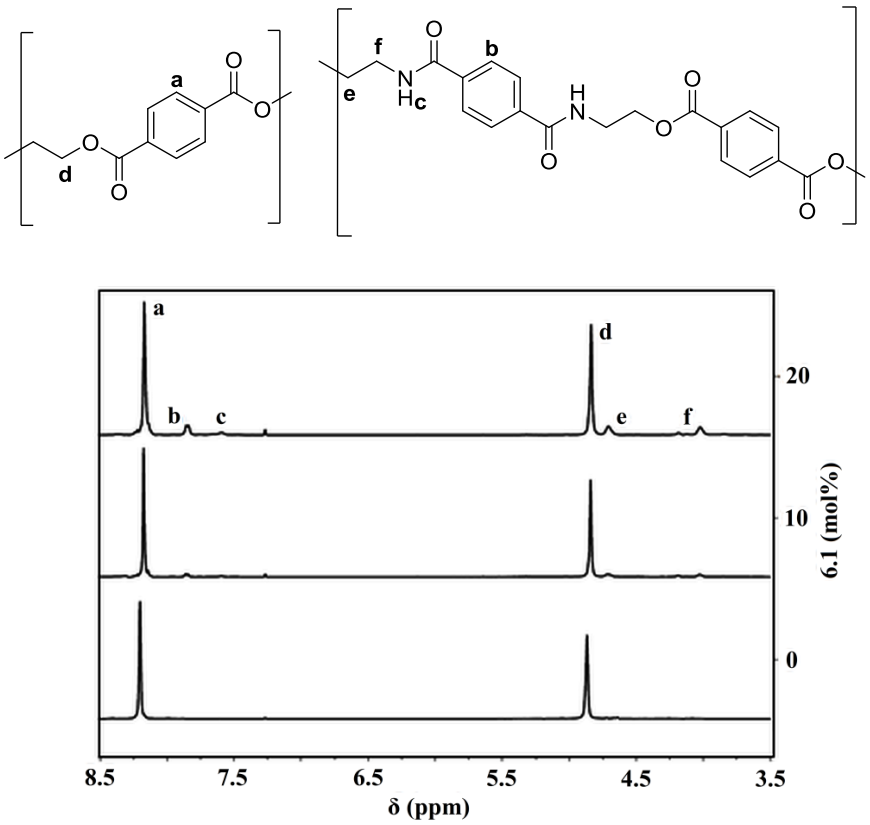

Figure 6.6 ^{1}H NMR spectrum, with assignments of a PET-based copoly(ester-amide) incorporating **6.1**, and comparison of ^{1}H NMR spectra for selected PET*co*(**6.1**) copolymers.

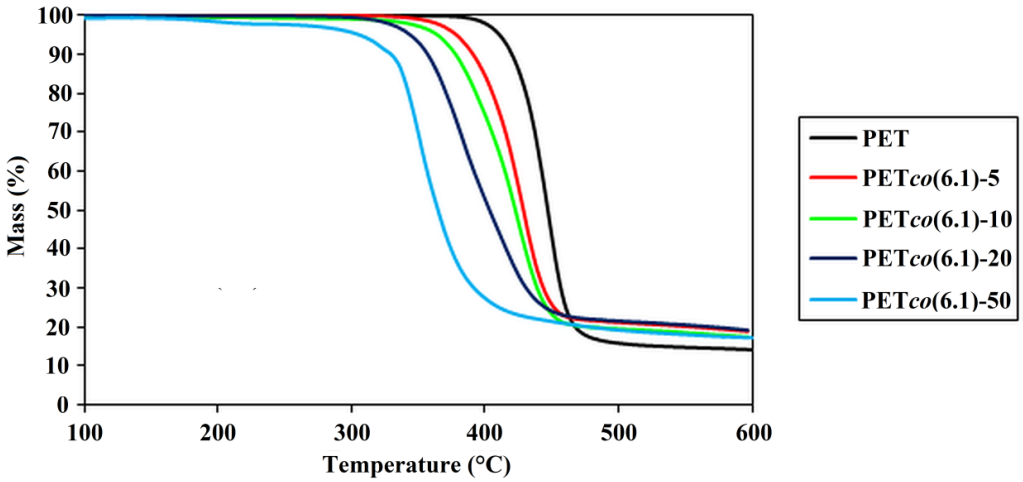

Figure 6.7 Comparative TGA scans (10 °C min^{-1}) of PET and the PET*co*(**6.1**) copolymer series.

It is noted that, in contrast to all of the thermally stable copoly(ester-imide)s previously synthesised in Chapters 3, 4 and 5, the T_d progressively decreases with increasing *amide* comonomer content. The thermal decomposition of semi-aromatic polyamides is proposed[14,19] to occur by the mechanism illustrated in Scheme 6.2. Here, a β-hydrogen transfer reaction accompanied by C-O scission in the ethylene unit forms carboxyl and *N*-vinylamide end groups. This process occurs via a 6-membered transition state as observed

for semi-aromatic polyesters such as PET,[20,21] but at lower temperatures, which in turn result in decreased T_ds for the PET*co*(**6.1**) copolymer series.

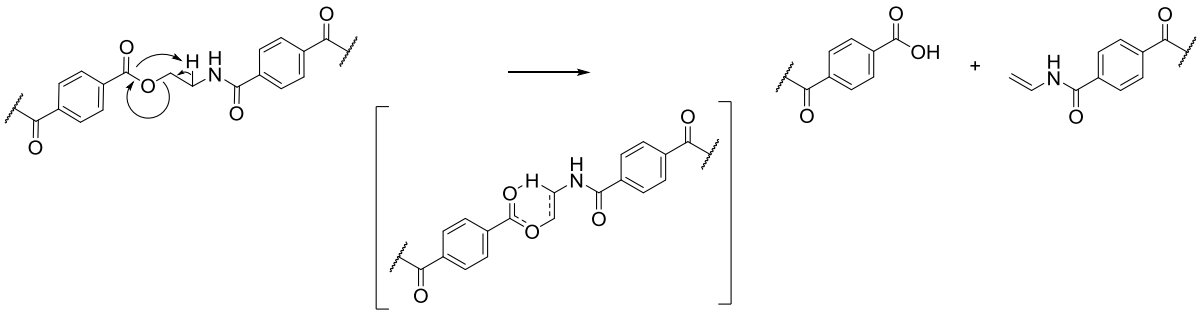

Scheme 6.2 Thermal decomposition mechanism for the PET*co*(**6.1**) copolymer series.

6.3.1.2 Thermal properties

Figure 6.8 illustrates the rise in T_g from PET itself, upon copolymerisation with **6.1**. All thermal properties for the PET*co*(**6.1**) copolymer series (with the exception of T_c) were determined from DSC 1st heating scans (20 °C min^{-1}), to avoid the risk of thermal degradation identified by TGA. It is observed that upon 20 mol% **6.1** content, there is a rise of 17 °C in the T_g. This is in rough agreement with the PET*co*(T2T)-30 copolymer synthesised by Gaymans *et al*.[8] which possessed a T_g of 112 °C, some 19 °C higher. Thus it is concluded that the T_g of PET may be significantly increased by the inclusion of amide residues.

In the PET*co*(**6.1**) copolymer series, the T_m initially decreases upon **6.1** incorporation, falling from 257 to 243 °C for PET and PET*co*(**6.1**)-20 respectively. A depressed T_m upon amide incorporation is in agreement with the work of Gaymans *et al*,[8] who observed a eutectic point at between 15-20 mol% T2T. It is therefore probable that PET*co*(**6.1**)-20 represents the eutectic point in this copolymer series, with the T_m rising substantially for the alternating copolymer, PET*co*(**6.1**)-50. The observed T_m of 333 °C for PET*co*(**6.1**)-50 is in good agreement with the literature value determined by Lu *et al*.[15] (332 °C). Upon annealing at 200 °C for 2 h, the ΔH_m values for PET*co*(**6.1**)-5 to 20 all exceed 45.45 J g^{-1} (χ_c > 32%).

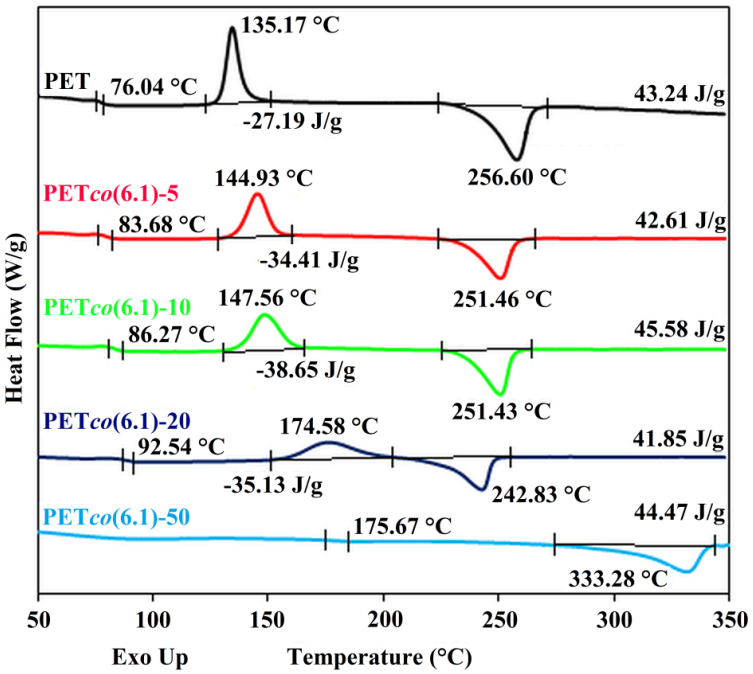

Figure 6.8 DSC 1st heating scans (20 °C min^{-1}) of PET and the PET*co*(**6.1**) copolymer series.

The entire PET*co*(**6.1**) copolymer series (when synthesised by melt-copolycondensation) exhibit T_{cc} exotherms indicating facile crystallisation upon heating. However, values for T_{cc} progressively increase upon **6.1** incorporation from 135 to 175 °C for PET and PET*co*(**6.1**)-20, respectively. This suggests a lowered crystallisation rate for the PET*co*(**6.1**) copolymer series in contrast to PET. Further evidence in support of slower crystallisation kinetics is illustrated in Figure 6.9 by the DSC 1st cooling scans of PET, PET*co*(**6.1**)-5 and 10. Although PET*co*(**6.1**)-5 and 10 are able to melt-crystallise to achieve a greater χ_c than PET (ΔH_c = -50.3 and -54.0 J g^{-1}, respectively), values for T_c decrease from 219 to 191 °C. It is noted that PET*co*(**6.1**)-20 also possesses the ability to melt-crystallise (T_c = 153 °C, ΔH_c = 15.9 J g^{-1}) but this is not shown in Figure 6.9 for reasons of scale.

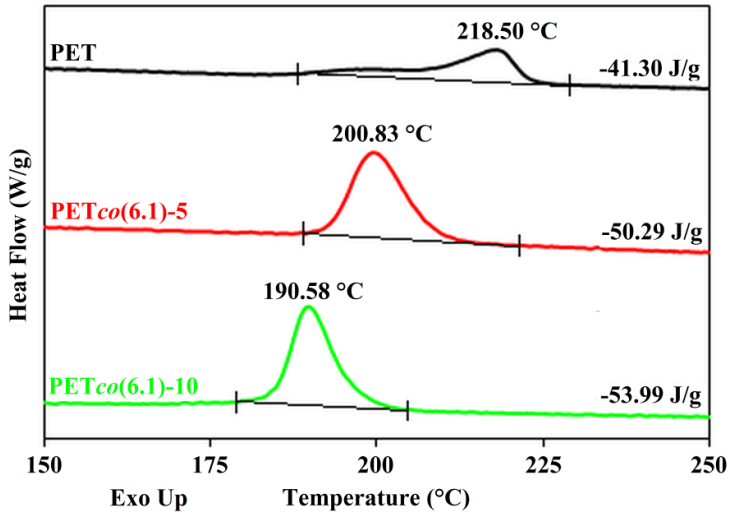

Figure 6.9 DSC 1st cooling scans (5 °C min^{-1}) of PET and selected PET*co*(**6.1**) copolymers.

The trends in T_c and T_{cc} for the PET*co*(**6.1**) copolymer series illustrated in Figure 6.8 and Figure 6.9 do not indicate enhanced crystallisation rates, despite an isomorphic amide comonomer having been incorporated. It is therefore likely that the crystallisation rate only increases for a PET-based copoly(ester-amide), relative to PET, when small amounts of amide comonomer are present. This feature was previously observed by Xiao *et al.*[22], who established that small amounts (< 2 mol%) of a rigid imide comonomer could act as a nucleating agent for PET and infact increase the crystallisation rate.

As crystallisation rates increase via the amide-adjacent melt-crystallisation model proposed by Gaymans *et al*., this mechanism is most likely only valid for copoly(ester-amide)s at low amide comonomer content. In practice, it appears more important to ensure that the two comonomers are of very similar chain length and therefore potentially isomorphic in character (which is stated as a prerequisite), in order to retain semi-crystalline behaviour and a comparable crystallisation rate. This phenomenon was previously observed for the PEN*co*(**3.1**) and PET*co*(**5.1**) copolymer series in Chapters 3 and 5, respectively. However, if the ester and amide comonomers are of similar chain length, then any increase in crystallisation rate may be facilitated by the proposed crystallisation mechanism.

6.3.1.3 X-ray powder diffraction and computational modelling

Analysis by X-ray powder diffraction suggests a subtle yet noticeable change in crystal structure for the PET*co*(**6.1**) copolymer series, upon progressive incorporation of comonomer **6.1** into PET. Figure 6.10 illustrates the shift in (011) and (100) peaks from 2θ = 22.8 and 26.2° to 23.2 and 24.9° respectively for PET*co*(**6.1**)-20. Furthermore, the $(01\bar{1})$ and (010) peaks coalesce to a single peak measured at 2θ = 17.3°.

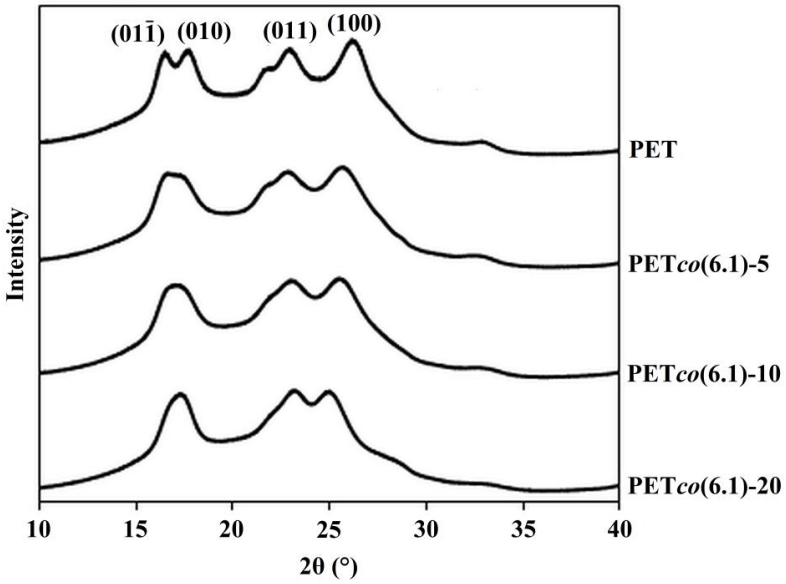

Figure 6.10 X-ray powder diffraction patterns of PET and the PET*co*(**6.1**) copolymer series.

PET*co*(**6.1**)-20 was consequently modelled as a polymorph of PET in space group $P\bar{1}$, utilising the same method as described for PET*co*(**5.1**)-15 in Chapter 5. Reitveld refinement (R_{wp} = 12%) of the manually adjusted, simulated PET*co*(**6.1**) model against the experimental powder pattern of PET*co*(**6.1**)-20 (Figure 6.11) gave a proposed crystal structure with cell parameters a = 4.56, b = 5.95, c = 10.75 Å, α = 99.2, β = 117.8, γ = 111.9°, ρ = 1.43 g cm^{-3}. With respect to the unit cell of PET, the cell parameters of PET*co*(**6.1**)-20 differ by < 1%. This suggests that **6.1** may be easily accommodated in the PET crystal lattice, with any change in powder diffraction being representative of only small changes in cell parameters. It is therefore reasonable to propose that cocrystallisation is occurring between PET and **6.1**, due to the retention of semi-crystalline behaviour exhibited upon analysis by DSC and X-ray powder diffraction.

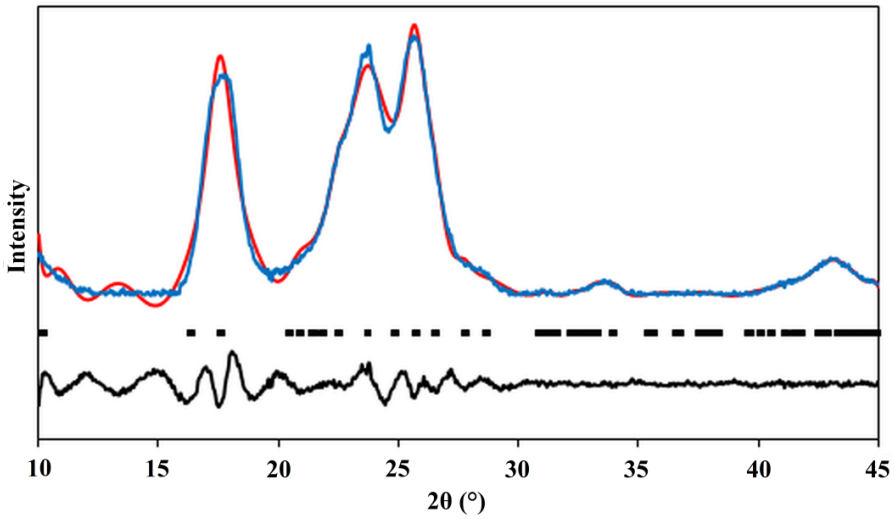

Figure 6.11 Reitveld refinement plot for PET*co*(**6.1**)-20 (R_{wp} = 12%), where red = simulated X-ray powder diffraction pattern, blue = experimental X-ray powder diffraction pattern, black rectangles = observed ticks and black = difference.

6.3.2 Synthesis of rigid copoly(ester-amide)s

6.3.2.1 Polymer synthesis and characterisation

Section 6.3.1 outlined the proportional rise in T_g for PET following copolymerisation with **6.1**. However, this enhancement in thermal properties was accompanied by a decrease in thermal stability attributed to an increased β-H transfer reaction rate. It is therefore reasonable to assume that a PET-based copoly(ester-amide) with a rigid amide comonomer that does *not* contain an amide-adjacent ethylene unit, would exhibit both an increased T_g *and* comparable thermal stability.

The isomorphic character displayed between PET and **5.1** in Chapter 5 demonstrated how the retention of semi-crystalline behaviour was achievable at high comonomer contents. This enabled the proposal of two new rigid amide comonomers (**6.2** and **6.3**) that possess similar chain lengths to the BHET dimer and **5.1**, where it was envisaged that similar morphological behaviour would be observed (Figure 6.12). The ester analogue of **6.2**, comonomer **6.4,** was also tested as a potential variant to investigate the effect of a rigid amide intermolecular network against a reference comonomer.

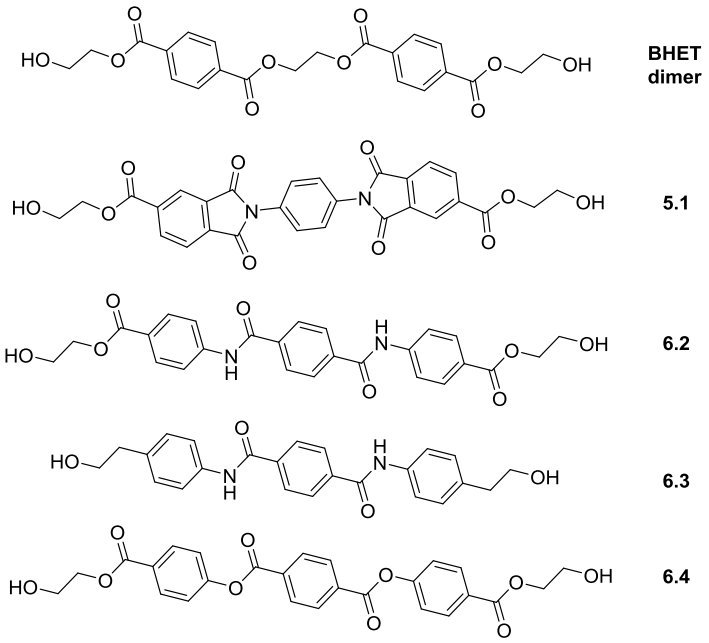

Figure 6.12 Comparative chain length of the BHET dimer against designed, rigid, amide comonomers.

The adapted[23] reaction of terephthaloyl chloride with 4-aminobenzoic acid and 4-aminophenethyl alcohol at room temperature afforded "**6.2** intermediate" and **6.3** in excellent yields of 90 and 89%, respectively. The glycolisation of **6.2** intermediate to afford **6.2** was achieved by the previously utilised 2-bromoethanol route as discussed in Chapter 5.

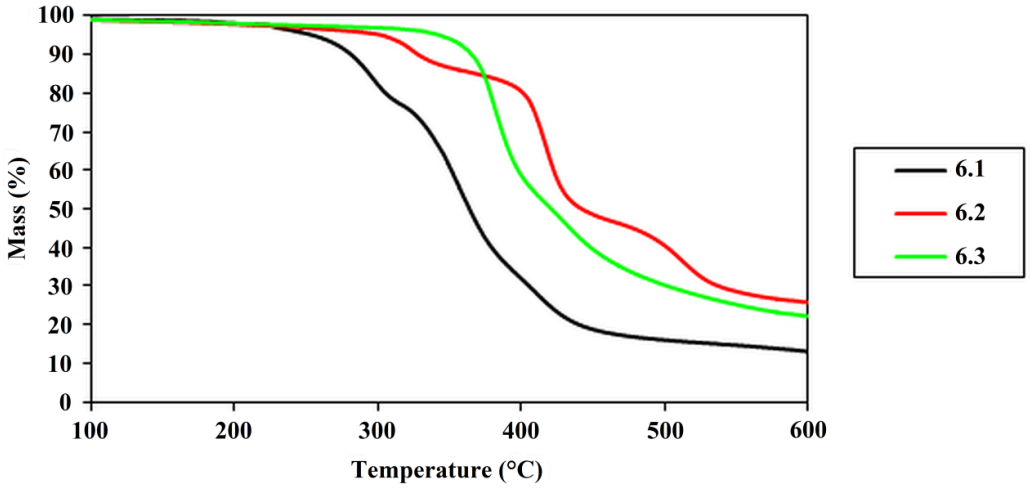

Figure 6.13 TGA heating scans (10 °C min^{-1}) of amide comonomers **6.1**-**6.3**.

In comparison to **6.1**, comonomers **6.2** and **6.3** display superior thermal stability as illustrated by the comparative TGA heating scans (10 °C min^{-1}) in Figure 6.13. Onset T_d values of > 300 °C are observed under a nitrogen atmosphere, inferring that degradation would not occur under the standard polycondensation operating conditions. This result confirms that the thermal stability of an amide comonomer may be increased by the removal of an aliphatic unit adjacent to the amide functional group, as observed for **6.1**.

PET-based copoly(ester-amide)s incorporating **6.2** and **6.3** were synthesised by the laboratory-scale melt-polycondensation route described in Chapter 2, with amide comonomer content ranging from 2-8 mol%. This is illustrated in Scheme 6.3 using **6.2** as the example comonomer. In contrast to the synthesis of PET-based copoly(ester-imide)s in Chapter 5, the bisester diamide units present in **6.2** and **6.3** introduce dicarboxyl functional groups that may be susceptible to transesterification reactions. Although the central bis-ester diamide unit would still be present post-interchange, the effective comonomer chain length of **6.2** and **6.3** would be shortened, reducing the rigidity relative to PET.

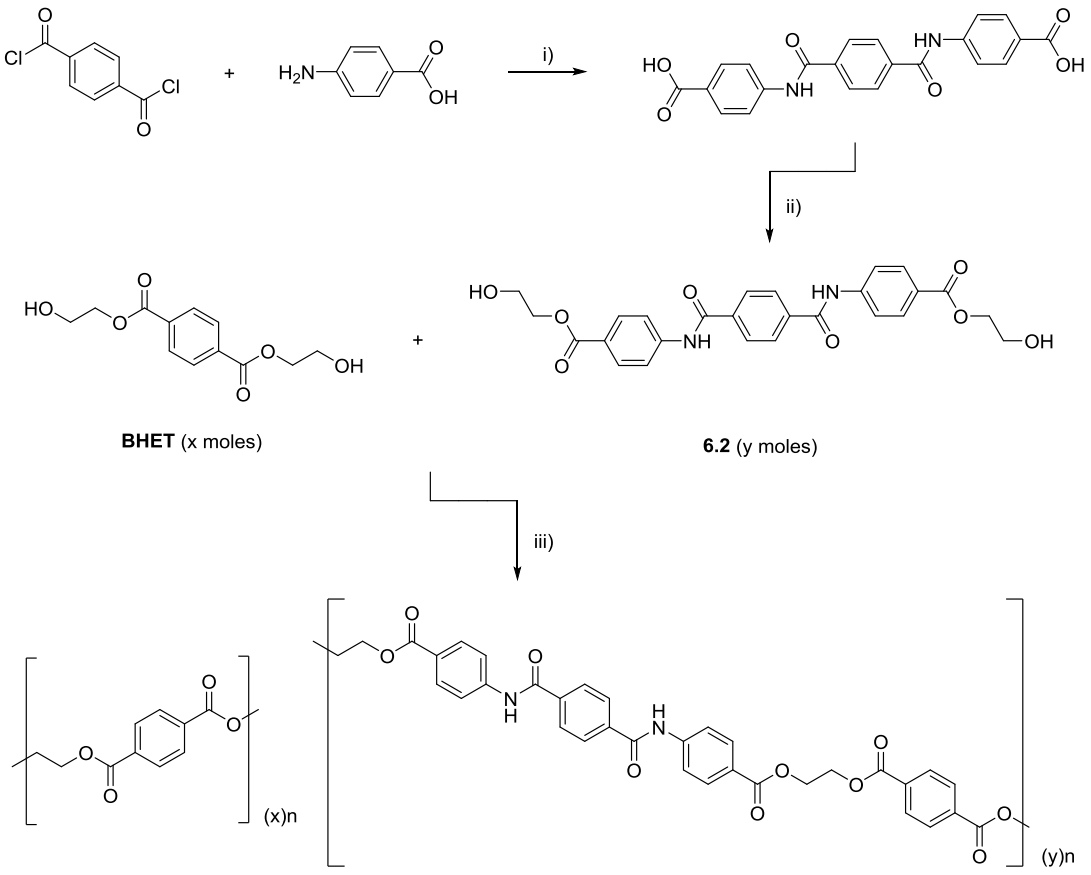

Scheme 6.3 Synthesis of PET-based copoly(ester-amide)s via melt-copolycondensation of bis(2-hydroxyethyl) terephthalate (BHET) with aromatic amide comonomers (**6.2** as example), where $y \leq x$. Reaction conditions: i) Pyridine, dioxane, RT, 16 h, 90%; ii) 2-Bromoethanol, TEA, DMF, 80 °C, 16 h, 57%; iii) Sb_2O_3, 280 °C, 2.5 h, < 1mbar.

Melt-copolycondensation reactions were therefore conducted for 0.5 h and at 280 °C to minimise the possibility of amide-ester interchange side reactions. Hence, the formation of amide blocks within a copoly(ester-amide) may be controlled by reducing the time for which the copolymer is at relatively high temperatures.[8] To ensure a sufficient molecular weight for the synthesised PET-based copoly(ester-amide)s, selected samples were subjected to SSP at 200 °C for 16 hours post-copolycondensation.

Figure 6.14 illustrates the comparative ^{13}C NMR spectra of PET, **6.2** and PET*co*(**6.2**)-8. It is clear that **6.2** has been successfully incorporated into PET, as the aromatic C=C resonances associated with PET*co*(**6.2**)-8 are in good agreement with those visible in comonomer form. The ^{13}C NMR spectrum of PET*co*(**6.2**)-8 indicates the presence of three resonances, denoted by blue asterisks, that do not correspond to PET or **6.2**. However, these resonances are relatively weak, suggesting that the majority of **6.2** has remained intact during copolycondensation. Analysis by ^{1}H NMR spectroscopy confirmed copolymerisation of **6.2** and **6.3** with PET, whereby the copolymer composition ratios largely matched the initial comonomer feed ratios of ester to amide. This further confirms the inclusion of rigid amide residues in PET with minimal disruption to the central bisester diamide units in **6.2** and **6.3**.

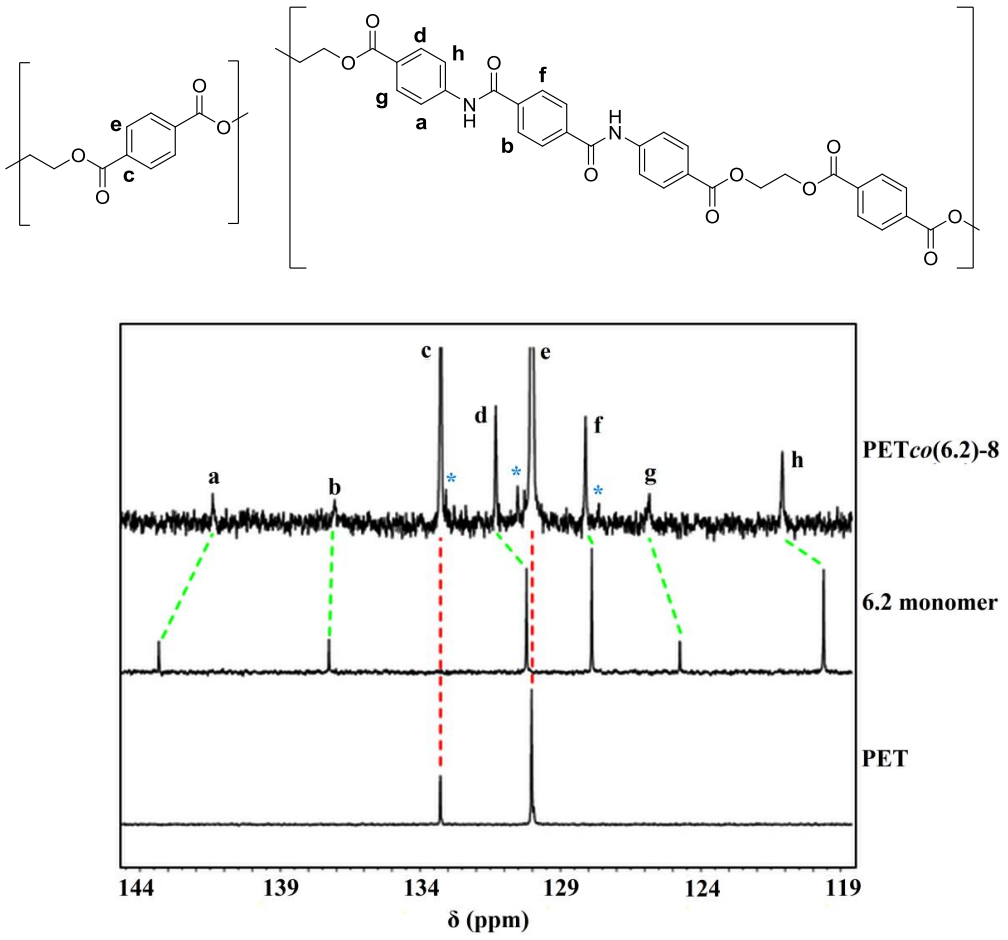

Figure 6.14 Comparative ^{13}C NMR spectra of PET, **6.2** and PET*co*(**6.2**)-8, together with the ^{13}C NMR assignments for a PET*co*(**6.2**) copolymer.

6.3.2.2 Polymer rheology and morphology analysis

The copolymerisation of rigid amide comonomers with PET had a pronounced effect on the polymer's melt-processability, relative to that of PET. Incorporation of **6.2** and **6.3** at 2 mol% afforded extrudable materials as copolymer fibres in the same manner as PET. However this

was not achievable above 4 mol% inclusion with respect to **6.2**. It was suspected that η* had been substantially raised following the introduction of a rigid hydrogen bonded network. This perceived increase in η* was seen experimentally, with the mechanical stirrer unable to agitate the copolymer melt for the entire polycondensation reaction time period (30 minutes) under vacuum at 280 °C. Melt-copolycondensation reactions for PET*co*(**6.2**)-6 and 8 were therefore stopped after 15 minutes at the extrusion temperature.

Figure 6.15 illustrates the comparative rheological properties of PET*co*(**6.2**)-2 and 8, confirming the experimental observations described previously. Both copolymers exhibit conventional rheological behaviour for semi-crystalline polymers with respect to temperature, whereby η* decreases sharply past the T_m indicating viscoelastic flow. However, this fall in η* is more prominent for PET*co*(**6.2**)-2. At the extrusion temperature of 280 °C, values of η* for PET*co*(**6.2**)-2 and 8 are ~ 150 and 1600 Pa s signifying processable and unprocessable materials, respectively.

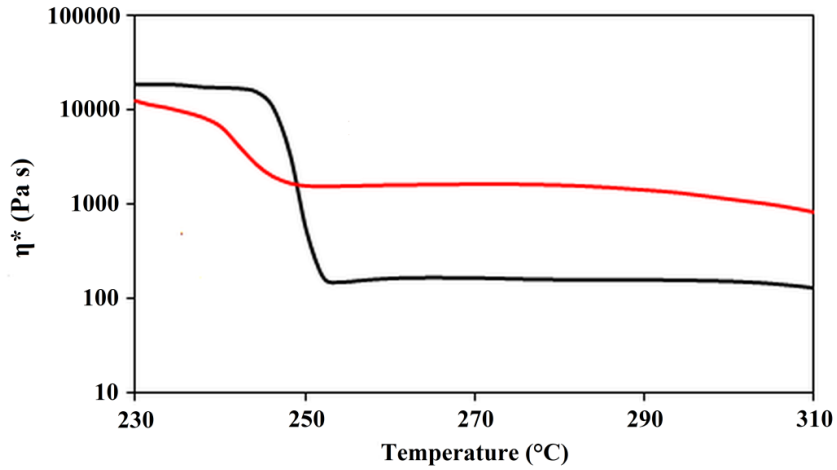

Figure 6.15 Comparative rotational rheology analysis of PET*co*(**6.2**)-2 (black) and PET*co*(**6.2**)-8 (red) performed in temperature sweep mode (heating rate of 4 °C min^{-1}, frequency of 10 rad s^{-1} and 5% strain).

In terms of molecular weight distributions for the PET-based copoly(ester-amide)s synthesised in the present work, there appears to be a general decrease in M_w upon increasing amide content. This is somewhat to be expected considering the shortened melt-copolycondensation reaction time relative to PET, especially for PET*co*(**6.2**)-6 and 8 which gave M_w values of 6,300 and 8,400 Da respectively. It is clear that the sequential step-growth copolycondensation is incomplete at the enforced reaction endpoint, thus restricting the concurrent removal of ethylene glycol.

The molecular weights of PET-based copoly(ester-amide)s containing 4 mol% amide may be increased by at least 60% by SSP. This increase in M_w is not to the detriment of the molecular

weight distribution, as Đ values decrease below their pre-SSP equivalents in both cases. However, each post-SSP M_w value is still inferior to that obtained for PET pre-SSP. This observation suggests that for future industrial purposes, amide incorporation may have to be limited to 2 mol% in order to manufacture copolymers that have sufficient molecular weights.

Table 6.1 Molecular weight distributions and dispersities of PET, the PET*co*(**6.2**) and PET*co*(**6.3**) copolymer series.

Polymer		M_w[a]	M_n[a]	M_z[a]	Đ
		Da	**Da**	**Da**	**-**
PET	pre-SSP	20,600	6,360	37,500	3.2
	post-SSP	32,800	9,800	60,900	3.3
PET*co*(**6.2**)-2		18,400	4,170	35,200	4.4
PET*co*(**6.2**)-4	pre-SSP	9,000	3,150	15,600	2.9
	post-SSP	14,700	5,750	30,400	2.6
PET*co*(**6.2**)-6		6,300	2,360	12,300	2.7
PET*co*(**6.2**)-8		8,400	2,780	15,700	3.0
PET*co*(**6.3**)-2		21,900	5,460	42,600	4.0
PET*co*(**6.3**)-4	pre-SSP	11,000	2,960	23,600	3.7
	post-SSP	20,000	5,800	60,200	3.4

The increase in η* following incorporation of a rigid amide comonomer is clearly an effect of the greater intramolecular stiffness and extent of intramolecular interactions (hydrogen bonds) in PET*co*(**6.2**)-8, relative to PET. This increased rigidity may also be viewed in terms of the polymer morphology. Semi-crystalline polymers are commonly described[24] by a two-phase model, consisting of only crystalline and amorphous fractions. In terms of heat capacity, this morphology results in the expression:[25]

Equation 6.1
$$\boldsymbol{C_p(T) = \alpha C_{p,SC}(T) + \beta C_{p,A}(T)}$$

where C_p(T), $C_{p,SC}$ (T), $C_{p,A}$ (T) are the temperature dependencies of the specific heat capacities of the semi-crystalline polymer, crystalline phase and amorphous phase respectively, α is the fractional χ_c, and β is the amorphous fraction. Therefore, in a two-phase model, α and β would sum to 100%. However, this was not observed[26] experimentally by DSC, leading to the proposal of a three-phase model to account for the missing C_p. The third fraction [denoted as the rigid amorphous fraction (RAF)] may be defined[27] as amorphous material *immobilised at the interface between the amorphous and crystalline phases*. Considerable experimental evidence has since been collated to support this three-phase model.[28–32]

Due to physical constraints on the RAF enforced by the adjacent crystalline phase, the RAF may not contribute to any heat capacity change at the T_g. The mobile amorphous fraction, MAF, is therefore calculated[33] from Equation 6.2:

Equation 6.2
$$\alpha_{MA} = \frac{\Delta C_{p,SC}}{\Delta C_{p,A}}$$

where $\Delta C_{p,SC}$ and $\Delta C_{p,A}$ represent the change in heat capacity at T_g for the semi-crystalline and amorphous equivalents of a semi-crystalline polymer. Values for ΔC_p were obtained from the 2nd HyperDSC heating scans (175 °C min^{-1}) following cooling scans from the melt at 5 and ~ 900 °C min^{-1}, which generated semi-crystalline and amorphous materials respectively. The χ_c was calculated as detailed in Chapter 2, enabling the calculation of the RAF:

Equation 6.3
$$\alpha_{RA} = 1 - \alpha_{MA} - \alpha_{\chi c}$$

Table 6.2 details the resulting values of the MAF, RAF and χ_c for PET and PET*co*(**6.2**)-4. Incorporation of the rigid amide comonomer **6.2** has resulted in a significantly increased RAF from 18 ± 6 to 62 ± 4%. As PET*co*(**6.2**)-4 is able to melt-crystallise at a comparable level to PET, a simultaneous decrease in the MAF is observed from 56 ± 5 to 18 ± 6%. It is therefore concluded that the inclusion of a rigid, intramolecular hydrogen bonded network has effectively immobilised a large proportion of the amorphous phase.

Table 6.2 Comparative rigid amorphous phase determination of PET and PET*co*(**6.2**)-4, where MAF = mobile amorphous fraction, RAF = rigid amorphous fraction and SD = standard deviation.

Polymer	Crystallinity		MAF		RAF	
	%	SD	%	SD	%	SD
PET	26	3	56	5	18	6
PET*co*(**6.2**)-4	17	2	21	5	62	4

6.3.2.3 Thermal properties

It is established[34,35] that the T_g of a semi-crystalline polyester will increase if a greater RAF is present. The rigidity imparted by the RAF restricts conformational changes in the MAF by hindering chain mobility and reducing the amount of free volume available. This is evident in Figure 6.16, which illustrates the DSC 2nd heating scans (20 °C min^{-1}) of PET and the PET*co*(**6.2**) copolymer series. For PET*co*(**6.2**)-2, the thermal properties of: T_g = 87 °C; T_m = 243 °C matched those previously obtained by Hibbs *et al.*[17].

However, due to the successful change in functionality to **6.2** from the dimethyl ester to the glycolised equivalent, the T_g may be increased beyond 95 °C. A maximum increase of 20 °C

in T_g is observed upon just 6 mol% amide incorporation. This value then falls slightly to 94 °C for PET*co*(**6.2**)-8, attributed to a fall in χ_c from 26 to 12%. In comparison to the thermal characteristics of the PET*co*(**6.1**) copolymer series, just 4 mol% incorporation of **6.2** is sufficient to match the rise in T_g for PET*co*(**6.1**)-20, which emphasises the rigidity imparted by **6.2**. Onset T_d values were determined to be in excess of 400 °C by TGA (10 °C min^{-1}) for the entire PET*co*(**6.2**) copolymer series. This concludes that the transition to a rigid aromatic amide comonomer from **6.1** has been successful in avoiding premature thermal degradation.

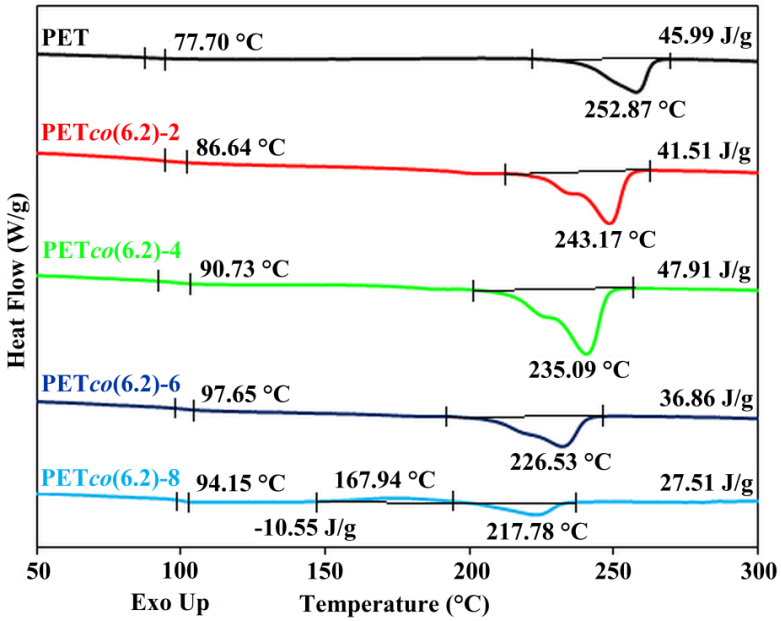

Figure 6.16 DSC 2nd heating scans (20 °C min^{-1}) of PET and the PET*co*(**6.2**) copolymer series.

The T_m is noted to decrease linearly across the PET*co*(**6.2**) copolymer series with respect to increasing **6.2** content, reaching 218 °C for PET*co*(**6.2**)-8. It is extremely unlikely that the theoretical **6.2** homopolymer would possess a T_m lower than PET, therefore suggesting that a 35 °C fall in T_m is not part of a eutectic trend as observed for the PET*co*(**5.1**) copolymer series. It appears more probable that **6.2** is somewhat compatible with the PET crystal lattice, which enables melt-crystallisation to still occur at 8 mol% **6.2** incorporation.

This theory is proposed under the assumption that cocrystallisation is not occurring, with a complete loss of crystallinity expected to occur at ~ 15 mol% comonomer content. The PET*co*(**6.2**) copolymer series therefore exhibits semi-crystalline behaviour across a larger composition range than the PET*co*(**5.5**) and PET*co*(**5.6**) copolymer series in Chapter 5, which produced amorphous materials at > 5 mol% imide. However, as observed for the non-isomorphic PET-based copoly(ester-imide)s, significant χ_cs may be achieved by annealing at 200 °C for 2 h. Values of χ_c > 30 % are obtained for PET*co*(**6.2**)-2, 4 and 6, but

this decreases to 14% for PET*co*(**6.2**)-8 hence displaying further evidence of the non-isomorphic behaviour exhibited at higher **6.2** content.

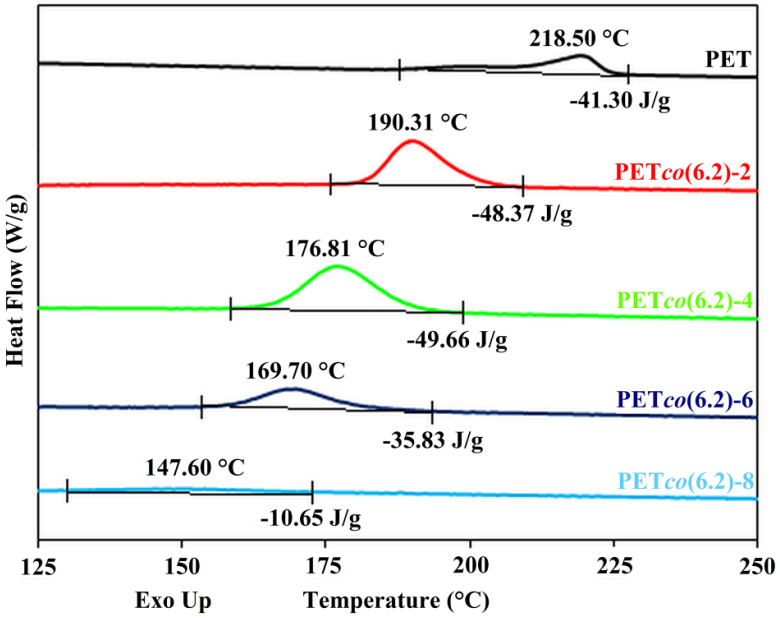

Figure 6.17 DSC 1st cooling scans (5 °C min^{-1}) of PET and the PET*co*(**6.2**) copolymer series.

Figure 6.17 illustrates the DSC 1st cooling scans (5 °C min^{-1}) of the PET*co*(**6.2**) copolymer series. A progressive depression in T_c from PET to PET*co*(**6.2**)-8 (219 and 148 °C respectively) is observed, thus demonstrating a similar trend in thermal properties to that seen in Figure 6.16. Although ΔH_c for PET*co*(**6.2**)-6 is comparable to PET (-41.3, c.f. -35.8 J g^{-1}), the ability of PET*co*(**6.2**)-8 to melt-crystallise is clearly diminished. This in turn results in an observed T_{cc} peak on the 2nd heating scan (168 °C at 20 °C min^{-1}), implying that the crystallisation rate of PET*co*(**6.2**)-8 is slower than that of PET.

Incorporation of comonomer **6.3** into PET produced comparable thermal behaviour to the PET*co*(**6.2**) copolymer series at equivalent levels of amide content (Figure 6.18), as might be anticipated from the similar structural rigidity between **6.2** of **6.3**. Copolymer PET*co*(**6.3**)-4 has a T_g of 92 °C [the T_g for PET*co*(**6.2**)-4 is 91 °C], yet it is unable to melt-crystallise to a similar extent as PET*co*(**6.2**)-4. It is probable this is due to the shorter chain length of **6.3** relative to **6.2** (Figure 6.12), resulting in a less compatible comonomer in terms of isomorphic character. This is reflected in the lower χ_c seen on reheat (21 against 34%, respectively).

Although not presented here, the T_c exotherms for PET*co*(**6.3**)-2 and 4 are only slightly depressed relative to PET, to 203 and 196 °C, respectively. Both copolymers are therefore able to melt-crystallise in a facile manner, with PET*co*(**6.2**)-2 in particular exhibiting a high ΔH_c value of -54.9 J g^{-1}. This is reflected in a raised T_g/T_m ratio of 0.73 from 0.67 for

PET*co*(**6.2**)-4, illustrating the enhancement in thermal performance from the inclusion of either novel rigid amide comonomer. The χ_c of PET*co*(**6.2**) copolymers may be also raised by annealing to achieve relatively high ΔH_m values, especially for PET*co*(**6.3**)-2 at 56.1 J g^{-1}.

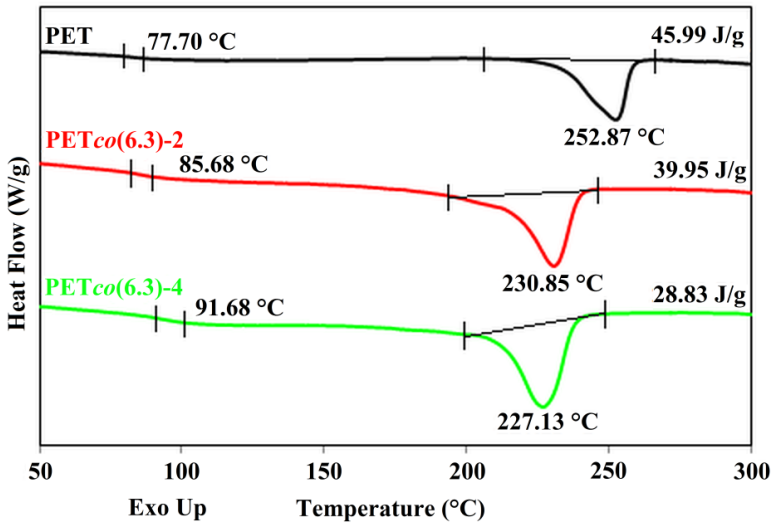

Figure 6.18 DSC 2nd heating scans (20 °C min^{-1}) of PET, PET*co*(**6.3**)-2 and 4.

The introduction of rigid, aromatic amide residues in PET has thus resulted in a pronounced effect on the thermomechanical properties of the resulting PET-based copoly(ester-amide)s. Uniaxially oriented fibre samples of PET, PET*co*(**6.2**)-2 and PET*co*(**6.2**)-4 were drawn until failure (and repeated at least 10 times) to establish load-extension curves and tensile moduli for each sample. Figure 6.19 illustrates the representative load-extension plots of such polymers as the median curve in each case.

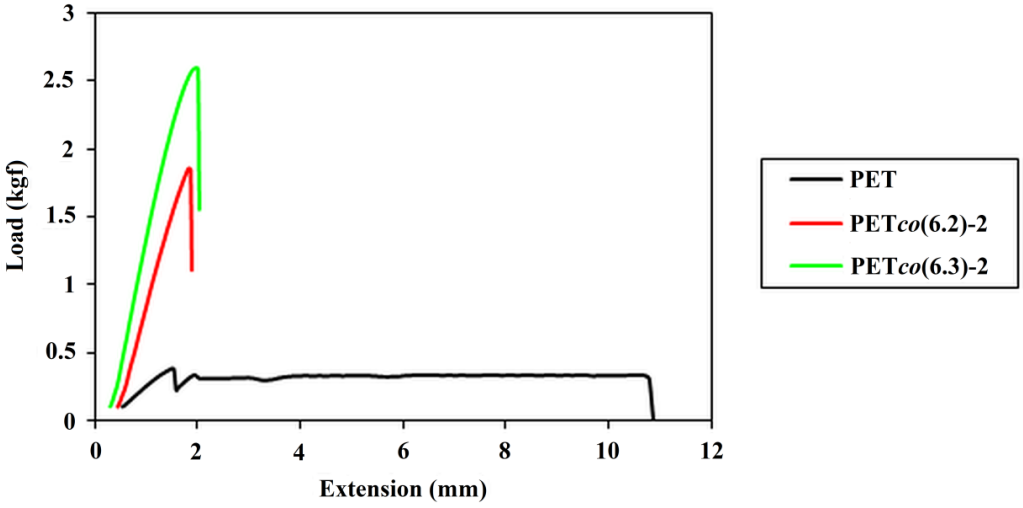

Figure 6.19 Representative load-extension curves for PET and selected PET-based copoly(ester-amide)s.

Table 6.3 Tensile moduli for PET and selected PET-based copoly(ester-amide)s.

Polymer	Tensile modulus (kgf mm^{-2})	
	Average	SD
PET	46	11
PET*co*(**6.2**)-2	110	28
PET*co*(**6.3**)-2	110	21

The transition from a relatively soft, elastic polymer to a hard, stiff and brittle material upon amide inclusion is clearly visible in Figure 6.19. PET exhibits a median elongation to break (ETB) ratio of 25%, far greater than median ETB values of 4 and 3% for PET*co*(**6.2**)-2 and PET*co*(**6.3**)-2 respectively. When in conjunction with an increased load applied before failure for the copoly(ester-amide)s, a very large increase in the tensile modulus is observed (Table 6.3).

This quantitatively confirms the production of more rigid materials, as may be expected when considering the molecular structures of the Kevlar®-based comonomers **6.2** and **6.3**. The observed trade-off between increased rigidity and decreased elongation could be important in producing novel, high-performance *fibres*, but may not be conducive for oriented film production, which would require isotropic forward and sideways draw behaviour.

It was proposed, in reference to Figure 6.16, that the PET*co*(**6.2**) and PET*co*(**6.3**) copolymer series do not contain isomorphic comonomers as near-amorphous materials were produced above 8 mol% **6.2** content. The X-ray powder diffraction patterns of PET, PET*co*(**6.2**)-4 and PET*co*(**6.3**)-4 support this idea. As illustrated in Figure 6.20, there is no significant difference between the respective powder patterns, suggesting that PET-based copoly(ester-amide)s at this content are not forming new copolymer crystal structures. The cell parameters for PET*co*(**6.1**)-20 were previously stated as differing by just < 1% with respect to PET, despite a subtle shift in powder patterns. It is therefore reasonable to assume that PET*co*(**6.2**)-4 and PET*co*(**6.3**)-4 melt-crystallise as PET, or in a very slightly distorted PET crystal lattice.

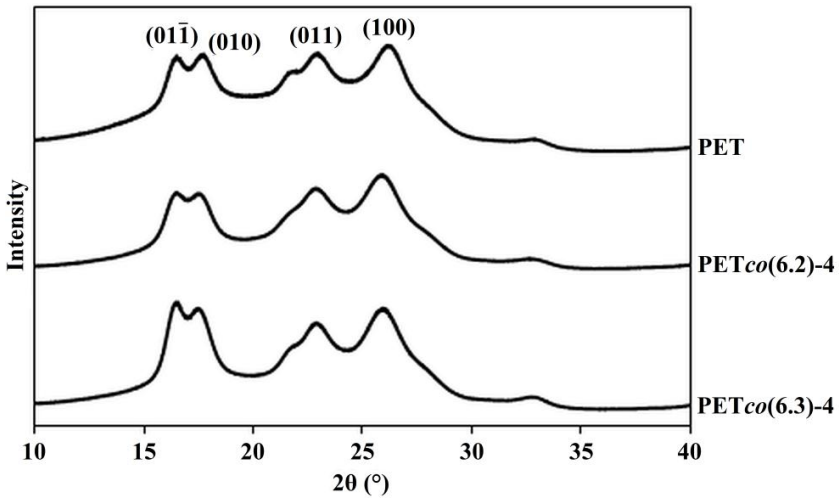

Figure 6.20 X-ray powder diffraction patterns of PET, PET*co*(**6.2**)-4 and PET*co*(**6.3**)-4.

6.3.3 Synthesis of copolyester analogues

The inclusion of rigid amide comonomers **6.2** and **6.3** in PET was successful in terms of raising the relative thermal performance, but afforded unprocessable materials at > 4 mol% amide content. It was envisaged that removal of the intermolecular hydrogen bonded network in the relevant PET-based copoly(ester-amide)s would improve melt-processability but might retain sufficient intramolecular rigidity for enhanced T_gs to be obtained.

Comonomer **6.4** was therefore synthesised as the ester analogue of **6.2**, in an equivalent two-step synthesis. This was achieved by reaction of terephthaloyl chloride and 4-hydroxybenzoic acid, followed by the glycolisation of the "**6.4** intermediate" dicarboxylic acid via the 2-bromoethanol route. Although satisfactory yields of the required products were obtained at each step (87 and 54% respectively), the glycolisation step produced impurities (< 3 mol%) not observed for the corresponding **6.2** intermediate diacid. This may be attributed to an extremely slow filtration step for **6.4** post-synthesis (> 48 h) and the relative insolubility of **6.4** in DMF at 90 °C during the reaction.

PET-based copolyesters incorporating **6.4** at 2, 4 and 8 mol% were consequently synthesised via the laboratory-scale melt-polycondensation route as illustrated in Figure 6.21. All PET*co*(**6.4**) copolymers were extrudable at 280 °C in a facile manner. Analysis by ^{1}H NMR spectrometry revealed that the PET*co*(**6.4**) composition ratios essentially matched the comonomer feed ratios at 2 and 4 mol%, but not at 8 mol%. It is again probable that this is due to the insolubility of **6.4** in BHET (as observed for **5.1**), which limits the amount of **6.4** that may undergo a polycondensation reaction. Molecular weights determined by GPC for the PET*co*(**6.4**) copolymer series lie between M_w = 13,200-15,400 Da, indicating respectable distributions compared to PET.

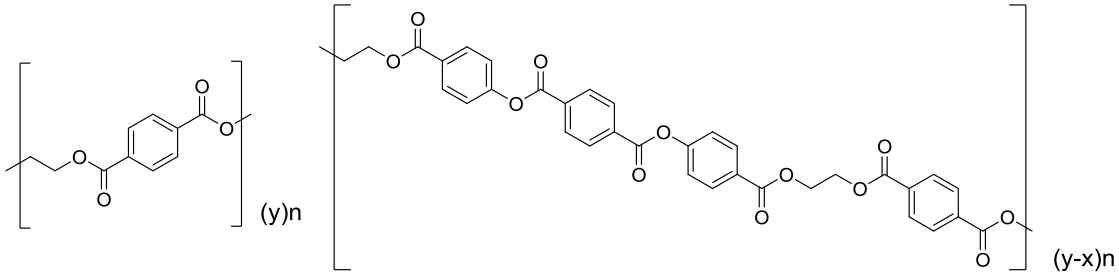

Figure 6.21 Representative chemical structure of PET*co*(**6.4**).

Figure 6.22 illustrates the DSC 2nd heating scans (20 °C min^{-1}) of PET and the PET*co*(**6.4**) copolymer series. It is observed that the T_g slowly increases upon increasing **6.4** content, to a maximum of 84 °C for PET*co*(**6.4**)-4 and 8. This confirms that removal of an intermolecular hydrogen bonded network has a pronounced effect on the T_g, with just 2 mol% inclusion of the analogous amide comonomer **6.2** ensuring superior performance (T_g = 86 °C). As the RAF is reduced by substitution of **6.2** for **6.4**, it is likely that the sizeable MAF and relative flexibility of the PET chain (of which a large proportion is no longer immobilised) contribute to the relatively lower T_g.

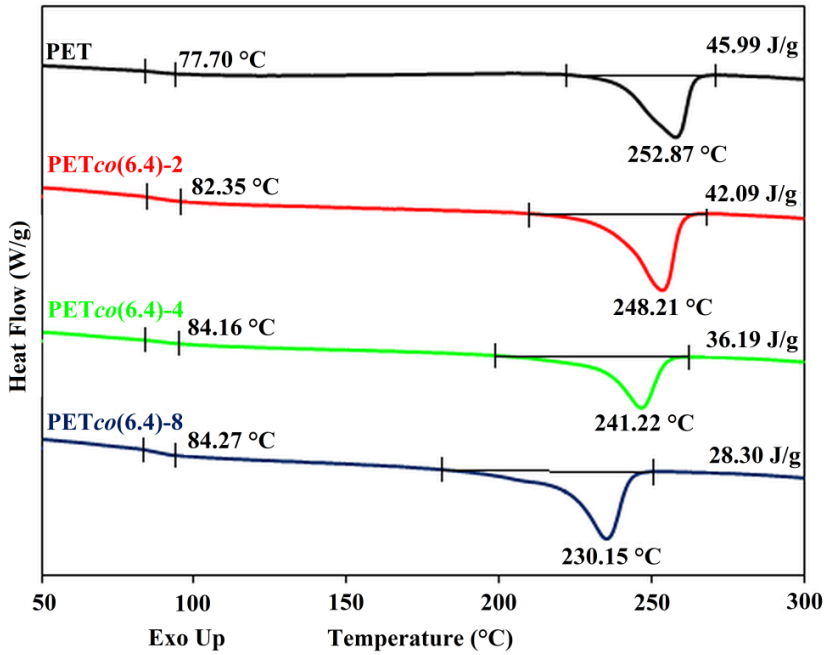

Figure 6.22 DSC 2nd heating scans (20 °C min^{-1}) of PET and the PET*co*(**6.4**) copolymer series.

6.4 Conclusions

In contrast to Chapters 3, 4 and 5, which focussed on copoly*imides*, the T_g of a semi-aromatic, semi-crystalline homopolyester was here successfully raised following copolymerisation with novel rigid *amide* comonomers. Related research from the literature

(Bouma *et al*. and Harashina *et al*.) was initially developed further, to validate the concept that an analogous amide comonomer to BHET could increase the T_g relative to PET.

Two rigid Kevlar®-type comonomers, **6.1** and **6.2**, of similar chain length to the BHET dimer were therefore synthesised and copolymerised with PET up to 8 mol%. The consequent introduction of an intermolecular hydrogen bonded network, in conjunction with increased rigidity along the copoly(ester-amide) chain, led to a maximum observed T_g of 98 °C for PET*co*(**6.2**)-8. Furthermore, tensile moduli were found to dramatically increase upon 2 mol% amide incorporation to levels more than twice that of PET.

Analysis of the PET*co*(**6.2**) copolymer series by rotational rheology and HyperDSC demonstrated that the increased T_g arose at the expense of melt-processability, whereby copolymers containing > 8 mol% of **6.2** were no longer extrudable at 280 °C. This was attributed to the inversion of the MAF and RAF fractions in a PET*co*(**6.2**)-4 copolymer relative to PET. Therefore, an analogous ester comonomer to **6.2** was synthesised (**6.4**) in an effort to produce a more melt-processable copolyester with comparable thermal properties. Incorporation of comonomer **6.4** at 8 mol% with PET, however, afforded only a relatively low T_g of 84 °C emphasising the intermolecular and intramolecular rigidity required to increase the thermal performance of PET.

6.5 Experimental

6.5.1 Materials

Dimethyl terephthalate and bis(2-hydroxylethyl) terephthalate were obtained from DuPont Teijin Films, U.K. Antimony trioxide was purchased from SICA, France. Ethanolamine, ethanol, diethyl ether, 4-aminobenzoic acid, dioxane, pyridine, terephthaloyl chloride, methanol, DMF, triethylamine, 2-bromoethanol, 4-aminophenethyl alcohol, 4-hydroxybenzoic acid, tetrachloroethane, 1M HCl solution, acetone, dimethylsulfoxide, deuterated dimethylsulfoxide and deuterated chloroform were purchased from Sigma Aldrich, U.K. Chloroform and sodium hydroxide were purchased from Fisher Scientific, U.K. Trifluoroacetic acid and 1,1,1,3,3,3-hexafluoro-2-propanol were purchased from Fluorochem, U.K. All materials were used as purchased.

6.5.2 Monomer synthetic procedures

6.5.2.1 *N,N*'-bis(2-hydroxyethyl) terephthalamide (6.1)[16]

A solution of dimethyl terephthalate (10.50 g, 0.05 mol) and ethanolamine (20.00 g, 0.33 mol) was heated to 120 °C for 16 h. The reaction solution was then cooled to room temperature, diluted with ethanol, and the product filtered off and washed with cold diethyl ether before being dried under vacuum at 100 °C for 24 h to afford **6.1** as a white powder (10.74 g, 85%).

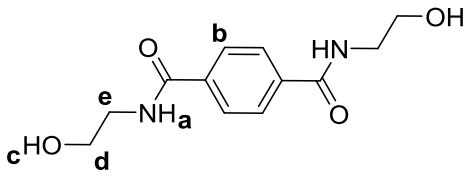

6.1

M.P. (DSC) = 240 °C. MS *m*/*z* = 253.1182 $[M+H]^+$ and 275.1002 $[M+Na]^+$, calculated 253.1188 and 275.1008. ^{1}H NMR (400 MHz, d_6-DMSO) δ_H (ppm) 8.55 (2H, t, J = 4.0 Hz, H_a), 7.91 (4H, s, H_b), 4.75 (2H, t, J = 4.0 Hz, H_c), 3.50 (4H, m, H_d), 3.34 (4H, m, H_e). ^{13}C NMR (100 MHz, d_6-DMSO) δ_C (ppm) 165.6, 136.6, 127.1, 59.6, 42.2. IR (ν_{max} cm^{-1}) 3361 (νO-H), 3281 (νN-H), 2951 (νC-H), 1617 (νC=O), 1050 (νC-N).

6.5.2.2 Bis(2-hydroxyethyl)-4,4'-[terephthaloyl bis(azanediyl)] dibenzoate (6.2)[23]

A solution of 4-aminobenzoic acid (13.72 g, 0.10 mol), dioxane (100 mL) and pyridine (7.86 g, 0.10 mol) was heated to 50 °C until the 4-aminobenzoic acid had dissolved and was then cooled to 0 °C. A solution of terephthaloyl chloride (10.16 g, 0.05 mol) in dioxane (100 mL) was then added dropwise over 10 mins. The reaction solution was warmed to room temperature and stirred for 16 h, before being filtered, washed with methanol and dried under vacuum at 100 °C for 24 h to afford the intermediate **6.2** product as a white powder (18.25 g, 90%).

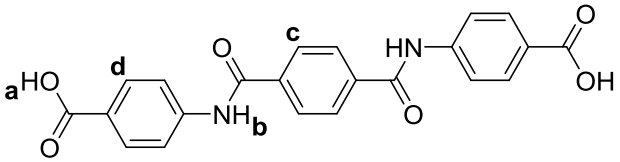

M.P. (DSC) = 389 °C. MS *m*/*z* = 405.0181 $[M+H]^+$, calculated 405.1095. ^{1}H NMR (400 MHz, d_6-DMSO) δ_H (ppm) 12.78 (2H, br, H_a), 10.69 (2H, s, H_b), 8.12 (4H, s, H_c), 7.95 (8H, m, H_d). ^{13}C NMR (100 MHz, d_6-DMSO) δ_C (ppm) 166.9, 165.2, 143.0, 137.3, 130.2,

127.9, 125.7, 119.6. IR (ν_{max} cm^{-1}) 3324 (νO-H), 2822 (νC-H), 1647 (νC=O), 1264 (νC-O), 1173 (νC-N).

A sample of the intermediate **6.2** product (15.00 g, 37.09 mmol) was dissolved in DMF (250 mL). 2-Bromoethanol (13.91 g, 0.11 mol) and triethylamine (11.26 g, 0.11 mol) were then added to the solution and the reaction was held at 80 °C for 16 h. The solution was cooled to room temperature and the product was precipitated in deionised water, filtered off, washed with methanol and dried under vacuum at 110 °C for 24 h to afford **6.2** as a white powder (10.45 g, 57%).

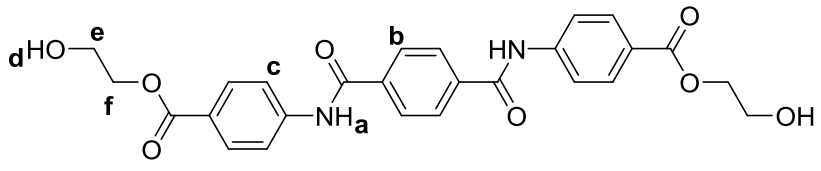

6.2

M.P. (DSC) = 328 °C. MS *m*/*z* = 491.1444 $[M-H]^+$, calculated 491.1455. ^{1}H NMR (400 MHz, d_6-DMSO) δ_H (ppm) 10.72 (2H, s, Ha), 8.12 (4H, s, H_b), 7.95 (8H, q, *J* = 8.0, 16.0 Hz, H_c), 4.94 (2H, s, H_d), 4.27 (4H, s, H_e), 3.70 (4H, s, H_f). ^{13}C NMR (100 MHz, d_6-DMSO) δ_C (ppm) 165.4, 165.2, 143.4, 137.3, 130.2, 127.9, 124.7, 119.6, 66.3, 59.1. IR (ν_{max} cm^{-1}) 3338 (νO-H), 2949 (νC-H), 1644 (νC=O), 1260 (νC-O), 1072 (νC-N).

6.5.2.3 *N*,*N*'-bis[4-(2-hydroxyethyl)phenyl] terephthalamide (6.3)

Synthesis as described for intermediate **6.2**. 4-Aminophenethyl alcohol (9.60 g, 0.07 mol) and pyridine (5.50 g, 0.07 mol) in dioxane (70 mL). Terephthaloyl chloride (7.11 g, 0.035 mol) in dioxane (70 mL) to afford product **6.3** as a brick-red powder (12.53 g, 89%).

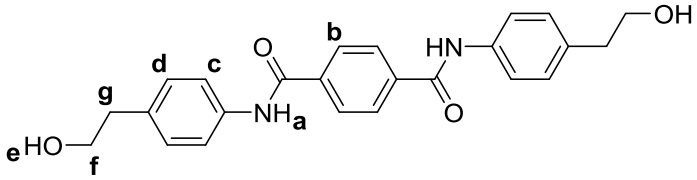

6.3

M.P. (DSC) = 341 °C. MS *m*/*z* = 405.1812 $[M+H]^+$, calculated 405.1814. ^{1}H NMR (400 MHz, d_6-DMSO) δ_H (ppm) 10.32 (2H, s, H_a), 8.08 (4H, s, H_b), 7.68 (4H, d, *J* = 8.0 Hz, H_c), 7.20 (4H, d, *J* = 8.0 Hz, H_d), 4.62 (2H, br, H_e), 3.59 (4H, t, *J* = 8.0 Hz, H_f), 2.70 (4H, t, *J* = 8.0 Hz, H_f). ^{13}C NMR (100 MHz, d_6-DMSO) δ_C (ppm) 164.5, 137.4, 136.8, 135.1, 129.0, 127.6, 120.4, 62.2, 38.5. IR (ν_{max} cm^{-1}) 3295 (νO-H), 2858 (νC-H), 1644 (νC=O), 1321 (νC-O), 1048 (νC-N).

6.5.2.4 Bis[4-((2-hydroxyethoxy)carbonyl)phenyl] terephthalate (6.4)[36]

A solution of 4-hydroxybenzoic acid (17.34 g, 0.126 mol) and sodium hydroxide (6.86 g, 0.172 mol, 1M solution) was cooled to 0 °C. A solution of terephthaloyl chloride (8.49 g, 0.042 mol) in tetrachloroethane (90 mL) was then added dropwise over 1 h. The reaction solution was then warmed to room temperature and stirred for 4 h. A precipitate was then formed by acidifying the solution to pH 2 with 1M HCl, which was then filtered, washed with water, acetone, diethyl ether and ethanol before being dried under vacuum at 60 °C for 24 h to afford the intermediate **6.4** product as a white powder (14.73 g, 87%).

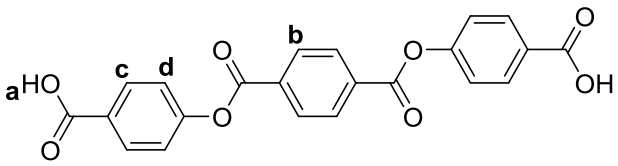

M.P. (DSC) = 355 °C. MS *m*/*z* = 405.0608 $[M-H]^+$, calculated 405.0602. ^{1}H NMR (400 MHz, d_6-DMSO) δ_H (ppm) 13.10 (2H, br, H_a), 8.34 (4H, s, H_b), 8.06 (4H, d, *J* = 8.0 Hz, H_c), 7.49 (4H, d, *J* = 8.0 Hz, H_d). ^{13}C NMR (100 MHz, d_6-DMSO) δ_C (ppm) 166.5, 163.4, 153.8, 133.2, 131.0, 130.3, 130.1, 128.7, 122.1. IR (ν_{max} cm^{-1}) 3078 (νO-H), 2553 (νC-H), 1723 (νC=O), 1162 (νC-O).

Synthesis as described for **6.2**. Intermediate **6.4** product (8.00 g, 19.69 mmol) in DMF (300 mL). 2-Bromoethanol (7.38 g, 59.06 mmol) and triethylamine (5.98 g, 59.06 mmol) to afford product **6.4** as a white powder (5.25 g, 54%).

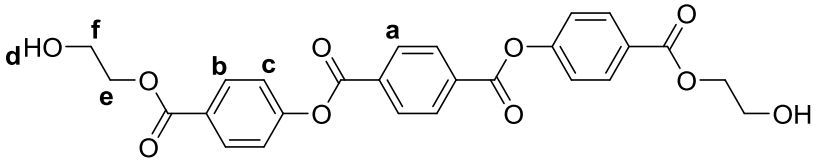

6.4

M.P. (DSC) = 321 °C. MS *m*/*z* = 495.1283 $[M+H]^+$, calculated 491.1291. ^{1}H NMR (400 MHz, d_6-DMSO) δ_H (ppm) 8.36 (4H, s, H_a), 8.12 (4H, d, *J* = 8.0 Hz, H_b), 7.53 (4H, d, *J* = 8.0 Hz, H_c), 4.97 (2H, br, H_d), 4.30 (4H, m, H_e), 3.72 (4H, m, H_f). ^{13}C NMR (100 MHz, d_6-DMSO) δ_C (ppm) 165.09, 163.40, 154.09, 133.23, 130.97, 130.36, 127.78, 122.28, 66.71, 59.01. IR (ν_{max} cm^{-1}) 3526 (νO-H), 2960 (νC-H), 1728 (νC=O), 1250 (νC-O).

6.5.3 Polymer synthetic procedures

Polymers were synthesised via the laboratory-scale melt-polycondensation procedure as described in Chapter 2, unless otherwise stated.

6.5.3.1 PET

Synthesis and characterisation detailed in Chapter 5.

6.5.3.2 PET*co*(6.1) copolymer series

Reagents			Comonomer feed ratio		Copolymer composition ratio	
(g)			(mol%)		(mol%)	
BHET	6.1	Sb_2O_3	BHET	6.1	PET	6.1
40.00	2.08	0.10	95	5	85	5
40.00	4.39	0.10	90	10	91	9
40.00	9.90	0.10	80	20	82	18

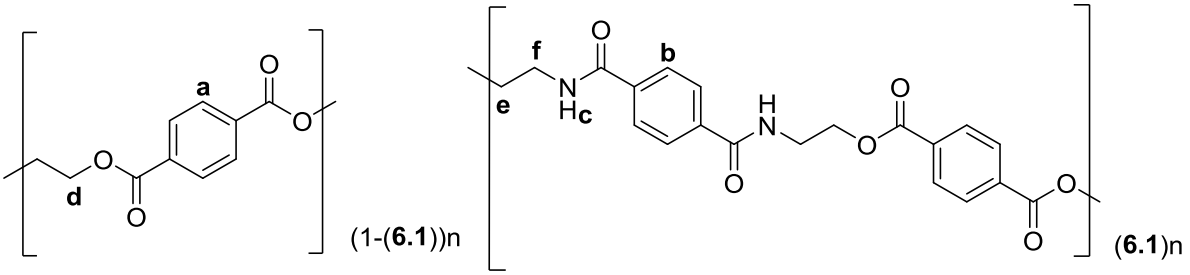

PET*co*(6.1)-5

^{1}H NMR [400 MHz, $CDCl_3$:TFA (2:1)] δ_H (ppm) 8.17 (8H, m, H_a), 7.86 (4H, m, H_b), 7.59 (2H, s, H_c), 4.84 (4H, s, H_d), 4.70 (4H, s, H_e), 4.02 (4H, s, H_f). ^{13}C NMR [100 MHz, $CDCl_3$:TFA (2:1)] δ_C (ppm) 168.0, 133.3, 130.4, 130.0, 127.4, 63.9. T_g = 84 °C, T_{cc} = 145 °C, T_c = 201 °C, T_m = 251 °C, T_d = 390 °C. M_w (GPC/HFIP) = 18,400 Da, M_n (GPC/HFIP) = 4,570 Da. IR (ν_{max} cm^{-1}) 2979 (νC-H), 1716 (νC=O), 1243 (νC-O), 1092 (νC-N).

PET*co*(6.1)-10

^{1}H NMR [400 MHz, $CDCl_3$:TFA (2:1)] δ_H (ppm) 8.18 (8H, m, H_a), 7.86 (4H, m, H_b), 7.59 (2H, s, H_c), 4.84 (4H, s, H_d), 4.70 (4H, s, H_e), 4.02 (4H, s, H_f). ^{13}C NMR [100 MHz, $CDCl_3$:TFA (2:1)] δ_C (ppm) 168.0, 137.0, 133.3, 132.3, 130.5, 130.4, 130.0, 127.4, 63.9, 40.0. T_g = 86 °C, T_{cc} = 148 °C, T_c = 191 °C, T_m = 251 °C, T_d = 377 °C. M_w (GPC/HFIP) = 21,100 Da, M_n (GPC/HFIP) = 3,910 Da. IR (ν_{max} cm^{-1}) 2980 (νC-H), 1713 (νC=O), 1241 (νC-O), 1089 (νC-N).

PET*co*(6.1)-20

^{1}H NMR [400 MHz, $CDCl_3$:TFA (2:1)] δ_H (ppm) 8.17 (8H, m, H_a), 7.84 (4H, m, H_b), 7.59 (2H, s, H_c), 4.84 (4H, s, H_d), 4.71 (4H, s, H_e), 4.02 (4H, s, H_f). ^{13}C NMR [100 MHz, $CDCl_3$:TFA (2:1)] δ_C (ppm) 168.0, 137.0, 133.3, 132.3, 130.5, 130.4, 130.0, 127.4, 64.3,

63.9, 40.0. T_g = 93 °C, T_{cc} = 177 °C, T_c = 153 °C, T_m = 243 °C, T_d = 358 °C. M_w (GPC/HFIP) = 48,900 Da, M_n (GPC/HFIP) = 3,620 Da. IR (ν_{max} cm^{-1}) 3383 (νO-H), 2960 (νC-H), 1716 (νC=O), 1242 (νC-O), 1093 (νC-N).

6.5.3.3 PET*co*(6.1)-50

A solution of terephthaloyl chloride (1.00 g, 4.93 mmol) and comonomer **6.1** (1.24 g, 4.93 mmol) in 1-chloronaphthalene (50 mL) was heated to 170 °C and held at this temperature for 1 h. The temperature was then increased to 210 °C over a 3 h period and then held at this temperature for 40 h. The reaction mixture was then cooled to room temperature, precipitated in methanol, filtered and dried under vacuum for at 110 °C for 24 h to afford the polymer product **PET*co*(6.1)-50** (1.46 g).

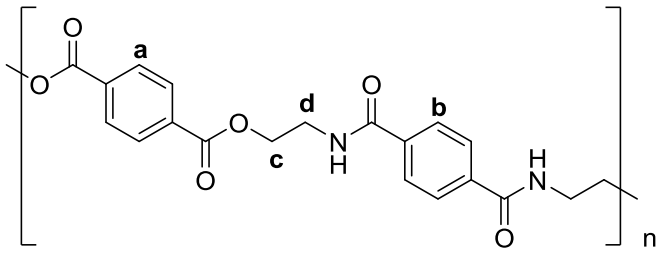

^{1}H NMR [400 MHz, $CDCl_3$:TFA (2:1)] δ_H (ppm) 8.13 (4H, s, H_a), 7.83 (6H, s, H_b), 4.69 (4H, s, H_c), 4.00 (4H, s, H_d). ^{13}C NMR [100 MHz, $CDCl_3$:TFA (2:1)] δ_C (ppm) 171.0, 168.3, 135.9, 133.2, 132.2, 130.3, 130.0, 127.8, 127.4, 64.4, 40.0. T_g = 176 °C, T_m = 332 °C, T_d = 330 °C. M_w (GPC/HFIP) = 47,200 Da, M_n (GPC/HFIP) = 5,500 Da. IR (ν_{max} cm^{-1}) 3321 (νN-H), 2967 (νC-H), 1637 (νC=O), 1265 (νC-O), 1103 (νC-N).

6.5.3.4 PET*co*(6.2) copolymer series

Reagents			**Comonomer feed ratio**		**Copolymer composition ratio**	
(g)			**(mol%)**		**(mol%)**	
BHET	**6.2**	**Sb_2O_3**	**BHET**	**6.2**	**PET**	**6.2**
30.00	1.19	0.10	98	2	99	1
30.00	2.42	0.10	96	4	96	4
30.00	3.40	0.10	94	6	95	5
30.00	5.04	0.10	92	8	93	7

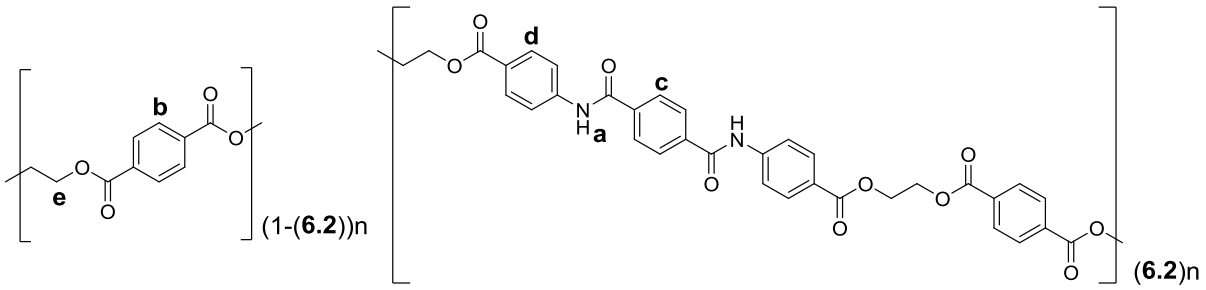

PET*co*(6.2)-2

^{1}H NMR [400 MHz, $CDCl_3$:TFA (2:1)] δ_H (ppm) 8.92 (2H, s, H_a), 8.17 (8H, s, H_b), 8.04 (4H, s, H_c), 7.82 (8H, s, H_d), 4.84 (12H, s, H_e). ^{13}C NMR [100 MHz, $CDCl_3$:TFA (2:1)] δ_C (ppm) 168.0, 133.3, 131.3, 129.9, 128.1, 63.9. T_g = 87 °C, T_c = 190 °C, T_m = 243 °C, T_d = 404 °C. M_w (GPC/HFIP) = 18,400 Da, M_n (GPC/HFIP) = 4,180 Da. IR (ν_{max} cm^{-1}) 2892 (νC-H), 1713 (νC=O), 1237 (νC-O), 1092 (νC-N).

PET*co*(6.2)-4

^{1}H NMR [400 MHz, $CDCl_3$:TFA (2:1)] δ_H (ppm) 8.94 (2H, s, H_a), 8.18 (8H, s, H_b), 8.04 (4H, s, H_c), 7.81 (8H, s, H_d), 4.84 (12H, s, H_e). ^{13}C NMR [100 MHz, $CDCl_3$:TFA (2:1)] δ_C (ppm) 168.0, 133.3, 131.3, 130.5, 130.0, 128.1, 121.1, 65.1, 63.9. T_g = 92 °C, T_c = 177 °C, T_m = 235 °C, T_d = 404 °C. M_w (GPC/HFIP) = 9,100 Da, M_n (GPC/HFIP) = 3,180 Da. IR (ν_{max} cm^{-1}) 2989 (νC-H), 1715 (νC=O), 1244 (νC-O), 1088 (νC-N).

PET*co*(6.2)-6

^{1}H NMR [400 MHz, $CDCl_3$:TFA (2:1)] δ_H (ppm) 8.93 (2H, s, H_a), 8.18 (8H, s, H_b), 8.04 (4H, s, H_c), 7.82 (8H, s, H_d), 4.84 (12H, s, H_e). ^{13}C NMR [100 MHz, $CDCl_3$:TFA (2:1)] δ_C (ppm) 168.0, 141.4, 133.3, 133.1, 131.3, 130.5, 130.0, 128.1, 121.1, 65.1, 63.9, 63.3. T_g = 95 °C, T_c = 170 °C, T_m = 227 °C, T_d = 401 °C. M_w (GPC/HFIP) = 6,400 Da, M_n (GPC/HFIP) = 2,390 Da. IR (ν_{max} cm^{-1}) 2971 (νC-H), 1718 (νC=O), 1243 (νC-O), 1099 (νC-N).

PET*co*(6.2)-8

^{1}H NMR [400 MHz, $CDCl_3$:TFA (2:1)] δ_H (ppm) 8.93 (2H, s, H_a), 8.18 (8H, s, H_b), 8.04 (4H, s, H_c), 7.82 (8H, s, H_d), 4.84 (12H, s, H_e). ^{13}C NMR [100 MHz, $CDCl_3$:TFA (2:1)] δ_C (ppm) 168.0, 141.4, 137.1, 133.3, 130.5, 130.0, 128.1, 125.8, 121.1, 65.1, 63.9, 63.3. T_g = 95 °C, T_{cc} = 168 °C, T_c = 150 °C, T_m = 218 °C, T_d = 402 °C.

M_w (GPC/HFIP) = 8,400 Da, M_n (GPC/HFIP) = 2,750 Da. IR (ν_{max} cm^{-1}) 3008 (νC-H), 1717 (νC=O), 1243 (νC-O), 1096 (νC-N).

6.5.3.5 PET*co*(6.3) copolymer series

Reagents			Comonomer feed ratio		Copolymer composition ratio	
(g)			(mol%)		(mol%)	
BHET	**6.3**	**Sb_2O_3**	**BHET**	**6.3**	**PET**	**6.3**
30.00	0.98	0.10	98	2	99	1
30.00	1.99	0.10	96	4	97	3

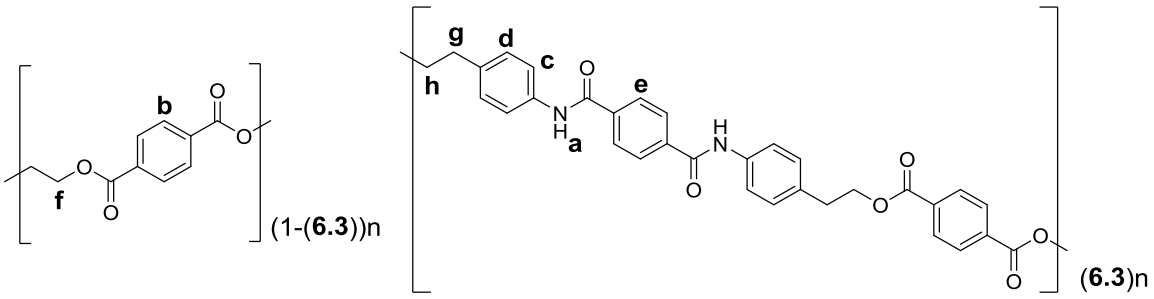

PET*co*(6.3)-2

^{1}H NMR [400 MHz, $CDCl_3$:TFA (2:1)] δ_H (ppm) 8.75 (2H, s, H_a), 8.17 (8H, s, H_b), 7.97 (4H, s, H_c), 7.55 (4H, s, H_d), 7.39 (4H, s, H_e), 4.84 (4H, s, H_f), 4.64 (4H, s, H_g), 4.21 (4H, s, H_h). ^{13}C NMR [100 MHz, $CDCl_3$:TFA (2:1)] δ_C (ppm) 168.0, 133.3, 130.0, 63.9. T_g = 86 °C, T_c = 203 °C, T_m = 231 °C, T_d = 404 °C. M_w (GPC/HFIP) = 21,900 Da, M_n (GPC/HFIP) = 5,540 Da. IR (ν_{max} cm^{-1}) 3014 (νC-H), 1710 (νC=O), 1244 (νC-O), 1096 (νC-N).

PET*co*(6.3)-4

^{1}H NMR [400 MHz, $CDCl_3$:TFA (2:1)] δ_H (ppm) 8.76 (2H, s, H_a), 8.17 (8H, s, H_b), 8.03 (4H, s, H_c), 7.55 (4H, s, H_d), 7.39 (4H, s, H_e), 4.84 (4H, s, H_f), 4.68 (4H, s, H_g), 4.19 (4H, s, H_h). ^{13}C NMR [100 MHz, $CDCl_3$:TFA (2:1)] δ_C (ppm) 165.8, 131.1, 128.4, 127.8, 127.6, 125.9, 125.4, 120.7, 120.6, 66.9, 64.9, 62.9, 61.7, 61.1, 31.9. T_g = 94 °C, T_c = 196 °C, T_m = 227 °C, T_d = 399 °C. M_w (GPC/HFIP) = 11,000 Da, M_n (GPC/HFIP) = 2,930 Da. IR (ν_{max} cm^{-1}) 2974 (νC-H), 1711 (νC=O), 1240 (νC-O), 1088 (νC-N).

6.5.3.6 PET*co*(6.4) copolymer series

Reagents			Comonomer feed ratio		Copolymer composition ratio	
(g)			(mol%)		(mol%)	
BHET	6.4	Sb_2O_3	BHET	6.4	PET	6.4
30.00	1.58	0.10	98	2	99	1
30.00	2.42	0.10	96	4	96	4
25.97	4.40	0.10	92	8	95	5

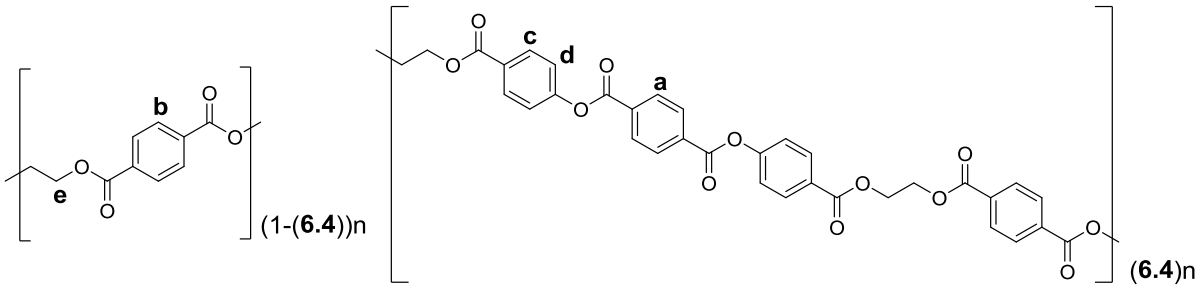

PET*co*(6.4)-2

^{1}H NMR [400 MHz, $CDCl_3$:TFA (2:1)] δ_H (ppm) 8.19 (8H, s, H_b), 4.85 (12H, m, H_e). ^{13}C NMR [100 MHz, $CDCl_3$:TFA (2:1)] δ_C (ppm) 167.9, 133.3, 132.3, 130.0, 69.1, 64.7, 63.9. T_g = 82 °C, T_c = 215 °C, T_m = 248 °C, T_d = 404 °C. M_w (GPC/HFIP) = 16,500 Da, M_n (GPC/HFIP) = 4,470 Da. IR (ν_{max} cm^{-1}) 2971 (νC-H), 1711 (νC=O), 1237 (νC-O), 1092 (νC-N).

PET*co*(6.4)-4

^{1}H NMR [400 MHz, $CDCl_3$:TFA (2:1)] δ_H (ppm) 8.45 (4H, m, H_a), 8.17 (8H, s, H_b), 8.14 (4H, s, H_c), 4.83 (12H, m, H_e). ^{13}C NMR [100 MHz, $CDCl_3$:TFA (2:1)] δ_C (ppm) 168.0, 133.3, 132.5, 132.2, 131.9, 130.8, 130.5, 130.0, 121.9, 63.9. T_g = 82 °C, T_c = 209 °C, T_m = 241 °C, T_d = 403 °C. M_w (GPC/HFIP) = 15,100 Da, M_n (GPC/HFIP) = 4,150 Da. IR (ν_{max} cm^{-1}) 2960 (νC-H), 1716 (νC=O), 1242 (νC-O), 1092 (νC-N).

PET*co*(6.4)-8

^{1}H NMR [400 MHz, $CDCl_3$:TFA (2:1)] δ_H (ppm) 8.34 (4H, m, H_a), 8.17 (8H, s, H_b), 8.14 (4H, s, H_c), 7.37 (4H, m, H_d), 4.83 (12H, m, H_e). ^{13}C NMR [100 MHz, $CDCl_3$:TFA (2:1)] δ_C (ppm) 167.9, 133.6, 133.3, 132.4, 132.2, 131.9, 130.6, 130.5, 130.0, 122.0, 118.5, 114.5, 64.6, 63.9. T_g = 83 °C, T_c = 199 °C, T_m = 230 °C, T_d = 401 °C. M_w (GPC/HFIP) = 13,200 Da, M_n (GPC/HFIP) = 3,640 Da. IR (ν_{max} cm^{-1}) 2984 (νC-H), 1711 (νC=O), 1238 (νC-O), 1096 (νC-N).

6.6 References

1 P. E. Cassidy, *Thermally stable polymers, synthesis and properties*, Marcel Dekker, New York, 1980.
2 H. H. Yang, *Aromatic High-Strength Fibres*, Wiley-Interscience, New York, 1989.
3 H. H. Yang, *Kevlar Aramid Fibres*, Wiley, New York, 1993.
4 S. H. Hsiao and W. T. Leu, *Polym. Int.*, 2005, **54**, 392–400.
5 S. Kwolek, *US Pat.*, US 3,287,323A, *Process for the production of a highly orientable, crystallizable, filamentforming polyamide*, 1966.
6 A. M. Issam, *Res. Chem. Intermed.*, 2014, **40**, 3033–3044.
7 DuPont, *Internal Communication*, 2015.
8 K. Bouma, G. M. M. Groot, J. Feijen and R. J. Gaymans, *Polymer*, 2000, **41**, 2727–2735.
9 K. Bouma, J. H. G. M. Lohmeijer and R. J. Gaymans, *Polymer*, 2000, **41**, 2719–2725.
10 K. Bouma, G. de Wit, J. H. G. M. Lohmeijer and R. J. Gaymans, *Polymer*, 2000, **41**, 3965–3974.
11 A. C. M. van Bennekom and R. J. Gaymans, *Polymer*, 1997, **38**, 657–665.
12 A. C. M. van Bennekom and R. J. Gaymans, *Polymer*, 1996, **37**, 5439–5446.
13 A. C. M. van Bennekom, P. A. A. T. Willemsen and R. J. Gaymans, *Polymer*, 1996, **37**, 5447–5459.
14 H. Harashina, T. Nakane and T. Itoh, *J. Polym. Sci. Part A: Polym. Chem.*, 2007, **45**, 2184–2193.
15 C. Lu, Q. Li and J. Pan, *J. Polym. Sci. Polym. Chem.*, 1985, **23**, 3031–3044.
16 G. J. E. Biemond, K. Brasspenning and R. J. Gaymans, *J. Appl. Polym. Sci*, 2011, **124**, 1302–1315.
17 M. R. Hibbs, J. Holtzclaw, D. M. Collard, R. Y. F. Liu, A. Hiltner, E. Baer, D. A. Schiraldi, *J. Polym. Sci. Part A: Polym. Chem.*, 2004, **42**, 1668–1681.
18 K. Yamada, *J. Appl. Polym. Sci*., 1987, **33**, 1649–1661.
19 A. Ballistreri, D. Garozzo, G. Montaudo, A. Pollicino and M. Giuffrida, *Polymer*, 1987, **28**, 139–146.
20 G. Grassie and N.Scott, *Polymer Degradation and Stabilisation*, Cambridge University Press, Cambridge, 1985.
21 G. Montaudo, C. Puglisi and F. Samperi, *Polym. Degrad. Stab.*, 1993, **42**, 13–28.
22 J. Xiao, H. Zhang, X. Wan, D. Zhang, Q. F. Zhou, E. M. Woo and S. R. Turner, *Polymer*, 2002, **43**, 3683–3690.
23 A. Le Guen, M. Klapper and K. Muller, *Macromolecules*, 1998, **31**, 6559–6565.
24 S. D. Mancini and M. Zanin, *J. Appl. Polym. Sci.*, 2000, **76**, 266–275.
25 J. D. Menczel, *J. Therm. Anal. Calorim.*, 2011, **106**, 7–24.
26 J. D. Menczel, *J. Polym. Sci. Polym. Lett. Ed.*, 1981, **19**, 261–264.
27 B. Wunderlich, *Prog. Polym. Sci.*, 2003, **28**, 383–450.
28 Y. Fu, B. Annis, A. Boller, Y. Jin and B. Wunderlich, *J. Polym. Sci, Part B: Polym. Phys*., 1994, **32**, 2289-2306.
29 Y. Fu, W. R. Busing, Y. Jin, K. A. Affholter and B. Wunderlich, *Macromol. Chem. Phys.*, 1994, **195**, 803–822.
30 A. Flores, M. Pieruccini, N. Stribeck, S. S. Funari, E. Bosch and F. J. Baltá-Calleja, *Polymer*, 2005, **46**, 9404–9410.
31 K. C. Cole, A. Ajji and E. Pellerin, *Macromolecules*, 2002, **35**, 770–784.
32 P. G. Karagiannidis, A. C. Stergiou and G. P. Karayannidis, *Eur. Polym. J.*, 2008, **44**, 1475–1486.
33 H. Xu, B. S. Ince and P. Cebe, *J. Polym. Sci. Part B: Polym. Phys.*, 2003, **41**, 3026–3036.
34 S. Z. D. Cheng, R. Pan and B. Wunderlich, *Makromol. Chem.*, 1988, **189**, 2443–2458.

35 R. Androsch and B. Wunderlich, *Polymer*, 2005, **46**, 12556–12566.
36 J. K. W. Chui, T. M. Fyles and H. Luong, *Beilstein J. Org. Chem*, 2011, **7**, 1562–1569.

Chapter 7

Conclusions and future work

7.1 Conclusions

The main aim of this research project was to increase the thermomechanical performance, primarily defined by the T_g, of semi-aromatic, semi-crystalline polyesters. This has been successfully achieved via copolymerisation with rigid imide, amide and ester comonomers that displayed isomorphic behaviour, enabling the maintenance of T_ms and retention of semi-crystalline behaviour. Such high performance polyester-based materials were initially synthesised on a bespoke laboratory-scale melt-polycondensation rig on a 20-50 g scale. In some cases, this was then succeeded by multiple syntheses on an industrial 7 kg scale to facilitate the production of cast, uniaxially and biaxially oriented film.

Novel biphenyldiimide comonomers (**3.1** and **4.1**) were readily incorporated into the naphthalate-based homopolyesters PEN and PBN, respectively. For each copoly(ester-imide) series, semi-crystalline materials were generated throughout all copolymer composition ratios studied and rationalised by a number of analytical techniques. With the single exception of the cocrystalline PBN*co*PBT copolymer series detailed by Jeong *et al.*,[1] this retention of crystallinity, in naphthalate polyester-based systems is unprecedented in the literature. Furthermore, increases in T_g of up to 56 and 23 °C were observed in comparison to PEN and PBN to afford materials that exhibited comparable thermal performance to PEEK and PET. The replacement of PEEK with PEN*co*(**3.1**)-18 is of great commercial interest, as illustrated by the successful production of heat-set PEN*co*(**3.1**)-18 biaxially oriented film, but the production of a PET analogue with liquid crystalline properties [PBN*co*(**4.1**)-20] is unlikely to warrant further development due to the relative monomer costs.

The same isomorphic copolymerisation strategy was applied to PET by designing a rigid imide comonomer, **5.1**, based on the widely utilised and commercially available trimellitic anhydride unit. It was proposed, and subsequently demonstrated, that incorporation of **5.1** would afford a cocrystalline copoly(ester-imide) series as observed in Chapters 3 and 4. Several attempts have been previously made, most notably by Xiao *et al.*[2] and Park *et al.*,[3] to enhance the thermal performance of PET. However, because of the inclusion of non-isomorphic imide comonomers, the T_gs of such materials that are *also* semi-crystalline were limited to 82 and 93 °C, respectively. In contrast, a maximum possible T_g of 163 °C was

observed for the PET*co*(**5.1**) copolymer series, which is also significantly greater than those of the PET*co*BB copolymers studied by Hu *et al*.[4] and Ma *et al*.[5]

A range of rigid imide comonomers based on tetracarboxylic diimide residues also increased the T_g of PET to above 105 °C. Although not isomorphic, inclusion of the comonomers **5.5**, **5.6** and **5.7** at up to 10 mol% still produced semi-crystalline PET-based copoly(ester-imide)s following either melt-crystallisation or thermal annealing. The incorporation of Kevlar®-based rigid amide comonomers, **6.2** and **6.3**, with PET *al*so achieved a similar rise in T_g to ~ 95 °C at just 4 mol% incorporation. Retention of semi-crystalline behaviour, in comparison to the PET-based copoly(ester-imide)s, was more evident due to the increased similarity in comonomer chain lengths with the BHET dimer. However, this concept could not be fully examined at higher levels of amide content due to the generation of thermally unprocessable materials, attributed to the formation of a rigid intermolecular hydrogen bonding network. It is therefore unlikely that these materials will be considered for future industrial scale-up in preference to the PET*co*(**5.1**) copolymer series.

The materials presented in this thesis therefore encompass an extremely wide operating temperature range (T_gs from 76 to 178 °C), which in turn implies their potential viability in flexible electronics, solar cells and data storage applications. Commercial success of these materials is likely to be dependent on the successful replacement of PEN and PEEK biaxially oriented film with cost-effective alternatives that exhibit comparable performance. This, in theory, should be achievable from the substitution for PET*co*(**5.1**)-5 and PEN*co*(**3.1**)-18, respectively, based upon their thermal performance and production from commercially available starting reagents. The limitations of copoly(ester-imide)s for usage in the desired applications is discussed below in reference to future work arising from this research project.

7.2 Future work

7.2.1 PEN-based materials

Instron hot-box tensile analysis of PEN*co*(**3.1**)-18 cast film in Chapter 3 established that the optimum drawing temperature is between 160-170 °C. However, this temperature is 20-30 °C above the current operating capacity on an industrial-scale film line preventing large scale production of PEN*co*(**3.1**)-18 biaxially oriented film, at least by DTF. Therefore, in the long term, further engineering work on the film line is required in order to create a process whereby such draw temperatures may be achieved. This is likely to include modification of the casting and forward draw units in order to prevent unnecessary cooling of the extruded

copolymer melt which causes brittleness, and to upgrade the heating units on the forward draw.

As a short term compromise, future scale-up work should aim to produce PEN*co*(**3.1**)-5 (T_g = 131 °C, T_m = 256 °C) or PEN*co*(**7.1**)-5 biaxially oriented film. PEN*co*(**7.1**)-5 could be a commercially viable alternative to PEN*co*(**3.1**)-5 due to the incorporation of *N*,*N*'-bis-(hydroxyalkyl)-pyromellitic diimide, **7.1**, as first copolymerised with PET by Mary *et al.*[6] The thermal properties of PEN*co*(**7.1**)-5 are very similar to PEN*co*(**3.1**)-5 in demonstrating an increase in T_g relative to PEN, to 134 °C. The required drawing temperatures would consequently be lower and achievable at ~ 140 °C.

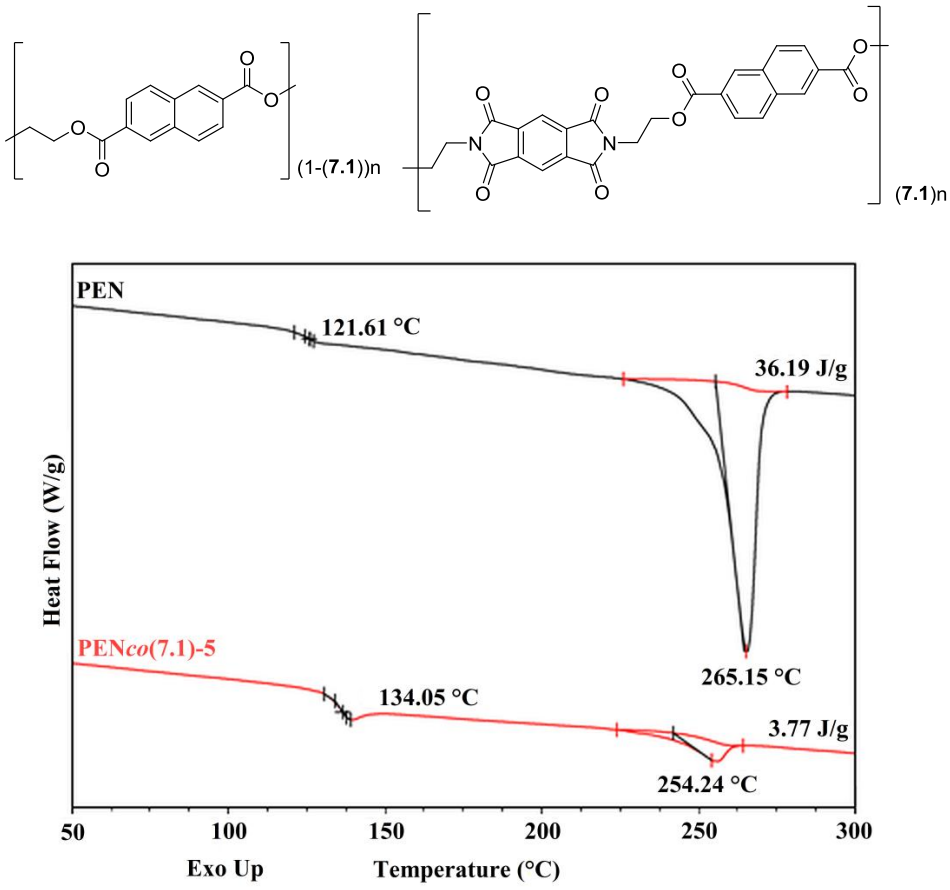

Figure 7.1 Molecular structure of the PEN*co*(**7.1**) copolymer (above) and the DSC 2nd heating scans (20 °C min^{-1}) of PEN and PEN*co*(**7.1**)-5 (below).

The molecular weights of PEN-based copoly(ester-imide)s may also be a contributing factor to the processing difficulties observed on the film line, whereby the M_ws of PEN*co*(**3.1**)-5 and PEN*co*(**7.1**)-5 are approximately 70% of PEN post-polymerisation. Current research is therefore focussed on the development of an industrial-scale SSP process for PEN*co*(**7.1**)-5, after demonstrating in Chapter 3 that the M_w of PEN*co*(**3.1**)-18 could be raised by over 50% via the laboratory-scale SSP process.

PEN*co*(**7.1**)-5 synthesised on an industrial-scale was first subjected to the SSP method developed by Heyworth[7] to check that the molecular weight could be improved. Samples were heated under dynamic vacuum to 160 °C at a rate of 0.25 °C min^{-1} where an isothermal hold was performed for 15 mins. The temperature was then raised to 230 °C at a rate of 0.1 °C min^{-1} and held at this temperature until the desired intrinsic melt viscosity (IV) was achieved.

Table 7.1 Molecular weight distributions, dispersities and viscosity analysis of PEN*co*(**7.1**)-5 pre and post-SSP.

Polymer		M_w[a]	M_n[a]	M_z[a]	Đ	η*[b]	IV[b]
		Da	**Da**	**Da**	**-**	**Pa s**	**dL g^{-1}**
PEN*co*(**7.1**)-5	pre-SSP	15,400	5,460	27,200	2.9	159	0.62
	post-SSP	15,400	2,410	29,000	6.7	263	0.69

[a] Determined by GPC (HFIP eluent). [b] Determined by rotational rheology temperature sweep mode at 290 °C.

Table 7.1 details the measured values of IV and η* for PEN*co*(**7.1**)-5 post-SSP. The viscosities certainly suggest an increase in molecular weight, but the GPC values for M_w and M_n are not consistent with this, which may be attributed to the insolubility of high molecular weight post-SSP material in HFIP. This SSP route is now being scaled up from the laboratory (~ 10 g) to an industrial-scale (~ 20 kg) by High Force Research Ltd. and DTF to be later assessed as a viable route to increasing the molecular weights of all future thermally enhanced copolymers.

Efforts to produce PEN*co*(**3.1**)-18 biaxially oriented film are currently concentrated upon the optimised Long stretcher route, as detailed in Chapter 3. Heat-set samples of approximately A4-size will be sent to the Holst Centre (Eindhoven, Netherlands) and the Centre for Process Innovation (Wilton, U.K), which both operate as open innovation centres that specialise in the development of materials for flexible electronic applications. This will enable specific consumer feedback and future progress on industrially produced film.

The most concerning characteristic of the PEN*co*(**3.1**) copolymer series, that will need further development, is the increased moisture uptake of the diimide copolymers relative to PEN itself. This trend is illustrated in Figure 7.2 by the almost linear correlation in moisture content with respect to increasing **3.1** content. Prior to analysis, PEN*co*(**3.1**) polymer chip samples were held in an environmental chamber for 168 hours at 50 °C and 30% relative humidity in order to reach their equilibrium moisture level.

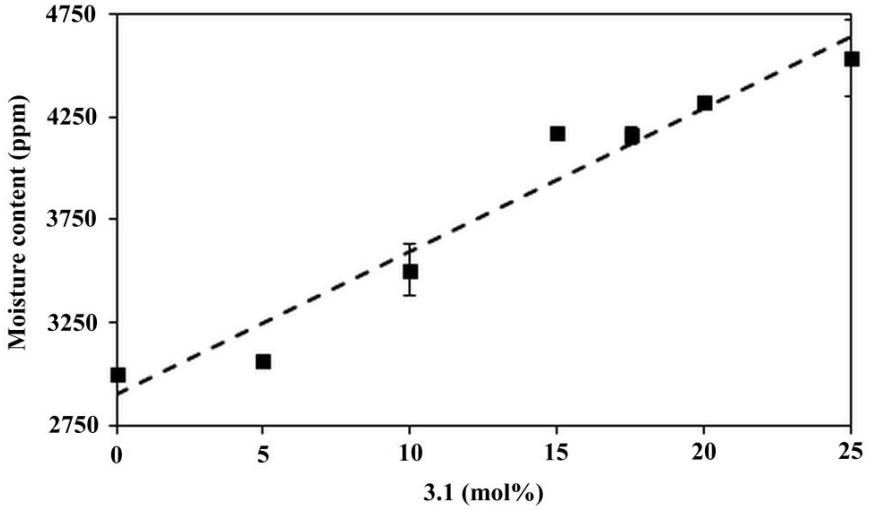

Figure 7.2 Moisture content levels of PEN and the PEN*co*(**3.1**) copolymer series.

Raised moisture content levels are reported[8] to increase the rate of hydrolytic degradation, which in this case may be attributed to the introduction of more polar and therefore hydrophilic imide residues. The utilisation of copoly(ester-imide)s synthesised in this thesis may therefore be restricted to applications which operate at relatively low humidity levels and/or under inert atmospheres. Analysis of PEN*co*(**3.1**) biaxially oriented film by weatherometer methods is required in order to repeatedly measure the optical and mechanical properties following simulated accelerated atmospheric conditions.

7.2.2 PET-based materials

It was established in Chapter 5 that despite the successful industrial-scale production of thermally enhanced PET-based biaxially oriented film [PET*co*(**5.5**)-10], the thermomechanical properties (G' and G'') were inferior to PET due to a lower χ_c. There is consequently a trade-off between obtaining the highest possible T_g and maximum retention of the χ_c. This is in comparison to producing a copolymer that displays an increased T_g relative to PET y*et al*so exhibits isomorphic behaviour, as observed for PET*co*(**5.1**)-5.

It is therefore clear that future work should primarily focus on the production of PET*co*(**5.1**)-5 biaxially oriented film, followed by extensive property analysis (DSC, tensile analysis, DMA etc.) to establish whether enhanced thermomechanical performance improvement may be achieved in comparison to PET. This would originate with Instron hot box tensile analysis of the forward draw behaviour in PET*co*(**5.1**)-5, to establish optimum film line conditions before pursuing industrial pilot production.

The incorporation of rigid amide comonomers had a more pronounced effect on the rheological properties of PET than their imide equivalents, with just > 4 mol% of comonomer

6.2 and **6.3** producing such high melt viscosities that the materials become unprocessable from the melt. As the inclusion of the ester analogue comonomer **6.4** was relatively unsuccessful in raising the T_g of PET, it may instead be preferable to use asymmetrical, semi-rigid amide comonomers that are capable of enhancing the thermal performance of PET. Scheme 7.1 illustrates the proposed synthesis route of a novel semi-rigid amide comonomer, **7.2**, that may be suitable for this purpose.

Adapted from syntheses by Kitson *et al.*[9] and Mehenni *et al.*,[10] the facile coupling of the commercially available reagents methyl 4-(chlorocarbonyl)benzoate and 3-(4-aminophenyl)-propionic acid may be achieved through stirring in acetone with the base potassium carbonate (Step i). Following hydrolysis of the methyl benzoate group (Steps ii and iii), the resultant diacid may then undergo an esterification reaction to form comonomer **7.2** (Step iv). The final product therefore contains bis(EG) functionality as observed for the synthesised comonomers in Chapters 5 and 6.

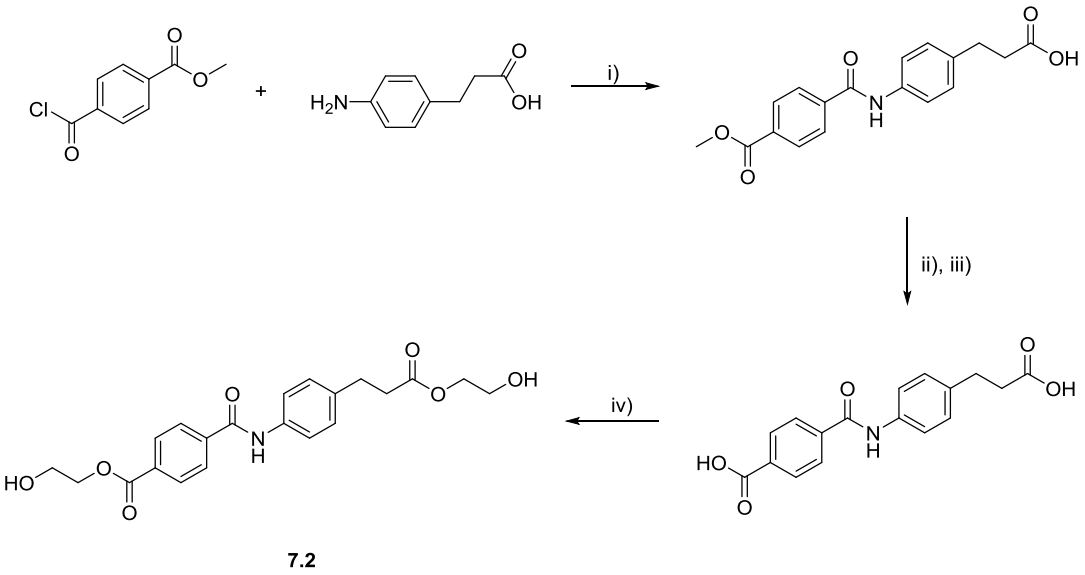

7.2

Scheme 7.1 Proposed reaction scheme for the synthesis of a semi-rigid amide comonomer, **7.2**. Reaction conditions: i) K_2CO_3, acetone, 16 h, RT; ii) NaOH, ethanol, H_2O, 16 h, reflux; iii) 2M HCl/H_2O, 3 h, RT; iv) TEA, 2-bromoethanol, 16 h, 90 °C.

The chain length of **7.2** is comparable to those observed for **6.2** and **6.3** and thus should retain semi-crystalline behaviour at content levels of at least 10 mol% in PET. Figure 7.3 illustrates the chain length of **7.2** against the BHET dimer to emphasise the potential for isomorphism. If there is sufficient tolerance demonstrated by the PET unit cell to incorporate **7.2** without a drastic fall in χ_c, then it may be favourable to shorten the length of the initial amino acid reagent. 4-Aminophenylacetic acid, 4-aminobenzoic acid and 4-aminobenzoic acid ethyl ester are all commercially available at lower cost than 3-(4-aminophenyl)-propionic acid,

providing greater variation to the final amide comonomer structure and potentially lowering any future scale-up costs.

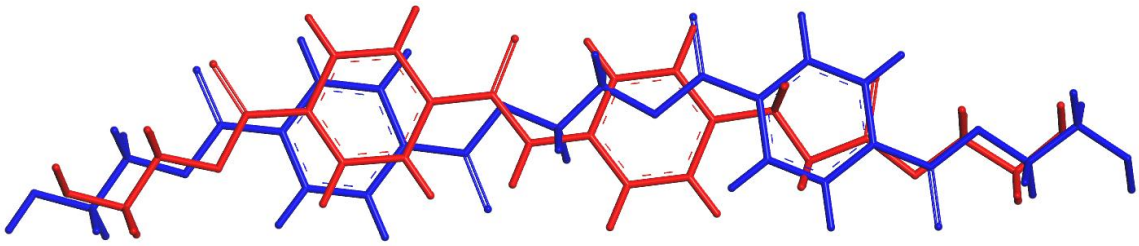

Figure 7.3 Overlaid energy-minimised chemical structures of the bis(2-hydroxyethyl)terephthalate dimer (blue) and **7.2** (red).

7.3 References

1 Y. G. Jeong, W. H. Jo and S. C. Lee, *Macromolecules*, 2000, **33**, 9705–9711.
2 J. Xiao, X. Wan, D. Zhang, Q. Zhou and S. R. Turner, *J. Polym. Sci. Polym. Chem.*, 2001, **39**, 408-415.
3 L. S. Park and D. C. Lee, *Polym. Eng. Sci*., 1995, **35**, 1629–1635.
4 Y. S. Hu, M. Rogunova, D. A. Schiraldi, A. Hiltner and E. Baer, *J. Appl. Polym. Sci.*, 2002, **86**, 98–115.
5 H. Ma, M. Hibbs, D. M. Collard, S. Kumar and D. A. Schiraldi, 2002, *Macromolecules*, **35**, 5123–5130.
6 L. J. F. Mary and P. Kannan, *Eur. Polym. J.*, 1999, **35**, 17–26.
7 P. Heyworth, *Internal Communication.*, 1995.
8 S. Al Abdulrazzak and S. A. Jabarin, *Polym. Int.*, 2002, **51**, 164–173.
9 P. J. Kitson, R. J. Marshall, D. Long, R. S. Forgan and L. Cronin, *Angew. Chem. Int. Ed.*, 2014, **53**, 12723–12728.
10 H. Mehenni, H. Guillou, C. Tessier and J. Brisson, *Can. J. Chem.*, 2008, **86**, 7–19.